UNIVERSITÉ DE SHERBROOKE

Faculté de génie
Département de génie électrique
et de génie informatique

electric – Transport, Energy Storage and Conversion laboratory
Canada

UNIVERSITÉ DE LILLE

École Doctorale des Sciences
Pour l'Ingénieur
(ED SPI)

Laboratoire d'Electrotechniques et d'Electronique de Puissance de Lille
France

STRATEGIES DE GESTION D'ÉNERGIE POUR VÉHICULES ÉLECTRIQUES ET HYBRIDE AVEC SYSTÈMES HYBRIDE DE STOCKAGE D'ÉNERGIE

ENERGY MANAGEMENT STRATEGIES OF ELECTRIC AND HYBRID VEHICLES SUPPLIED BY HYBRID ENERGY STORAGE SYSTEMS

Thèse de doctorat

Spécialité : génie électrique

par

NGUYỄN Bảo-Huy

Soutenue le 18 septembre 2019 devant le jury composé de :

M. Loïc BOULON	Professeur, Université du Québec à Trois-Rivières, QC, Canada	Rapporteur
M. Alain BOUSCAYROL	Professeur, Université de Lille, France	Directeur de thèse
M. Ruben GONZALEZ-RUBIO	Professeur, Université de Sherbrooke, QC, Canada	Rapporteur UdeS
M. Ronan GERMAN	Maître de conférences, Université de Lille, France	Co-encadrant
Mme Marie-Cécile PÉRA	Professeur, Université de Franche-Comté, France	Rapporteur
Mme Manuela SECHILARIU	Professeur, Université de technologie de Compiègne, France	Président du jury
M. Rochdi TRIGUI	Directeur de recherche, IFSTTAR, France	Examinateur
M. João Pedro F. TROVÃO	Professeur, Université de Sherbrooke, QC, Canada	Directeur de thèse

Lille, France – Sherbrooke (Québec), Canada

A problem well put is half solved.

John Dewey

Everything should be made as simple as possible, but not simpler.

(supposed to be) Albert Einstein

Của tin, gọi một chút này làm ghi.

Nguyễn Du

MEMBRES DU JURY

M. Loïc BOULON, Rapporteur
Professeur, Université du Québec à Trois-Rivières, QC, Canada

M. Alain BOUSCAYROL, Directeur de thèse
Professeur, Université de Lille, France

M. Ruben GONZALEZ-RUBIO, Rapporteur UdeS
Professeur, Université de Sherbrooke, QC, Canada

M. Ronan GERMAN, Co-encadrant
Maître de conférences, Université de Lille, France

Mme Marie-Cécile PÉRA, Rapporteur
Professeur, Université de Franche-Comté, France

Mme Manuela SECHILARIU, Président du jury
Professeur, Université de technologie de Compiègne, France

M. Rochdi TRIGUI, Examinateur
Directeur de recherche, Institut français des sciences et technologies des transports, de l'aménagement et des réseaux, France

M. João Pedro F. TROVÃO, Directeur de thèse
Professeur, Université de Sherbrooke, QC, Canada

Acknowledgements

I am writing these acknowledgements shortly with simple words. It is due to the Asian philosophy: let the blanks tell more.

This thesis has been carried out in four years under the supervision of my advisory board, whom my first words of acknowledgements are dedicated to. I would like to thank M. Alain BOUSCAYROL to supervise my thesis at L2EP, Université de Lille, France. I cannot count how many things I have learnt from him. With me, Alain is the best teacher in the world. I would like to thank M. João Pedro F. TROVÃO to supervise my thesis at e-TESC laboratory, Université de Sherbrooke, Canada. I cannot imagine how I could deal with the difficulties during my PhD life without him. With me, João is the kindest professor in the world. I would like to thank M. Ronan GERMAN to advise me on the work of the thesis. Ronan is the most interesting advisor I have ever known.

I would like to acknowledge the jury of my thesis defense. I would like to thank Mme Manuela SECHILARIU, Professor at Université de technologie de Compiègne, France for being the president of the jury. I would like to thank Mme Marie-Cécile PÉRA, Professor at Université de Franche-Comté, France and M. Loïc BOULON, Professor at Université du Québec à Trois-Rivières, Canada for being the reviewers (rapporteurs) of the thesis. I would like to thank M. Ruben GONZALEZ-RUBIO, Professor at Université de Sherbrooke, Canada for being the UdeS reviewer of the thesis. I would like to thank M. Rochdi TRIGUI, Director of research at IFSTTAR, France for being the examiner of the thesis. All of their questions, discussions, and suggestions are in the positive directions to help me improving my work. I also appreciate their encouragements with positive comments on the reports and during the thesis defense.

In France, I have worked in L2EP which is a dynamical and comfortable research environment. I would like to thank Mme Betty LEMAIRE-SEMAIL – the Director of the laboratory – and all the professors and staffs of L2EP for developing this environment.

I have been also with Hanoi University of Science and Technology (HUST), Vietnam. Hanoi is where I was born; and HUST is the hometown of my academic life. I would like to thank thầy TẠ Cao Minh – the father of my academic life. My thanks go to chị Hà, anh Thành, anh Quang, Hùng, and all my teachers and friends at HUST.

I have had a great time of joyfulness at L2EP with my friends, especially in P2 and ESPRIT. Thank you, Abdoulaye, Anatole, Clément, David, Emna, Florentin, Florian, Gianluca, Guillaume, Hugo, Houssein, Jérôme, Jalal, Jian, Kaibo, Kévin, Laure, Laurent, Loris, Marc, Meryeme, Nicolas, Oriol, Rihab, Ryan, Shingo, Smail, Sylvain, and you guys in L2EP. I will miss our time, especially with lunch, coffee, and Tarot!

My life in Lille has been colorful thanks to my Vietnamese friends. Thank you, anh Kỳ, anh Bình, anh Long, Tân; and thank Jinlin. Thank you, Trang and Huy, my so-sweet neighbors. Thank you too, Lê.

It has been also a great time at e-TESC lab with my friends there. Thank you, Adrien, Ahmad, Alexandre, Félix, Mandé, Mebrahtom, Pascal. Special thanks to you, Chadi!

My thanks go to the Vietnamese community in Sherbrooke. Thank you, chú Hiến, chị Vân, anh Cường, chị Hà, chị Hiền, anh Khôi, Bảo, Dũng, Huệ, Kiên, Long, Thuỷ, Tính, Tuyền.

My family always backs me without any need of thank-you words. This thesis is dedicated to the two women of my life: my mother and my wife.

Résumé

Les véhicules électriques et hybrides font partie des éléments clés pour résoudre les problèmes de réchauffement de la planète et d'épuisement des ressources en combustibles fossiles dans le domaine du transporte. En raison des limites des différents systèmes de stockage et de conversion d'énergie en termes de puissance et d'énergie, les hybridations sont intéressantes pour les véhicules électriques (VE). Dans cette thèse, deux hybridations typiques sont étudiées

- un sous-système de stockage d'énergie hybride combinant des batteries et des supercondensateurs (SC) ;
- et un sous-système de traction hybride parallèle combinant moteur à combustion interne et entraînement électrique.

Ces sources d'énergie et ces conversions combinées doivent être gérées dans le cadre de stratégies de gestion de l'énergie (SGE). Parmi celles-ci, les méthodes basées sur l'optimisation présentent un intérêt en raison de leur approche systématique et de leurs performances élevées. Néanmoins, ces méthodes sont souvent compliquées et demandent beaucoup de temps de calcul, ce qui peut être difficile à réaliser dans des applications réelles.

L'objectif de cette thèse est de développer des SGE simples mais efficaces basées sur l'optimisation en temps réel pour un VE et un camion à traction hybride parallèle alimentés par des batteries et des SC (système de stockage hybride). Les complexités du système étudié sont réduites en utilisant la représentation macroscopique énergétique (REM). La REM permet de réaliser des modèles réduits pour la gestion de l'énergie au niveau de la supervision. La théorie du contrôle optimal est ensuite appliquée à ces modèles réduits pour réaliser des SGE en temps réel. Ces stratégies sont basées sur des réductions de modèle appropriées, mais elles sont systématiques et performantes. Les performances des SGE proposées sont vérifiées en simulation par comparaison avec l'optimum théorique (programmation dynamique). De plus, les capacités en temps réel des SGE développées sont validées via des expériences en « hardware-in-the-loop » à puissances réduites. Les résultats confirment les avantages des stratégies proposées développées par l'approche unifiée de la thèse.

Mots-clés : véhicule électrique hybride, véhicule électrique, stratégie de gestion de l'énergie, optimisation en temps réel, batterie, supercondensateur (SC), système de stockage d'énergie hybride, représentation énergétique macroscopique (REM), simulation « hardware-in-the-loop (HIL) ».

Abstract

Electric and hybrid vehicles are among the keys to solve the problems of global warming and exhausted fossil fuel resources in transportation sector. Due to the limits of energy sources and energy converters in terms of power and energy, hybridizations are of interest for future electrified vehicles. Two typical hybridizations are studied in this thesis:

- hybrid energy storage subsystem combining batteries and supercapacitors (SCs); and
- hybrid traction subsystem combining internal combustion engine and electric drive.

Such combined energy sources and converters must be handled by energy management strategies (EMSs). In which, optimization-based methods are of interest due to their high performance. Nonetheless, these methods are often complicated and computation consuming which can be difficult to be realized in real-world applications.

The objective of this thesis is to develop simple but effective real-time optimization-based EMSs for an electric car and a parallel hybrid truck supplied by batteries and SCs. The complexities of the studied system are tackled by using Energetic Macroscopic Representation (EMR) which helps to conduct reduced models for energy management at the supervisory level. Optimal control theory is then applied to these reduced models to accomplish real-time EMSs. These strategies are simple due to the suitable model reductions but systematic and high-performance due to the optimization-based methods. The performances of the proposed strategies are verified via simulations by comparing with off-line optimal benchmark deduced by dynamic programming. Moreover, real-time capabilities of these novel EMSs are validated via experiments by using reduced-scale power hardware-in-the-loop simulation. The results confirm the advantages of the proposed strategies developed by the unified approach in the thesis.

Keywords: Hybrid electric vehicle (HEV), electric vehicle (EV), energy management strategy (EMS), real-time optimization, battery, supercapacitor (SC), hybrid energy storage system (H-ESS), Energetic Macroscopic Representation (EMR), Hardware-In-the-Loop (HIL) simulation.

Table of contents

List of figures

List of tables

Nomenclature

DP	Dynamic Programming
ECMS	Equivalent Consumption Minimization Strategy
ED	Electrical Drive
EM	Electrical Machine
EMR	Energetic Macroscopic Representation
EMS	Energy Management Strategy
ESR	Equivalent Series Resistance
EV	Electric Vehicle
H-ESS	Hybrid Energy Storage System/Subsystem
HEV	Hybrid Electric Vehicle
HIL	Hardware-In-the-loop
ICE	Internal Combustion Engine
IM	Induction Machine
LPF	Low-Pass Filter
LQR	Linear Quadratic Regulator/Regulation
MPC	Model Predictive Control
NEDC	New European Driving Cycle
OCV	Open-Circuit Voltage

PMP	Pontryagin's Minimum Principle
PMSM	Permanent Magnet Synchronous Machine
SC	Supercapacitor
SoC	State-of-Charge
UDDS	Urban Dynamometer Driving Schedule
WLTC	Worldwide harmonized Light vehicles Test Cycles

Introduction

The world is facing critical issues of environmental pollution and exhaust of fossil fuel resources. Meanwhile transportation systems play an important role in the both figures of environmental care and fuel consumption [Bauer 2016]. Electric and hybrid vehicles are among the most promising solutions for these problems.

In fact, electric vehicles (EVs) have a long history counted from the 19th century [DoE 2014]. At their early days, EVs were suitable urban transportations with short traveling distances. However, EVs then dramatically lost their market due to the competition of gasoline cars. The main factors are mature internal combustion engine (ICE) technology and cheap oil mass production. Since 2000s, EVs have been becoming more and more promising. It is a result of technology developments in energy storage systems, power electronics, and electrical drives (in terms of power and energy). It can be predicted that EVs will be an important part of the future of sustainable green transportation.

Nevertheless, there are still gaps between energy storage devices and ICE (with fuel tank) in terms of power and energy densities [Whittingham 2012]. Hence, today has not been yet the day of full EVs without any fossil fuel consumption. Thus, hybridizations are of interest in this transition stage. This thesis studies two types of hybridizations:

- different electrical energy storages (battery/supercapacitor) are combined to form hybrid energy storage subsystem (H-ESS); and

- mechanical converters (ICEs) combine with electrical converters (electrical drives) to form hybrid traction subsystem of hybrid electric vehicles (HEVs).

The different H-ESSs and hybrid traction subsystems must be handled by energy management strategies (EMSs). This topic has been attracting numerous efforts from both academics and industry [Salmasi 2007; Tie 2013]. In this context, the thesis is conducted in the collaborations between French and Canadian research programs and institutions. Firstly, it is within the French network on hybrid and electric vehicles (MEGEVH) and Canada Research Chair (CRC) in Efficient Electric Vehicles with Hybridized Energy Storage Systems. In MEGEVH, the work is conducted at the Laboratory of Electrical Engineering and Power Electronics (L2EP), University of Lille, France. Whereas in CRC, the thesis is carried out at the electric – Transport, Energy Storage and Conversion laboratory (e-TESC lab.), University of Sherbrooke (UdeS), Québec, Canada. This thesis has inherences and interactions with several works developed at MEGEVH, L2EP and CRC, e-TESC on energy management, energy storage systems, optimization methods, power electronics, and electrical drives. Moreover, the studied systems of the thesis are of the common interest between the French program CE2I (Integrated Intelligent Energy Converters) and the Canadian one Mitacs Accelerate which is multi-source hybrid vehicles.

EMS development methods – the topic of this thesis – can be classified into two main groups: rule-based and optimization-based methods [Salmasi 2007]. Rule-based methods are developed based on human knowledge and experiences on the behaviors of the systems. For instance, it is known that batteries prefer smooth current while supercapacitors (SCs) can work with fluctuated power profile [Christen 2000]. Thus, a rule for battery/SC H-ESSs is defined that high-frequency parts of the demanded power should be provided by the SCs, while the low-frequency parts are the duty of the batteries. A low-pass filter is often employed to realize this rule, e.g., [Schaltz 2009]. The rules can be deterministic, like filtering, or based on artificial intelligence such as fuzzy logic [Li X. 2009; Martinez 2011] and neural networks [Moreno 2006; Tian 2016]. Rule-based methods are often intuitive, straightforward, and suitable for real-time implementation. However, they depend on human expertise which are not always the most proper. Furthermore, methods like neural networks often require long training time with huge data and strong computational resources.

Optimization-based methods are developed in the way that the energy management problems are formulated in forms of optimization problems; then optimization techniques are applied to solve the problems. For example, to save fuel of an HEV, the studied vehicle is modeled as a dynamical system and the fuel consumption is defined as the cost function. The batteries energy variation is also charged as a penalty in the cost function. For that, an equivalent factor must be introduced. Then, optimal control theory is applied to solve that problem to obtain the so-called equivalent consumption minimization strategy (ECMS) [Sciarretta 2004]. The strategies can be off-line optimal [Vinot 2014] or real-time sub-optimal [Ettihir 2016]. The most advantage of the optimization-based methods is that it allows developing EMSs by an organized approach. That means the developer just has to follow an "automatic" procedure to obtain the strategy. Moreover, since the EMSs are based on optimization techniques, they are optimal (off-line strategies) or often close-to-optimal (real-time strategies) with high performances reported. The drawbacks are often due to the complexities of the methods and high computational efforts which may prevent them from real-world applications.

Within this context, the thesis aims to develop simple but effective real-time optimization-based EMSs for an electric car and a hybrid truck supplied by battery/SC H-ESS. In order to tackle the complexity of the studied systems, Energetic Macroscopic Representation (EMR) [Bouscayrol 2013; EMR 2019] will be employed as a unified formalism. The approach is to use EMR to systematically deduce suitable reduced models for energy management; then applying optimal control theory to develop real-time strategies. These strategies, on one hand, inherit the systematic approach and high performances of optimization-based methods; on the other hand, benefit the simplifications due to EMR-based model reduction. The performances of the developed strategies will be verified by comparing with the off-line optimal strategies as the benchmarks. Dynamic programming (DP) will serve as these benchmarks due to its ability to deduce optimal solutions [Kirk 1970; Sundström 2009]. Since DP is an off-line method, the comparisons will be done by simulations. Moreover, the real-time ability of the developed EMSs will be validated via experiments by using reduced-scale power hardware-in-the-loop (HIL) simulation [Bouscayrol 2011].

The thesis will be presented in three chapters. Chapter 1 will address the background of the thesis and a literature review on energy management methods. In which, the global context and the scientific context of the thesis will be presented. Based on that, the issue of energy

management for the studied systems which are a battery/SC EV and a battery/SC hybrid truck will be figured out. Then, the chapter will review the state-of-the-art developments in EMSs of HEVs and H-ESS where the pros and cons of each method will be analyzed. Finally, the objective and approach of the thesis will be addressed.

Chapter 2 will present the development and validations of a real-time optimization-based current distribution strategy for a battery/SC EV based on Hamiltonian minimization. The studied system will be modeled and controlled by using EMR and inversion-based control scheme. Then model reduction and transformations steps will be done to obtain a reduced mathematical model. Next, the third necessary condition of Pontryagin's minimum principle will be applied to deduce a real-time strategy. With the EMR-based reduced model and by using only the condition of Hamiltonian minimization, the proposed strategy is simple and does not require any more feedback adaptation scheme for real-time implementation. The new EMS will be compared to the conventional real-time strategies, the DP-based optimal benchmark, and the case of battery-only EV by simulations. Finally, the power HIL experiments will validate the real-time ability of the novel strategy.

In Chapter 3, a real-time optimization-based torque distribution strategy for a parallel hybrid truck supplied by batteries and SCs will be proposed and validated. Modeling, EMR, and inversion-based control scheme of the studied system will be presented. Next, the reduced mathematical model will be achieved after several steps of model reduction and transformations. Thereafter, to simultaneously accomplish the objective of fuel consumption and the requirement of charge sustaining, the cost function will be reformulated. As a result, the optimal control problem can be solved by using linear quadratic regulation (LQR) technique. The obtained solution will be in the form of a closed-loop control of the battery state-of-charge (SoC) which is ready to serve as a real-time EMS. DP-based optimal solution and the conventional ICE truck will be used to define the performances of the proposed strategy. The real-time ability of the new EMS will then be experimentally validated by using power HIL simulation.

1. Background and literature review

This chapter aims to address the context, the objective, and the approach of the thesis. The global context will be firstly presented to point out the necessity of developing electric and hybrid vehicles. Then the hybridizations of mechanical and electrical sources will be addressed. Next, it will be the scientific and technical context of research networks and programs which the thesis is based on. Afterwards a state-of-the-art review on methods to develop energy management strategies (EMSs) will be presented. Based on that, the objective and the approach of the thesis will be figured out.

1.1. Context of the thesis

1.1.1. Electrified vehicles: why electric and why not yet full electric?

a. Why electric vehicles?

Electric vehicle (EV) is not a new concept. The history of EVs can be counted from the late 19th century [DoE 2014; Ehsani 2010] (Figure 1.1). At that time, long-distance traveling was being responsible of trains with steam locomotive, as a result of the first industrial revolution. Urban transportations, however, were still dominated by horse-drawn vehicles (steam-engine cars existed, nevertheless, their limits on efficiency, sizes and masses of boilers prevented them from the market.) There was a need of machines to replace horses on the roads. With previous inventions of lead-acid battery and electrical DC machine, electric cars appeared as a solution. The first commercial electric car in New York could reach a maximal speed of 32 km/h and an autonomy range of 40 km [Ehsani 2010]. That was suitable for urban transportations that days. EVs therefore rapidly developed and had a "golden age" during the first decade of the 20th century.

EVs were not the only solution for automotive industry at that time, but also gasoline cars. The first commercial internal combustion engine (ICE)-powered car was released in 1886 in Germany [Melosi 2010]. Nonetheless, ICE vehicles had significant drawbacks. One of the most important problems was that ICEs needed manual starting by a hand crank. Besides, manual gearshift was difficult to be handled. Their noise and emission also mattered. Thus, at the beginning, EVs were advanced over gasoline cars. The game-changer was Henry Ford's Model-T released in 1908, which was a reliable and cheaper ICE car. Then the electric starter, patented in 1911 and implemented in the year after, completed the mature ICEs since hand crank was no longer needed. Other factors also contributed to the downgrading of EVs. Oil became cheaper thanks to the discovery of massive fossil fuel resources and effective oil productions. Besides, long-distance traveling via roads, instead of only railways as before, was more and more in demand due to the developments of cities-connecting roads. Battery and charging technologies at that time did not allow EVs satisfying such traveling. As a consequence, EVs totally lost the market by about 1935 [DoE 2014].

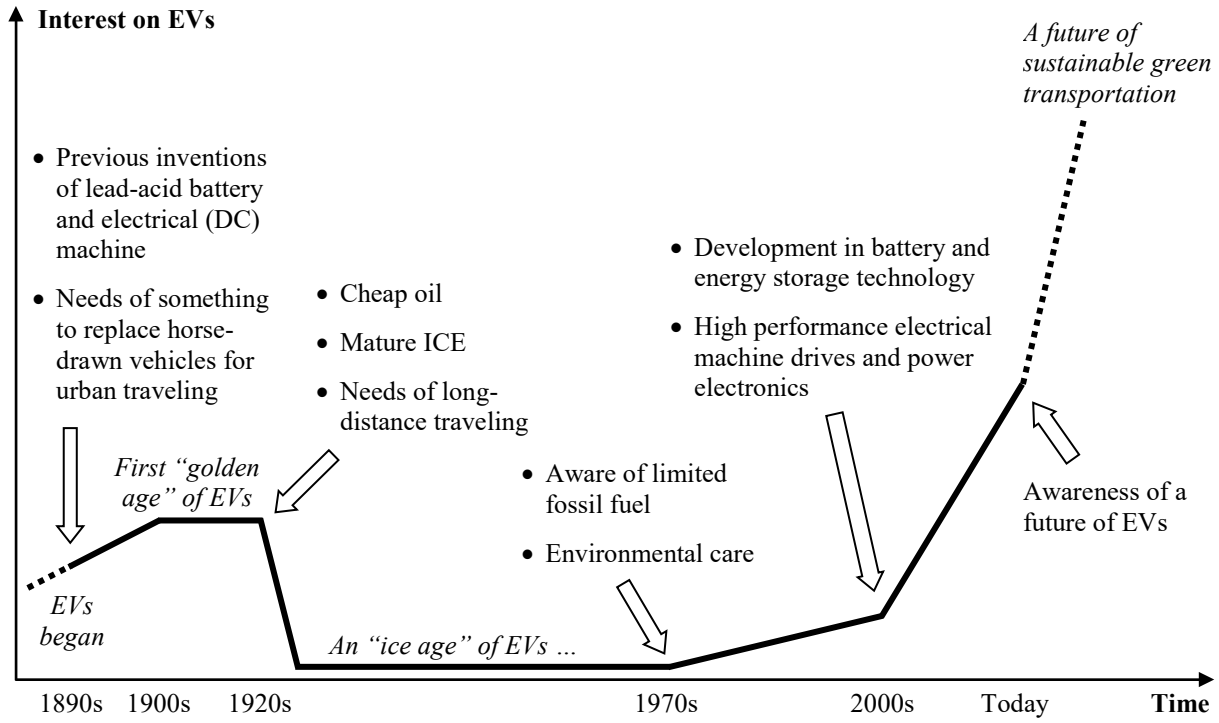

Figure 1.1: A brief history of the interest on EVs in terms of power and energy.

The "ice age" of EVs had been continuing until 1970s. The oil crisis made people aware of the risk of depending on that sort of energy. It was also realized the fact that fossil fuel is not unlimited. Additionally, environmental issues raised concerns of pollution caused by cars [Chan 2009; Ehsani 2010]. The interests on EVs came back; the "ice" began melting. Automotive manufactures started producing versions of electric cars, such as GM EV1, the most notable electric car at that time. However, EVs were still low-speed short-range cars, mostly due to the limits of battery technology. Lead-acid and even nickel metal hydride batteries are not capable for EVs to be close to gasoline cars, in terms of both power (in recharge) and energy. Thus, the interests on EVs was growing, but not yet so strongly.

Tesla, Inc. has been a game-changer by making EV a reliable car with Tesla Roadster released in 2008 in the United States. Right after that, Mitsubishi i-MiEV (2009) and Nissan Leaf (2010) were introduced in Japan have been being the examples of successful EVs accepted by customers. Then, EVs of European automotive manufacturers have been in market such as BMW i3 and Renault ZOE. The most important factor for a reliable EV, which means in fact highway-capable EV, has been the developments in battery technologies. Lithium-ion (Li-ion) batteries have become mature for EVs applications. Batteries capacity this day can allow vehicle autonomy ranges up to 400 km (Renault ZOE, since 2016)[1], and even more than 500 km (Tesla Model S, since 2017). Battery charging technologies, including batteries management and power electronics chargers, enable quick-charge mode which can charge batteries up to 80% of SoC within about 30 minutes[2]. Besides, high-performance electrical drives contribute on providing attractive characteristics for EVs, such as very high efficiency powertrains and in-

[1] With New European Driving Cycle (NEDC).
[2] However, fast charging normally degrades batteries life-time.

wheel machines. EV now is the important trend, in which most of big automotive manufacturers have been producing their versions of electric cars. A future of sustainable green transportation worldwide is growing.

b. Why not yet electric vehicles?

It has been concluded that EVs are the possible future of the world for personal vehicles. However, today, or even near future, is still not the day of pure EVs without any fossil fuel-powered vehicles. On the engineering aspect, the reason mostly lies on the limits of energy storage devices.

Figure 1.2 illustrates these limits in terms of power and energy adapted from [Trovão 2017; Werkstetter 2015]. The horizontal axis is specific power measured in W/kg. The vertical axis represents specific energy with the unit of Wh/kg. The crossed lines depict typical dynamics of these sources and storages. For example, it shows that fuel cells are the electrical energy source that can store the highest energy per mass but has mostly the lowest ability to generate power.

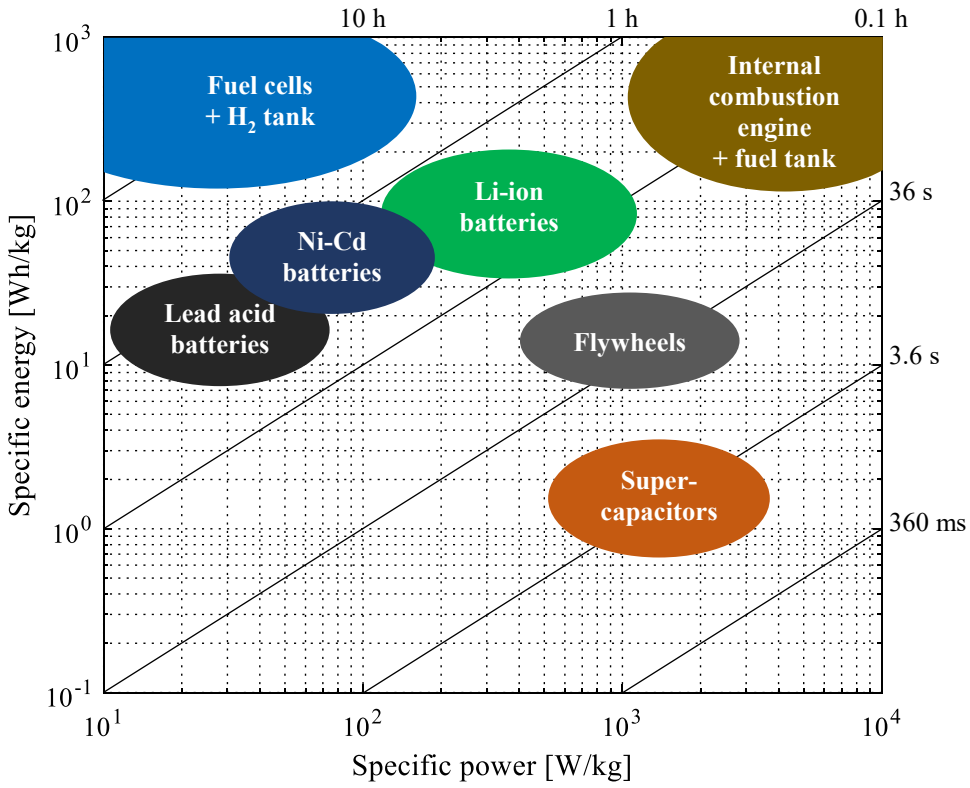

Figure 1.2: Power and energy densities comparison of common sources used for vehicles (adapted from [Trovão 2017; Werkstetter 2015]).

It is shown by Figure 1.2 that so far none of electrical energy source or storage can completely replace ICE. The most common ESSs used in modern EVs are Li-ion batteries, which have less capability than ICE in terms of energy. The autonomy range of one of the most luxury EVs (Tesla model S, up to more than 500 km) is just close to a common conventional gasoline car (up to 600 km). To produce the same power, batteries packs are more heavy and larger than ICEs with fuel tanks, due to the difference in specific power. In terms of customers convenience, it takes commonly about five minutes to totally fill-up the fuel tank of a gasoline car; whereas it is 30 minutes for an EV to charge about 80% of its batteries in case of fast charging mode. The number is about 7 to 8 hours for EVs in case of normal charge at home.

c. Hybridizations of energy sources and storages

Electrification of vehicles is necessary but not yet completed as discussed above. While waiting breakthrough technologies on energy storage devices that can be commercialized, hybridizations are solutions for current electrified vehicles. Two sorts of hybridizations are addressed in this thesis:

- hybridization of mechanical converters (ICEs) and electrical converters (electrical drives) to form hybrid traction subsystem in hybrid electric vehicles (HEVs); and
- hybridization of different electrical energy storages (battery/SC) to form hybrid energy storage subsystem (H-ESS) used in EVs and/or HEVs.

Hybrid electric vehicles configurations

HEVs can be classified into three configurations: series, parallel, and series-parallel as illustrated in Figure 1.3, Figure 1.4, and Figure 1.5, respectively [Chan 2010]. Each topology has its own pros and cons which are suitable for different applications.

Series HEVs are composed of an ICE and two electrical machines (EM) (see Figure 1.3). The drivetrain is propelled by EM 1 which is supplied by power electronics converter 1. The DC power, which supplies converter 1, is provided by the DC bus. The ICE mechanically coupled with EM 2 serving as a generator; the generated electrical power is then supplied to the DC bus via converter 2. The DC bus is the parallel coupling between converter 2 and the ESS.

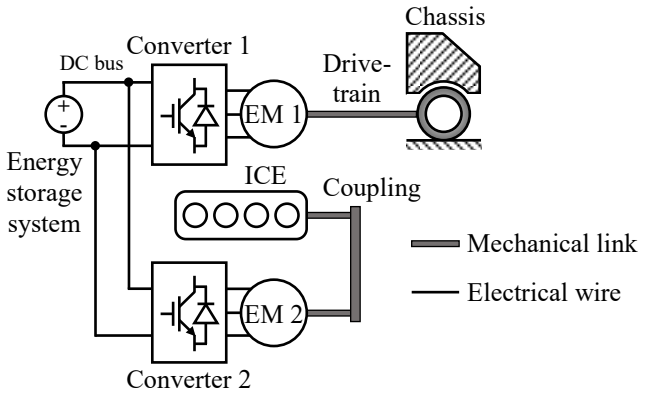

Figure 1.3: General configuration of series HEVs.

In the series configuration (see Figure 1.3), there is no mechanical coupling between the vehicle drivetrain and the ICE. That enables the ICE to work at its optimal operation region. The disadvantage lies on the size of the EMs. EM 1 must provide all the traction power required by the drivetrain. EM 2 must be able to convert all the power generated by the ICE. Sizing the ESS is also challenging. Series HEVs are therefore efficient but expensive and bulky. Thus, this configuration is suitable for large vehicles, e.g., buses [Hu 2014; Li J. 2017], locomotive [Mayet 2014b], and military vehicle [Boulon 2010, 2013].

In parallel HEVs, the ICE, the EM, and the drivetrain are mechanically coupled (see Figure 1.4). The machine is supplied by the converter and the ESS. Because the mechanical power is provided by the machine and the engine, they can provide higher power than their own maximal capabilities. This configuration has drawback in term of efficiency since the ICE speed is directly linked to the vehicle velocity. That prevent the ICE working in its optimal operation region. Clutch and variable transmission (e.g., multi-speed gearbox) are therefore often required. Due to its pros and cons, the applications of the parallel configuration are on cars and on the heavy-duty vehicles working mainly in stationary driving conditions, such as trucks [Biasini 2013; Mayet 2019; Mullem 2010; Suzuki 2008].

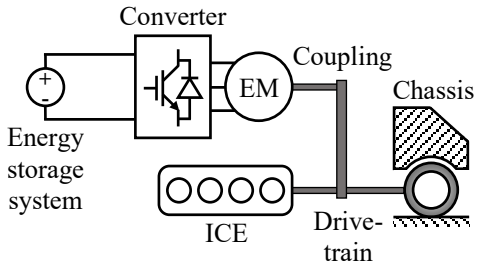

Figure 1.4: General configuration of parallel HEVs.

Series-parallel HEVs, as its name, are the combination of series and parallel configurations, in which the ICE and the EMs are coupled both mechanically and electrically (see Figure 1.5). A typical mechanical device, called planetary gear set, can be used to connect EM 1, EM 2, the ICE, and the drivetrain. The DC bus is also the electrical coupling of the ESS and the generation subsystem like series HEVs.

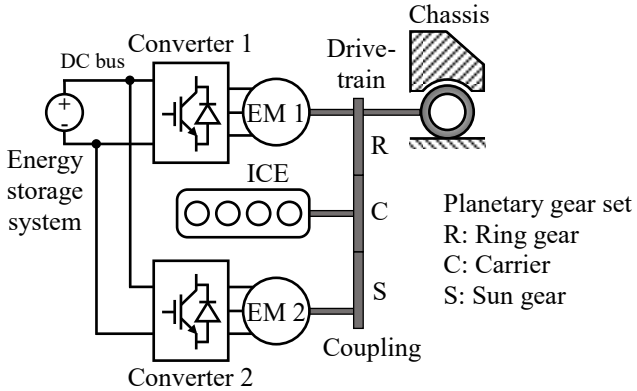

Figure 1.5: A configuration of series-parallel HEVs.

This sort of HEVs can gain advantages of both series and parallel configurations. Due to the mechanical parallel connection, the drivetrain can be driven by both the EM 1 and the ICE. Besides, the planetary gear set allows controlling speed of the ICE within its optimal operation range. However, the gear set is complex and difficult to be sized for heavy-duty vehicles (multiple sets are required, that is even more complex, e.g., [Lhomme 2017; Xiang 2017]). Thus, series-parallel configuration is most suitable for cars [Borhan 2012; Chen Zh. 2014a] (such as Toyota Prius [Montazeri-Gh 2015]).

Hybrid energy storage subsystems configurations

H-ESS is the combinations of two or several electrical ESSs and/or sources to gain advantages of both high-power-density and high-energy-density sorts of devices. An H-ESS uses the different ESS as a function of the situation. The goal can be to extend the main ESS lifetime. Hybridization between batteries and SCs is among the most promising solutions for H-ESSs for electrified vehicles (EVs and HEVs) [Allègre 2013; Trovão 2015a]. Batteries are the most expensive component of an electric or hybrid vehicle nowadays. Degradations of batteries over driving cycles are therefore costly. Hence, adding SCs to reduce the aging stresses on batteries is of interest. In fact, the battery/SC H-ESS has been installed in commercial products such as Bolloré Bluecar® [Bolloré 2012]. Batteries and SCs can be combined by mainly three ways: passive, semi-active, and active topologies (Figure 1.6, Figure 1.7, and Figure 1.8, respectively).

Passive configuration (see Figure 1.6) is the simplest topology of battery/SC H-ESSs. The batteries and the SCs are directly connected in parallel at the DC bus and supply power to the traction subsystem. Since the internal impedance of the SCs is much lower and the dynamics of the SCs are much faster than those of the batteries, the SCs can compensate the high fluctuated current demanded by the traction part.

The solution is relatively cheap for H-ESSs. It is simple, highly reliable, and there is no need of control and energy management. However, the current compensation is passive, instead of being controlled. Moreover, the SCs voltage is fixed to the batteries voltage, hence very few of SCs energy, which is directly related to their voltage, can be used. Thus, this topology is commonly used for application requiring simplicity and high reliability such as [Ehsani 2006; Henson 2008; Pagano 2007; Trovão 2016].

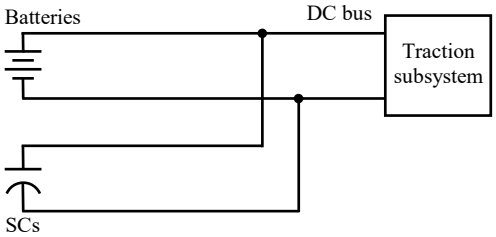

Figure 1.6: General configuration of passive battery/SC H-ESS.

To effectively use SCs to support batteries, a bidirectional DC/DC converter should be added to control the SCs power; that forms the semi-active configuration (see Figure 1.7). The SCs are connected in series with an inductor which is followed by the low-voltage side of a power

electronics chopper. The high-voltage side of the chopper is connected in parallel with the batteries. The DC bus voltage is fixed by the batteries voltage.

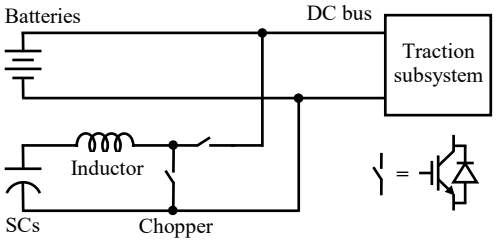

Figure 1.7: General configuration of semi-active battery/SC H-ESS.

This topology allows the SCs power being controlled to obtain optimal power profile of the batteries with only one DC/DC converter added. This solution offers good trade-off between performance and price and/or complexity. Hence, it is widely used in many applications such as [Ibrahim 2016; Kollmeyer 2014; Vinot 2013; Vulturescu 2013]. The drawback of semi-active configuration is that the batteries voltage must be high enough to supply the traction subsystem. Heavy-duty vehicles like truck or bus need high DC bus voltages which can be challenging for batteries sizing. Additionally, uncontrolled DC bus voltage can lead to non-optimal operation of EM drive of the traction subsystem.

To overcome the above drawback of the semi-active topology, active configuration is often of interest (see Figure 1.8). One more DC/DC converter is added to batteries and coupled in parallel with the chopper of the SCs branch. They supply power to the traction subsystem via a DC bus capacitor. The DC bus voltage must therefore be controlled.

With this configuration, the batteries voltage is lower than the DC bus one; that cause the batteries sizing less challenging for high voltage applications. The DC bus voltage can be controlled to be stationary, or to vary following the optimal operation of the machine drive subsystem. Due to its high performances, the active topology is popular in many applications e.g., [Dai 2016; De Castro 2012; Hredzak 2014]. Its disadvantages lie on the complexity of control scheme with more voltage and current controls and the cost of additional devices.

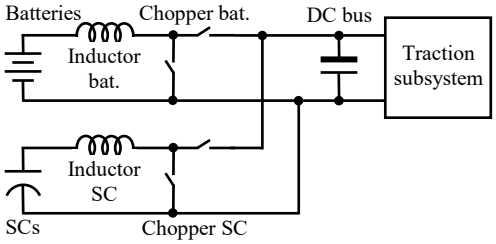

Figure 1.8: General configuration of active battery/SC H-ESS.

1.1.2. Energy management strategies: why and where is the thesis?

As previously discussed, hybridization is promising for efficient electrified vehicles nowadays, in both mechanical and electrical parts of the vehicles. However, the hybridized systems must be coordinated so that their subsystems cooperate correctly and effectively to achieve certain

objectives. Such mandatory coordination is energy management strategy (EMS) which is the focus of this thesis.

Due to the importance of EMSs in hybridized electrified vehicles, they are of study interest of various research institutions, networks, and programs. This thesis is within a collaborated framework of the French network on hybrid and electric vehicles (MEGEVH) and the Canada Research Chair in Efficient Electric Vehicles with Hybridized Energy Storage Systems. In MEGEVH, the thesis is conducted at the Laboratory of Electrical Engineering and Power Electronics of Lille (L2EP), University of Lille, France. For Canada side, the thesis is conducted at the electric – Transport, Energy Storage and Conversion laboratory (e-TESC lab.), University of Sherbrooke (UdeS), Québec, Canada.

MEGEVH stands for Energy Modeling and Energy Management of Hybrid and Electric Vehicles [MEGEVH 2019]. The network, initiated in 2004, is composed of 10 academic laboratories and 8 industrial partners in France (Figure 1.9). It aims to develop modeling and energy management methods for electric and hybrid vehicles which are validated in laboratory experimental platforms with real reference vehicles.

The common formalism used in MEGEVH is Energetic Macroscopic Representation (EMR) which is a formalism for modeling, control, and energy management of complex and multi-physical energetic systems [Bouscayrol 2000, 2013; EMR 2019]. EMR highlights the interactions between subsystems in terms of power flows respecting the principles of causality and interaction [Hautier 2004; Iwasaki 1994]. More details on EMR are given in Appendix A.1. In MEGEVH and in this thesis, EMR is used as the unified formalism for modeling, control, and EMSs development.

Figure 1.9: The map of MEGEVH network [MEGEVH 2019].

This thesis is in the intersection of MEGEVH "Strategy" and MEGEVH "Multi-source" (Figure 1.10). The framework MEGEVH "Strategy" is the researches on modeling, control and EMSs of HEVs [Letrouvé 2013; Lhomme 2007] and multi-source EVs [Dépature 2017; Marx 2017]. The framework MEGEVH "Multi-source" focuses on the EMSs for EVs and HEVs supplied by multiple sources (Hybrid-ESS). Studied H-ESSs have been fuel cells and SCs [Dépature 2017], multi-stack fuel cells [Marx 2017], and fuel cell/battery/SC subsystem [Castaings 2016b], all for EVs. Interests on EMSs of fuel cell/battery H-ESSs have been also addressed in a scientific contest [Dépature 2018a] organized by MEGEVH.

Additionally, this thesis shares the common research interest with MEGEVH "Storage" on the studied systems of energy storages [Allègre 2010a; Castaings 2016b; Gauchia 2011]. Furthermore, the thesis inherits from MEGEVH "Optim" the methods on development of global optimization and real-time optimization-based EMSs for HEVs [Horrein 2015; Kermani 2009]. Within this framework, this thesis studies development methods of optimization-based EMSs for EVs and HEVs supplied by batteries and SCs.

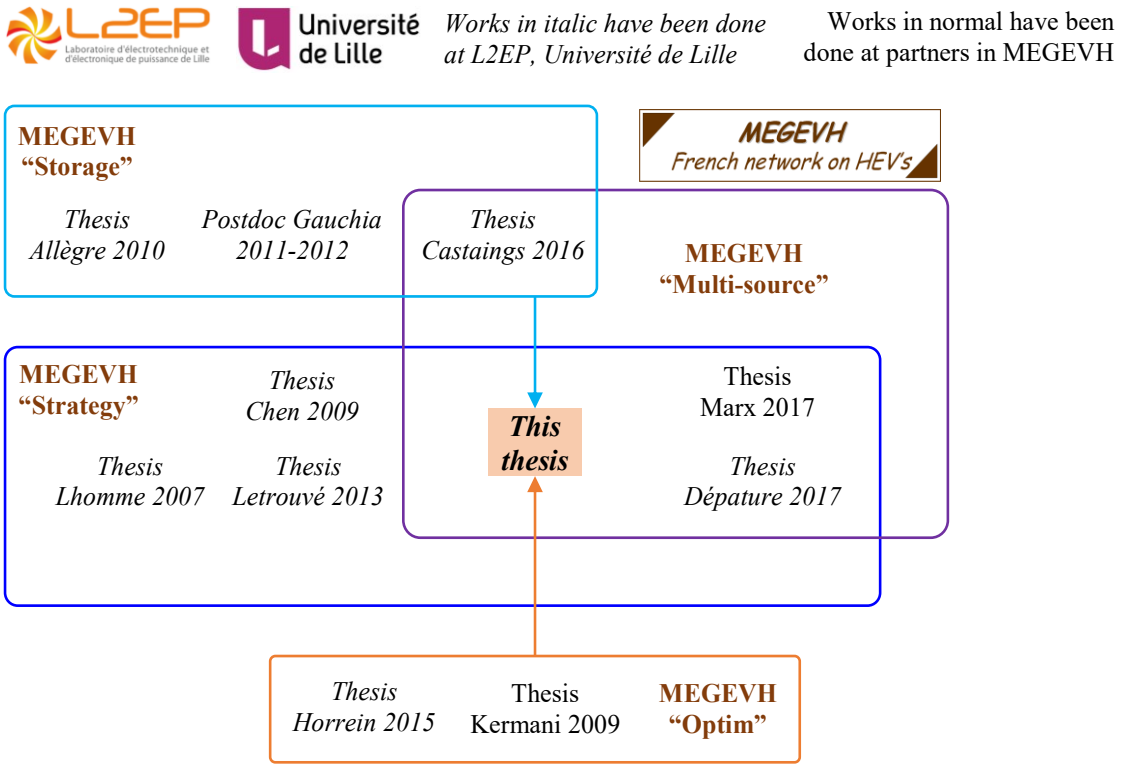

Figure 1.10: Scientific context of the thesis within MEGEVH network.

The thesis is also under the Canada Research Chair program in Efficient Electric Vehicles with Hybridized Energy Storage Systems conducted in UdeS [CRC 2017] (Figure 1.11). The research project aims to study the subsystems of EVs including electrical machines [Shah Mohammadi 2018], power electronics [Beraki 2017; Daouda 2018], and batteries and H-ESSs

[LeBel 2018; Pelletier 2018]. To coordinate these subsystems in an efficient EV, there are works on energy management [De Castro 2012; Gomozov 2017; Machado 2016; Trovão 2013b, 2015b, 2017] those the thesis is based on.

The technical context of the thesis is also in the common interest of French and Canadian research programs, under CE2I (Integrated Intelligent Energy Converters) and Mitacs Accelerate, respectively. Within CE2I program, a multi-source hybrid truck is studied as a concept of integrated intelligent transportation. Meanwhile, within Mitacs Accelerate program, the project focuses on multi-machine multi-source vehicles. That context leads to the studied systems of this thesis those are an EV and a hybrid truck supplied by H-ESSs combining Li-ion batteries and SCs.

This section has already discussed the global context of studying EVs and HEVs, the needs of hybridizations, the scientific context of the research networks and programs, and the technical context on the studied systems of the thesis. It has been figured out that energy management plays an essential role in hybridized electrified vehicles. In the next section, a state-of-the-art review on methods for EMSs development will be presented.

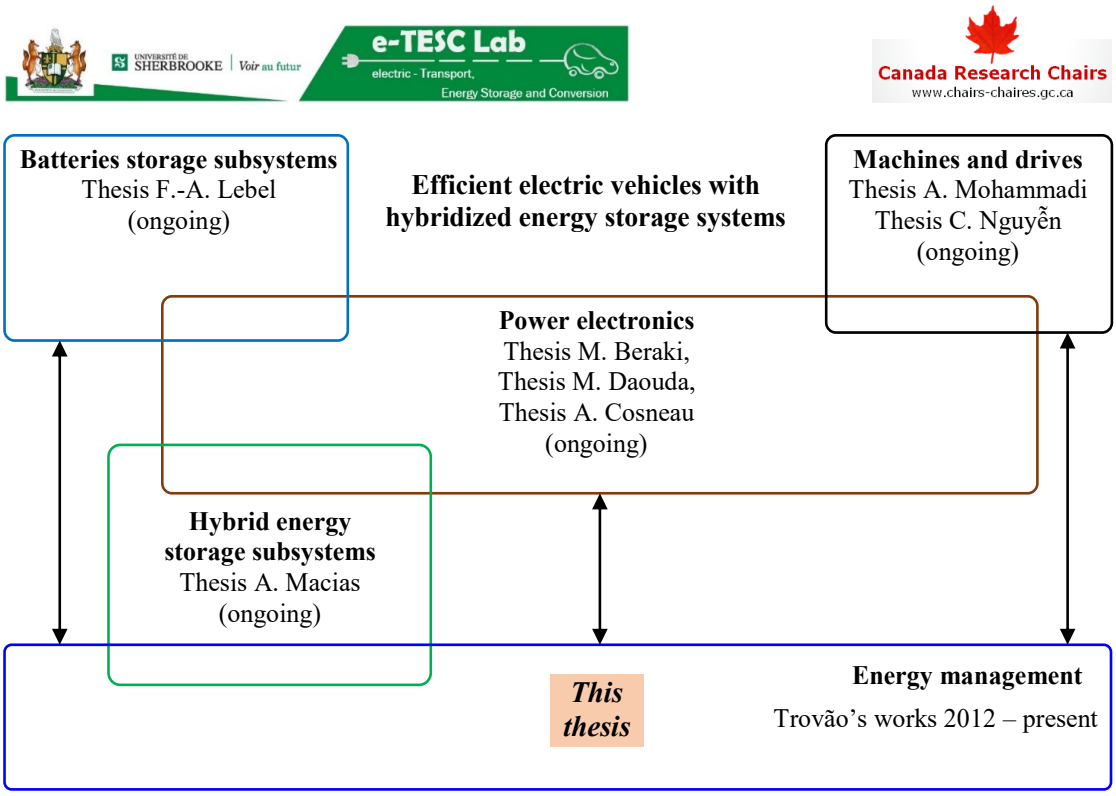

Figure 1.11: Scientific context of the thesis within Canada Research Chair program.

1.2. State-of-the-art review on energy management strategies

Before addressing the energy management methods, a general description of studied hybrid systems with EMSs could be useful (Figure 1.12). The general system can be considered as a combination of a primary source and a secondary source. The former is the energy source or storage that provides the main long-term energy to guarantee the driving range of the vehicle. For example, in an HEV, the ICE is the primary source, whereas in an EV, the batteries play this role. The secondary source is the ESS that can be frequently charged/discharged during the operations of the vehicles. The role of the secondary source is to support the primary source to achieve energy management objectives. For instance, in HEVs, batteries are secondary source that provide electrical power to help the ICEs to reduce fuel consumption and/or emission. Meanwhile in battery/SC EVs, SCs are the secondary one to extend batteries life-time by compensating high fluctuated power request.

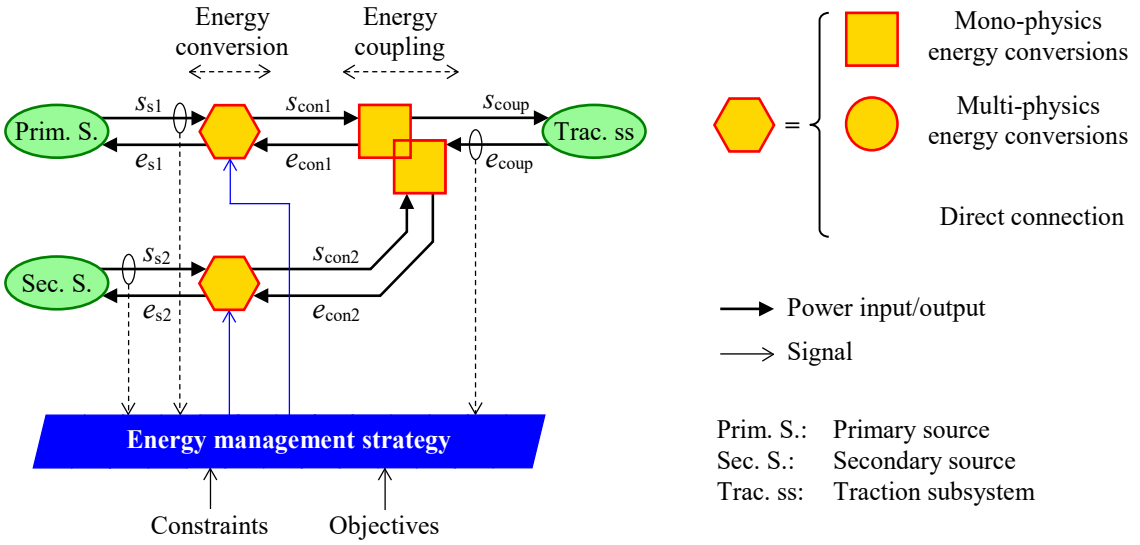

Figure 1.12: EMR-based general description of multi-source vehicles with EMSs.

Energy sources and storages can produce and store energy in different physical forms, e.g., ICEs impose mechanical energy whereas batteries exchange electrical energy. To work in a system, they need to be associated with multi-physical energy converters. For example, electrical machines convert electrical energy to mechanical energy and vice versa, so that batteries can work with ICEs in HEVs. Furthermore, to effectively operate multi-source systems, the energy flows should be controlled (by EMSs). The energy conversions should be controllable, such as electrical drives (electric machines, power electronics converters, and their control). The controlled energy flows combine at the energy coupling to supply energy to the traction subsystem or the drivetrain. EMSs are implemented in the strategy block. The EMSs measure and/or estimate the system variables to impose the energy flows references in order to obtain the objectives while satisfying the constraints.

In this study, the development methods are organized based on the traditional classification proposed in [Salmasi 2007]. In this work, a more detailed classification of energy management methods is presented (Figure 1.13).

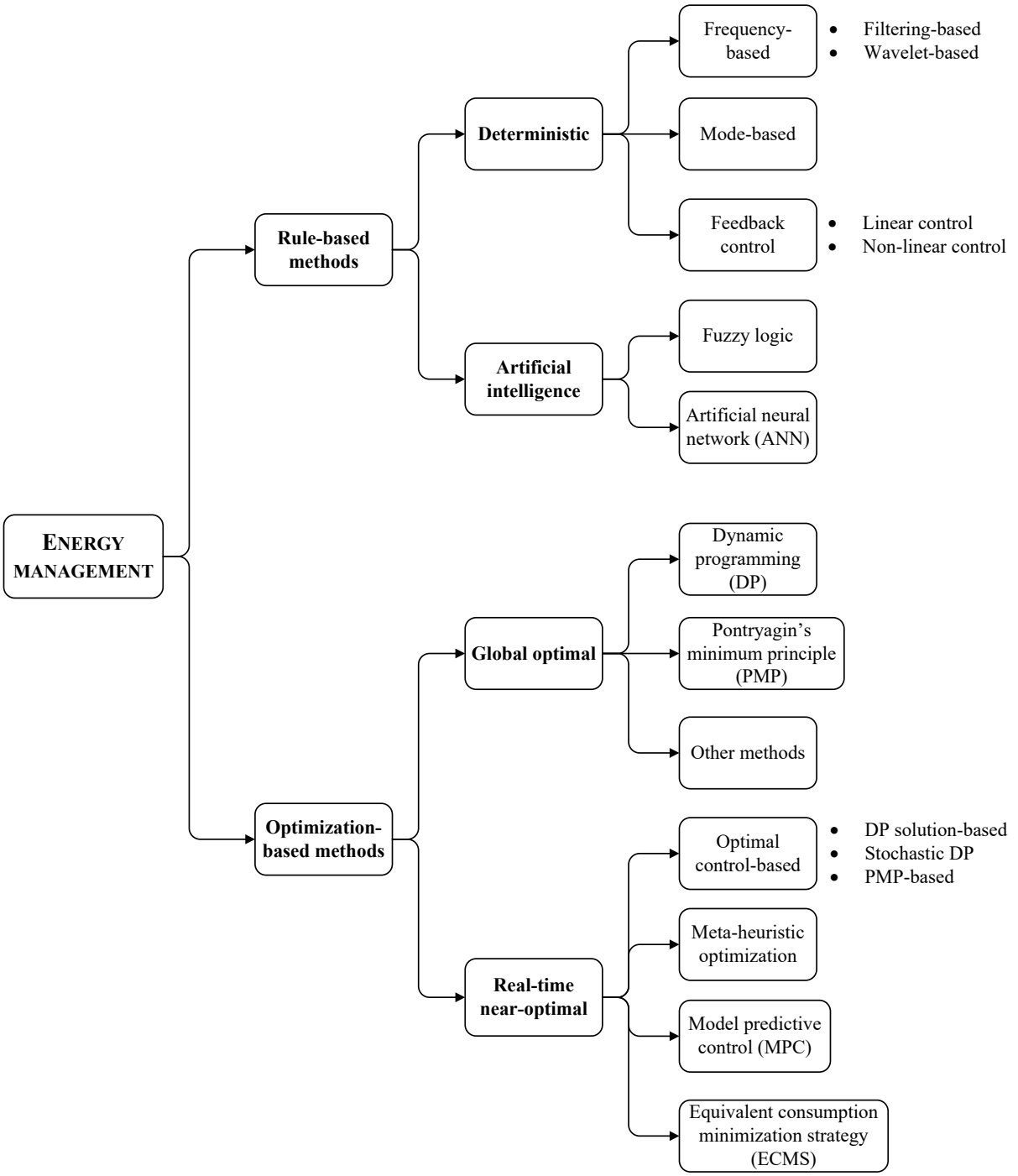

Figure 1.13: Classification of energy management methods.

1.2.1. Rule-based methods

Rule-based methods are classified into deterministic and artificial intelligent (AI)-based groups. The former ones are explicit rules deduced from user's knowledge of the systems behaviors. Whereas the rules of the latter ones are based on AI methods to simulate the human behaviors and learning abilities. Rule-based strategies are often easy to be implemented in real-time which

is suitable for real-world applications. However, they are not optimal and dependent on human expertise.

a. Deterministic rule-based methods

Frequency-based methods

H-ESS and HEVs are the combinations of energy sources; in which there are often sources preferable to work at low frequency (LF) and the other ones more suitable for high frequency (HF). Hence, it is straightforward to develop EMS based on frequencies of power references (Figure 1.14). LF power demand corresponds to the steady state driving and HF power demand corresponds to the variations (acceleration and regenerative braking). The methods can be classified as filtering-based and wavelet-based regarding the most common used techniques of frequency separation.

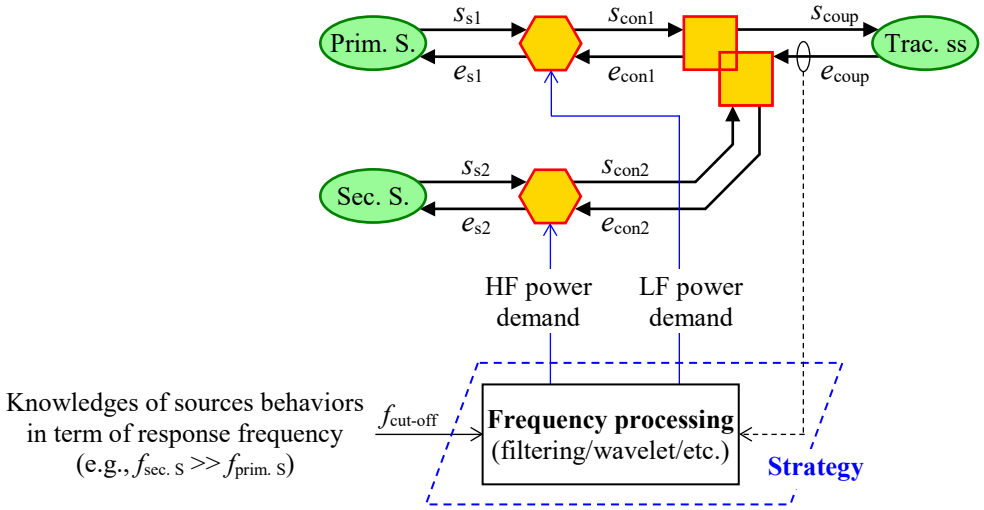

Figure 1.14: General description of EMSs with frequency-based methods.

Filtering-based methods

Frequency separation can be realized by using low-pass or high-pass filters (LPFs/HPFs) to generate the power references for energy storage devices. This is a very simple but effective method for energy management.

Two LPFs are used for a fuel-cell/battery/SC energy storage subsystem, in which one is for fuel-cell and one is for batteries power references [Schaltz 2009]. Two EMSs, which are with or without batteries, are investigated. The objective of batteries life-time extension is examined in terms of number of cycles and depth-of-discharge (DoD). Two configurations of fuel-cell/SC and battery/SC H-ESSs are studied in [Tani 2012] using LPFs. The performances of DC bus voltage control, storage devices currents control, and EMS are verified by experiments.

An adaptive mechanism for the time constant of the LPF of battery/SC H-ESS energy management is proposed in [Florescu 2015]. The time constant is adapted regarding the SCs voltage. The time constants of the LPFs can be chosen based on the Ragone plot [Christen 2000] as addressed in [Akli 2009] for flywheel, batteries, and SCs, in [Dépature 2018b] for fuel-cells and SCs, and in [Allègre 2013; Nguyễn 2016] for battery/SC H-ESS.

Not only for energy storage subsystems, filtering-based strategy can be also applied to energy management of HEVs. In [Kim Y. 2014], the so-called frequency-domain power distribution strategy is investigated for hybrid powertrains. The studied system is examined by several hardware-in-the-loop experiments including the so-called battery-in-the-loop and engine-in-the-loop.

Wavelet-based methods

To separate the frequencies of the energy sources, wavelet transformation technique can be used. The Haar wavelet is used in [Zhang 2008] for energy management of a fuel-cell/battery/SC H-ESS. The three-level wavelet-based scheme decomposes the demanded traction power into 3 frequency components for fuel-cells, batteries, and SCs. A similar multi-level decomposition is also applied in [Uzunoglu 2008] for a fuel-cell/SC system. Wavelet transformation is used in cooperation with a nonlinear auto-regressive neural network for a battery/SC military hybrid vehicle in [Ibrahim 2016]. The neural network predicts the requested power for the wavelet transformation to decompose the power frequency.

The advantage of wavelet technique is the localized signal decomposition in both time and frequency domain. This sort of methods requires wavelet transformations which make it more complicated to be implemented in on-board embedded systems in comparison to the filtering-based approach.

Mode-based methods

This group addresses the mode-based methods which are developed by heuristic approaches. They are normally in a general form like “if the system is in this state then the strategy should be in that mode” (Figure 1.15). Mode-based methods can be considered as the simplest approach to develop EMSs. The strategies can be easily implemented thanks to their intuitive approach. There is, however, almost no systematic methodology to develop them.

Baseline control strategy, which is used in ADVISOR, is applied in [Johnson 2000] for HEVs. Maximal and minimal torque envelopes are defined. The operation of the engine depends on these envelopes and batteries SoC levels. An 8-state mode-based strategy is proposed for energy management of a full-active fuel-cell/battery H-ESS for a tramway [Garcia 2010]. The operation modes are defined based on the batteries SoC and the load power. A similar 7-state EMS is presented in [Hannan 2012] for a multi-source system combining fuel-cells, batteries, and SCs. A series HEV using H-ESS combining batteries and SCs are studied in [Yoo 2008]. The mode-based EMS manages both mechanical and electrical couplings. Hence, the strategy is considered as composition approach even though the voltage and current controls are separated from the EMS. Mode-based strategies are also of interest for managing the operations of batteries and SCs in other applications like smart DC grid [Sechilariu 2013; Yin 2017].

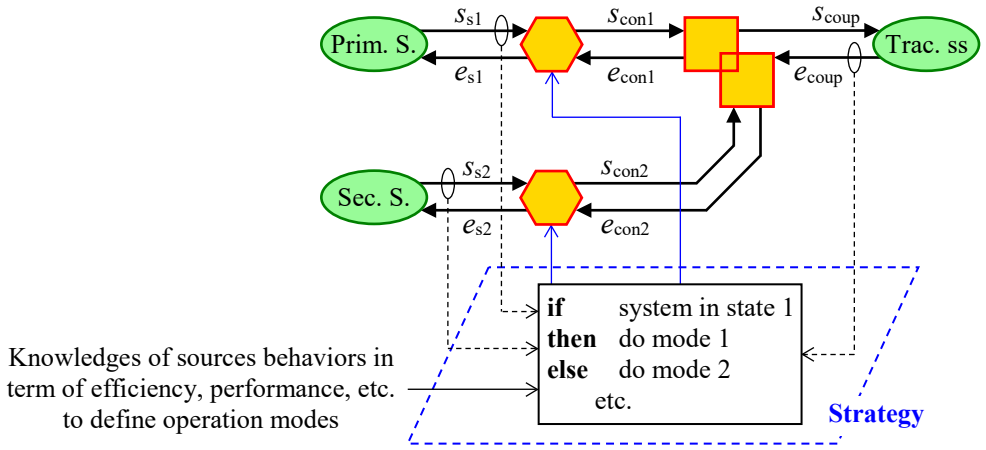

Figure 1.15: General description of EMSs with mode-based methods.

Feedback control-based methods

The subject of energy management is dynamical systems. It is therefore reasonable to develop EMSs using automatic control theory (Figure 1.16). The methods can be classified as linear and non-linear control. In which, linear control is often applied with decomposition approach; while non-linear control frequently goes with composition approach.

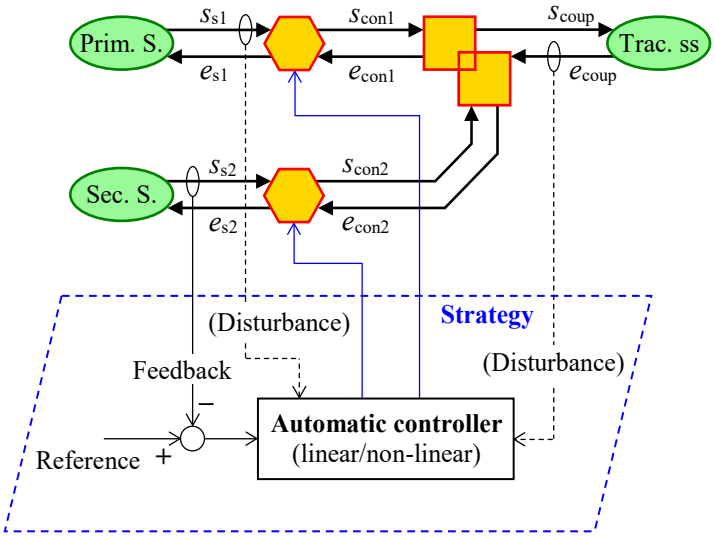

Figure 1.16: General description of EMSs with feedback control-based methods.

Linear control

The linear control scheme is applied for energy management of the H-ESS combining fuel-cells, batteries, and SCs in [Thounthong 2009]. The proportional controllers are employed for SCs and batteries voltage control. The studied systems are well examined by experiments. However,

it could be noted that while the SCs voltage directly relates to their SoC, the batteries voltage does not. Hence, the batteries voltage control loop could be appropriately replaced by their SoC control with the estimation of the batteries SoC from their voltage.

Proportional-integral (PI) controller with anti-windup mechanism is used to control the SCs voltage that is called "compensation loop" for fuel-cell/SC H-ESS in [Azib 2010]. DC bus voltage and SCs current control loops are developed independently with the outer supervisory control of SCs voltage. PI controller for batteries and SCs SoC management are also investigated for a hybrid vehicles in [Wang L. 2011].

In [Nguyễn 2018b], the author proposed a merging control of an H-ESS for EVs. It is developed based on the principle of inversion of EMR. A closed-loop voltage control for SCs has been introduced to couple with the traditional open-loop current control of the batteries. The trade-off between the two different objectives is addressed by a weighting factor.

Non-linear control

In [Thounthong 2010], the DC bus and the SCs voltages are considered in the same framework of non-linear flatness-based control for a fuel-cell/SC system. Similarly, non-linear control is also applied in [Ayad 2010; Benmouna 2018; Hilairet 2013] with the passivity-based control technique.

A fuel-cell/battery/SC H-ESS is considered as a multi-input multi-output (MIMO) system that is controlled by a control Lyapunov function (CLF) in [Rajabzadeh 2016]. Non-linear control with CLF and sliding mode control technique are also investigated by the authors of [Song 2017] for battery/SC EVs. With the similar composition approach, an H-ESS can be treated as a port-controlled Hamiltonian system as in [Dai 2016]. Disturbance rejection for energy management of the system is then developed.

Feedback control-based methods are model-based strategies which can be systematically deduced by using control theory and system dynamical models. They are therefore promising for EMSs development. Nevertheless, it often causes confusions when the low-level (local) controls are mixed with high-level (supervisory) EMSs. The plants can therefore become huge non-linear MIMO systems which make the control laws very complicated. It could be better if the two levels are decomposed regarding their objectives, functions, and dynamics. It is also interesting to note that there is a lack of feedback control-based strategies developed for HEVs energy management. This could be therefore promising to initiate applications of advanced control technique to EMSs of HEVs.

b. Artificial intelligence-based methods

Fuzzy logic-based methods

It is reasonable that fuzzy logic is widely used for EMSs development since it is close to human decision making. It can be stated that fuzzy logic-based EMSs are mode-based strategies but in the language of fuzzy logic. The mode-based approach has been already addressed in the

previous subsection. Hence, works on fuzzy logic-based strategy development are not presented in detail here, despite numerous works using this method.

Artificial neural network-based methods

Beside fuzzy logic, artificial neural network (ANN) is also an artificial intelligent method that can be used for EMSs development (Figure 1.17). Normally, ANN-based EMSs can achieve high performances; however, they often require hard computational efforts.

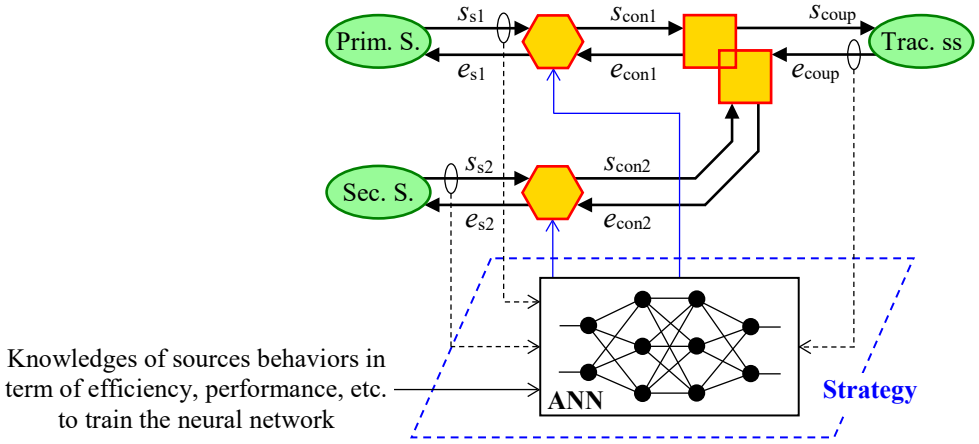

Figure 1.17: General description of EMSs with artificial neural network-based methods.

A simple two-layer network is used to calculate the SCs current reference for a battery/SC H-ESS in [Moreno 2006]. The results are compared with an optimal EMS based on PMP. One of the strong abilities of ANN is pattern recognition; thus, it is often used for identification and/or prediction. The two-part papers [Murphey 2012, 2013] propose an intelligent energy management approach for power-split HEVs. ANNs are used for both driving conditions predictions and for power distribution. The first-part paper presents the driving environment learning and DP optimal control-based training of the ANNs. The second-part paper addresses the on-line implementation of the developed ANN-based EMS. Even though the authors demonstrated well the real-time implementation of the proposed EMS, its complexities make it challenging to be realized for real-world applications.

Using DP to deduce optimal solutions for training the ANN to be implemented in real-time is also the approach presented in [Tian 2016]. The studied system is a parallel HEV supplied by a battery/SC H-ESS. The optimization problem is to minimize the total cost of fuel consumption and electrical consumption with a penalty of the final energy state of the H-ESS. A length ratio-based ANN is implemented with the claim of reduction of computational efforts for real-time realization in micro-controller.

1.2.2. Optimization-based methods

The objective of energy management is to minimize/maximize certain performance criteria. Optimization-based methods are therefore naturally of interest. They are classified into two main groups: off-line global optimal and real-time near-optimal methods. The former can

deduce optimal solutions; however, they are off-line computation methods which cannot be directly used for real-world applications. The optimal solutions are therefore often used as benchmarks to evaluate the real-time strategies. The latter give only sub-optimal solutions but can be implemented in real-time. The real-time optimization-based methods are complicated, but they can be closer to the optimal than rule-based strategies. Methods of the both groups are widely used and are attracting more and more interests from researchers.

Before addressing optimization-based EMSs, the optimal control problem formulation should be presented. An energy management problem can be formulated by adopting the form of optimal control [Kirk 1970; Sciarretta 2007] as follows:

Find the control laws $\underline{u}(t)$ for the system

$$\frac{d}{dt}\underline{x}(t) = \underline{f}\left[\underline{x}(t), \underline{u}(t), \underline{w}(t), t\right]; \tag{1.1}$$

in which $\underline{x}(t)$ is the state variables and $\underline{w}(t)$ is the disturbances; that minimize the cost functions $\{J_1 \cdots J_n\}$ given as:

$$\underline{J} = [J_1 \cdots J_n]^T \tag{1.2}$$

with the constraints:

$$\begin{cases} \underline{p}\left[\underline{x}(t), \underline{u}(t), t\right] \leq 0 \\ \underline{q}\left[\underline{x}(t), \underline{u}(t), t\right] = 0 \end{cases}; \tag{1.3}$$

where $\underline{p}$ and $\underline{q}$ are sets of functions expressing the inequality and equality constraints of the system, respectively. The cost functions (1.2) are expressed by:

$$J_i = \underbrace{h_i\left[\underline{x}(t_f), t_f\right]}_{\text{Cost of the final state}} + \underbrace{\int_{t_0}^{t_f} g_i\left[\underline{x}(t), \underline{u}(t), t\right] dt}_{\text{Cost of the whole procedure}} \tag{1.4}$$

$$\text{with } i \in \{1,2, \dots, n\};$$

where g and h denote arbitrary functions; t_0 and t_f are the initial and the final time, respectively.

When the problem is properly formulated, one can use various types of methods to solve it depending upon the study purpose. It could be worth to note that optimization methods can be used not only for EMSs, but also for sizing problems, e.g. [Hu 2015b]. The two problems, energy management and sizing, can be combined into multi-layer design problems as surveyed in [Sylvas 2017]. In which, the combinations are classified as alternating, nested, and simultaneous coordination. Whereas the multi-layer architecture is considered as topological optimization, sizing optimization, and optimization-based strategy. This combination could be a trend; however, this thesis focuses on EMSs development, thus, the sizing problem is not discussed.

a. Global optimal methods

Global optimal EMSs using optimal control and optimization techniques are addressed here. Two main approaches of optimal control frequently in use are dynamic programming (DP) and Pontryagin's minimum principle (PMP). Besides, the other optimization techniques are also employed for off-line energy management.

Dynamic programming

DP is based on the Bellman principle of optimality [Kirk 1970]. Considering the above general system (1.1) the discrete form, DP is expressed by Bellman equation as follows:

$$J^*_{k,N}\left[\underline{x}(k)\right] = \min_{\underline{u}(k)} \left\{ \underbrace{g_{\mathrm{D}}\left[\underline{x}(k), \underline{u}(k)\right]}_{\substack{\text{Cost-to-go from current stage} \\ k \text{ to next stage } k+1}} + \underbrace{J^*_{k+1,N}\left[\underline{f}\left(\underline{x}(k), \underline{u}(k)\right)\right]}_{\substack{\text{Optimal cost-to-go from next stage} \\ k+1 \text{ to final stage } N}} \right\}; \tag{1.5}$$

in which the subscript k, N denotes the procedure going from the k^{th} stage to the final N^{th} stage, similar for $k+1, N$; g_{D} is the discrete form of the function g mentioned in (1.4). The optimal control $\underline{u}^*(k)$ is deduced as a control law with the feedback of the state variable [Kirk 1970]:

$$\underline{u}^*(k) = \underline{u}\left[\underline{x}(k), k\right]. \tag{1.6}$$

The Bellman equation (1.5) is normally solved by numerical computation. The optimal control (1.6) is then stored as a look-up table. Figure 1.18 illustrates the solving procedure for an arbitrary scalar component of $\underline{x}$. It is to find the optimal path from the current state $x_i(k)$ to the final state $x(N)$. The optimal paths from all possible next states $x(k+1)$ to $x(N)$ must be *a priori* known. The operation of DP is to repeat this procedure from $x(N)$ to the initial state $x(0)$. Due to computation in discrete time, the system must be discretized and quantized.

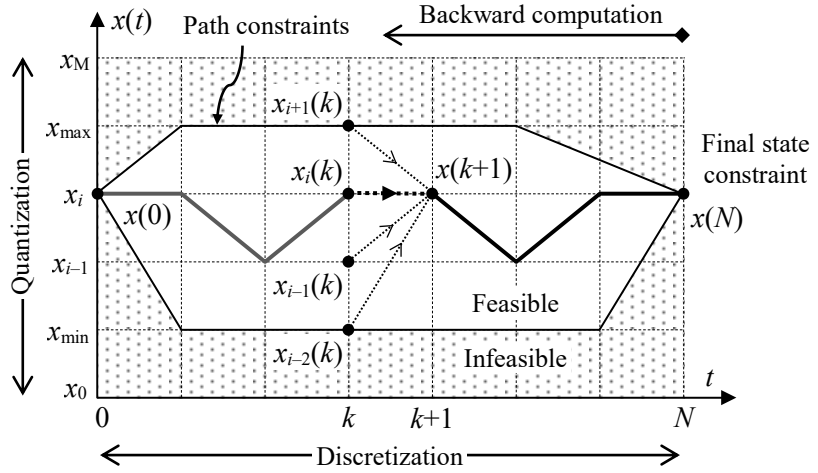

Figure 1.18: General description of EMSs with dynamic programming.

An improved DP was proposed with a fixed states number for better numerical calculation in [Fares 2015]. Multiple costs of a fuel-cell/battery system are considered: fuel-cell hydrogen consumption, its life-time and batteries energy consumption. However, the compromises between these costs are not addressed. A real-time EMS using PID controller is used for comparison with the DP solution.

In [Santucci 2014], DP is used to generate a benchmark for a parallel HEV supplied by a semi-active battery/SC H-ESS. The decomposition methodology is adopted for energy management of the mechanical coupling, while the composition approach is used for power sharing between batteries and SCs. MPC and mode-based strategies are developed for the H-ESS. An ECMS is deduced for HEV. The MPC strategy addresses two objectives of SoC tracking errors and batteries power with corresponding weighting matrices. A battery aging model is put in the cost function of DP to minimize the batteries degradation. The cost functions of MPC and DP are therefore different, whereas, they should be the same for performance comparison.

Power-split HEV using Toyota hybrid system is studied in [Liu 2008]. Both deterministic and stochastic DP strategies address two objectives: fuel consumption and battery SoC variation with a fixed penalty factor. ECMS is used to minimize a total fuel consumption combining engine fuel consumption and equivalent fuel consumption of the electric machine. They are considered equally.

By using EMR, the complex model of multi-physical systems can be systematically organized in backward representations (proposed in [Horrein 2015a]) for DP problem statement and solving. The approach has been used for optimal benchmark solutions deductions for battery/SC H-ESS-based EVs [Nguyễn 2017b], parallel HEVs [Nguyễn 2018c; Pam 2017], and HEVs supplied by batteries and SCs [Nguyễn 2018a].

Most of previous works in H-ESSs develop improved EMSs with only one objective (batteries life–time). However, at least the costs on SCs operation also could be considered. Generally, a methodology to develop multi-objective EMS is demanded. In this thesis, Appendix A.2 presents a procedure to develop multi-objective EMS of H-ESS for an EV. SCs system losses are considered as the second cost function. The DP generates a Pareto front to be used in order to compare with another on-line EMS.

Thanks to its ability to generate global optimal solutions regarding all types of constraints for all types of dynamical systems, DP is the most used method to deduce the optimal benchmark for energy management problems. The drawback of DP is that it is costly in term of computation. Moreover, this method requires the *a priori* known disturbances which is not realistic for vehicular applications. Thus, DP is used only for off-line simulation. In order to be applied for real-time EMSs, it must be modified as will be presented later in this subsection.

Pontryagin's minimum principle

To solve the optimal control problem stated by (1.1)–(1.4), PMP was proposed as necessary conditions of the optimal solutions [Athans 1966; Bryson 1975; Kirk 1970]. An m-dimension co-state vector $\underline{\lambda}(t)$ is defined to form the Hamiltonian expressed as:

$$H = g\left[\underline{x}(t), \underline{u}(t), t\right] + \sum_{i=1}^{m} \lambda_i(t) f_i\left[\underline{x}(t), \underline{u}(t), t\right] \tag{1.7}$$

where m is the order of the system (1.1). PMP states that if a control $\underline{u}^*(t)$ is the optimal control that cause the optimal state trajectory $\underline{x}^*(t)$, there must exist an optimal co-state $\underline{\lambda}(t)$ so that they satisfy the following three necessary conditions:

$$\frac{d}{dt}\underline{x}^*(t) = \frac{\partial H}{\partial \underline{\lambda}(t)}; \tag{1.8}$$

$$\frac{d}{dt}\underline{\lambda}^*(t) = -\frac{\partial H}{\partial \underline{x}(t)}; \tag{1.9}$$

$$H\left[\underline{u}^*(t), \underline{x}^*(t), \underline{\lambda}^*(t), t\right] \leq H\left[\underline{u}(t), \underline{x}^*(t), \underline{\lambda}^*(t), t\right]. \tag{1.10}$$

By solving the above equations, one can find a set of solutions which can be compared to find the global optimal solution. Normally, the disturbance $\underline{w}(t)$ must be known in advance to determine the co-state variable $\underline{\lambda}(t)$. When there exist constraints, numerical computations are required for solving the differential equations. Generally, the solutions are in open-loop form.

PMP is widely used to develop off-line strategies for energy management of HEVs and H-ESSs. In [Hou 2014], an approximate PMP with the restricted five Hamiltonian candidates is proposed for energy management of a plug-in parallel HEV. A reduction of calculating time from six hours to four minutes is reported. However, the method still required the driving cycle known in advance. Thus, it is considered an off-line method even though the authors claim the feasibility of real-time implementation.

The authors of [Fontaine 2013] study a parallel HEV supplied by a battery/SC H-ESS. Two strategies are proposed to minimize either fuel consumption or battery power using PMP. A novel numerical solution for PMP is applied for HEV energy management problem [Van Keulen 2014]. Results are compared with DP solution. The study seems to be focused on the mathematical optimal control theory that EMS is just a case study to examine the applicability of the theoretical method.

An HEV using battery/SC H-ESS is investigated in [Vinot 2013]. PMP is used to develop an EMS that minimizes both fuel consumption and battery root-mean-square (rms) current. The optimal control problem with two independent control laws is solved simultaneously. Pareto fronts in the cases without and with battery are generated. A simple mode-based strategy for determining engine power requirement is implemented. Filtering-based strategy for battery/SC H-ESS with various cut-off frequencies is examined.

Normally, PMP can deduce the close results in comparison with DP. The advantage of PMP is that it is less computationally demanding than DP. However, PMP requires the guess of initial value of the co-state variable that makes it not a total systematic approach.

The other methods

Beside DP and PMP, several other optimization methods are also of interest for off-line EMS development. The authors of [Wei 2017] studied a series HEV with bi-directional DC/DC converter connecting battery to the DC bus. The Radau pseudo-spectral method is used to translate the optimal control problem to a non-linear programming problem. The conjugate gradient-based BPTT-like optimal control algorithm is used to develop an EMS for a power-split HEV in [Cipek 2013]. For the same kind of vehicle, in [Wu 2014], the optimal control problem is formulated and solved in form of a mixed-integer linear programming problem. Battery state-of-health model is considered in [Hu 2015a] for energy management of a fuel-cell/battery/SC H-ESS. A convex optimization framework is proposed to solve the energy management problem.

b. Real-time near-optimal methods

The global optimization approaches mentioned above give only off-line solutions for energy management problems that cannot be realized for real-world applications. To develop real-time EMSs, sub-optimal methods are investigated. There are five groups addressed in this report: the methods based on global optimal control, model predictive control (MPC), meta-heuristic optimization, equivalent consumption minimization strategy (ECMS), and the other methods.

Global optimal control-based methods

One way to develop the real-time strategies is to adapt the off-line EMSs produced by global optimal control methods. They can be categorized as DP solution-based, stochastic DP, and PMP-based methods as presented in the followings.

DP solution-based methods

Optimal solutions can be computed off-line, then implemented in some forms like look-up table as real-time strategies (Figure 1.19). DP solution-based methods combine the systematic approach of optimization-based methods and the real-time implementable ability of rule-based approaches. However, the DP solution is obtained from one or several specific driving conditions. Hence, it is hard to ensure that real-time adaptations can work well with the real-world driving cycles.

In [Chen Zh. 2014], an intelligent EMS for a power-split plug-in HEV is developed using DP and ANN. DP deduce the optimal solutions for six standard driving cycles that are used to train the neural networks. Two ANNs are developed with and without specific trip information. The proposed EMS is validated by simulation. The lack of experimental results in this paper implies the difficulty to realize the ANNs in a real-time platform. DP is computed via off-line simulation to generate data for training the ANNs. The off-line training processes do not affect the real-time implementation but increase the complexity of the method.

The fuel consumption of plug-in HEVs is minimized using DP in [Qiuming 2008]. Traffic-data-based trip modeling is used to give information about the future traffic condition. However, the ability of on-board implementation for real-time energy management has not been fully

discussed. In [Song 2015], DP is used for designing of a battery/SC H-ESS and then for development of an optimal EMS. After that, a near-optimal mode-based strategy is produced based on the DP solutions. Results confirm the good performances of the proposed strategy in comparison to the DP optimal solution. However, the strategy is tested with the same two driving cycles used for development of DP solutions. Whereas the rule-based strategy is deduced based on these solutions. It could be more convinced to evaluate the proposed strategy with the other unknown driving cycles.

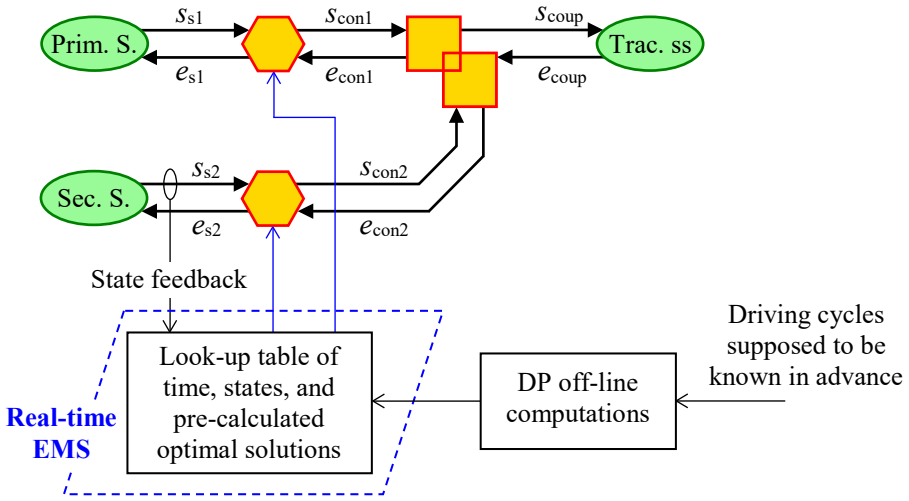

Figure 1.19: General description of real-time EMSs with DP solution-based methods.

Stochastic DP-based methods

The DP mentioned previously is deterministic DP in which all the disturbances must be *a priori* known in finite horizon. Meanwhile, real-time strategies must be in infinite horizon with unknown disturbances. In order to adopt DP for real-time EMS, stochastic DP is a suitable approach. In this method, unknown disturbances are modeled as random processes. Statistical techniques like Markov chain are normally employed. The drawbacks of this approach lie on the high computational efforts of both DP calculation and stochastic model prediction.

Stochastic DP with Markov chain forecast is used for energy management of a fuel-cell/battery H-ESS in [Kim M. 2007]. The hydrogen mass and battery energy usage are minimized with equal weighting factors. Sets of initial parameters and variable are provided as inputs to a Markov chain model of which the output is used to build a cost table. The optimal control problem is then solved by DP based on this cost table. Based on this process, the authors proposed a close-to-optimal "pseudo stochastic DP" that can be implemented in real-time. In [Moura 2013], a plug-in HEV is managed using multi-objective stochastic DP with varied weighting factor to trade-off the batteries life-time and the fuel consumption. Electrical consumption is also taken into account by a fixed penalty factor.

Due to the essence of random-process simulated disturbances, stochastic DP strategies are very suitable to be applied for fixed-routine vehicle like trains, buses, and delivery trucks.

PMP-based methods

As examined previously, PMP is often used to solve the energy management problem as an optimal control one. Nevertheless, this principle is originally suitable only for development of off-line strategies since it requires all the knowledge of disturbances in advance. To overcome the mentioned drawback, works on PMP-based real-time EMSs have been studied. Adaptive and/or predictive techniques are often employed (Figure 1.20).

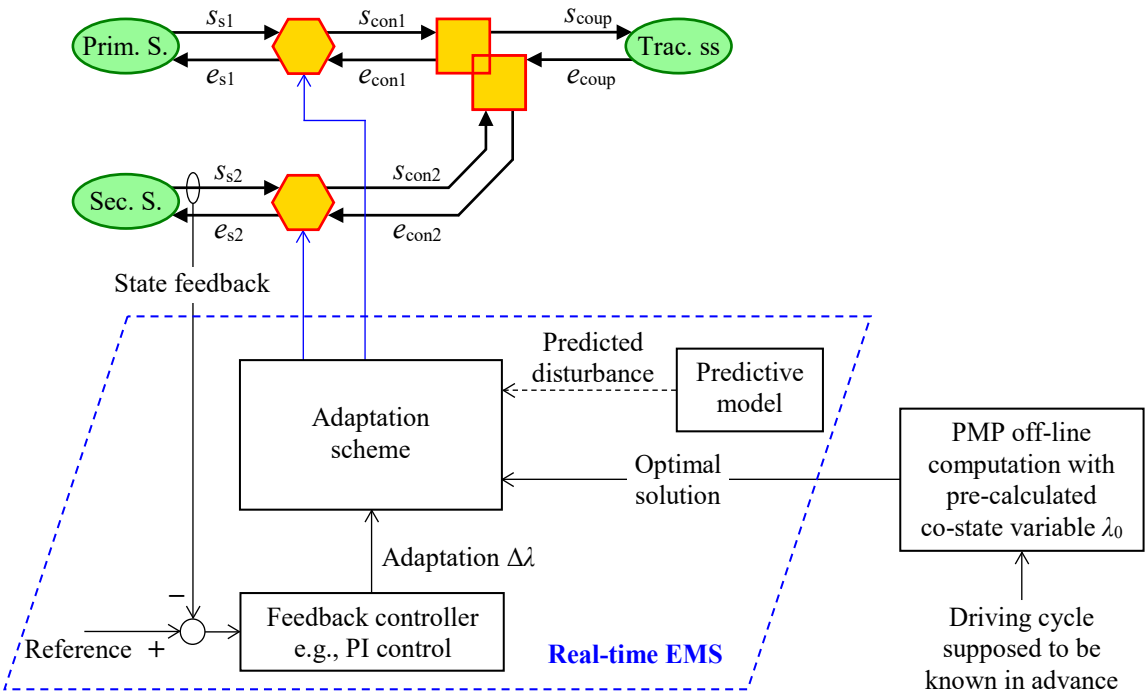

Figure 1.20: General description of real-time EMSs with PMP-based methods.

The most frequently used approach is λ-control initiated in [Delprat 2002] then developed by [Kermani 2011; Kessels 2008] for energy management of HEVs. The main idea of λ-control can be summarized as followings:

- PMP is used to solve the optimal control problem of energy management.
- An optimal value of the co-state variable λ^* is calculated by off-line computation. Normally, λ^* is claimed to be constant. The control law is in open-loop form that consider only the initial value of the state variable $x(t_0)$.
- To be implemented in real-time, the control law should be in closed-loop form. It is the feedback of the state variable $x(t)$ to deal with real-world constraints and unpredicted disturbances. The co-state variable is then in form of $\lambda_0 + \Delta\lambda(t)$ in which $\Delta\lambda(t)$ is imposed by a PI controller and λ_0 is initial "guessed" [Kessels 2008]. This value can be the optimal λ^* which is calculated for a known driving cycle [Castaings 2016a].

The authors of [Nguyen 2014] used this method to realize an on-line optimal control-based strategy for battery/SC storage system supplying for HEVs. In [Castaings 2016a], λ-control is examined and compared with the conventional filtering strategy for H-ESS using battery and SC. Recently, this method is applied for energy management of a fuel-cell/battery vehicle [Ettihir 2016].

λ-control is an interesting way to develop an on-line adaptive mechanism for PMP-based strategies. However, it still requires an initial calculated value of the co-state variable which is not very straightforward for real-world applications. Furthermore, the adaptive mechanism acts only for charge sustaining and for constraints assurance [Castaings 2016a; Nguyen 2014]. The real-time dynamical behavior of the state variable is therefore not fully considered for the whole working progression. The method requires off-line iterative simulations to determine λ_0 for a learning driving cycle. Then the obtained solution can be implemented in on-board processor with a simple feedback adaptational scheme. Thus, this method is suitable for real-time implementation. The complexity is mostly on the step of the off-line optimal solution for a learning cycle known in advance. Improvement in this step could make the method more realistic for real-world applications.

Other methods have been also proposed. An ANN-based adaptive mechanism is developed for an optimal control-based EMS of fuel-cell/SC systems [Lin 2011]. The ANN predicts the next-stage variables then updates the information to the optimal controller. In [Hemi 2015], a Markov chain is used to predict the required fuel-cell power regarding the future demanded traction power. This prediction is then added to the optimal fuel-cell power calculated by PMP. The EMS is then validated by simulation. The approaches are advanced but complicated. ANN and Markov chain both require high computational efforts that challenges the ability of real-time realization.

PMP is attractive thanks to its analytical approach. It can be adopted to deduce close-form analytical solution which can be easily implemented in real-time. Such a solution could be of interest despite the sub-optimal essence of real-time strategies. This approach has been applied in [Nguyễn 2019] and will be presented in the next chapter of this thesis.

Model predictive control

Model predictive control (MPC) is a promising approach to develop real-time optimization-based EMS. The idea of MPC is to convert the original optimal control problem into an optimization problem, then solve it for a predicted time horizon in each discrete control step.

Figure 1.21 describes the MPC scheme and Figure 1.22 illustrates the principle of receding horizon control which is the core of MPC. At the current k^{th} step, a predictive model forecasts the future disturbance $\underline{w}$ in N_{p} next predicted steps. Based on this prediction and the information of the current state $x(k)$, an optimization solver computes the optimal control $\underline{u}$ for N_{c} control steps. Only the first computed control $\underline{u}(k)$ is imposed on the system. The prediction horizon and the control horizon are then receded one step (see Figure 1.22). The procedure is repeated for the next $(k+1)^{\text{th}}$ step. Many predictive methods can be employed in MPC framework [Zhou 2019].

The article [Gomozov 2017] proposes a non-uniform sampling method for MPC for energy management of semi-active H-ESS combining battery and SC. The sampling is distributed from small to large sampling time to achieve long horizon with precise prediction. This work considers both batteries and SCs SoCs as state variables. Linear MPC is used for EMS of a fuel-cell/SC H-ESS in [Greenwell 2010]. It is developed with a model in which only SCs SoC is treated as the state variables. The local control level is independently decomposed from the energy management (supervisory) level. Multi-objective approach is investigated with two cases of weighting factor of the SCs SoC called “low SoC penalty” and “high SoC penalty”.

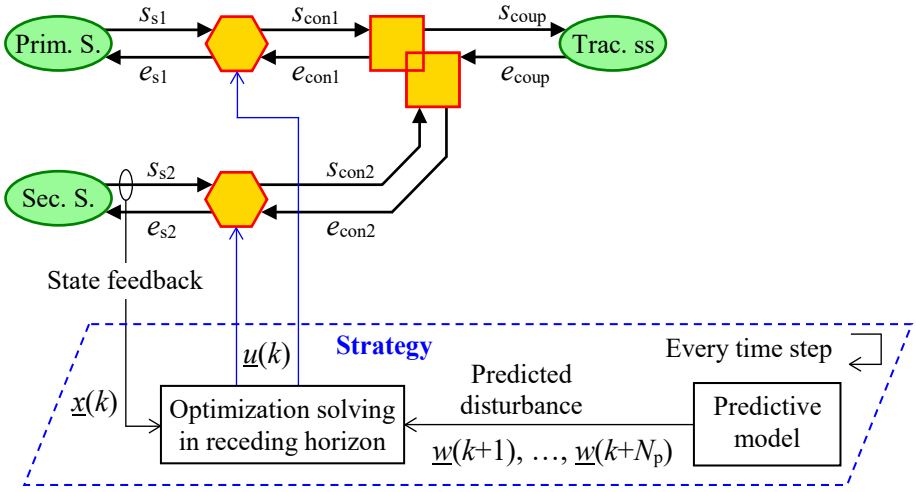

Figure 1.21: General description of EMSs with model predictive control.

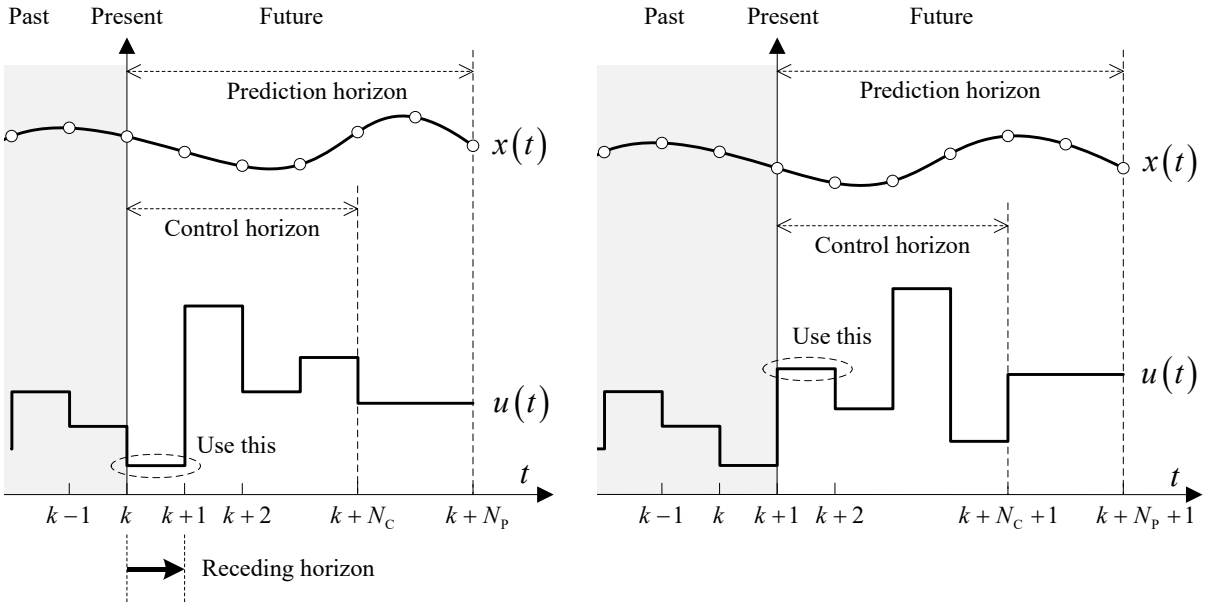

Figure 1.22: Illustration of receding horizon principle.

Non-linear MPC and linear time-varying MPC are developed and compared in [Borhan 2012] for energy management of power-split HEVs. Only batteries SoC is controlled as the state variable. Fuel consumption and SCs SoC are minimized simultaneously. In the linear time-varying MPC, the quadratic form of cost function is formulated, and then quadratic programming is used to solve the problem. With the non-linear MPC, PMP is used to reformulate the cost function, then DP is used to solve the problem in the prediction horizon.

In [Pant 2014] the EMS of a battery/SC H-ESS is decomposed into two levels. The high-level control defines a peak threshold for battery power. This level is realized by using MPC. The low-level control is a rule-based strategy to decide the power references to batteries and SCs based on the defined peak threshold. In [Sun 2015], the MPC strategy takes into account the traffic-data for battery SoC planning for HEVs, in which the computational effort is much reduced. The EMS is decomposed into the long-term level with traffic flow velocity information for SoC planning and the short-term level with horizon velocity prediction. The batteries SoC trajectory and the predicted velocity are inputted to the MPC to calculate the engine torque and speed references. Fuel consumption and the engine state switching are aimed to be minimized.

MPC is a promising technique due to its unique principle of solving optimization problems in predicted scopes. The main challenge lays on the high required computational performance to solve the optimization problems every sampling period. It could be noted that MPC-based EMSs are often validated by off-line simulations or signal HIL simulations. That indirectly shows the difficulty of real-time implementation of MPC strategies. Besides, many current MPC strategies are based on third-party optimization solvers which limit them from real-world applications. Fast optimization solving and disturbance predicting are still of interest to do research to make MPC possible for on-board embedded systems.

Meta-heuristic optimization

Beside MPC mentioned above, for solving optimization problems in real-time, it is also of interest to employ meta-heuristic methods (Figure 1.23). They are numerical searching techniques that can be considered as beyond heuristic searching. These methods are often inspired from natural phenomena such as metal annealing or swarm behaviors. In the followings, a number of works on energy management using meta-heuristic optimization methods are addressed.

A dynamic neighborhood particle swarm optimization algorithm is used to calculate the optimal value of the engine power for plug-in series HEVs [Chen Ze. 2015]. It is to minimize the energy consumption including the cost of engine energy, the cost of electrical grid energy to charge the battery, and the cost of engine energy to charge the battery. These costs are summed with a proportionality factor. A fuzzy logic controller is used to evaluate the performances of the prediction of the driving cycle by a correction factor. When the prediction performance is poor, a mode-based strategy is used to ensure the robustness of the system. In [Chen S. 2015], improved particle swarm optimization is implemented and compared to a mode-based strategy and an ECMS strategy for HEVs. The improvement is to consider the worst experience of the particles to increase the convergent performance of the search algorithm. To maximize the efficiency of the battery/SC H-ESS, simulated annealing optimization is used to improve the performances of a mode-based strategy [Wang B. 2016].

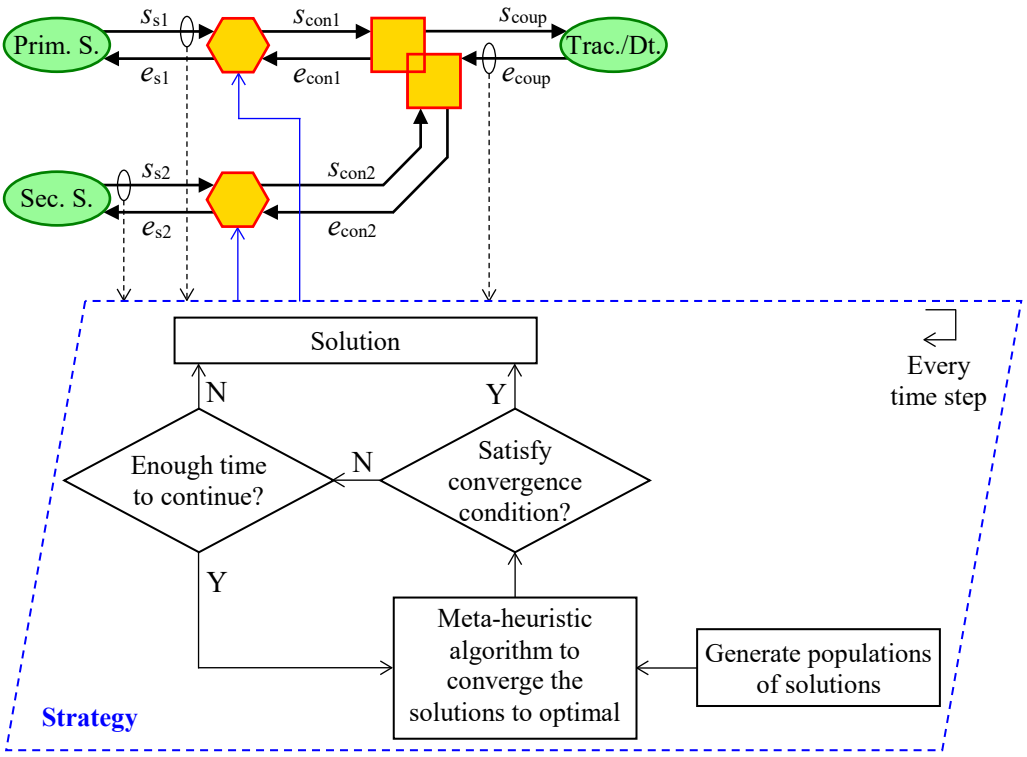

Figure 1.23: General description of EMSs with meta-heuristic optimization.

Several meta-heuristic real-time EMSs for battery/SC H-ESS are studied with a multi-level hierarchical structure [Denis 2018; Trovão 2013a, 2015b]. The strategies are decomposed into two layers which are tactical and strategical, respectively. The strategical layer is responsible for energy planning, while the tactical layer manages the power behavior of the system. Energy planning is realized by certain rules to restrict the search space of the optimization-based lower layer for power planning. Thanks to decomposing the strategies into layers, these developed EMSs can be realized via power HIL simulation despite of their complexity.

Meta-heuristic optimization techniques are of interest because they do not require to know the systems models. Whereas in complex applications like vehicles, these models are often not easy to be exactly deduced. However, there are drawbacks. One is on the computational complexity. This sort of methods is generally based on the generation and evaluation of a population of great number of candidates in every single sampling time step. This approach can overcome the complexity of system model, but unfortunately not suitable for common embedded electronics control units in vehicles. The another is on the convergence of the searching algorithms. Due to the relatively short sampling time step, it is hard to ensure the algorithms can converge to the optimal solutions.

Equivalent fuel consumption minimization strategy

ECMS was originally proposed as an instantaneous optimization-based energy management approach for HEVs [Paganelli 2000, 2002]. It is then extended for the fuel-cell-based H-ESS e.g. [Han 2014]. The idea is to minimize an instantaneous cost function containing the fuel rate

and an equivalent electrical consumption. That means, instead of minimizing the fuel consumption:

$$J_{\text{fuel}} = \int_{t_0}^{t_f} \dot{m}_{\text{fuel}}(t)dt\,; \tag{1.11}$$

where $\dot{m}_{\text{fuel}}$ is the fuel mass flow rate, an instantaneous cost function can be defined by:

$$J_{\text{inst}} = \dot{m}_{\text{fuel}}(t) + p(t)\dot{SOC}(t); \tag{1.12}$$

in which $\dot{SOC}$ is the derivative of the SoC of the electrical energy storage; $p(t)$ is the equivalent factor to calculate the equivalent electrical consumption. The instantaneous cost function has a similar form with the Hamiltonian (see (1.7)). Hence, PMP is often used to develop ECMS.

A pre-transmission parallel HEV is studied in [Nüesch 2014] with a multi-objective ECMS by minimizing fuel consumption and NOx emissions. Trade-offs are given with different values of the weighting factor. The emissions and batteries SoC are considered as the state variables. It is therefore the blend of control and energy management. A fuel-cell/battery H-ESS is investigated in [Han 2014]. The authors use DP to calculate the equivalent factor for ECMS by off-line computation. The ECMS then can be applied on-line by a map-based generated equivalent factor. Both DP and PMP are used to evaluate the performances of the proposed method.

ECMS was originally proposed intuitively as a rule-based method, however, it was soon transformed to an optimal control problem which is solved by using PMP. The method therefore has mostly the same pros and cons as PMP. A notable point of ECMS is that the fuel consumption rate $\dot{m}_{\text{fuel}}$ is often given by a look-up table. Thus, it requires numerical computations which are a drawback in term of real-time ability. This problem is often overcome by approximating the look-up table by polynomial functions, e.g. [Kermani 2011].

1.3. Objective and approach of the thesis

1.3.1. Objective of the thesis

Within the research context of MEGEVH network and Canada Research Chair program and with the applications of the CE2I and Mitacs programs, the studied systems of the thesis have been figured out. They are an EV and a parallel hybrid truck supplied by battery/SC H-ESS (Figure 1.24). The semi-active H-ESS configuration is used due to its good trade-off between performance and cost.

It can be seen from the state-of-the-art review that among numerous methods, real-time optimization-based strategies have been attracting the most researchers' efforts. There are several reasons of this attractiveness. Firstly, the EMSs can be implemented in real-time that is able for real-world applications. Secondly, optimization approaches offer systematical ways to develop EMSs. Once the strategies developers can formulate the energy management problems in terms of optimization problems, various optimization methods can be applied to solve the

problems. These methods normally do not depend on the expertise of the developers on the studied system. Finally, thanks to optimization methods, the EMSs are of high performances which are often close to optimal.

However, it is also figured out in the review that optimization-based methods are usually complex. They are complicated to develop, often computational consuming, and hard for on-board implementation. These drawbacks could limit them from real-world applications.

Hence, within the context addressed above, the objective of this thesis is to develop simple but effective real-time optimization-based EMSs for an EV and a hybrid truck supplied by battery/SC H-ESS.

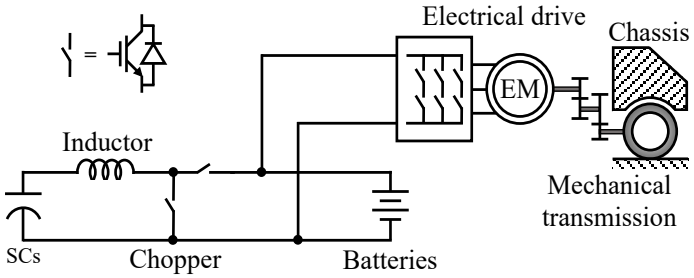

(a) EV supplied by battery/SC H-ESS

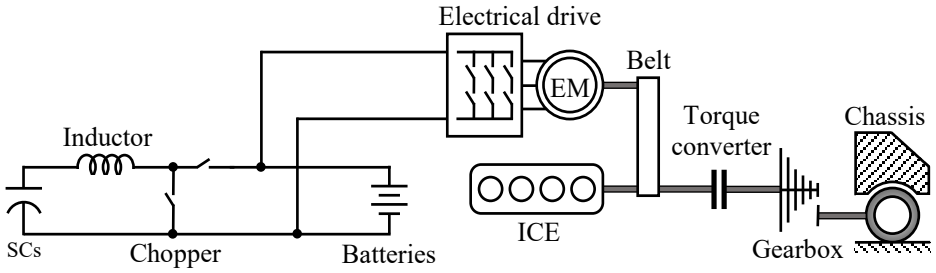

(b) Parallel hybrid truck supplied by battery/SC H-ESS

Figure 1.24: Studied systems of the thesis.

1.3.2. Methodology of the thesis

a. System representation

In order to develop real-time optimization-based EMSs, optimal control methods should be applied. For that, the following terms must be figured out:

- State variables to be controlled;
- Control variables to be imposed;
- Disturbances to be compensated;
- Constraints (physical limitations) to be respected;
- Objectives, i.e., cost functions, to be minimized.

Furthermore, the aim of the thesis is to develop simple easy-to-implement EMSs. To deal with the complexity of the studied systems and to overcome the drawbacks of using optimization methods, EMR is used. It is an effective formalism to deal with complex systems (see Appendix A.1 for more details on the EMR). The approach is using EMR to formulate the systems in term of optimal control to develop real-time optimization-based EMSs which are easy-to-implement.

Hence, an EMR-based representation of the studied system, shown in Figure 1.25, is deduced. The output of the strategy block is the control variables. The constraints and objectives are defined by technical requirements. The output of the primary source can be either controllable (e.g., ICE torque) or uncontrollable (e.g., batteries voltage). In case of uncontrollable, it could be optionally measured or estimated which is depicted as a dashed line.

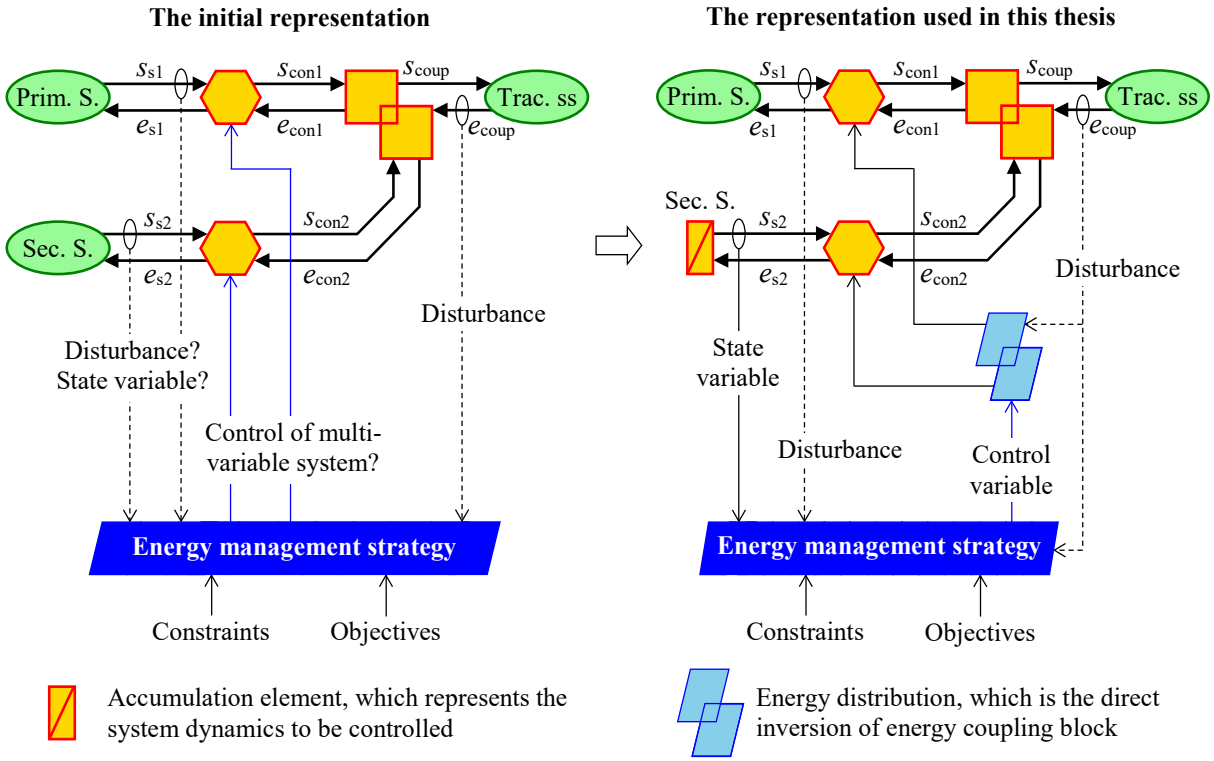

Figure 1.25: EMR-based general system representation used in the thesis.

The secondary source always has its state-of-energy varying during the system operation. This variation must be controlled to ensure the constrains and to achieve the objectives. The secondary source is therefore depicted as an accumulation element (crossed rectangle) of which the output is the state variable to be controlled. Thus, the feedback measurement of this variable is mandatory which is represented by a solid line.

The coupling element (overlapped squares) is the "node" which is vital for energy management. Based on the principle of inversion, its inverted element (overlapped parallelograms) distribute the power requirement between the primary and the secondary

sources. This distribution is based on respecting the control variable and compensating the disturbances. These disturbances can be measured, or estimated, or injected as references from the drivetrain. The signal for compensation is therefore presented as a dashed line.

b. Thesis development approach

Energy management is at the supervisory level, which is higher than local control [Bouscayrol 2005; Salmasi 2007; Trovão 2013a]. The systems will therefore be firstly modeled and controlled. Afterwards they will be transformed to the mentioned above representation for developing EMSs. From the transformed representations, mathematical models will be deduced for optimal control formalism. These steps, which are based on EMR, are modeling for energy management.

An advantage of real-time optimization-based strategies is that they are close to optimal. To validate this performance, optimal solutions should be deduced. Hence, DP will be applied to obtain off-line optimal benchmarks to evaluate the performances of the developed real-time EMSs. Since DP is a backward computational method, EMR-based backward representations ([Horrein 2015; Mayet 2014a], see Figure 1.26) of the systems will be deduced. The representations are used to organize the DP program implemented by using an available toolbox developed in [Sundström 2009].

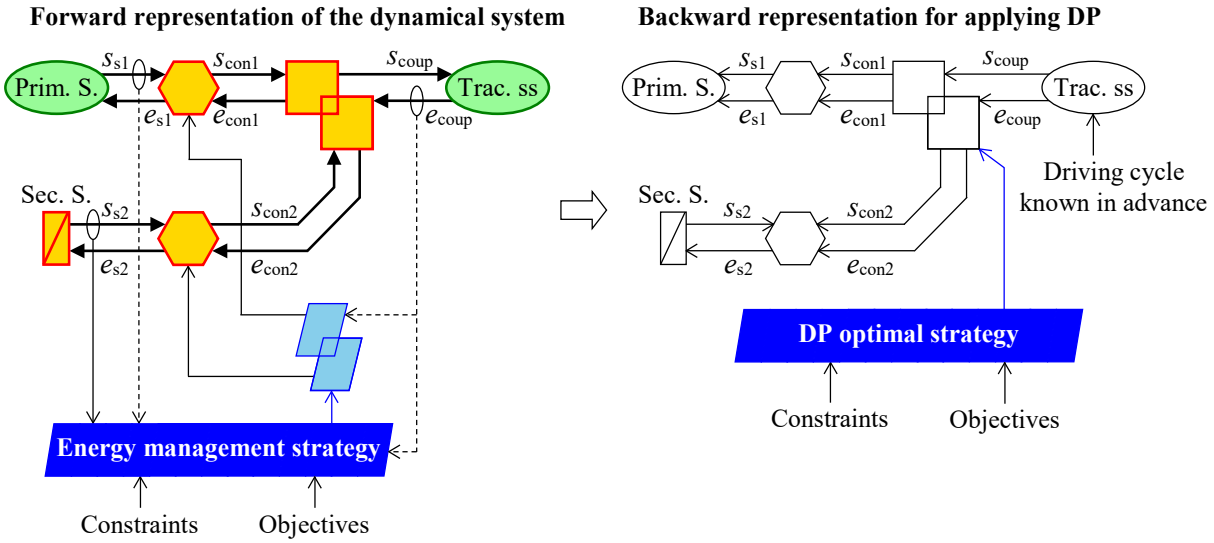

Figure 1.26: Backward representation deduction from forward representation in the thesis.

Then optimal control theories will be applied to deduce real-time optimization-based EMSs. Theses EMSs will be validated by simulations and then experiments. Experiments will be carried out by using reduced-scale power hardware-in-the-loop (HIL) simulation. The objective of experimental validations is to verify the real-time implementation ability of the developed EMSs. Simulations and experiments will be conducted using MATLAB/Simulink-based EMR library [EMR 2019]. Figure 1.27 presents a summary of the methodology for thesis development.

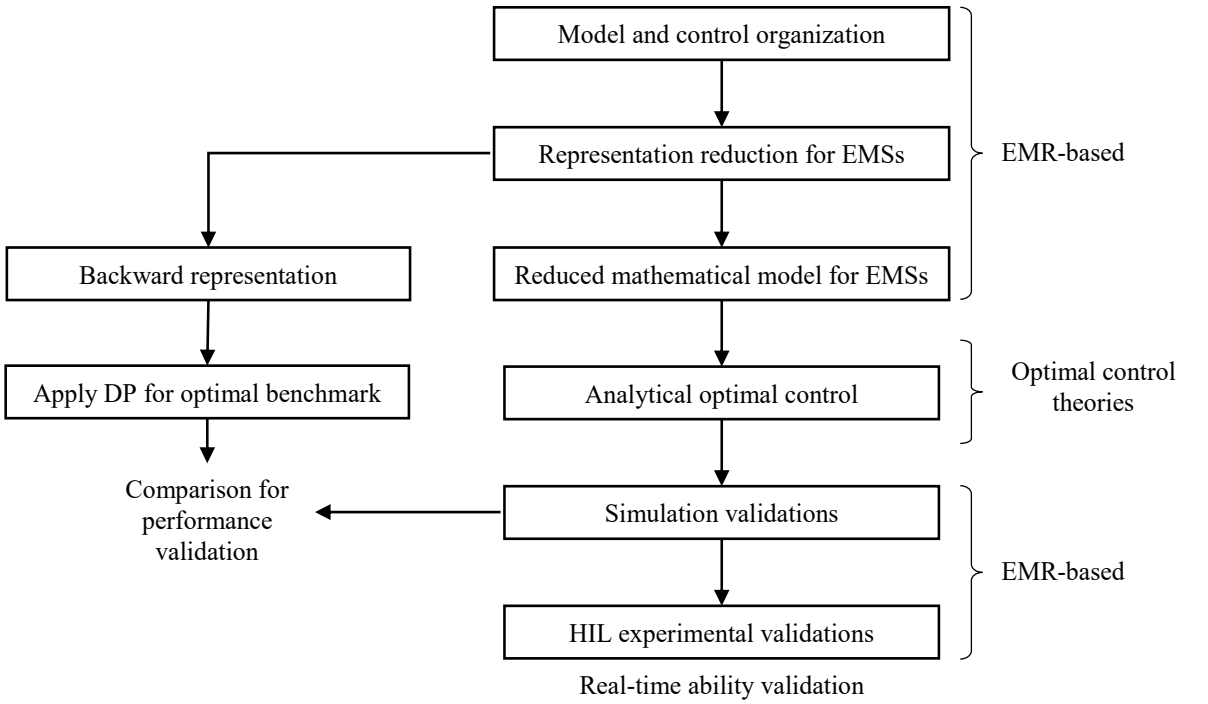

Figure 1.27: Methodology for thesis development.

1.4. Conclusion

In this chapter, it has been figured out that due to the trend of electrified vehicles and the limits of electrical ESSs, hybridizations are promising. In which, H-ESSs and HEVs configurations have been addressed to point out the necessity of EMSs. The scientific context of the thesis within collaborated research networks and programs has been given. It defines the studied problems on EMSs of EV and a hybrid truck supplied by battery/SC H-ESS. Then, the state-of-the-art review has considered various strategies development methods. It could be concluded that real-time optimization-based EMSs are of interest but often complicated. The objective of the thesis has been therefore stated to develop less complex but effective real-time optimization-based EMSs for the studied system. Based on these context and objective, the approach to develop the thesis has been presented.

2. Real-time optimization-based energy management strategy for a battery/supercapacitor electric vehicle

The objective of this chapter is to develop a less complex but effective real-time optimization-based energy management strategy for a battery/supercapacitor electric vehicle. Firstly, the system model for energy management will be deduced. For that, the full dynamical model of the studied system will be modeled and controlled using energetic macroscopic representation and inversion-based control. Model reduction and transformation will be done to obtain the reduced mathematical model. Secondly, a novel method based on Hamiltonian minimization will be proposed to develop a near-optimal strategy. This method will deduce an analytical closed-form control law which can directly serve as a real-time strategy. The performances of the proposed strategy will be validated by simulations and reduced-scale power hardware-in-the-loop experiments. Dynamic programming will serve as an off-line optimal benchmark whereas conventional real-time filtering and λ-control strategies will be used for comparisons.

2.1. Model for energy management strategy

2.1.1. Studied system

The studied system is an EV supplied by an H-ESS combining Li-ion batteries and SCs (Figure 2.1). It is a semi-active configuration in which the batteries directly connected to the DC bus. Hence, the DC bus voltage is fixed by the batteries one. The SCs are added to the system via a bi-directional DC/DC converter composed by an inductor and a power electronics chopper. Since SC capacitance drops dramatically when the current frequency increases [Devillers 2014], SCs are often connected in series with a power inductor for current smoothing. Thus, the boost DC/DC converter topology is usually used for SCs, in which the SCs are connected to the low-voltage side of this converter.

The battery/SC H-ESS supplies the electrical drive composed by the electrical machine and its inverter. This electrical drive propels the vehicle via a mechanical transmission driveline which is the combination of shafts, fixed gearbox, and wheels. The driveline transmits mechanical power to drive the chassis, which is assumed to represent all the mechanical dynamics of the vehicle. The resistive force is imposed by the environment which is normally air and road.

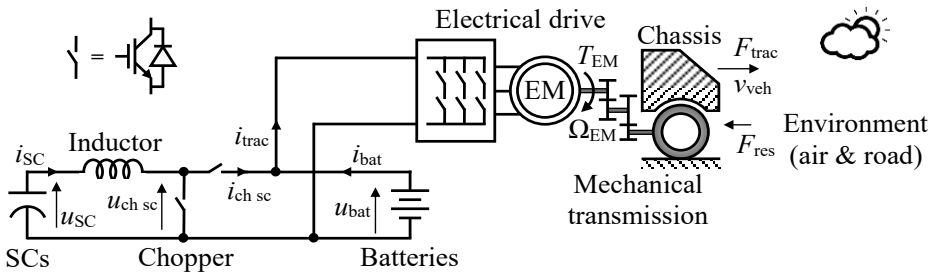

Figure 2.1: Studied system: an EV supplied by a battery/SC H-ESS.

2.1.2. Modeling and energetic macroscopic representation of the studied system

a. Components modeling and representation

Following the EMR philosophy of "divide and conquer," a complex system can be decomposed into subsystems to be controlled. Components of the studied system can thereby be represented by EMR pictograms as shown in Figure 2.2.

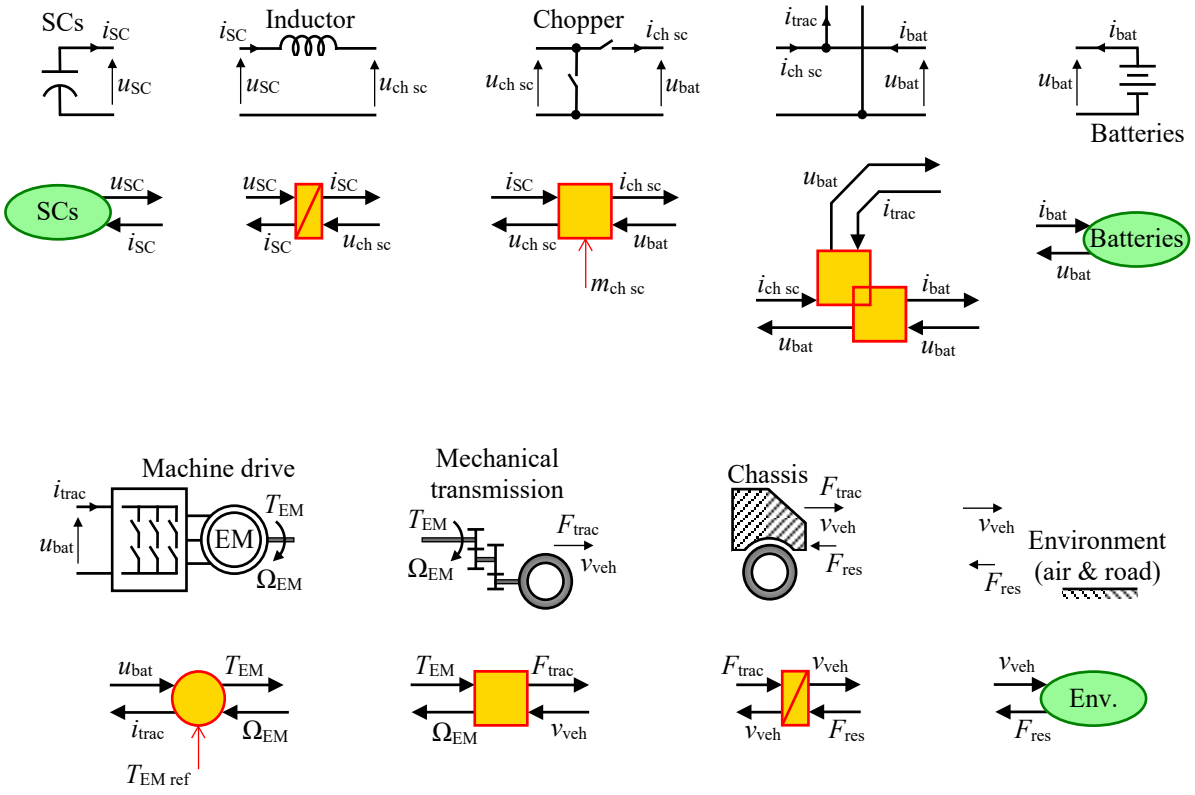

Figure 2.2: EMR of the studied EV components.

Batteries

The equivalent circuit of batteries model is given in Figure 2.3. The batteries output the voltage u_{bat} and inputs the current i_{bat}. There is a voltage drop in the equivalent series resistance (ESR) r_{bat}. The ESR is in fact different in charging and discharging modes; and it is a non-linear function of the state-of-charge (SoC). The open-circuit voltage (OCV) $u_{\mathrm{bat\,OC}}$ is also a non-linear function of the batteries SoC SoC_{bat}. In this work, the relationships $r_{\mathrm{bat}}(SoC_{\mathrm{bat}})$ and $u_{\mathrm{bat\,OC}}(SoC_{\mathrm{bat}})$ are given by look-up tables. The SoC is calculated by Coulomb counting with the capacitance C_{bat}. Hence, the batteries model is given as follows:

$$\begin{cases} u_{\mathrm{bat}} = u_{\mathrm{bat\,OC}}(SoC_{\mathrm{bat}}) - r_{\mathrm{bat}}(SoC_{\mathrm{bat}})i_{\mathrm{bat}} \\ SoC_{\mathrm{bat}} = SoC_{\mathrm{bat\,init}} - \dfrac{1}{C_{\mathrm{bat\,eq}}}\displaystyle\int_0^t i_{\mathrm{bat}}\,dt \end{cases}; \tag{2.1}$$

in which

$$C_{\mathrm{bat\,eq}} = 3600C_{\mathrm{bat}} \tag{2.2}$$

where C_{bat} is the batteries capacitance in Ah; $C_{\mathrm{bat\,eq}}$ the equivalent capacitance in Farad. The batteries are represented by a source element (oval) which receives the current i_{bat} as the input and outputs the voltage u_{bat} (see Figure 2.2).

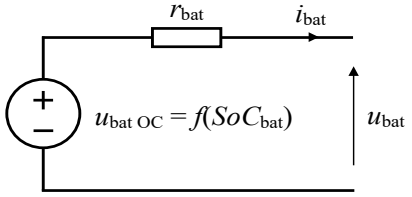

Figure 2.3: Batteries equivalent circuit model.

Supercapacitors

Unlike battery, the SoC of SC is almost proportional to its voltage. Thus, the SCs model can be simply given by the equivalent circuit model (Figure 2.4). The current i_{SC} charges/discharges the SCs with the capacitance C_{SC}. The SCs capacitance can be considered to vary with their voltage as modeled in [Grbovic 2011]. However, the coefficient of the capacitance variation is neglectable. In this work, for energy management purpose, the capacitance C_{SC} is considered a constant. The SC resistance r_{SC} causes an internal voltage drop and is quite independent of the SCs SoC. The mathematical model is expressed as:

$$u_{\mathrm{SC}} = u_{\mathrm{SC\,init}} - \frac{1}{C_{\mathrm{SC}}}\int_0^t i_{\mathrm{SC}}\,dt - r_{\mathrm{SC}}i_{\mathrm{SC}} \tag{2.3}$$

where u_{SC} is the SCs output voltage and $u_{SC\,init}$ their initial voltage. For local control development, the SCs energy does not aim to be controlled. Thus, the SCs is here depicted by a source element[3], similar to the batteries (see Figure 2.2). It is a voltage source in which the SCs voltage u_{SC} is the output.

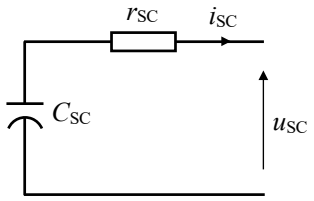

Figure 2.4: SCs equivalent circuit model.

Inductor

The inductor equivalent circuit model is considered as a pure inductance L and its parasitic resistance r_L (Figure 2.5). The inductor is assumed to work in linear conditions (unsaturated). Their parameters L and r_L are therefore constant. The inductor voltage is set by the difference between the SCs voltage u_{SC} and the chopper voltage $u_{ch\,sc}$. Since the inductor is connected in series with the SCs, its current is the SCs current i_{SC}. The inductor model is therefore given by:

$$u_{SC} = L\frac{d}{dt}i_{SC} + r_L i_{SC} + u_{ch\,sc}. \tag{2.4}$$

The inductor introduces a delay on the current response. It is therefore represented by an accumulation element[4] (crossed rectangle). In this sort of elements, the principle of causality must be respected. The output is an integral function of the input. Thus, the inductor inputs are the voltages u_{SC} and $u_{ch\,sc}$ and its output is the current i_{SC} (see Figure 2.2).

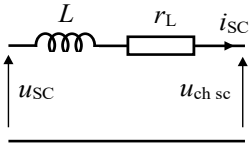

Figure 2.5: Inductor equivalent circuit model.

Chopper

The chopper modulates the low-side voltage $u_{ch\,sc}$ from the high-side voltage u_{bat} by its modulation function $m_{ch\,sc}$. The chopper current $i_{ch\,sc}$ is therefore linked to the SCs current i_{SC} via this function. In this study, the average model of the chopper is used as follows:

[3] In EMR, a source element is a terminal of the studied system.
[4] The output of the accumulation element is the state variable of the system model. Each accumulation element has only one output.

$$\begin{cases} u_{\text{ch sc}} = m_{\text{ch sc}} u_{\text{bat}} \\ i_{\text{ch sc}} = m_{\text{ch sc}} \eta_{\text{ch sc}}^{k_{\text{ch sc}}} i_{\text{sc}} \end{cases} \text{ with } k_{\text{ch sc}} = \begin{cases} 1 \text{ if } u_{\text{bat}} i_{\text{ch sc}} \geq 0 \\ -1 \text{ if } u_{\text{bat}} i_{\text{ch sc}} < 0 \end{cases}; \tag{2.5}$$

in which $\eta_{\text{ch sc}}$ is the chopper efficiency; the coefficient $k_{\text{ch sc}}$ depends on the power flow direction. The chopper modulates electrical power at its both sides. Thus, it is depicted by a mono-physical conversion element (square) with an input signal (modulation function $m_{\text{ch sc}}$) to tune the system (see Figure 2.2).

Parallel connection

The parallel connection is simply the summation of the batteries current i_{bat} and the chopper current $i_{\text{ch sc}}$ to yield the traction current i_{trac} as follows:

$$\begin{cases} u_{\text{bat}} \text{ common} \\ i_{\text{trac}} = i_{\text{bat}} + i_{\text{ch sc}} \end{cases}. \tag{2.6}$$

The batteries voltage u_{bat} is commonly shared between the three sides. The parallel connection is depicted by a coupling element (overlapped squares) which couples the power flows of subsystems in EMR (see Figure 2.2).

Electrical drive

The drive converts the electrical power into the mechanical power and vice versa. It is therefore represented by a multi-physical element (circle, see Figure 2.2). In this study, the electrical drive is considered to be properly controlled. Thus, the drive is given by the static model as:

$$\begin{cases} T_{\text{EM}} = T_{\text{EM ref}} \\ i_{\text{trac}} = \dfrac{T_{\text{EM}} \Omega_{\text{EM}}}{\eta_{\text{ED}}^{k_{\text{ED}}} u_{\text{bat}}} \end{cases} \text{ with } k_{\text{ED}} = \begin{cases} 1 \text{ if } T_{\text{EM}} \Omega_{\text{EM}} \geq 0 \\ -1 \text{ if } T_{\text{EM}} \Omega_{\text{EM}} < 0 \end{cases}; \tag{2.7}$$

in which the machine torque T_{EM} is considered responding perfectly to the reference $T_{\text{EM ref}}$; Ω_{EM} is the machine rotational speed; η_{ED} the electrical drive efficiency; the coefficient k_{ED} depends on the power flow direction.

Mechanical transmission

The mechanical transmission is modeled by a constant ratio k_{tran}, combining the final drive ratio and wheel transmission as follows:

$$\begin{cases} F_{\text{trac}} = T_{\text{EM}} \eta_{\text{tran}}^{k_{\text{eff tran}}} k_{\text{tran}} \\ \Omega_{\text{EM}} = v_{\text{veh}} k_{\text{tran}} \end{cases} \text{ with } k_{\text{eff tran}} = \begin{cases} 1 \text{ if } F_{\text{trac}} v_{\text{veh}} \geq 0 \\ -1 \text{ if } F_{\text{trac}} v_{\text{veh}} < 0 \end{cases} \tag{2.8}$$

where F_{trac} is the traction force; v_{veh} the vehicle velocity; η_{tran} the efficiency; the coefficient $k_{\text{eff tran}}$ depends on the power flow direction. A mono-physical element is used to depict the mechanical transmission, which links the mechanical power at its both side (see Figure 2.2).

Chassis

The vehicle chassis dynamics is addressed by the second Newton law of the relationship between the traction force F_{trac}, the resistant force F_{res}, and the vehicle velocity v_{veh} as:

$$v_{\text{veh}} = \frac{1}{M_{\text{veh}}} \int_0^t (F_{\text{trac}} - F_{\text{res}}) dt. \tag{2.9}$$

The total mass M_{veh} is considered as the summation of the vehicle net weight and passengers. An accumulation element represents the chassis due to its dynamical behaviors (see Figure 2.2). Regarding the principle of causality, the chassis inputs are the forces F_{trac} and F_{res} and its output is the vehicle velocity v_{veh}.

Environment

The environment imposes the total resistant force on the vehicle as a combination of rolling resistant force, air drag resistant force, and gravitational resistant force cause by slope as:

$$F_{\text{res}} = k_{\text{roll}} M_{\text{veh}} g + 0.5 \rho c_{\text{x}} A (v_{\text{veh}} + v_{\text{wind}})^2 + M_{\text{veh}} g \sin \alpha \,; \tag{2.10}$$

in which k_{roll} is the rolling coefficient; g the gravitational acceleration; ρ the air density; c_{x} air drag coefficient; A the efficient front area of the vehicle; v_{wind} the wind velocity; and α the slope angle. The environment terminates the system under study; hence it is represented by a source element (see Figure 2.2).

b. Studied system representation

EMR elements depict components and subsystems, then they are connected to represent the system as the interactions of subsystems. EMR of the studied system is shown in Figure 2.6.

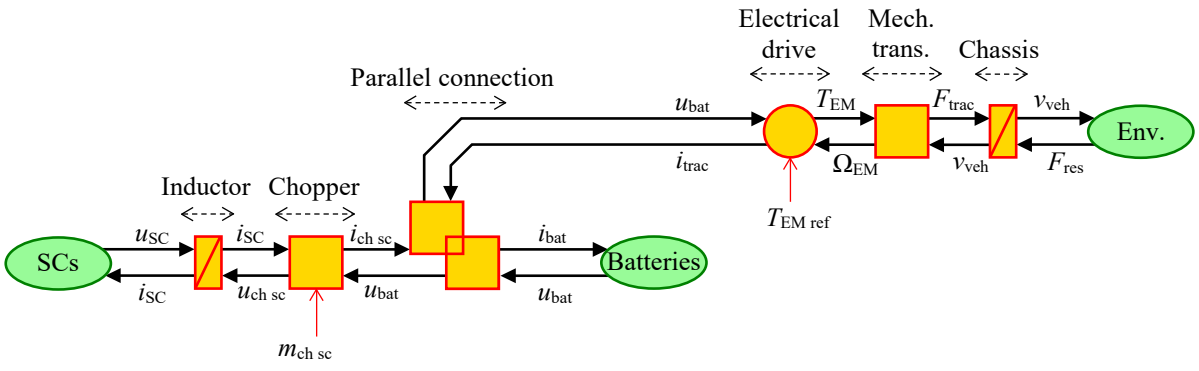

Figure 2.6: EMR of the studied battery/SC EV.

2.1.3. Local control of the studied system

EMR method offers a systematic approach to deduce control scheme from the system representation. Firstly, the tuning paths and control paths should be figured out. Then, the control element of each subsystem is obtained. Finally, the complete control scheme is accomplished.

a. Tuning paths and control paths

Tuning paths are the routes going from the tuning variables to the objective variables. The tuning variables are the ones which can be tuned to control the system. In this studied system (see Figure 2.6), there are two tuning variables which are the modulation functions $m_{\text{ch sc}}$ and the machine torque reference $T_{\text{EM ref}}$. The objective variables are the ones to be controlled. Here, there are two objective variables which are the batteries current i_{bat} and the vehicle velocity v_{veh}. Meanwhile the latter is clear, the former should be more explained. The objective of adding the SCs subsystem is to support the batteries, so the aim of controlling the SCs subsystem should be to indirectly control the batteries current i_{bat}.

There are two tuning paths of the studied system defined as in Figure 2.7. In the H-ESS, the $m_{\text{ch sc}}$ modulates the chopper voltage $u_{\text{ch sc}}$ to control the SCs current i_{SC} for tuning the chopper current $i_{\text{ch sc}}$ to control the batteries current i_{bat}. For the traction part, the reference $T_{\text{EM ref}}$ tunes the machine torque T_{EM} to obtain the traction force F_{trac} for controlling the vehicle velocity v_{veh}.

From the tuning paths of the system, the control paths can be constructed by the principle of inversion. The control paths are the routes going from the references of the objective variables to the tuning variables to impose the references on the system. They are like symmetrical via a "mirror" (see Figure 2.7).

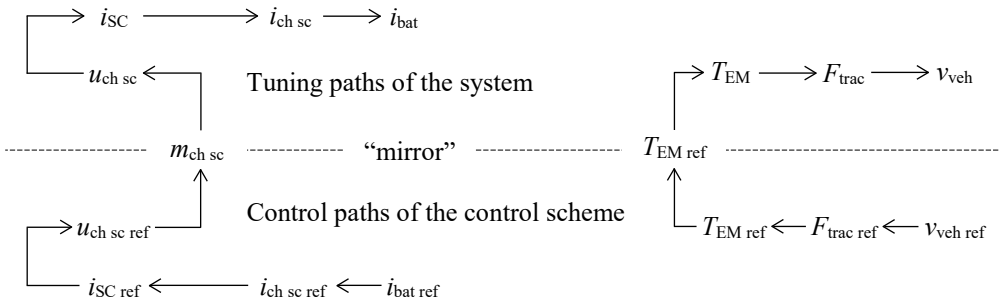

Figure 2.7: Tuning paths and control paths for local control of the studied battery/SC EV.

b. Control element as an inversion of system model element

The control of the system is built along the control paths defined above. Each subsystem represented by an EMR element is controlled by a control element which is the inversion of the model element[5]. There are two types of inversions:

- Direct inversion used for the elements containing no dynamical delay; thus, the mathematical models can be directly inverted;
- Indirect inversion used for the accumulation elements which contain the dynamical delays of the system; the direct inverted mathematical model is therefore non-causal. Hence indirect inversions are normally realized by feedback controllers.

Here, the vehicle speed controller is presented to illustrate how an indirect inversion is deduced and realized. The left part of Figure 2.8 is the chassis and its controller represented in EMR. Inversion of the accumulation element is a crossed parallelogram.

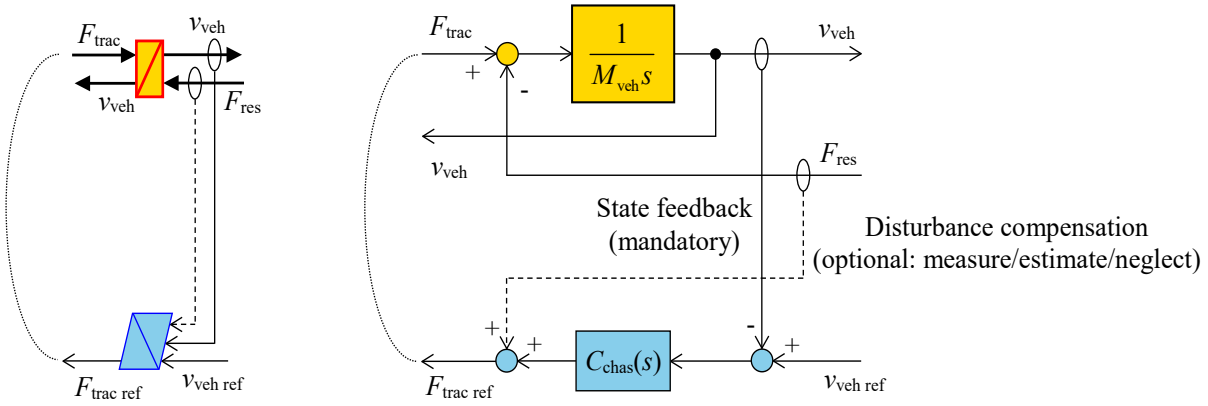

Figure 2.8: Velocity controller as an indirect inversion of the vehicle chassis.

The right part of Figure 2.8 illustrate the realization of indirect inversion by a velocity feedback controller $C_{chas}(s)$ as:

$$F_{trac\ ref} = C_{chas}(s)(v_{veh\ ref} - v_{veh}) + F_{res\ meas}; \quad (2.11)$$

In real-world applications, the resistive force cannot be measured; instead, they can be estimated or neglected.

c. Local control scheme of the studied system

Following the defined control paths, by inverting the subsystems models as illustrated above, the inversion-based control scheme of the system can be deduced by mirror effect as shown in Figure 2.9.

[5] Except the source element. It is the terminal of the system which is never inverted to be controlled.

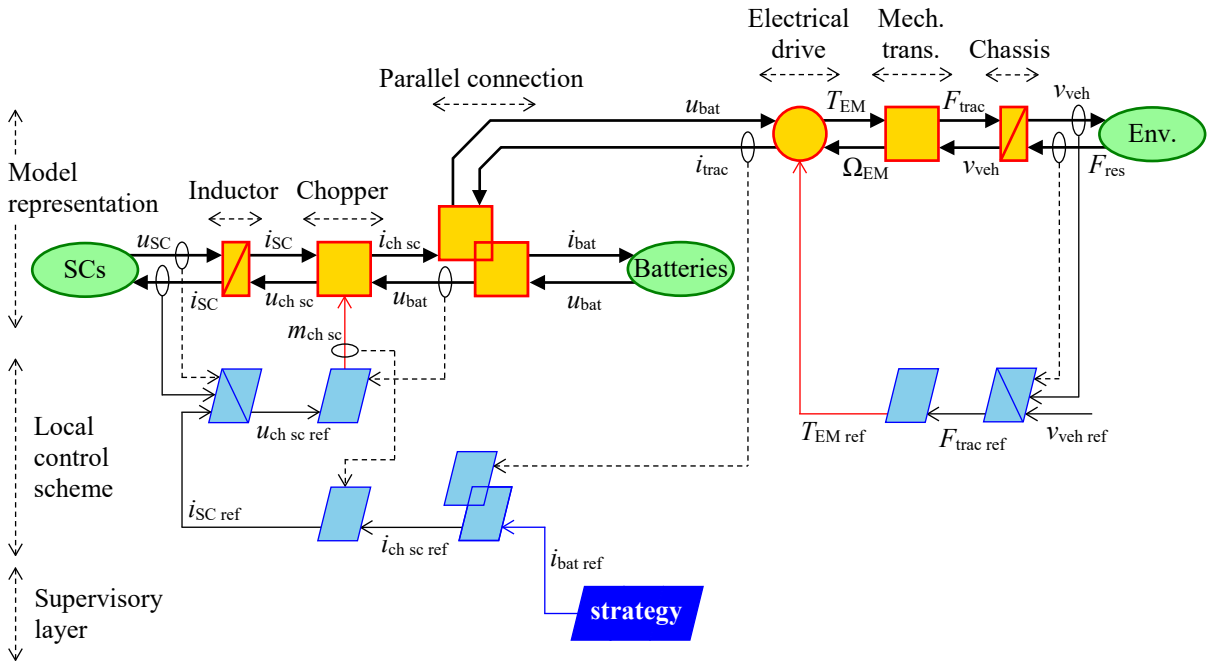

Figure 2.9: EMR and inversion-based control of the studied battery/SC EV.

Traction subsystem

The velocity control has been introduced above. The mechanical transmission is a conversion element which can be directly inverted as:

$$T_{\text{EM ref}} = \frac{F_{\text{trac ref}}}{k_{\text{tran}}}. \tag{2.12}$$

The machine drive is assumed that the torque responds perfectly to the reference, thus there is no need of controller. The $T_{\text{EM ref}}$ is imposed to the drive.

H-ESS subsystem

The parallel connection is directly inverted (overlapped parallelograms) as follows:

$$i_{\text{ch sc ref}} = i_{\text{trac meas}} - i_{\text{bat ref}}. \tag{2.13}$$

In this inversion, the traction current is the measurable disturbance to be compensated.

The current relationship of the chopper is inverted (parallelogram) by:

$$i_{\text{SC ref}} = \frac{i_{\text{ch sc ref}}}{m_{\text{ch sc}}}; \tag{2.14}$$

in which the modulation function $m_{\text{ch sc}}$ is considered as a disturbance.

The inductor is an accumulation element with dynamical delay, hence the inversion must be indirect (crossed parallelogram). It is realized by a closed-loop controller $C_{\text{ind}}(s)$ as follows:

$$u_{\text{ch sc ref}} = u_{\text{SC meas}} - C_{\text{ind}}(s)(i_{\text{SC ref}} - i_{\text{SC meas}}). \tag{2.15}$$

Here, the SCs voltage is measured as a disturbance to be compensated.

Finally, the modulation function is obtained by the direct inversion of the chopper voltage relationship given by:

$$m_{\text{ch sc}} = \frac{u_{\text{ch sc ref}}}{u_{\text{bat meas}}}. \tag{2.16}$$

The batteries voltage is measured as a disturbance.

The local control scheme has been developed. The batteries current reference $i_{\text{bat ref}}$ is imposed by a strategy block which is at the higher layer than local control. This is where EMSs are realized.

2.1.4. Model modification for energy management strategy development

In the previous subsections, the full dynamical system has been considered to develop local dynamical control. The EMSs should be then developed at the supervisory level. However, this full dynamical model may not be suitable for EMSs development. The EMSs impose references to the local control; thus, they correspond to the slower dynamics. Model modification for energy management is thereby introduced.

a. Model reduction

Since energy management is at the higher level than the local control, considering all dynamics of the system may not be effective[6]. There are three reasons:

- First, the full dynamical model is complex which is often a multi-variable high-order model. That can make the EMSs development complicated and hard to be realized.

- Second, dynamics of the system at each level are different. The dynamics at the higher level (strategy) are normally slower than the one at the lower level (control) [Bouscayrol 2005; Trovão 2013a]. Addressing all the fast dynamics can cause huge computational consuming for the EMSs which could be difficult for on-board implementation.

- Third, when the local control is properly developed, the controlled variables can be considered as being perfect response to the references. Thus, it is unnecessary to address these fast dynamics at the supervisory level.

[6] That is not obvious. Some previous works, e.g., [Dai 2016], have addressed all the dynamics in a single model to develop control and energy management simultaneously.

Hence, the model should be reduced to eliminate the fast dynamics at the local control level [Castaings 2016b; Horrein 2015; Mayet 2014a]. In the studied system, the bidirectional DC/DC converter can be reduced as illustrated in Figure 2.10.

When the current controller perfectly performs, the inductor, the chopper, and their inversions can be reduced to an equivalent converter, in which:

$$i_{\text{ch sc}} = i_{\text{ch sc ref}}. \tag{2.17}$$

The SCs current is given by:

$$i_{\text{SC}} \frac{u_{\text{bat}} i_{\text{ch sc}}}{u_{\text{SC}}} \tag{2.18}$$

in which, the converter efficiency is neglected. It is because the reduced model is used only for developing real-time strategy. Whereas the efficiency depends on the power flow direction. In real-time implementation, that may cause the chattering phenomenon when the current is around zero. When validating the developed strategy, the simulation is implemented with the full dynamical model which addresses all the efficiencies of the system.

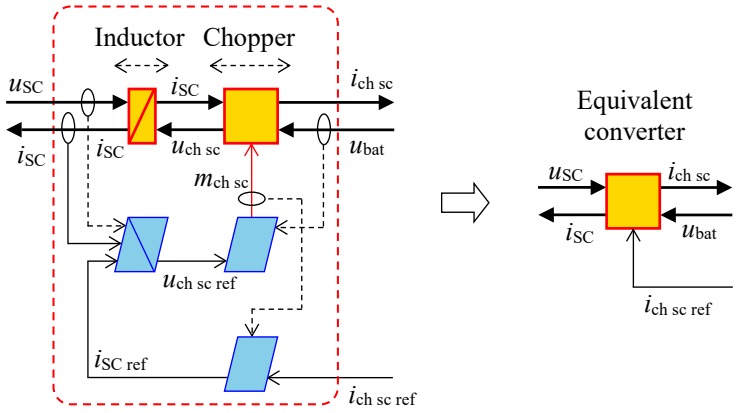

Figure 2.10: Model reductions of DC/DC converter assuming perfect control performances.

b. Model transformation

The system fast dynamics have been addressed at the local control level and have been therefore reduced. The EMSs, at the supervisory level, deal with the dynamical behaviors which are the dynamics of the secondary source, i.e., the SCs. The SCs model representation is therefore transformed to address these considered dynamics as shown in Figure 2.11.

When the SCs are modeled for local control purpose, their energy variation is not considered. The SCs are therefore represented as a source element of which the voltage u_{SC} is the disturbance of the current control loop. At the supervisory level, the energy variation of the secondary source is treated by the EMSs. Hence the SCs should be depicted by an accumulation element which represents the system dynamics under study. The SCs voltage u_{SC} is therefore the state variable

to be controlled by the EMSs (since it is the output of the accumulation element). The mathematical model here remains.

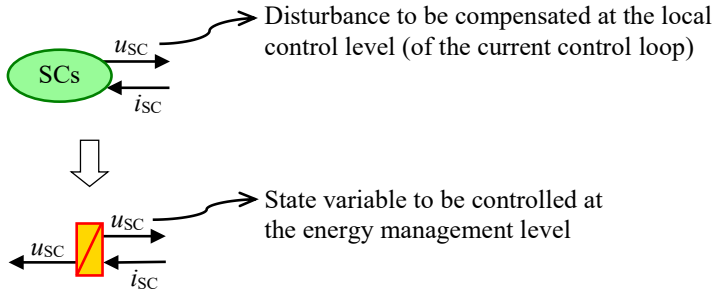

Figure 2.11: Model transformation to highlight the considered dynamics at supervisory level.

On the other hand, the strategy, at the supervisory level, deals with current distribution problem of the H-ESS. In which, the traction current i_{trac} is the disturbance input. Thus, the traction subsystem can be considered as an equivalent current source which enforces the current i_{trac} to the H-ESS (Figure 2.12). It should be noted that here there is no need of assuming that the vehicle velocity v_{veh} perfectly follows its reference $v_{\text{veh ref}}$. Furthermore, inside the equivalent source element of the traction subsystem, the vehicle dynamics can still be fully considered. Hence, the model here is transformed rather than reduced as the case of the DC/DC converter.

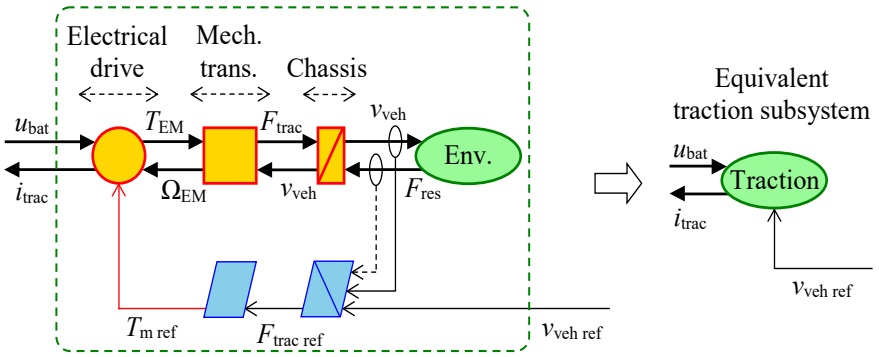

Figure 2.12: Model transformation to highlight the disturbance at supervisory level.

c. Model for energy management strategy development

Reduced EMR of the studied system

Applying model modifications addressed above, the system model can be reduced (Figure 2.13). The traction subsystem enforces the traction current i_{trac} as a disturbance to the H-ESS, in which the batteries couple with the equivalent converter and the SCs. The EMS, in the strategy block, imposes the batteries current reference $i_{\text{bat ref}}$. The coupling inversion element (overlapped

parallelograms) compensates the measured disturbance i_{trac} to deduce the chopper current reference $i_{\text{ch sc ref}}$ imposed to the converter.

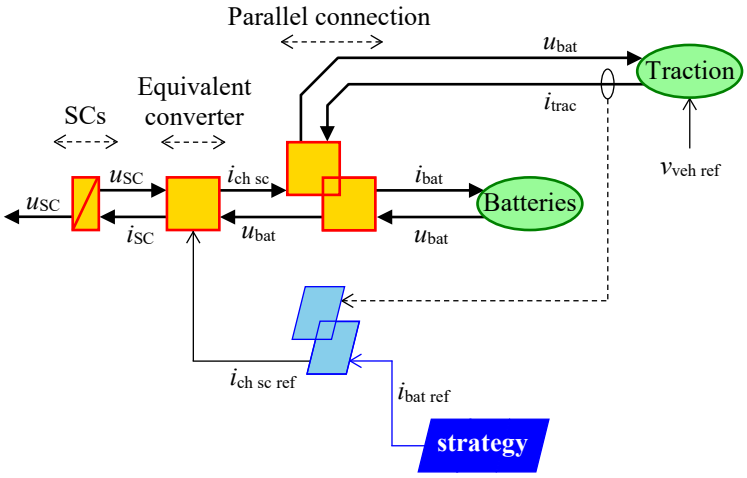

Figure 2.13: Reduced EMR of the studied battery/SC EV.

Reduced mathematical model for optimal control-based strategy development

From the reduced EMR, a reduced mathematical model can be obtained to apply optimal control for strategy development. The mathematical model is obtained by step-by-step combining the models of EMR system elements except the source elements which are terminal of the system. Here, they are the models of the SCs, the equivalent converter, and the parallel connection (see Figure 2.13). The process should be started from the accumulation element of which the output is the state variable to be controlled. The reduced mathematical model is therefore deduced as the follows. From (2.3), assuming that the SCs series resistance r_{SC} is neglectable, the SCs main dynamics are given by:

$$\frac{d}{dt}u_{\text{SC}} = -\frac{1}{C_{\text{SC}}}i_{\text{SC}}. \tag{2.19}$$

Besides, from (2.18), the SCs current can be calculated as:

$$i_{\text{SC}} = \frac{u_{\text{bat}}i_{\text{ch sc}}}{u_{\text{SC}}}. \tag{2.20}$$

As a result, the SCs dynamics can be expressed as:

$$\frac{d}{dt}u_{\text{SC}} = -\frac{u_{\text{bat}}i_{\text{ch sc}}}{C_{\text{SC}}u_{\text{SC}}}. \tag{2.21}$$

From (2.13) and (2.17), the chopper current is given by:

$$i_{\text{ch sc}} = i_{\text{trac}} - i_{\text{bat ref}}. \tag{2.22}$$

Finally, that leads to the reduced mathematical model of the studied system by combining (2.21) and (2.22) as the follows:

$$\frac{d}{dt}u_{\mathrm{SC}} = \frac{u_{\mathrm{bat}}}{u_{\mathrm{SC}}C_{\mathrm{SC}}}(i_{\mathrm{bat\,ref}} - i_{\mathrm{trac}}). \tag{2.23}$$

This mathematical model can be express as:

$$\frac{d}{dt}u_{\mathrm{SC}} = \underbrace{\frac{1}{u_{\mathrm{SC}}}}_{\substack{\text{State}\\ \text{variable}}} \quad \underbrace{\frac{1}{C_{\mathrm{SC}}}}_{\text{Parameter}} \left(\underbrace{i_{\mathrm{bat\,ref}}}_{\substack{\text{Control}\\ \text{variable}}} - \underbrace{i_{\mathrm{trac}}}_{\text{Disturbance}} \right) \underbrace{u_{\mathrm{bat}}}_{\text{Disturbance}} \tag{2.24}$$

in order to give some remarks:

- This model is in non-linear structure (see Appendix A.3) but less complex than the full dynamical model;
- There is only one parameter which is given by system datasheet;
- There are only two disturbances which are both measurable.

Cost function

With the above model, various control methods can be applied for different purposes. Since the objective is to develop an optimization-based EMS, optimal control theory is used. Optimal control is to find a control law for a dynamical system so that the cost function is minimized while satisfying the constraints. The cost function of the studied optimal control problem should therefore be defined.

The objective of adding the SCs subsystem is to extend the batteries life-time. There are various factors affecting batteries life-time [Barré 2013]. From the viewpoint of control and energy management, the rms value of batteries current is an appropriate stress index factor:

$$I_{\mathrm{bat\,rms}} = \sqrt{\frac{1}{t_{\mathrm{f}} - t_0}\int_{t_0}^{t_{\mathrm{f}}} i_{\mathrm{bat}}^2 dt}. \tag{2.25}$$

In fact, for a certain interval from t_0 to t_{f}, the minimization of the integration term leads to the minimization of the rms value. Furthermore, quadratic functions are of interest for many optimization techniques [Bryson 1975]. Hence, the cost function of the studied energy management problem can be defined by:

$$J = \int_{t_0}^{t_{\mathrm{f}}} i_{\mathrm{bat}}^2 dt. \tag{2.26}$$

2.2. Optimal benchmark using dynamic programming

The objective of the thesis is to develop real-time optimization-based EMSs. The EMSs are expected having near-optimal performances which should be validated by comparing to the optimal strategies. In order to deduce such benchmarks, DP is used thanks to its ability to obtain optimal solutions.

2.2.1. Backward representation

In this thesis, EMR is used as the unified formalism for modeling, control, and energy management. However, it is a forward representation respecting physical causality, meanwhile, DP is a non-causal backward method. Thus, the EMR-based backward representation [Horrein 2015; Mayet 2014a] is used to organize the system model for DP computation.

The backward representation (Figure 2.14) is transformed from the reduced EMR of the studied system (see Figure 2.13) by the following rules:

- Merging the system elements and their inversions;
- Changing the directions of the variables needed to be controlled to the directions of their references. Here, only the chopper current $i_{\text{ch sc}}$ is changed to the backward direction.

With these rules, the coupling element of the backward model has the relationship given by:

$$\begin{cases} i_{\text{bat}} = i_{\text{bat ref}} \\ i_{\text{ch sc}} = i_{\text{trac}} - i_{\text{bat}} \end{cases}. \tag{2.27}$$

This backward representation is used to organize the model of the system in the numerical program for problem solving.

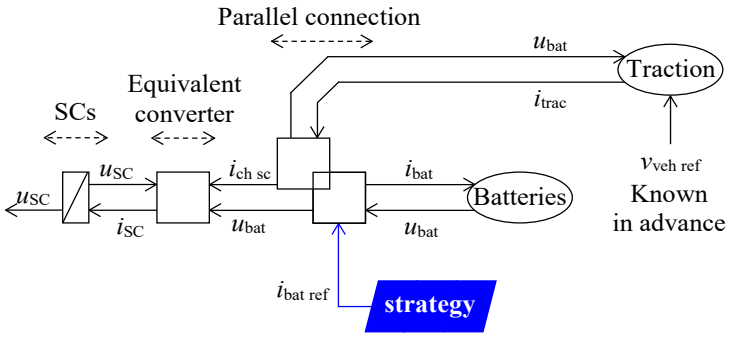

Figure 2.14: EMR-based backward representation of the studied system.

2.2.2. Dynamic programming implementation

The DP problem is implemented and solved by using the MALTB-based dpm function toolbox [Sundström 2009]. The EMR and the backward representation of the system help to organize the system model as illustrated in Figure 2.15.

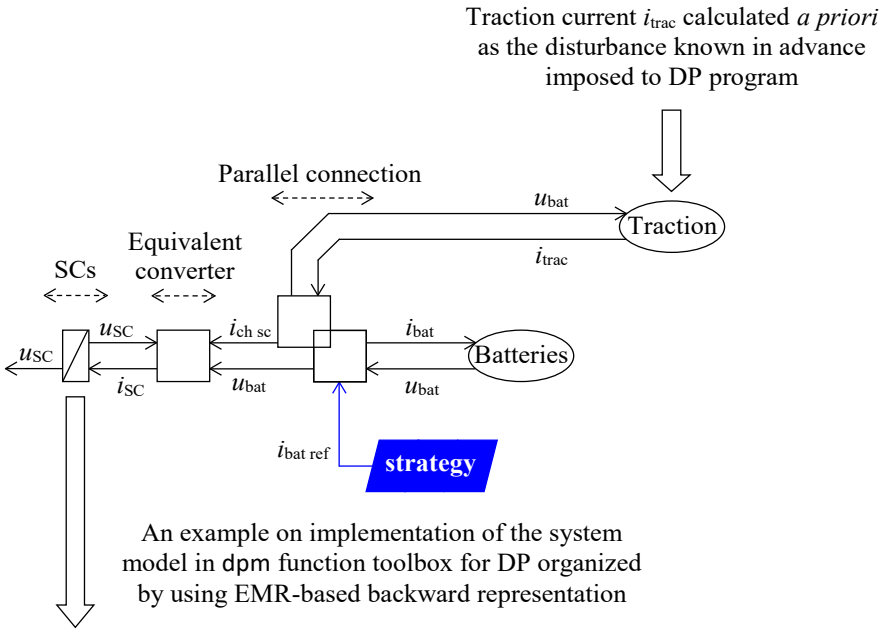


```
% SCs MODEL
% SCs open circuit voltage u_sc_ocv as the state variable
u_sc_ocv  =  u_sc_ocv + inp.Ts.*(- i_sc / (SC_C)) ;
% Update the state variable x(t)
X{1} = u_sc_ocv ;
% SCs terminal voltage u_sc
u_sc = u_sc_ocv - i_sc.*SC_r ;
% Infeasible case (for limitation)
in_SCs = (u_sc > SC_umax) + (u_sc < SC_umin) ;
```

Figure 2.15: Implementation of DP using EMR-based backward representation and dpm function toolbox [Sundström 2009].

The traction subsystem is simulated in advance to obtain the traction current i_{trac} as the disturbance enforced to the H-ESS. For that, the traction subsystem is assumed to be supplied by batteries as the approximation of the H-ESS. The system model is then implemented in form of MATLAB scripts which are organized by the backward representation (see Figure 2.15).

2.3. Real-time strategy based on Hamiltonian minimization

In this section, a novel real-time optimization-based EMS is proposed based on Hamiltonian minimization, which is an adaptation of PMP [Nguyễn 2019]. The methodology will be addressed first to explain the main idea of the method. Then the strategy development will be

presented to deduce an analytical close-form near-optimal control law. Next, the co-state variable will be determined based on its physical meaning. Finally, the strategy implementation will be described to show how simple it is.

2.3.1. Approach

Since the studied system is a single-variable system, the PMP, generally described in (1.7)–(1.10), can be stated with the Hamiltonian defined by scalar variable as:

$$H = g[x(t), u(t), t] + \lambda(t) f[x(t), u(t), t]. \tag{2.28}$$

The PMP claims that if u^* is an optimal control law, it must satisfy the following three necessary conditions:

$$\frac{d}{dt}x^*(t) = \frac{\partial H[u^*(t), x^*(t), \lambda^*(t), t]}{\partial \lambda(t)}; \tag{2.29}$$

$$\frac{d}{dt}\lambda^*(t) = -\frac{\partial H[u^*(t), x^*(t), \lambda^*(t), t]}{\partial x(t)}; \tag{2.30}$$

$$H[u^*(t), x^*(t), \lambda^*(t), t] \leq H[u(t), x^*(t), \lambda^*(t), t]. \tag{2.31}$$

Conditions (2.29) and (2.30) compose the dynamics of a Hamiltonian system. Condition (2.31) means the minimization of the Hamiltonian function[7]. Conventional methods satisfy all conditions to obtain an off-line open-loop control law; an additional state feedback scheme is then used for implementation in real-time. The strategies are therefore no longer optimal.

Here, an alternative approach is proposed [Nguyễn 2019]. Only condition (2.31) is used to directly deduce a real-time strategy. The Hamiltonian function contains a relationship between the control variable $i_{\text{bat ref}}$ and the state variable u_{SC}. Hence, applying (2.31) by a partial derivative with respect to the control variable can eventually carry out an analytical closed-form strategy. The co-state variable λ is then determined based on its physical meaning without considering the Hamiltonian system dynamics (2.29) and (2.30).

The obtained strategy is indeed sub-optimal as the PMP theory is not strictly satisfied. However, since the obtained control law is analytical closed-form with state feedback, no more additional feedback scheme is required. The close-to-optimal performance of the proposed strategy will be examined by comparing to the DP-based optimal benchmark addressed in the previous section.

2.3.2. Strategy development

From (2.23), (2.26), and (2.28), the Hamiltonian of the studied system is given as the combination of the cost and the dynamics of the system as the follows:

[7] To be mathematically strict, Hamiltonian is a functional, which is a function of functions.

$$H = i_{\text{bat}}^2 + \lambda \frac{1}{u_{\text{SC}} C_{\text{SC}}} (i_{\text{bat ref}} - i_{\text{trac}}) u_{\text{bat}}. \tag{2.32}$$

Since the $i_{\text{ch sc ref}}$ is given by the $i_{\text{bat ref}}$ compensating the i_{trac} (see Figure 2.13), it is suitable to obtain the control law $i_{\text{ch sc ref}}$ then to deduce the $i_{\text{bat ref}}$. The condition (2.31) can therefore be realized by:

$$\frac{\partial H}{\partial i_{\text{ch sc ref}}} = 0. \tag{2.33}$$

The i_{trac} is the disturbance enforced from the traction subsystem which is totally independent on the chopper current. Hence, considering (2.22) and by assuming perfect response of the chopper current control, that leads to:

$$\frac{\partial (i_{\text{bat}}^2)}{\partial i_{\text{ch sc}}} = -2 i_{\text{bat}}. \tag{2.34}$$

The partial derivative to be calculated therefore becomes:

$$\frac{\partial H}{\partial i_{\text{ch sc}}} = -2 i_{\text{bat}} - \lambda \frac{u_{\text{bat}}}{C_{\text{SC}}} \frac{i_{\text{ch sc}} \frac{\partial u_{\text{SC}}}{\partial i_{\text{ch sc}}} - u_{\text{SC}}}{u_{\text{SC}}^2}. \tag{2.35}$$

The partial derivative of u_{SC} with respect to $i_{\text{ch sc}}$ is calculated by:

$$\begin{aligned} \frac{\partial u_{\text{SC}}}{\partial i_{\text{ch sc}}} &= \frac{1}{\frac{\partial \left(\frac{u_{\text{SC}}}{u_{\text{bat}}} i_{\text{SC}} \right)}{\partial u_{\text{SC}}}} \\ &= \frac{1}{\frac{i_{\text{SC}}}{u_{\text{bat}}} + \frac{u_{\text{SC}}}{u_{\text{bat}}} \frac{\partial i_{\text{SC}}}{\partial u_{\text{SC}}}}. \end{aligned} \tag{2.36}$$

In which, the partial derivative of i_{SC} with respect to u_{SC} is adopted from [Nguyen 2014]. In which, the relationship between SCs current and voltage is given by:

$$i_{\text{SC}} = \frac{u_{\text{SC}} - \sqrt{u_{\text{SC}}^2 - 4 r_{\text{SC}} P_{\text{SC}}}}{2 r_{\text{SC}}} \tag{2.37}$$

where P_{SC} is the SCs terminal power. Thus,

$$\frac{\partial i_{\text{SC}}}{\partial u_{\text{SC}}} = -\frac{i_{\text{SC}}}{\sqrt{u_{\text{SC}}^2 - 4 r_{\text{SC}} P_{\text{SC}}}}. \tag{2.38}$$

That leads to:

$$\frac{\partial u_{\mathrm{SC}}}{\partial i_{\mathrm{ch\ sc}}} = \frac{u_{\mathrm{bat}}\sqrt{u_{\mathrm{SC}}^2 - 4r_{\mathrm{SC}}P_{\mathrm{SC}}}}{i_{\mathrm{SC}}\sqrt{u_{\mathrm{SC}}^2 - 4r_{\mathrm{SC}}P_{\mathrm{SC}}} - P_{\mathrm{SC}}}. \tag{2.39}$$

Applying (2.39) to (2.35), the partial derivative of the Hamiltonian is then carried out:

$$\frac{\partial H}{\partial i_{\mathrm{ch\ sc}}} = -2i_{\mathrm{bat}} - \lambda\frac{u_{\mathrm{bat}}}{C_{\mathrm{SC}}}\frac{i_{\mathrm{ch\ sc}}\dfrac{u_{\mathrm{bat}}\sqrt{u_{\mathrm{SC}}^2 - 4r_{\mathrm{SC}}P_{\mathrm{SC}}}}{i_{\mathrm{SC}}\sqrt{u_{\mathrm{SC}}^2 - 4r_{\mathrm{SC}}P_{\mathrm{SC}}} - P_{\mathrm{SC}}} - u_{\mathrm{SC}}}{u_{\mathrm{SC}}^2}. \tag{2.40}$$

Considering that (by neglecting efficiency):

$$\frac{u_{\mathrm{bat}}i_{\mathrm{ch\ sc}}}{i_{\mathrm{SC}}} = u_{\mathrm{SC}}; \tag{2.41}$$

and by applying the Hamiltonian minimization condition (2.33), it follows as:

$$2i_{\mathrm{bat}} + \lambda\frac{u_{\mathrm{bat}}}{C_{\mathrm{SC}}}\frac{\dfrac{u_{\mathrm{SC}}\sqrt{u_{\mathrm{SC}}^2 - 4r_{\mathrm{SC}}u_{\mathrm{SC}}i_{\mathrm{SC}}}}{\sqrt{u_{\mathrm{SC}}^2 - 4r_{\mathrm{SC}}u_{\mathrm{SC}}i_{\mathrm{SC}}} - u_{\mathrm{SC}}} - u_{\mathrm{SC}}}{u_{\mathrm{SC}}^2} = 0. \tag{2.42}$$

The control law is therefore obtained as:

$$i_{\mathrm{bat\ ref}} = \lambda\frac{u_{\mathrm{bat}}}{2C_{\mathrm{SC}}}\frac{u_{\mathrm{SC}} - \dfrac{u_{\mathrm{SC}}\sqrt{u_{\mathrm{SC}}^2 - 4r_{\mathrm{SC}}u_{\mathrm{SC}}i_{\mathrm{SC}}}}{\sqrt{u_{\mathrm{SC}}^2 - 4r_{\mathrm{SC}}u_{\mathrm{SC}}i_{\mathrm{SC}}} - u_{\mathrm{SC}}}}{u_{\mathrm{SC}}^2}. \tag{2.43}$$

It can be seen that the control law $i_{\mathrm{bat\ ref}}$ is a function of the state variable u_{SC}. Thus, the control law is closed-form which does not require any additional state feedback adaptation scheme. Once the co-state variable λ is determined, (2.43) is ready to serve as a real-time strategy.

2.3.3. Co-state variable physical meaning and determination

This approach determines λ not by the Hamiltonian dynamics (2.29) and (2.30), but by its physical meaning. The physical essence of the co-state variable has been pointed out in the literature [Ross 2015]. It is an equivalent factor to convert the dynamical function of the system to an equivalent cost to be minimized. Such a physical explanation has been also figured out by previous works, e.g. [Nguyen 2014]. It is used here to calculate λ.

The Hamiltonian (2.32) can be analyzed in terms of physical units as the follows:

$$H = \underbrace{i_{\mathrm{bat}}^2}_{\mathrm{A}^2} + \lambda\frac{u_{\mathrm{bat}}}{u_{\mathrm{SC}}}\underbrace{\frac{1}{C_{\mathrm{SC}}}}_{1/\mathrm{F}}\underbrace{(i_{\mathrm{bat\ ref}} - i_{\mathrm{trac}})}_{\mathrm{A}}; \tag{2.44}$$

whereas the cost term i_{bat}^2 has a dimension of Ampere squared, the dimension of the dynamics term is Ampere per Farad. To perform a proper subtraction, the co-state variable, as an equivalent factor, should have a form of λ equals Capacitance times Current. On the right-hand side, the former term can be chosen as the SCs capacitance which is the only capacitive quantity of the studied system.

The latter term of current is more flexible to be determined. In [Nguyễn 2017a], it is given by the expected maximal batteries current when the SCs can no longer support the batteries. This value is set by the proportions of the batteries C-rate regarding the driving modes. This approach leads to a high-performance strategy validated by the reported simulation results. However, C-rate is an indicator of batteries energy rather than their power. The justification of this approach is therefore not so convinced.

To overcome the issue mentioned above, λ is determined from the traction rms current:

$$\lambda = C_{\text{SC}} i_{\text{trac rms}}; \tag{2.45}$$

in which, $i_{\text{trac rms}}$ depends on the driving modes and should be pre-calculated. The pre-calculation can be done with a standard driving cycle. In this work, the Worldwide harmonized Light duty driving Test Cycle (WLTC) is used. Based on the studied vehicle, the WLTC class 2 (Figure 2.16) is used for the pre-calculation of the $i_{\text{trac rms}}$. It can be classified as three parts "Low," "Middle," and "High" according to [Tutuianu 2014]. They are corresponding to urban, rural, and highway driving modes of the studied vehicle, respectively.

In a summary, the co-state variable λ is determined as follows. The traction subsystem of the vehicle is simulated off-line with the WLTC class 2 driving cycle. The three values of $i_{\text{trac rms}}$, as well as λ, are computed regarding the three parts of the cycle mentioned above. The co-state variable is then implemented in the EMS as a function of driving modes. In this study, the driving modes (urban, rural, and highway) in real-time implementations are determined manually. In real-world applications, it is reasonable to assume that the driver knows what kind of driving modes the vehicle is working. An intelligent automatic recognition of the driving modes could be interesting; however, it is out of the scope of this study.

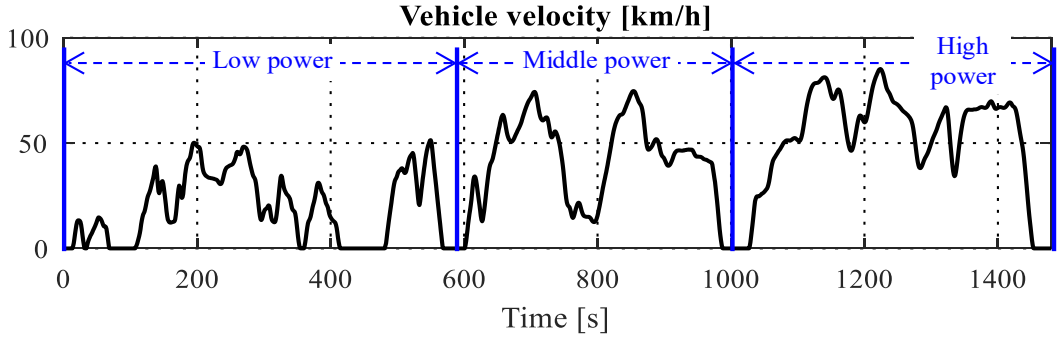

Figure 2.16: WLTC class 2 used for co-state variable λ determination.

2.3.4. Strategy implementation

The proposed EMS is implemented as illustrated in Figure 2.17. Four sensors are required for the measurements of the SCs voltage u_{SC}, the batteries voltage u_{bat}, the SCs current i_{SC}, and the traction current i_{trac}. The three former variables are imposed to (2.43) and (2.45) to conduct the calculated batteries current reference $i_{bat\ ref\ cal}$. The last measured variable, i.e., i_{trac}, is used only when the SCs voltage reaches maximal or minimal limitations. When the u_{SC} is between the two boundaries, the $i_{bat\ ref}$ is the $i_{bat\ ref\ cal}$; otherwise, it is switched to the $i_{trac\ meas}$. The smooth switching can be realized by using conventional method presented in [Lhomme 2009].

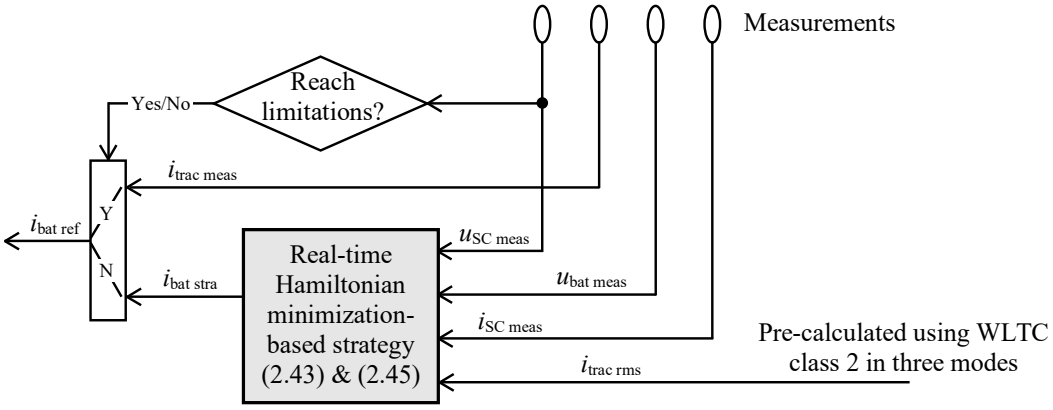

Figure 2.17: Implementation of the proposed Hamiltonian minimization-based EMS.

2.4. Simulations and results

2.4.1. Examined system

The reference vehicle used for this work is Tazzari Zero with the main parameters given in Table 2.1. The car is originally supplied by a pack of Li-ion batteries TS-LFP160AHA from Thunder Sky. The batteries have been sized for a real driving range around 100 km. For studies of H-ESSs, it is modified to the semi-active configuration by adding a SCs subsystem with the module BMOD0165 P048 BXX from Maxwell Technologies. SCs and batteries sizes are constant during the study to fairly compare the different EMS strategies.

Three standard driving cycles are considered for testing:

- WLTC class 2, which is utilized to determine the co-state variable λ, with urban, rural, and highway parts. This is the result of a statistical study that addressed various standard and real-world driving cycles from different countries in Europe, Asia, and America [Tutuianu 2014].
- NEDC with urban and highway parts. This driving cycle is used in many studies because it can clearly examine the acceleration and deceleration behaviors of vehicles. This cycle is however too smooth in comparison with real world-based cycles.
- ARTEMIS urban which is an urban cycle. This cycle addresses better than NEDC the fluctuations especially in urban areas.

Table 2.1: Examined system parameters for simulation of the battery/SC EV.

Parameters		Values
Vehicle (Tazzari Zero)		
Vehicle total mass	M_{veh}	692 kg
Aerodynamic standard	$c_{\text{x}}A$	0.7 m^2
Rolling coefficient	k_{roll}	0.02
Air density (at 20°C)	ρ	1.223 kg/m^3
Electrical drive (induction machine)		
Maximal power	$P_{\text{ED max}}$	15 kW
Nominal efficiency	$\eta_{\text{ED nom}}$	85 %
Batteries (Thunder Sky TS-LFP160AHA cells)		
Battery bank capacitance	C_{bat}	160 Ah
Battery bank resistance (at 80% SoC)	r_{bat}	28 mΩ
Battery bank OCV (at 80% SoC)	$u_{\text{bat OC}}$	78 V
SCs subsystem (Maxwell BMOD0165 P048 BXX module)		
Inductor inductance	L	0.2 mH
Inductor parasitic resistance	r_{L}	10.0 mΩ
SC series resistance	r_{SC}	6.3 mΩ
SC nominal voltage	$u_{\text{SC nom}}$	48 V
SC nominal capacitance	C_{SC}	165 F

Moreover, a real-world driving cycle was recorded through driving around the campus of University of Lille. It can be considered as a rural cycle.

The evaluation criterion is the batteries rms current; the lower the $i_{\text{bat rms}}$ is, the better the battery life-time is. It is because the rms current cause self-heating in batteries due to Joule losses in their internal resistance. Whereas the degradation of the batteries increases with the rise of temperature [Baghdadi 2016; Waldmann 2014]. Five cases are compared:

- conventional EV with batteries only;
- filtering strategy as a popular rule-based EMS;
- λ-control as an adaptive PMP-based real-time EMS;
- the proposed real-time near-optimal strategy;
- DP as an off-line optimal benchmark.

Considering a previous work with the same examined system [Castaings 2016a], this study uses the cut-off frequency $f_{\mathrm{LPF}} = 48$ mHz and the same λ-control parameters for adaptive PMP-based EMS. The parameters for DP problem solving is given in Table 2.2 which is implemented by using the available toolbox [Sundström 2009]. The simulations are carried out in MATLAB/Simulink™ with the EMR library [EMR 2019] shown in Figure 2.18.

Table 2.2: Parameters for DP problem solving of the battery/SC EV.

Parameters		**Range**	**Step**
State variable	u_{SC}	24 to 48 V	0.1 V
Control variable	$i_{\mathrm{bat\ ref}}$	−350 to 350 A	1 A
Time	t	0 to t_{f}	1 s
Initial state	$u_{\mathrm{SC\ init}}$	48 V	-
Final state constraint	$u_{\mathrm{SC\ final}}$	48 V	-

t_{f} is the length of the driving cycle under study

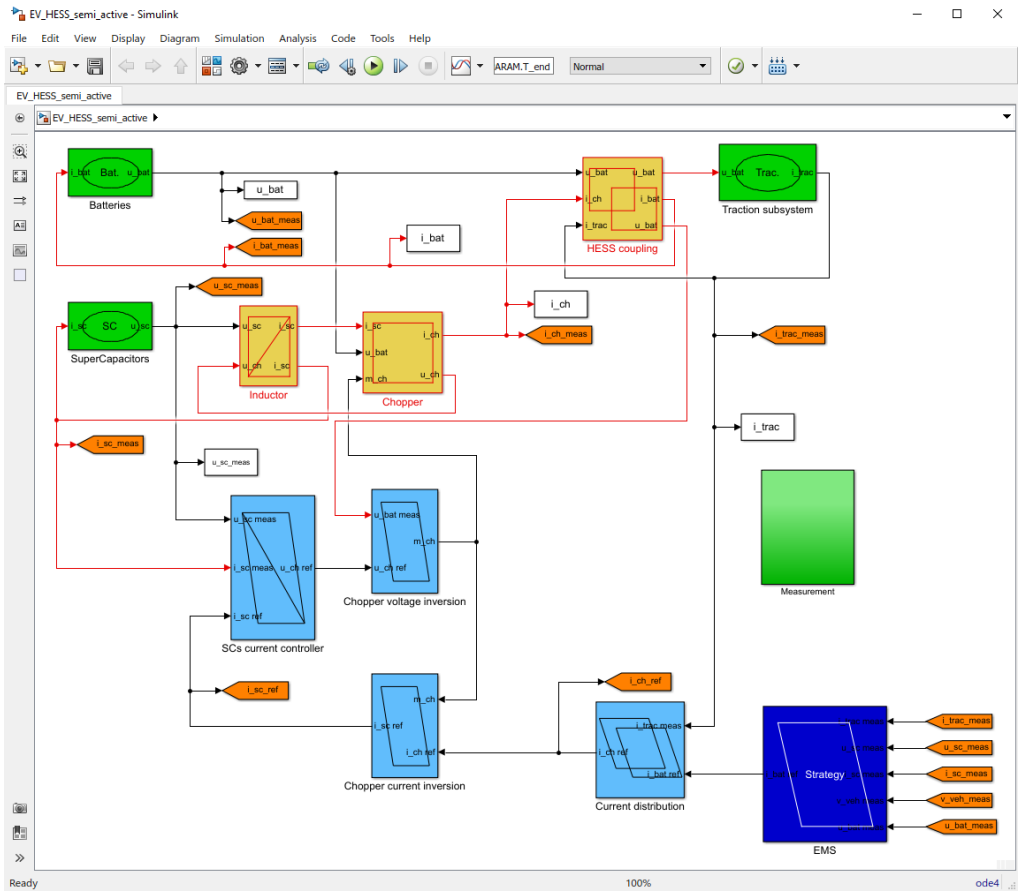

Figure 2.18: Simulation of the battery/SC EV in MATLAB/Simulink™ with the EMR library.

2.4.2. Results and discussions

The goal of the H-ESS is to minimize the batteries rms current which is stress index factor for batteries. By simulations, the different strategies for H-ESS power distribution are compared with the rms value of the batteries current during the full cycles. Figure 2.19 reports a comparative evaluation of the studied strategies with four driving cycles. The cycles can be classified by their velocity dynamics:

- NEDC which is the smoothest cycle;
- WLTC class 2 which is more fluctuated than NEDC in all parts;
- ARTEMIS urban which has more oscillations than WLTC class 2 in urban areas;
- The real-world cycle which is the highest fluctuated cycle recorded in a real driving.

Main results are presented and discussed in this subsection. Additional results are also provided in Appendix A.4, see Figure A.7–Figure A.9. Figure 2.19 shows a comparative evaluation of the four examined EMSs and the case of battery EV. The pure battery EV always leads to the highest battery rms current; meanwhile, the DP offers the lowest $i_{\mathrm{bat\,rms}}$ thanks to its optimal solution. These tests are used as a double benchmark for maximal (battery EV) and minimal (DP) batteries rms current.

The strategies used in combination with the defined H-ESS (see Table 2.1) has significant effectiveness with driving cycles having high-dynamics velocity profile (ARTEMIS urban and the tested real-world cycle). The proposed strategy can reduce up to 50% of the $i_{\mathrm{bat\,rms}}$ that means noteworthy life-time extension for this fluctuated real-world cycle. In the less oscillated cycles like NEDC and WLTC, the H-ESS is less effective. For the case of NEDC, even the ideal solution given by DP can reduce only 11.4% of the $i_{\mathrm{bat\,rms}}$; whereas it is 10% by using the proposed real-time strategy. It could therefore be seen that the battery/SC H-ESS is more suitable for city cars than for the other sorts of vehicles working with smoother driving conditions.

The most important is that the proposed strategy obtains the lowest batteries rms current in comparison to the other real-time strategies with all the tested driving cycles. By comparing to the optimal benchmark given by DP, the near-optimal performance of the new strategy can be verified.

Figure 2.20–Figure 2.22 show the detailed results of the five studied cases with the real-world driving cycle. The vehicle is controlled to follow the velocity reference (Figure 2.20). Figure 2.21 gives the SCs voltage evolutions of four examined strategies. Figure 2.22 presents the batteries current evolutions in the case of pure battery EV and the four strategies.

DP, serving as a benchmark, obtains a very smooth batteries current i_{bat} and guarantees charge sustaining of the SCs. The proposed strategy achieves the i_{bat} close to the one from DP with smooth variation and low peak values. Moreover, this EMS get the final value of u_{SC} equal to the initial value like the case of DP. Besides, it can be also seen that the evolution of the SCs voltage of the proposed strategy follows quite closely the one obtained by using DP. Even

though the proposed method is totally independent of DP. The strategy is therefore close-to-optimal not only in terms of batteries current, but also in terms of SCs voltage variation.

In λ-control, initially PMP also aims to satisfy the final state constraint of the SCs voltage. However, when it is adapted for unknown cycles, the constraint is not ensured to be satisfied. As a result, at the end of the cycle, the SCs voltage is not charged to the initial value. In [Castaings 2016a], the feedback control loop of the SCs voltage is developed to respect the voltage limitations rather than to ensure charge sustaining. Furthermore, the batteries current suffers from several peaks since the SCs often reach the lower boundary of their voltage.

In the case of filtering strategy, this method smoothens the oscillations of the i_{bat}, however, it is still more fluctuated than the other EMSs. Charge sustaining is also not achieved. (In fact, an additional rule-based recharging scheme is added, but it takes a period after the end of the driving cycle to recharge the SCs.)

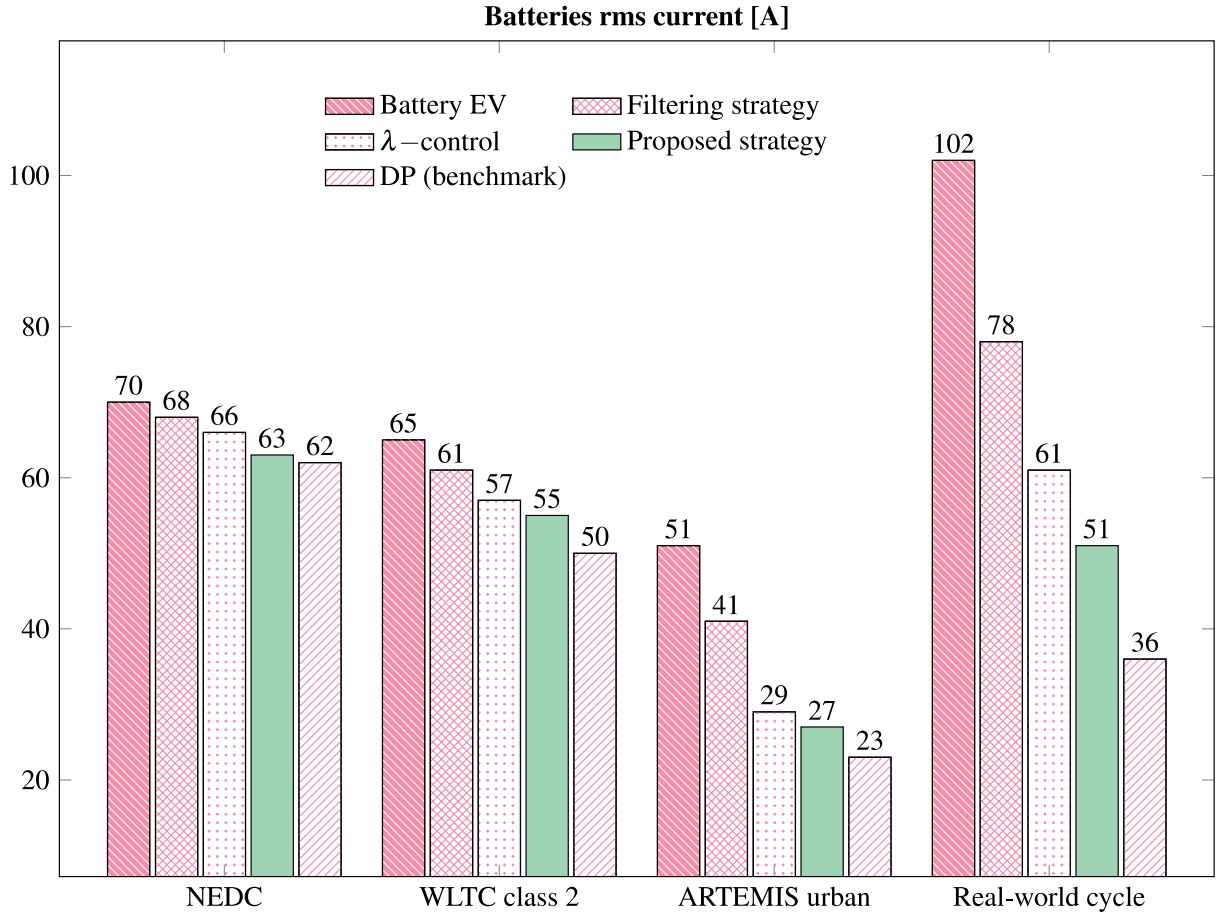

Figure 2.19: Comparative evaluation of the studied EMSs for battery/SC EV by simulations.

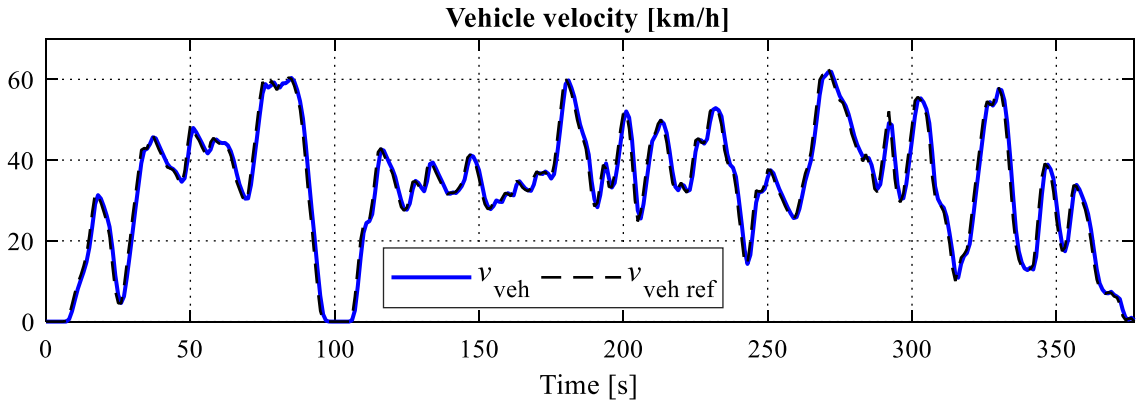

Figure 2.20: (Simulation results) the real-world driving cycle under study.

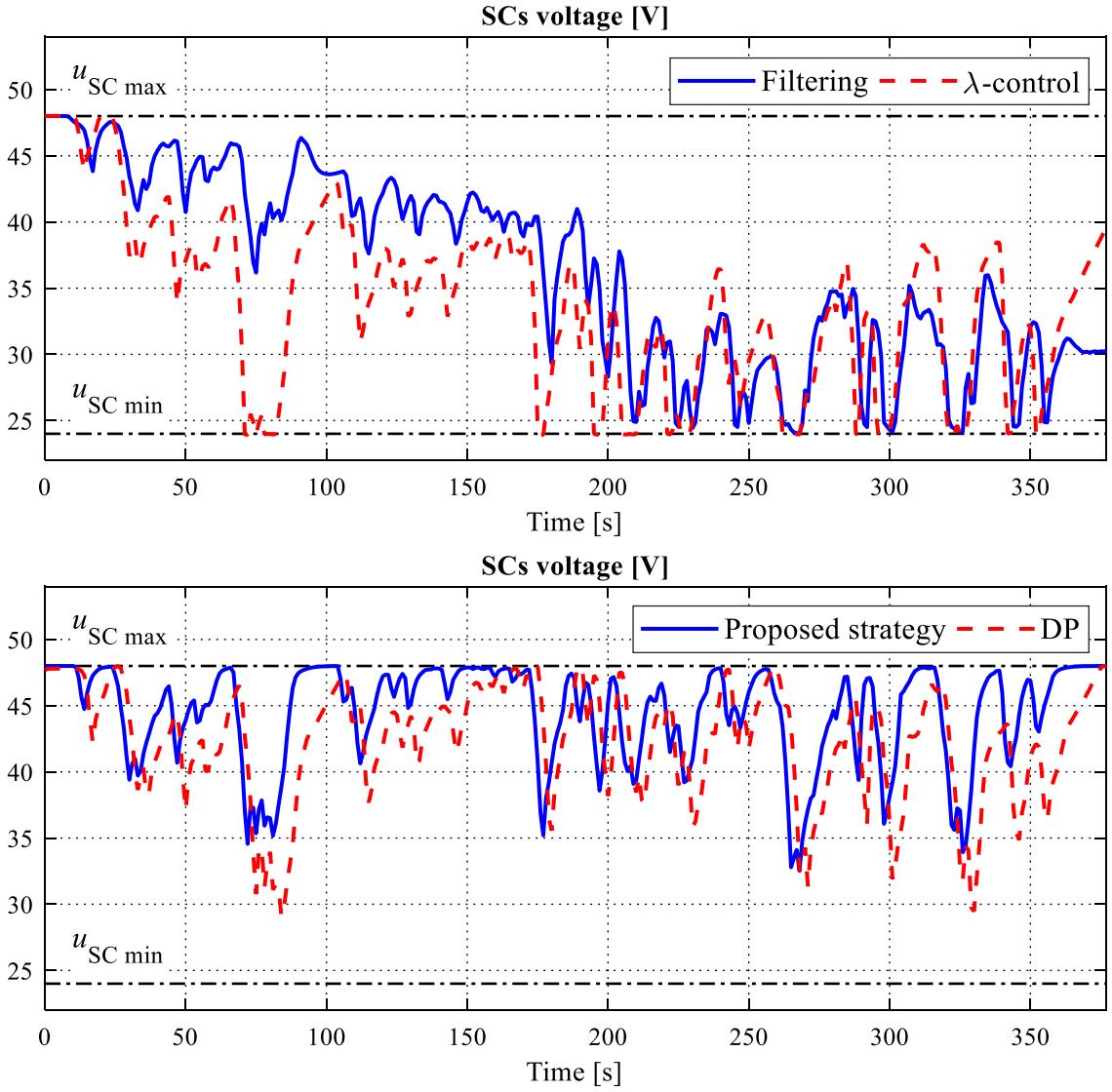

Figure 2.21: (Simulation results) SCs voltage evolutions with examined strategies.

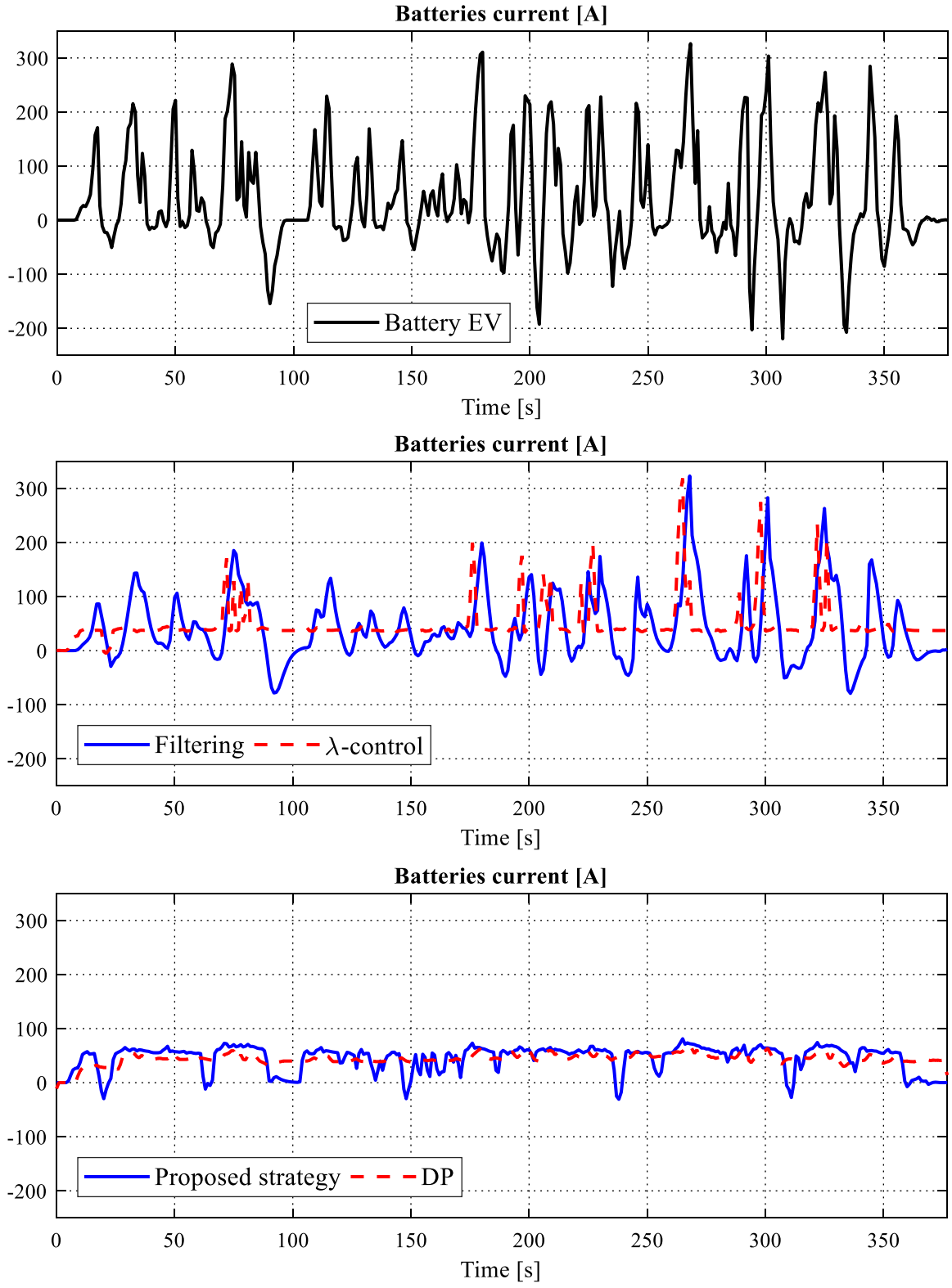

Figure 2.22: (Simulation results) batteries current evolutions with examined strategies.

2.5. Experiments and results

2.5.1. Experimental system

Experimental validations are carried out by using reduced-scale power hardware-in-the-loop (HIL) simulation [Bouscayrol 2011]. Figure 2.23 illustrates the principle of the reduced-scale power HIL simulation used in this work. The full-scale studied system can be considered as composed by three parts: the SCs subsystem, the batteries, and the traction subsystem. In order to validate EMSs by experiments, the system should be simulated by a reduced-scale power system available in the laboratory. Since the impact of SCs subsystem is under study, its topology is remained. This study focuses on the EMSs of the H-ESS; the traction subsystem therefore plays the role of generating the traction current which is the disturbance of the studied system. Thus, the traction subsystem, including the vehicle dynamics, can be emulated by using a controllable current source. Similarly, a controllable voltage source is used to emulate the batteries since batteries are not under study and their behaviors are assumed to be known perfectly. Moreover, it is to ensure that the studied SCs subsystem and the EMS is tested in the same conditions for each driving cycle.

The HIL simulation is realized by using the experimental setup illustrated in Figure 2.24. Main parameters of the components are given in Table 2.3. The experimental setup in the laboratory is shown in Figure 2.25. The software control panel is implemented in dSPACE ControlDesk as shown in Figure 2.26.

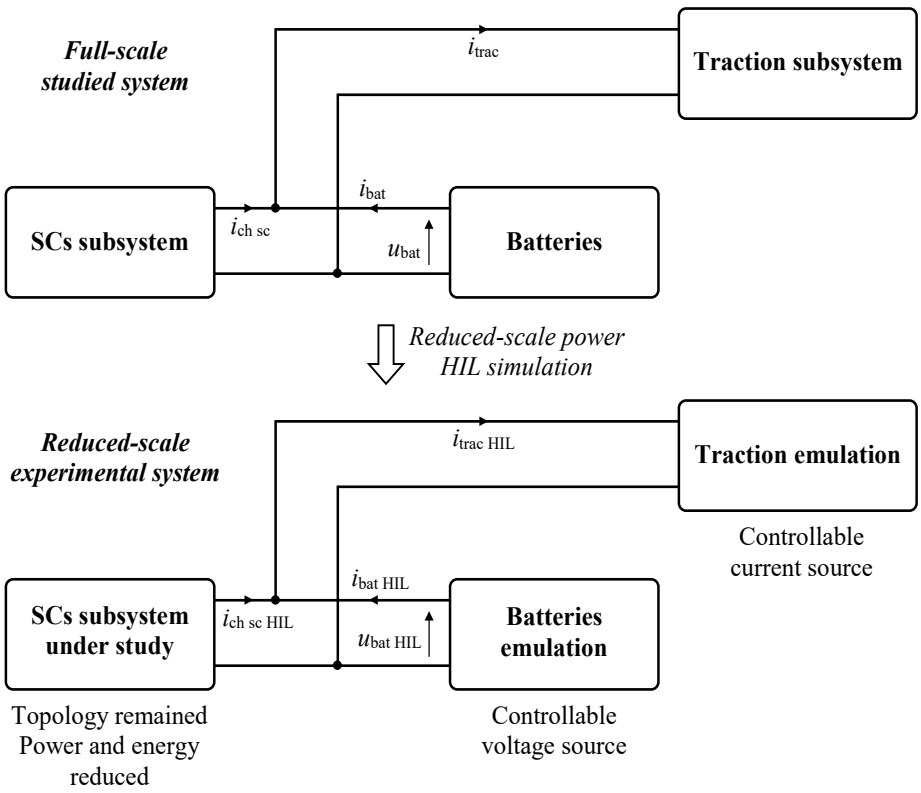

Figure 2.23: Principle of reduced-scale power HIL simulation for the battery/SC EV.

The controllable current source to emulate the traction subsystem is composed by a SCs pack, an inductor, and a chopper. The SCs consume the traction power by being charged during the experiments. The emulator is controlled by a current controller to follow the reference generated by the traction model. The full-scale traction model, including the vehicle inertia, generates the traction current reference. Via the power adaptation block, this reference is imposed to the current controller. If the current of the emulator follows the reference generated by the traction model, the emulator can emulate well the traction dynamics, as will be verified in Subsection 2.5.2.

The controllable voltage source to emulate the batteries is composed by a SCs pack, an inductor, a chopper, and a DC bus capacitor. The voltage of the emulator is controlled to follow the voltage reference generated by the batteries model via a power adaptation block.

Voltage and currents controllers are realized by using the classical PI controllers. The models and the controllers are implemented in the controller board (dSPACE DS1103). The SCs are used to emulate the batteries and the traction subsystems thanks to their fast dynamics. It is noteworthy that the dynamics of the components used for emulation should be faster than that of the emulated system.

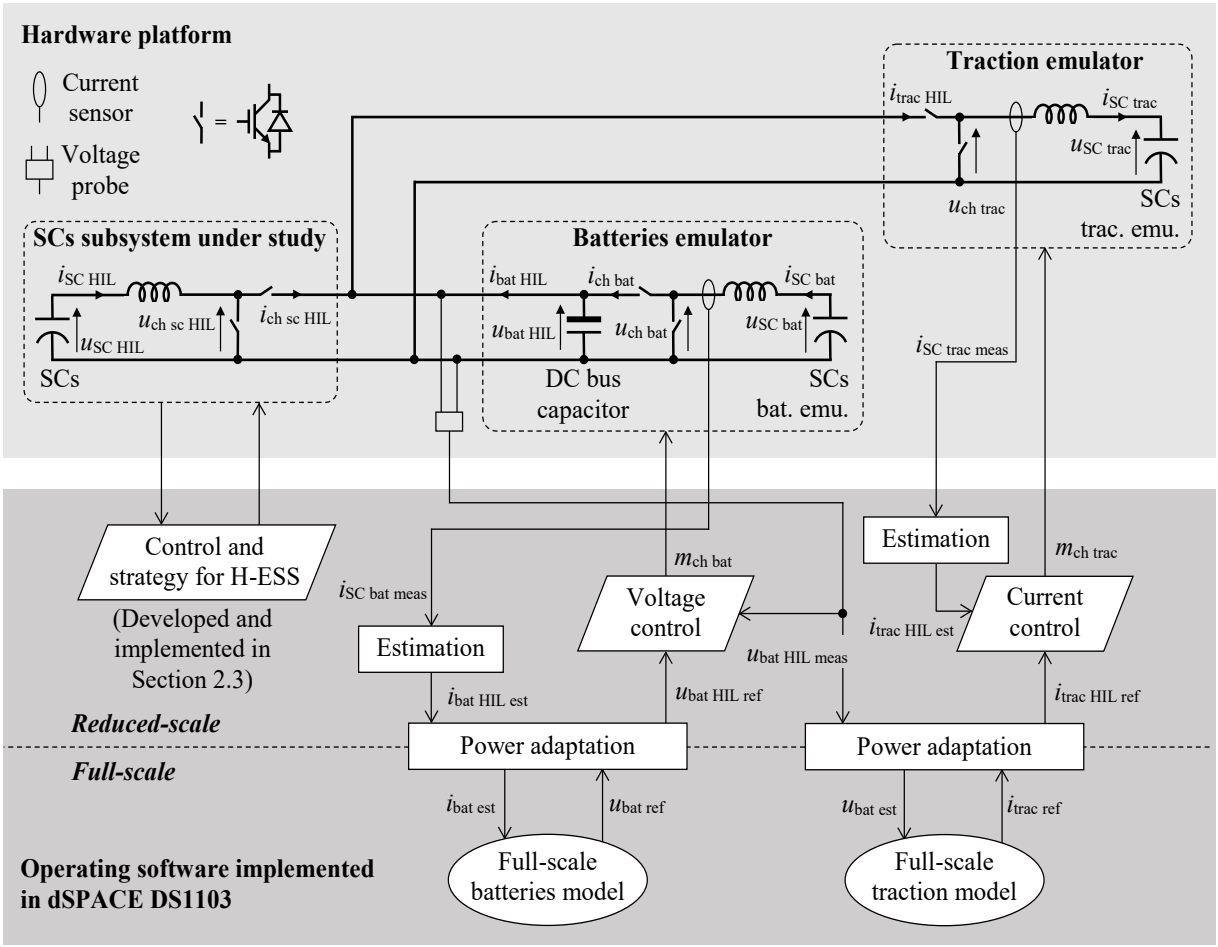

Figure 2.24: Experimental system configuration for the battery/SC EV.

Table 2.3: Reduced-scale power HIL system parameters for the battery/SC EV.

Parameters		Values
Adaptation ratio		35
SCs for batteries and traction emulators		
SCs capacitance	$C_{\text{SC bat/trac}}$	130 F
SCs nominal voltage	$u_{\text{SC bat/trac nom}}$	54 V
SCs subsystem		
SCs capacitance	C_{SC}	14.5 F
SCs nominal voltage	$u_{\text{SC nom}}$	60 V
SCs internal resistance	r_{SC}	73.0 mΩ
Inductor		
Inductor inductance	L	0.751 mH
Inductor parasitic resistance	r_{L}	0.18 Ω
Inductor of the batteries emulator		
Inductor inductance	$L_{\text{bat emu}}$	0.758 mH
Inductor parasitic resistance	$r_{\text{L bat emu}}$	0.20 Ω
Inductor of the traction emulator		
Inductor inductance	$L_{\text{trac emu}}$	0.752 mH
Inductor parasitic resistance	$r_{\text{L trac emu}}$	0.20 Ω
DC bus capacitor of the batteries emulator		
Capacitor capacitance	$C_{\text{bat emu}}$	2200 µF

The power HIL simulation is a complex system. EMR is therefore used for modeling and control of the system as given in Figure 2.27. The SCs packs, the inductors, the choppers, and the DC bus capacitor are represented by using the corresponding EMR pictograms. The control scheme of the HIL system is conducted by inversions of EMR elements. The DC bus capacitor is an accumulation element of which the output is a voltage; its inversion is therefore a closed-loop voltage control. The other of the control scheme is similar to the control of the SCs subsystem presented in Subsection 2.1.3.

The full-scale models of the batteries and the traction subsystem are depicted by the model/estimation elements (purple ovals). The full-scale models interact with the reduced-scale system via power adaptation blocks. In practice, i.e., practical control scheme, the currents $i_{\text{bat HIL}}$ and $i_{\text{trac HIL}}$ cannot be directly measured because they are choppers currents (which are pulses, and there is no sensor installed). These currents are therefore estimated by using the corresponding measured SC currents $i_{\text{SC bat}}$ and $i_{\text{SC trac}}$. That is obtained by the estimation blocks

(purple squares) which are model-copy of the chopper. The voltages and the currents of all the SC banks and the emulated batteries voltage (on the capacitor $C_{\text{bat emu}}$) are measured by voltage probes and current sensors.

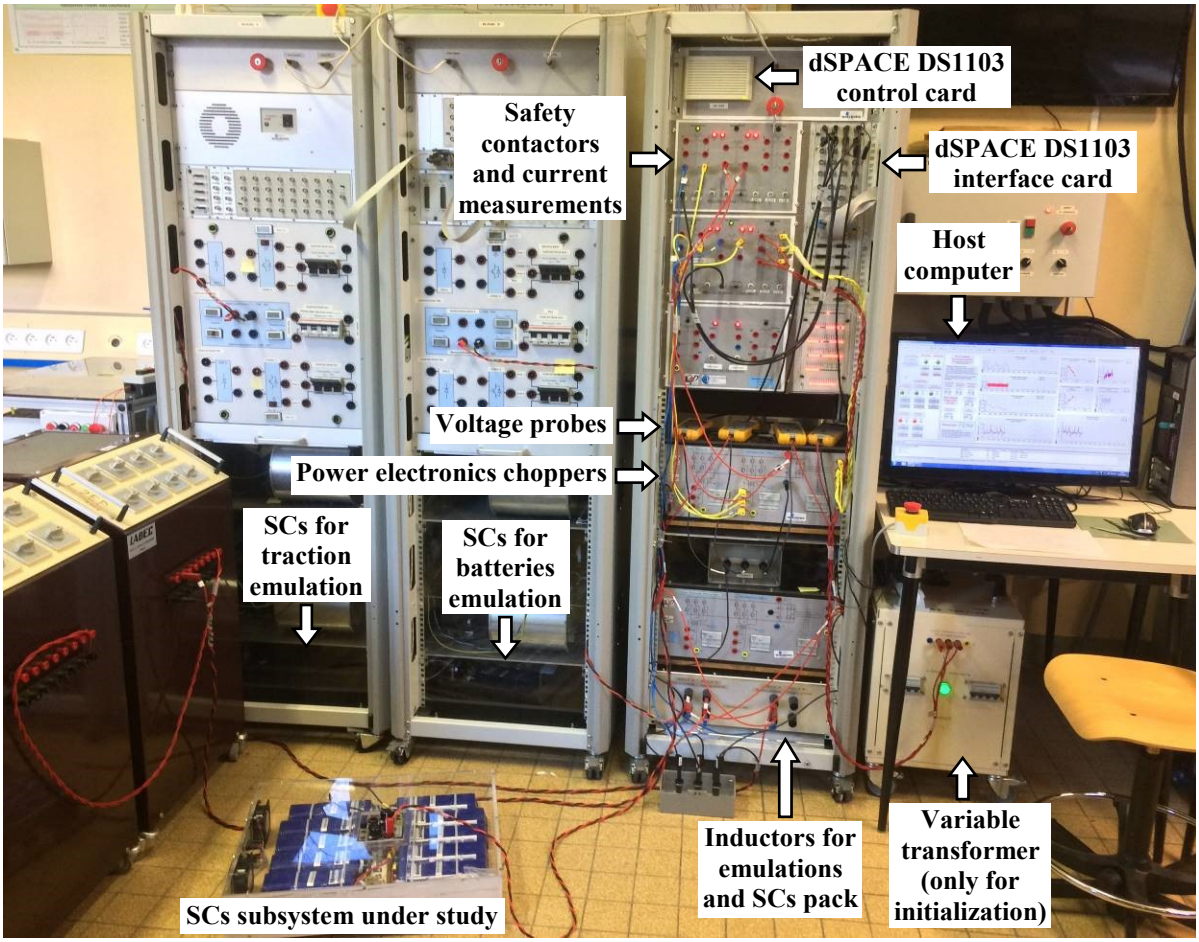

Figure 2.25: Experimental test bench for the battery/SC EV.

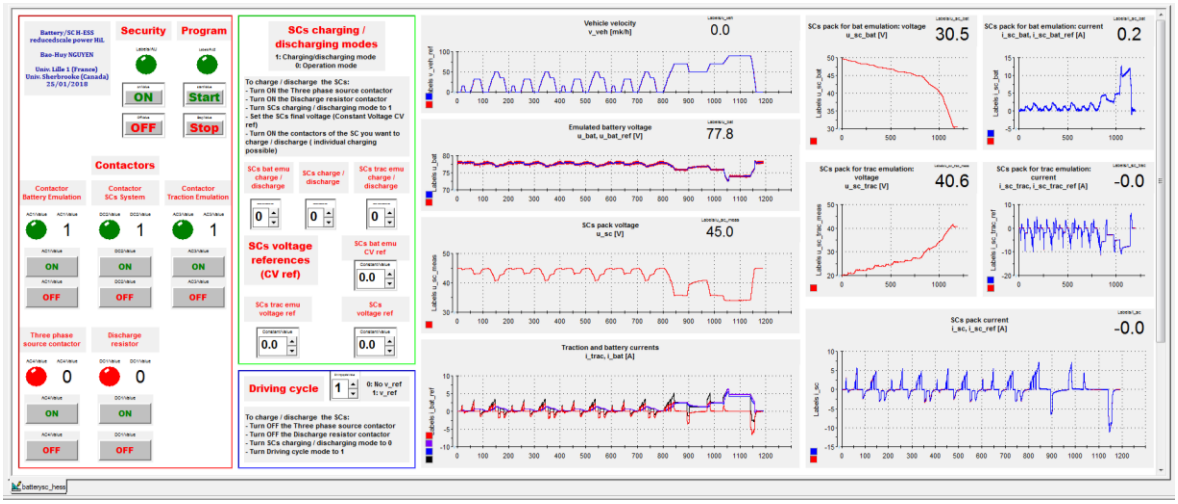

Figure 2.26: Control panel of the experimental system in dSPACE ControlDesk.

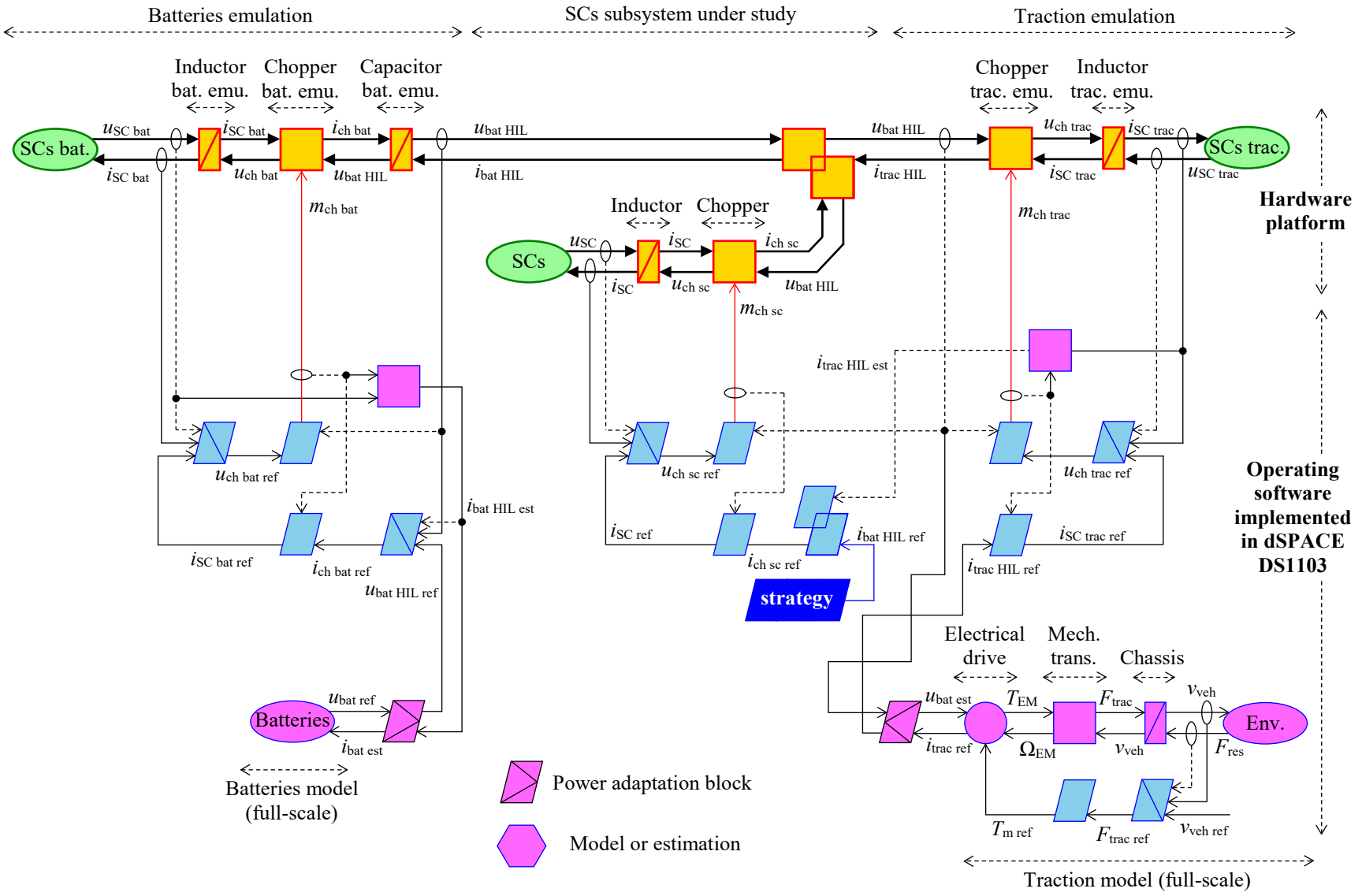

Figure 2.27: EMR of the reduced-scale power HIL experimental system for the battery/SC EV.

2.5.2. Results and discussions

The main results are presented and discussed in this subsection. Additional results are given in Appendix A.4, see Figure A.7–Figure A.9.

The real-time simulation (in dSPACE card) of the vehicle velocity control is presented in Figure 2.28. The simulation and experimental emulated batteries voltages $u_{\text{bat simu}}$ and $u_{\text{bat HIL}}$ are respectively plotted in Figure 2.29. This figure also provides the SCs voltages evolutions in full-scale simulation $u_{\text{SC simu}}$ and in reduced-scale HIL experiment $u_{\text{SC HIL}}$. Finally, traction and batteries currents, in both simulation and experiment, are given (Figure 2.30).

The first objective of experiment is to demonstrate the real-time implementation ability of the proposed EMS. It can be seen that the developed strategy operates successfully in the real-time platform for the real-world driving cycle (and all the other cycles, see Appendix A.4). Moreover, experimental results can validate if the simulations examine well the system performances. For that purpose, simulation and experimental results should be plotted in the same figure respecting the reduction ratios as being explained in the follows.

The power and the energy of the studied system are scaled down by a reduction ratio for power HIL implementation [Allègre 2010b]. The adaptation ratio is determined regarding the power and energy limitation of the available power components. It must ensure that the SCs used for traction emulation can absorb all the energy delivered by the SCs for the batteries emulation. The required energy storage capabilities are calculated with the WLTC class 2, which is the longest driving cycle under study. Regarding that, the adaptation ratio is set to 35 (see Table 2.3).

The emulated batteries voltage is equal to that voltage of the full-scale system (they can be plotted in the same axis). Thus, the currents i_{trac} and i_{bat}, (and $i_{\text{ch sc}}$) are scaled down exactly by the power ratio (see the scale between the two y-axes of the plot of the batteries and the tractions currents, Figure 2.30). It is noteworthy that the batteries emulator emulates not only the nominal batteries voltage (78 V) but also the fluctuations caused by the batteries current (see Figure 2.29). That confirms the reduced-scale power HIL simulation can emulate properly the behaviors of the studied full-scale system.

It is more complicated for scaling the SCs voltage. The SCs energy must be scaled down by the same reduction ratio as that of the power. The simplest way is to reduce the SCs capacitance by that ratio. The SCs voltage range can be therefore remained as in the full-scale system. Unfortunately, the SCs pack available in the laboratory has higher capacitance than it should do. Thus, the SCs voltage range must be reduced. The upper boundary $u_{\text{SC max}}$ are set the same for both full-scale simulations and reduced-scale experiments. Yet the lower boundary $u_{\text{SC min}}$ of the reduced-scale system is higher than that of the full-scale system. (See the two y-axes of the plot of the SCs voltage, Figure 2.29.)

The well-matched results between simulation and experiment verify the advantages of the proposed real-time EMS and accuracy of the examination method.

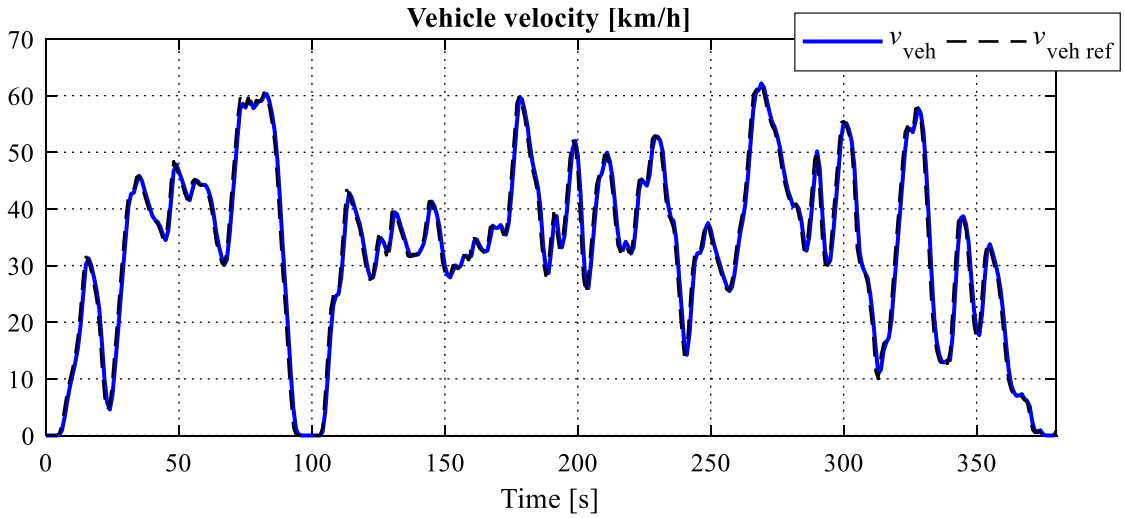

Figure 2.28: (Experimental results) vehicle velocity obtained by real-time simulation in dSPACE DS1103 card.

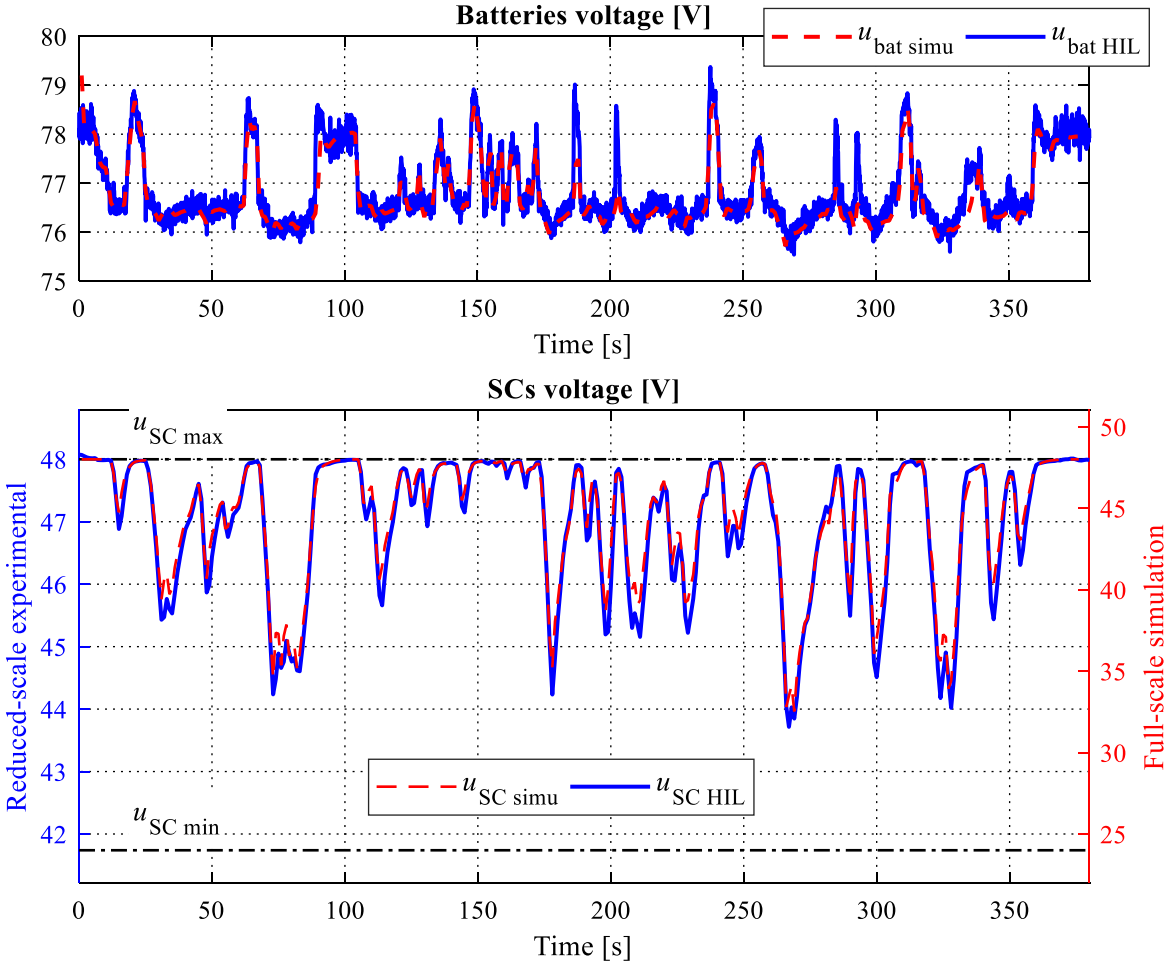

Figure 2.29: (Experimental results) batteries and SCs voltages with the proposed strategy.

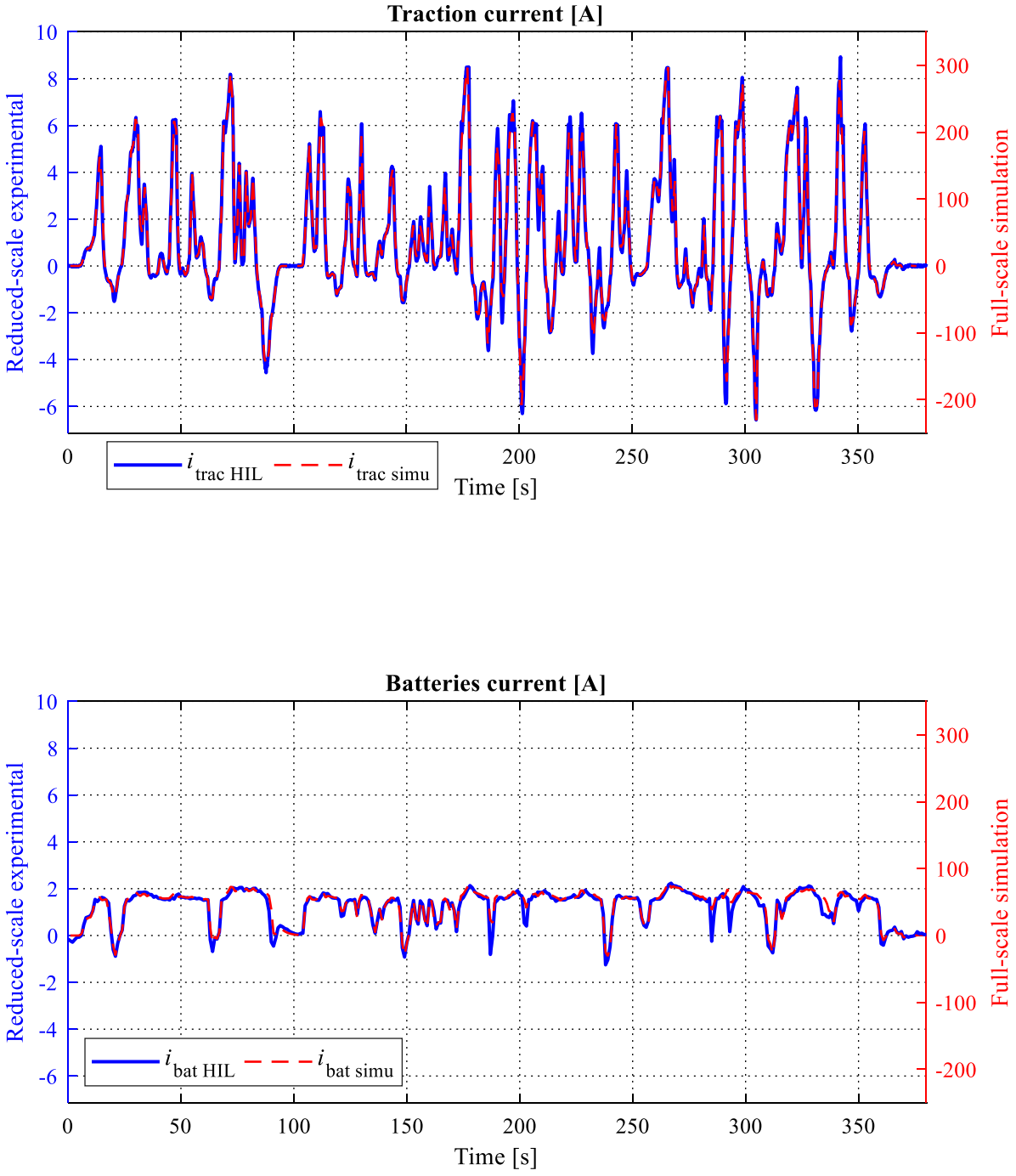

Figure 2.30: (Experimental results) traction and batteries currents with the proposed strategy.

2.6. Conclusion

This chapter has proposed and validated a new approach of using PMP to develop a real-time EMS for battery/SC H-ESSs in EVs. The near-optimal strategy has been obtained with the following process:

- Modeling and control of the full dynamical system.
- Model reduction and transformation steps for reduced mathematical model deduction. In fact, most of previous works have to deduce a reduced mathematical model. The authors have done this step by using various ways in literature. In this study, the reduction, transformation, and mathematical deduction follow the rules of EMR. That helps to deduce a simple model respecting physical meaning.
- Applying analytical optimal control theory to the obtained reduced mathematical model to deduce the strategy.

The first two steps are based on EMR. Meanwhile modeling and control are classical, the step of model reduction and transformation contributes to the advantages of the proposed method. In which, the reduced mathematical model allows the simplification of strategies development. That benefits to overcome the issue of complexity of optimization-based methods.

At the step of optimal control applying, the traditional methodology is to get the off-line optimal solution by fully using PMP, then to add an extra adaptive mechanism. This chapter has proposed an alternative approach. By only applying the Hamiltonian minimization condition of PMP, an analytical closed-form solution containing the state variable can be deduced. Thus, no additional adaptation of the co-state variable is required for real-time applications.

This novel strategy has been compared to the conventional EMSs including filtering, λ-control, and DP. The filtering and λ-control strategies are inherited from the previous works of the research group due to the common studied system for fair comparison. DP for the studied system has been developed and implemented using the EMR-based backward model representation and an available toolbox.

Simulation results have figured out that the proposed EMS gives the highest benefit in term of batteries rms current reduction (up to 50% on a real-world driving cycle compared to the battery EV). By comparing to the off-line optimal benchmark given by DP, the proposed EMS has been verified to be close-to-optimal. Furthermore, the real-time performances of the proposed strategy have been demonstrated by reduced-scale power HIL experiments organized by using EMR.

3. Real-time optimization-based energy management strategy for a battery/supercapacitor parallel hybrid truck

This chapter aims to develop a real-time optimization-based energy management strategy for a parallel hybrid truck with the electrical drive supplied by batteries and supercapacitors. Energetic macroscopic representation will be used for modeling and control of the system. Thereafter, this full dynamical model will be reduced to achieve the reduced mathematical model for energy management strategy development. A torque distribution strategy will be developed for energy management of the hybrid traction subsystem. The hybrid energy storage system will be handled by the strategy developed in Chapter 2. Since the obtained model of the studied hybrid traction subsystem is linear, linear quadratic regulator method will be used to develop a real-time optimization-based strategy. An off-line optimal benchmark based on dynamic programming will be used to evaluate the real-time strategy. Simulations and reduced-scale hardware-in-the-loop experiments will confirm the performances of the proposed method.

3.1. Model for energy management strategy

3.1.1. Studied system

The studied system is a parallel hybrid truck supplied by a semi-active H-ESS combining batteries and SCs (Figure 3.1). The chassis, with the wheels and the brake, is driven through a 6-level gearbox. The gearbox is connected with the ICE and the EM via a torque converter which can be considered working as a clutch. The torque converter is driven by a shaft connected with the ICE. The EM, supplied by an inverter, is coupled with the engine via a belt. The electrical drive is supplied by DC power from a semi-active H-ESS which is already studied in Chapter 2 (see Subsection 2.1.1).

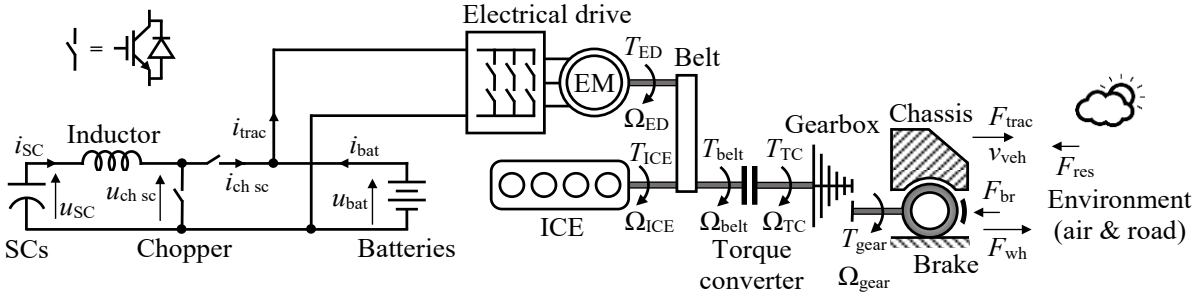

Figure 3.1: Studied system: a parallel hybrid truck supplied by a battery/SC H-ESS.

3.1.2. Modeling and energetic macroscopic representation of the studied system

The studied battery/SC parallel hybrid truck is mathematically modeled and graphically represented by using EMR (Figure 3.2).

Battery/supercapacitor hybrid energy storage system

The H-ESS has been studied in Chapter 2. Modeling, control, and energy management of this subsystem are conserved (see Subsection 2.1.2 for modeling and EMR). The H-ESS imposes the battery voltage u_{bat} to the electrical drive of the hybrid traction subsystem; the drive reacts by imposing the traction current i_{trac} to the H-ESS.

Electrical drive

The electrical drive consists of a permanent magnet synchronous machine and a three-phase inverter. By assuming that the drive is correctly controlled, it can be addressed by using a static model as follows:

$$\begin{cases} T_{\mathrm{ED}} = T_{\mathrm{ED\,ref}} \\ i_{\mathrm{trac}} = \dfrac{T_{\mathrm{ED}}\Omega_{\mathrm{ED}}}{u_{\mathrm{bat}}\eta_{\mathrm{ED}}^{k_{\mathrm{ED}}}} \end{cases} \text{ with } k_{\mathrm{ED}} = \begin{cases} 1 \text{ if } T_{\mathrm{ED}}\Omega_{\mathrm{ED}} \geq 0 \\ -1 \text{ if } T_{\mathrm{ED}}\Omega_{\mathrm{ED}} < 0 \end{cases} \tag{3.1}$$

where T_{ED} is the electrical drive torque; $T_{\mathrm{ED\,ref}}$ the reference torque; Ω_{ED} the rotational speed; and η_{ED} the efficiency of the drive. The factor k_{ED} depends on the power flow direction. The drive is represented by a multi-physical conversion element (circle).

Internal combustion engine

In this study, the ICE is examined by using a static model as a mechanical source of torque (oval). In which, the engine torque T_{ICE} is considered to perfectly follow the torque reference $T_{\mathrm{ICE\,ref}}$. The engine imposes its torque while the system reacts the rotational speed Ω_{ICE} to the engine. The inertia of the engine shaft is assumed to be reported with the mass of the vehicle.

Besides, the fuel consumption of the ICE is computed by using a map of consumption rate $\dot{m}_{\mathrm{fuel}}$ which is a function of the engine torque and speed. The static model of the ICE is given as follows:

$$\begin{cases} T_{\mathrm{ICE}} = T_{\mathrm{ICE\,ref}} \\ m_{\mathrm{fuel}} = \displaystyle\int_{t_0}^{t} \dot{m}_{\mathrm{fuel}}(T_{\mathrm{ICE}}, \Omega_{\mathrm{ICE}})dt \end{cases}; \tag{3.2}$$

in which $\dot{m}_{\mathrm{fuel}}(T_{\mathrm{ICE}}, \Omega_{\mathrm{ICE}})$ is given by a look-up table.

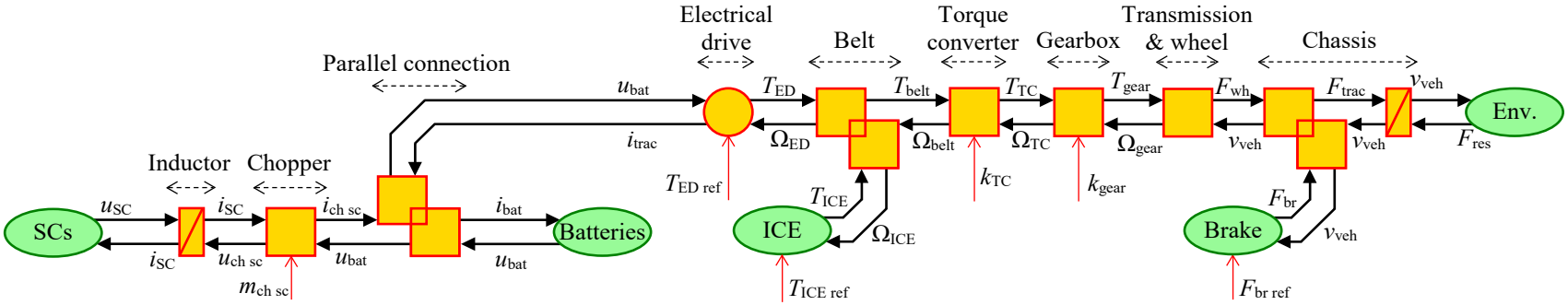

Figure 3.2: EMR of the studied battery/SC parallel hybrid truck.

Belt

The ICE directly drives the vehicle via its shaft; whereas the electrical drive is coupled via a belt (see Figure 3.1). The belt is represented by a coupling element (overlapped squares) with the following model:

$$\begin{cases} T_{\text{belt}} = T_{\text{ICE}} + T_{\text{ED}} k_{\text{belt}} \eta_{\text{belt}}^{k_{\eta\,\text{belt}}} \\ \Omega_{\text{ICE}} = \Omega_{\text{belt}} \\ \Omega_{\text{ED}} = \Omega_{\text{belt}} k_{\text{belt}} \end{cases} \quad \text{with} \quad k_{\eta\,\text{belt}} = \begin{cases} 1 \text{ if } T_{\text{ED}}\Omega_{\text{ED}} \geq 0 \\ -1 \text{ if } T_{\text{ED}}\Omega_{\text{ED}} < 0 \end{cases} \tag{3.3}$$

where T_{belt} is the belt torque; Ω_{belt} the belt speed; k_{belt} the fixed belt ratio; η_{belt} the belt efficiency; $k_{\eta\text{belt}}$ the efficiency factor depending on the power direction.

Torque converter

The torque converter engages the engine shaft to the gearbox. The full dynamical model of the torque converter can be complicated. However, its dynamical behaviors matter only during the gear transmissions [Lhomme 2008]. In this study, a simple model of the torque converter, depicted by a mono-physical conversion element (square), is adopted as:

$$\begin{cases} T_{\text{TC}} = T_{\text{belt}} k_{\text{TC}} \eta_{\text{TC}}^{k_{\eta\,\text{TC}}} \\ \Omega_{\text{belt}} = \Omega_{\text{TC}} k_{\text{TC}} \end{cases} \text{with} \quad k_{\eta\,\text{TC}} = \begin{cases} 1 \text{ if } T_{\text{belt}}\Omega_{\text{belt}} \geq 0 \\ -1 \text{ if } T_{\text{belt}}\Omega_{\text{belt}} < 0 \end{cases}; \tag{3.4}$$

in which T_{TC} is the torque of the torque converter; Ω_{TC} the torque converter rotational speed; k_{TC} the controlled engagement ratio; η_{TC} the torque converter efficiency; and the coefficient $k_{\eta\,\text{TC}}$ depends on the power direction.

Gearbox

The traditional discrete gearbox is employed with the model as follows:

$$\begin{cases} T_{\text{gear}} = T_{\text{TC}} k_{\text{gear}} \eta_{\text{gear}}^{k_{\eta\,\text{gear}}} \\ \Omega_{\text{TC}} = \Omega_{\text{gear}} k_{\text{gear}} \end{cases} \text{with} \quad k_{\eta\,\text{gear}} = \begin{cases} 1 \text{ if } T_{\text{TC}}\Omega_{\text{TC}} \geq 0 \\ -1 \text{ if } T_{\text{TC}}\Omega_{\text{TC}} < 0 \end{cases} \tag{3.5}$$

where T_{gear} is the gearbox torque; Ω_{gear} the gearbox speed; k_{gear} the controlled gearbox ratio; η_{gear} the gearbox efficiency; and the coefficient $k_{\eta\,\text{gear}}$ is a function of the power direction. The gearbox is assumed to be shifted immediately (no shifting delay). It is represented by a mono-physical conversion element (square).

Mechanical transmission and wheels

The mechanical transmission and the wheels are considered as a mechanical transmission with the model:

$$\begin{cases} F_{\text{wh}} = T_{\text{gear}} k_{\text{tran}} \eta_{\text{tran}}^{k_{\eta\,\text{tran}}} \\ \Omega_{\text{gear}} = v_{\text{veh}} k_{\text{tran}} \end{cases} \text{with } k_{\eta\,\text{tran}} = \begin{cases} 1 \text{ if } T_{\text{gear}}\Omega_{\text{gear}} \geq 0 \\ -1 \text{ if } T_{\text{gear}}\Omega_{\text{gear}} < 0 \end{cases}; \tag{3.6}$$

in which F_{wh} is the force of the wheels; v_{veh} the vehicle velocity; k_{tran} the fixed transmission ratio combining the final drive ratio and the wheels radius; η_{tran} the transmission efficiency; and $k_{\eta\,\text{tran}}$ the factor depending on the power direction. They are represented by a mono-physical conversion element (square).

Brake

The mechanical brake imposes the braking force F_{br} to the wheel of the vehicle by following the reference $F_{\text{br ref}}$ as:

$$F_{\text{br}} = F_{\text{br ref}} \tag{3.7}$$

with $F_{\text{br ref}} \leq 0$. Here it is assumed that there is no dynamical delay between the reference and the response of the braking force. The brake is depicted by a source element (oval) which receives the reaction v_{veh} from the system.

Chassis and environment

The force of the wheel F_{wh} and the braking force F_{br} are coupled during the braking mode of the vehicle as follows:

$$\begin{cases} F_{\text{trac}} = F_{\text{wh}} + F_{\text{br}} \\ v_{\text{veh}} \text{ common} \end{cases} \text{with } F_{\text{br}} \leq 0 \tag{3.8}$$

where F_{trac} is the traction force.

The chassis dynamics are the total equivalent mass of the vehicle (including goods, driver, and the equivalent rotational masses of the ICE and the electrical drive). The environment, including air and road, imposes the resistive force F_{res} to the system. Their model has been already addressed in Chapter 2 (see Subsection 2.1.2) as well as their EMR.

3.1.3. Local control of the studied system

Based on the EMR of the studied system (see Figure 3.2), there are two objective variables to be controlled which are the vehicle velocity v_{veh} and the batteries current i_{bat}. There are two independent tuning paths, and therefore two control paths, to control them (Figure 3.3). Since the control of the H-ESS has been already developed in Chapter 2 (see Subsection 2.1.3), this subsection mainly discusses the development of the local control scheme for the hybrid traction subsystem.

a. Tuning paths and control paths

There are five tuning variables to control the objective variable v_{veh}; which are $T_{\text{ED ref}}$, $T_{\text{ICE ref}}$, k_{TC}, k_{gear}, and $F_{\text{br ref}}$. The reference torques $T_{\text{ED ref}}$ and $T_{\text{ICE ref}}$ enforce the corresponding torques T_{ED} and T_{ICE} which are coupled to conduct the belt torque T_{belt}. This torque is then converted to the T_{TC} via the torque converter governed by the k_{TC}. Thereafter, shifting the gearbox by turning the k_{gear} produce the torque T_{gear}. The gearbox torque is then transformed to the force F_{wh} via the final drive and the wheel. Whereas the braking force reference $F_{\text{br ref}}$ imposes the F_{br} during the braking mode. The braking force, in this mode, is then coupled with the force produced in the wheel F_{wh} to produce the traction force F_{trac} which controls the vehicle velocity v_{veh}.

The control paths are then deduced from the tuning paths by inverting them via the "mirror effect" (Figure 3.3). For the traction subsystem, the control path is the route from the vehicle velocity reference $v_{\text{veh ref}}$ to the drive and the engine torques references $T_{\text{ED ref}}$ and $T_{\text{ICE ref}}$.

b. Local control scheme of the studied system

The local control scheme is built based on the control paths as shown in Figure 3.4. The closed-loop velocity control, as an indirect inversion of the chassis, is the same as the one presented in Subsection 2.1.3 (see Figure 2.8 and (2.11)).

The braking coupling is directly inverted (overlapped parallelogram) as follows:

$$\begin{cases} F_{\text{wh ref}} = F_{\text{trac ref}} k_{\text{br}} \\ F_{\text{br ref}} = F_{\text{trac ref}} (1 - k_{\text{br}}) \end{cases} \tag{3.9}$$

where k_{br} is the braking ratio computed from a braking strategy. In which $k_{\text{br}} = 1$ means fully electrical, i.e., regenerative, braking while $k_{\text{br}} = 0$ means fully mechanical braking. In fact, with this studied parallel hybrid truck, the electrical drive power is not enough to perform fully electrical braking.

The gearbox torque reference $T_{\text{gear ref}}$ is deduced by directly inverting the final drive and wheel (parallelogram) as:

$$T_{\text{gear ref}} = \frac{F_{\text{wh ref}}}{k_{\text{tran}}}. \tag{3.10}$$

The gearbox is then inverted (parallelogram) by:

$$T_{\text{TC ref}} = \frac{T_{\text{gear ref}}}{k_{\text{gear}}} \tag{3.11}$$

where k_{gear} is the disturbance denoted by the dashed arrow. The ratio k_{gear} is imposed by a gearshift strategy.

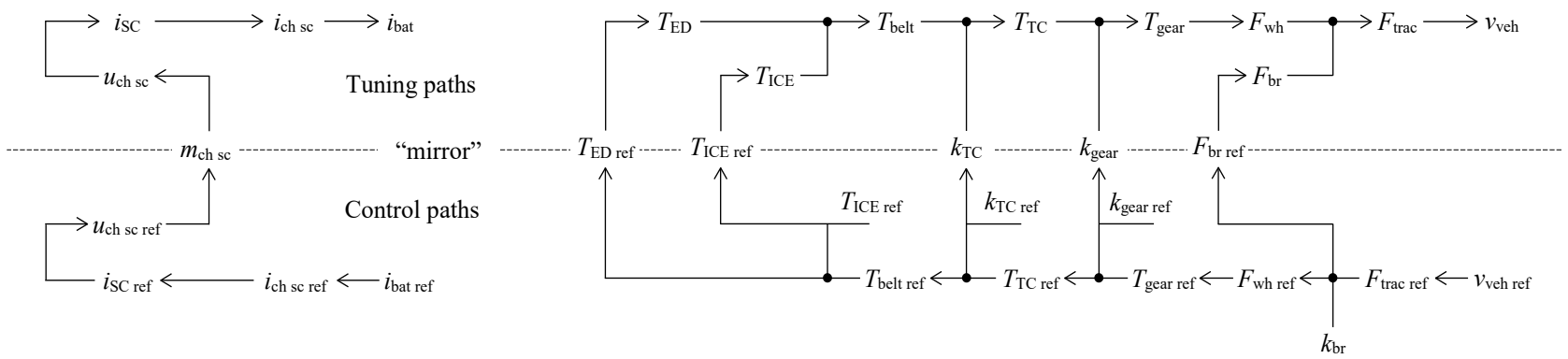

Figure 3.3: Tuning paths and control paths for local control of the studied battery/SC parallel hybrid truck.

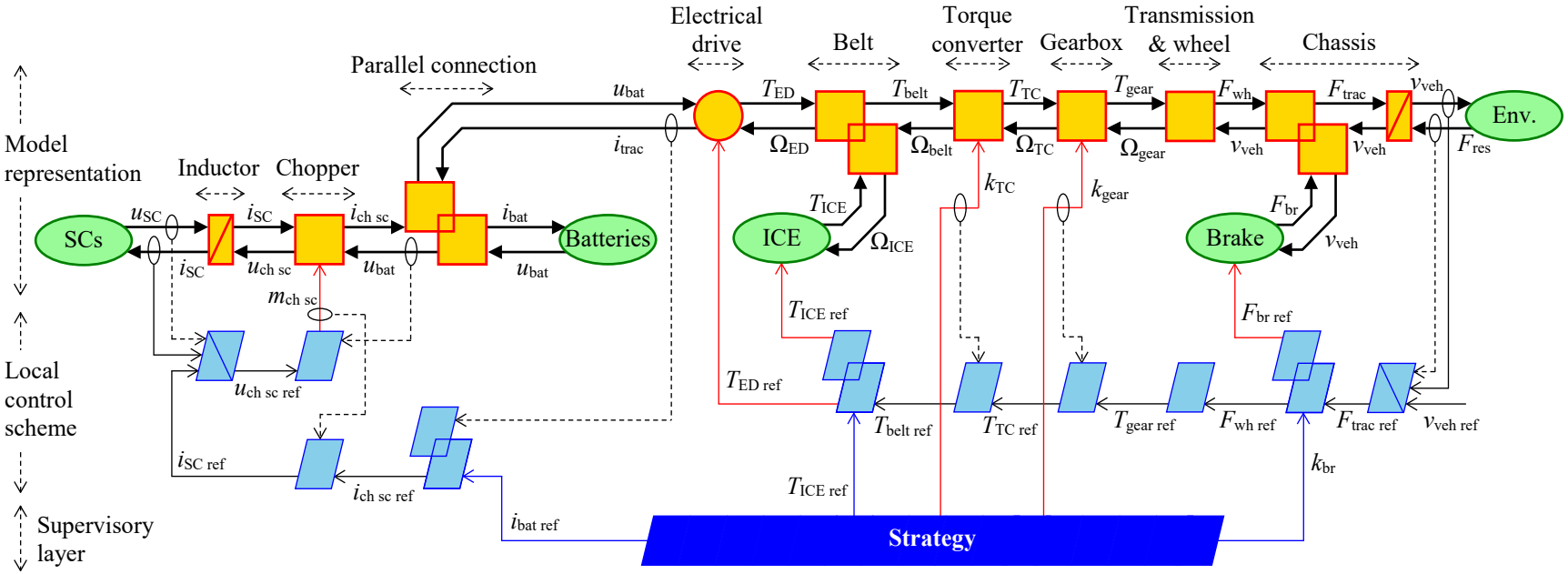

Figure 3.4: EMR and inversion-based control of the studied battery/SC parallel hybrid truck.

Similarly, the k_{TC} plays the role of a disturbance for computing the belt torque reference $T_{\mathrm{belt\ ref}}$ by inverting the torque converter as follows:

$$T_{\mathrm{belt\ ref}} = \frac{T_{\mathrm{TC\ ref}}}{k_{\mathrm{TC}}}. \tag{3.12}$$

A torque converter engagement strategy defines the ratio k_{TC}.

Finally, the belt is inverted to distribute its torque reference $T_{\mathrm{belt\ ref}}$ into the electrical drive and the engine:

$$T_{\mathrm{ED\ ref}} = \frac{T_{\mathrm{belt\ ref}} - T_{\mathrm{ICE\ ref}}}{k_{\mathrm{belt}}} \tag{3.13}$$

where the engine torque reference $T_{\mathrm{ICE\ ref}}$ is computed by a torque distribution strategy which is the objective of this study.

3.1.4. Model modification for energy management strategy development

Model modification is a key point of efficient EMS development (see Subsection 2.1.4). It is even more important due to the complexity of the studied H-ESS-based parallel hybrid truck. In this subsection, the system model is reduced to obtain a proper mathematical model for developing an optimal control-based EMS.

a. Model reduction assuming perfect control performances

By assuming that the inductor and the chopper are perfectly controlled, they and their inversions can be reduced to an equivalent converter (Figure 3.5). The reduction of this bidirectional DC/DC converter is the same as presented in Subsection 2.1.4. In which the equivalent conversion element represents a static model of the DC/DC converter.

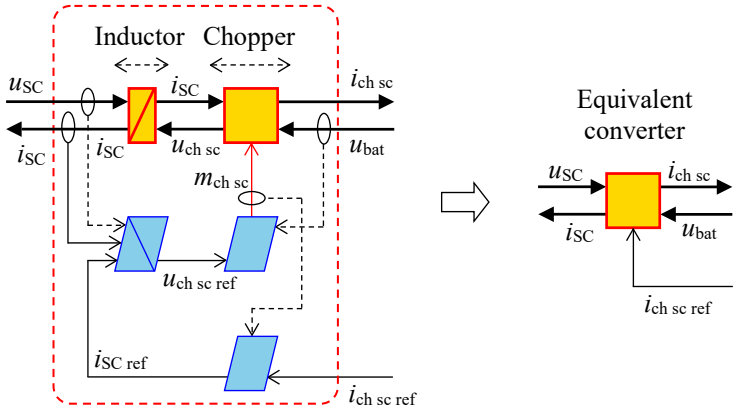

Figure 3.5: Model reductions of the DC/DC converter assuming perfect control performances.

b. Model transformation

Model transformation regarding concerned dynamics

Similar to Subsection 2.1.4, the EMSs, at the supervisory level, in this study do not deal with the dynamics of the chassis. Those dynamics are handled by the inversion-based controller at the local control level. Thus, the chassis and its velocity controller can be considered as an equivalent mechanical source (Figure 3.6). This subsystem imposes the traction current force reference $F_{\text{trac ref}}$ as a disturbance input.

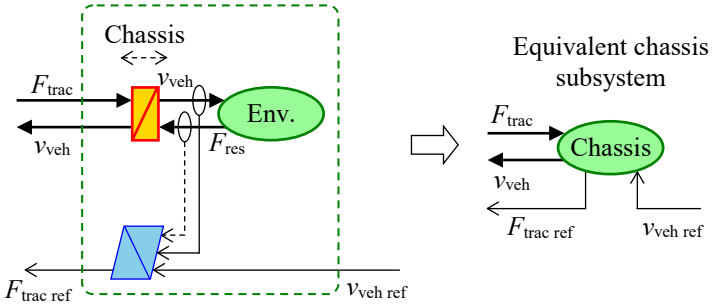

Figure 3.6: Model transformation of the chassis subsystem to highlight the disturbance.

The EMS does not consider the dynamics of the inductor or the chassis, which are already controlled at the local control layer. Instead, the dynamics of the SCs and the batteries are taken into account at the supervisory layer. Thus, their representations are transformed from source elements to accumulation elements (Figure 3.7). The model transformation of the SCs has been already addressed in Subsection 2.1.4.

In the case of the batteries, in fact, the state variable to be controlled is the SoC. However, SoC is not an energetic variable, i.e., it cannot produce power. It is just a dimensionless indicator of energy level. Hence, SoC is not a variable to be represented by using EMR. On the other hand, batteries voltage u_{bat} is a function of their SoC meanwhile the SoC is an integral of batteries current i_{bat} (see batteries model (2.1)). That is why batteries can be represented by an accumulation element with i_{bat} as the input and u_{bat} as the output. Furthermore, in fact, the SoC is always estimated by measuring batteries current. Thus, the objective of controlling the SoC as a state variable is warranted.

As a result, the first step reduced EMR of the studied system is given in Figure 3.8.

Model transformation regarding decomposed strategies

A global multi-objective multi-variable strategy for the studied system (Figure 3.8) is complex. There are two objectives with two state variables and five control variables which cause a complicated problem. To achieve the objective of developing a simple-but-effective EMS, decomposition method [Castaings 2016b; Horrein 2015] is adopted. The global strategy is decomposed into five local mono-objective strategies as shown in Figure 3.9.

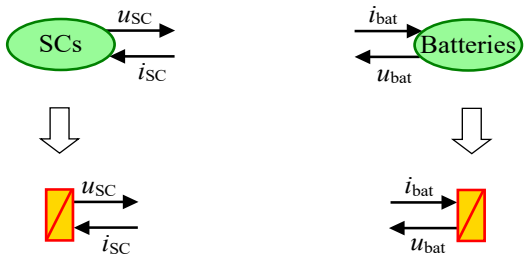

Figure 3.7: Model transformations of the energy storages to represent the dynamics considered at supervisory level.

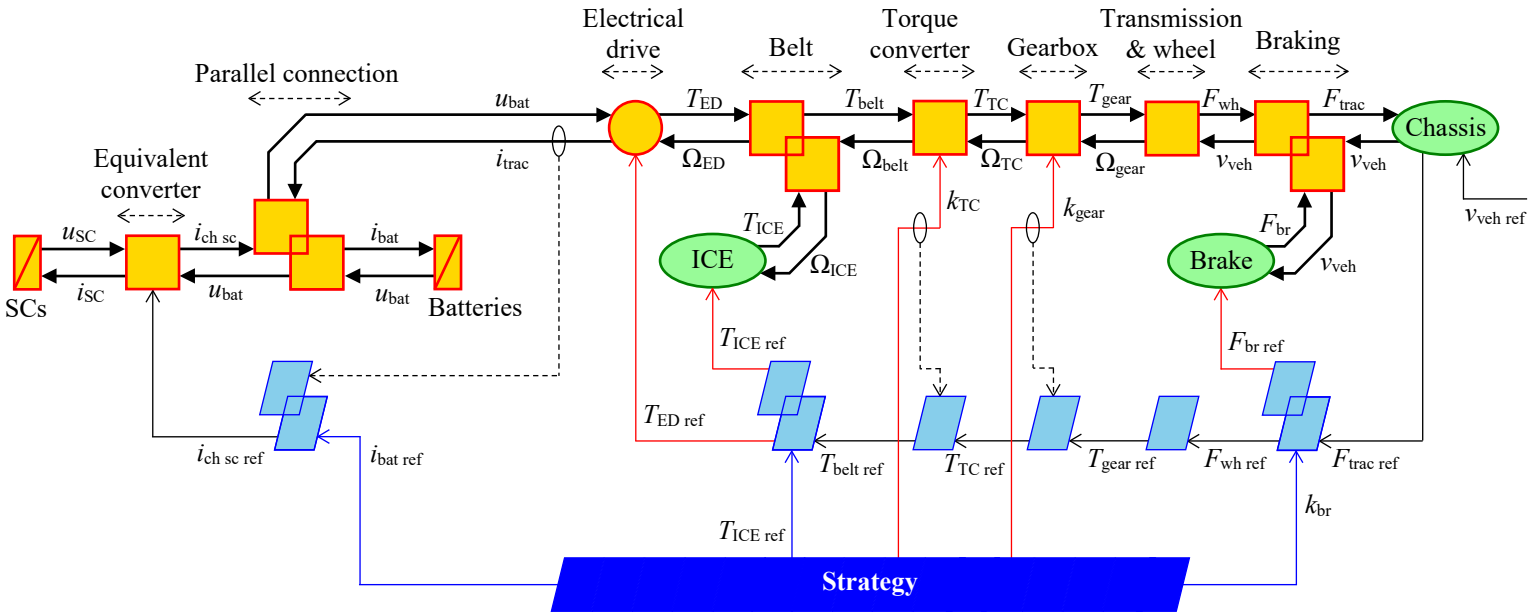

Figure 3.8: Reduced EMR of the studied battery/SC parallel hybrid truck by assuming perfect control performances.

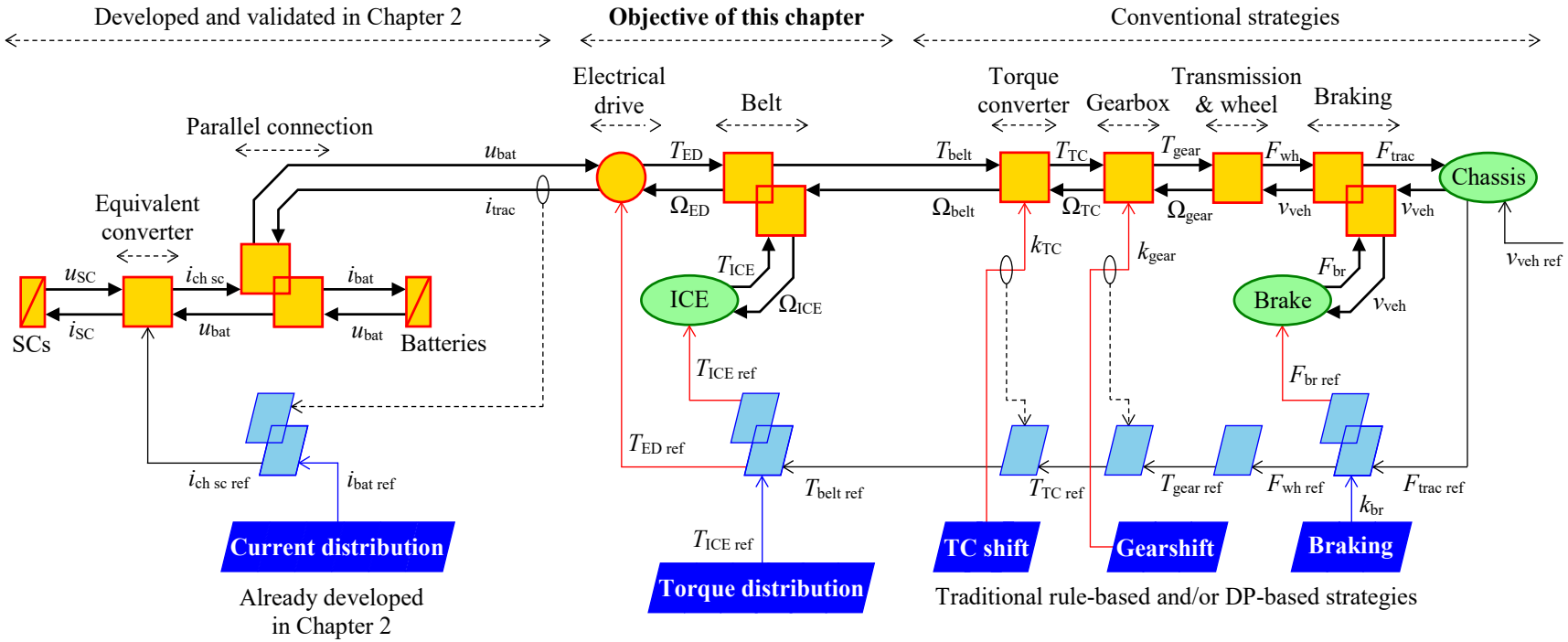

Figure 3.9: Decomposed EMSs for the studied battery/SC parallel hybrid truck.

The current distribution strategy has been developed in Chapter 2. For torque converter engagement (TC shift), gearshift, and braking strategies, traditional rule-based and/or DP-based optimal strategies can be used. By assuming that the gearbox can be shifted immediately, the torque converter disengagement can be neglected. Thus, in this study, the clutch of the torque converter is considered always being closed.

Besides, gearshift strategy has effects on the engine fuel consumption. The objective is to keep the ICE operating within its optimal efficiency region while the vehicle velocity and torque demand varies in a wide range. In case of parallel HEV, it has been shown that a decomposition of gearshift and power distribution strategies is a suitable approach [Ngo 2012]. Hence, it is suitable to inherit this decomposed cascade scheme. In which the gearshift strategy decides the engine speed and the total torque reference. Then the torque distribution strategy computes the torques references for the engine and the electrical drive. In this study, DP is used to develop an optimal gearshift strategy, then it is realized in real-time by using look-up table.

Finally, the objective of braking strategy is to regenerate as much as possible the energy during braking mode. In this work, a DP-based strategy is adopted, like gearshift, for fair comparison. In fact, it has been shown that a rule-based braking strategy can be combined (hybridized) with optimization-based power distribution strategy for HEVs to obtain the optimal results [Horrein 2015b]. So, real-time implementation, in any case, is not a problem for the braking strategy.

Once these strategies are correctly developed, the torque converter, the gearbox, and the brake can be considered working properly. Thus, the model of the drivetrain subsystem, including these components, the final drive and wheel, and the chassis, can be reduced to an equivalent mechanical source (see Figure 3.10).

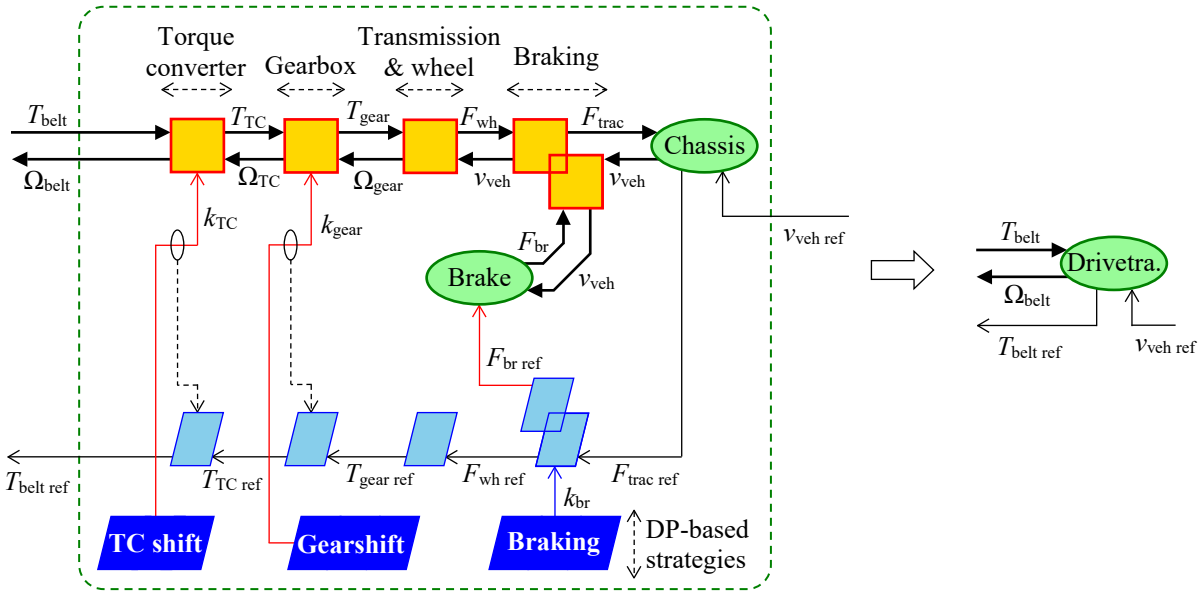

Figure 3.10: Model transformation of the drivetrain subsystem; assuming perfect control performances and properly developed strategies.

Also, the H-ESS model can be reduced to an equivalent ESS with the capacitance $C_{\text{ESS eq}}$ expressed in Farad (Figure 3.11). Since the SCs capacitance (in Farad) is much smaller than that of the batteries (in kilo-Farad), the equivalent ESS capacitance $C_{\text{ESS eq}}$ can be considered to equal the batteries capacitance $C_{\text{bat eq}}$.

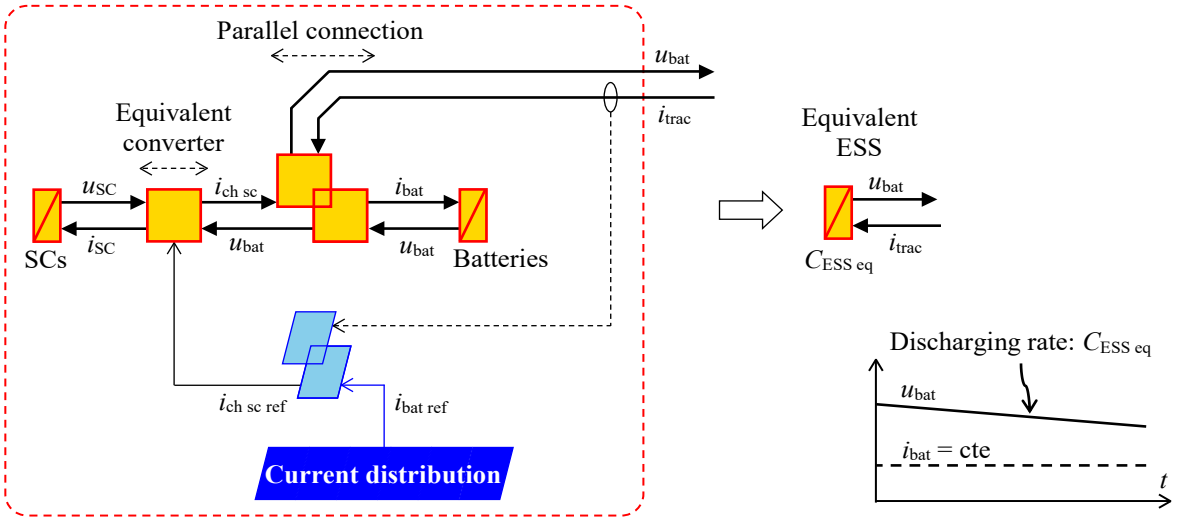

Figure 3.11: Model reduction of the H-ESS; considering dominant capacitance of the batteries.

c. Model adaptation for energy management strategy development

Reduced EMR of the studied system for torque distribution strategy development

By reducing the H-ESS and the drivetrain subsystem, the EMR of the studied system for developing torque distribution strategy can be deduced as shown in Figure 3.12. The drivetrain imposes the rotational speed Ω_{belt} and the belt torque reference $T_{\text{belt ref}}$ to the system. In which, the electrical drive speed Ω_{ED} and the engine speed Ω_{ICE} are fixed to that belt speed by the constant ratio k_{belt} (see (3.3)). Meanwhile the torque distribution strategy defines the control law to distribute the $T_{\text{belt ref}}$ into the $T_{\text{ED ref}}$ and the $T_{\text{ICE ref}}$.

In non-plug-in HEVs, the EMS should ensure the charge sustaining of the ESS; which means the final SoC should be close to its initial value.

Reduced mathematical model for optimal control-based strategy development

A mathematical model can be deduced from the aforementioned reduced EMR of the studied system. By neglecting the parasitic resistances and losses of the H-ESS, the equivalent ESS can be modeled as follows:

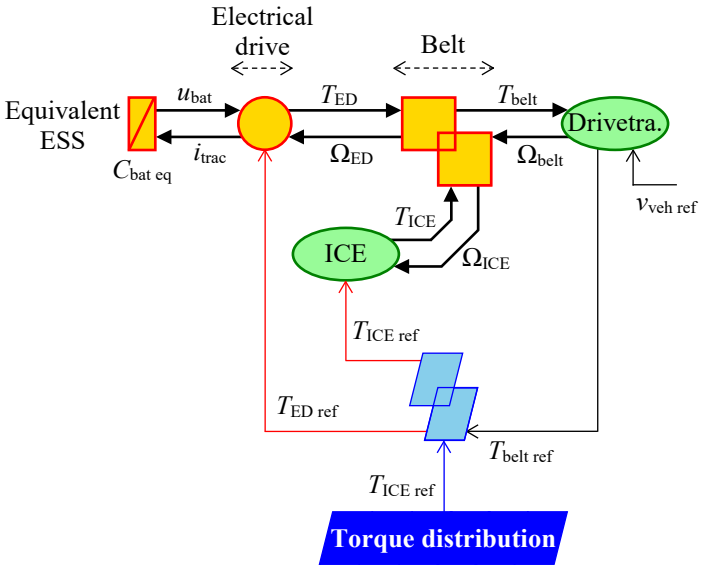

Figure 3.12: Reduced EMR for torque distribution strategy development.

$$\frac{d}{dt}SoC_{\text{ESS}} = \frac{-i_{\text{trac}}}{C_{\text{ESS eq}}}; \tag{3.14}$$

where SoC_{ESS} is the equivalent SoC of the H-ESS. In fact, by considering the dominant capacitance of the batteries in comparison to the SCs, the SoC_{ESS} can be approximated by the SoC_{bat}. Thus, the model of the equivalent ESS can be given by:

$$\frac{d}{dt}SoC_{\text{bat}} = \frac{-i_{\text{trac}}}{C_{\text{bat eq}}}. \tag{3.15}$$

From the electrical drive model (3.1) and the belt model (3.3), by neglecting the efficiency, the traction current can be calculated as follows:

$$\begin{aligned} i_{\text{trac}} &= \frac{\Omega_{\text{ED}} T_{\text{ED}}}{u_{\text{bat}}} \\ &= \frac{k_{\text{belt}} \Omega_{\text{ICE}} T_{\text{ED}}}{u_{\text{bat}}}. \end{aligned} \tag{3.16}$$

Considering the belt coupling with the assumptions of perfect response of the drive and the engine torque, that leads to:

$$i_{\text{trac}} = \frac{k_{\text{belt}} \Omega_{\text{ICE}}}{u_{\text{bat}}} (T_{\text{belt ref}} - T_{\text{ICE ref}}). \tag{3.17}$$

Replacing the i_{trac} in (3.17) to (3.15), the reduced mathematical model of the system can be deduced as follows:

$$\frac{d}{dt}SoC_{\text{bat}} = \frac{k_{\text{belt}}\Omega_{\text{ICE}}}{C_{\text{bat eq}}u_{\text{bat}}}(T_{\text{ICE ref}} - T_{\text{belt ref}}); \tag{3.18}$$

in which, the Ω_{ICE} and the u_{bat} are measurable disturbances; the $T_{\text{belt ref}}$ determined; the k_{belt} the given data; the SoC_{bat} the state variable; and the $T_{\text{ICE ref}}$ the control variable. This is a linear model (see Appendix A.3) which is convenient for optimal control application.

Cost function

The objective of the EMS is to reduce the fuel consumption of the ICE. Thus, the cost function to develop the strategy is:

$$\begin{aligned} J &= m_{\text{fuel}} \\ &= \int_{t_0}^{t} \dot{m}_{\text{fuel}}(T_{\text{ICE}}, \Omega_{\text{ICE}})dt \end{aligned} \tag{3.19}$$

where the fuel consumption rate $\dot{m}_{\text{fuel}}(T_{\text{ICE}}, \Omega_{\text{ICE}})$ is computed by using a look-up table.

3.2. Optimal benchmark using dynamic programming

DP is used to achieve the off-line optimal benchmark to evaluate the developed real-time strategies. Decomposition approach is continued to be applied to form a bi-level scheme EMS [Nguyễn 2018]. The DP optimization problem of the hybrid traction subsystem is solved first. Then the electrical traction power is the disturbance input to solve the DP optimization problem of the H-ESS.

3.2.1. Backward representation

The reduced EMR of the system, i.e., forward representation, (Figure 3.12) is transformed to the backward representation [Horrein 2015a] (Figure 3.13). The belt and its inversion are merged to form a backward coupling element (overlapped squares) with the following model:

$$\begin{cases} T_{\text{ICE}} = T_{\text{ICE ref}} \\ T_{\text{ED}} = \dfrac{T_{\text{belt}} - T_{\text{ICE}}}{k_{\text{belt}}\eta_{\text{belt}}^{k_{\eta\,\text{belt}}}} \\ \Omega_{\text{ICE}} = \Omega_{\text{belt}} \\ \Omega_{\text{ED}} = k_{\text{belt}}\Omega_{\text{belt}}. \end{cases} \tag{3.20}$$

In which, the belt torque and speed T_{belt} and Ω_{belt} are known in advance since it is imposed by the drivetrain with the vehicle velocity reference $v_{\text{veh ref}}$ *a priori* known. The torque distribution of the electrical drive and the ICE are therefore determined by backward computations (see the arrows directions in Figure 3.13). The backward representation of the H-ESS is inhered from Chapter 2 (see Figure 2.14 in Subsection 2.2.1).

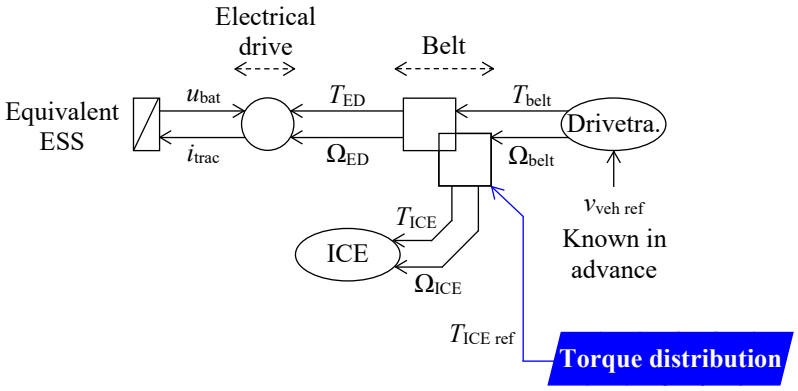

Figure 3.13: EMR-based backward representation of the studied system.

3.2.2. Dynamic programming implementation

Figure 3.14 illustrates the implementation and solving process of DP problem by using the EMR-based backward representations and the dpm function toolbox [Sundström 2009].

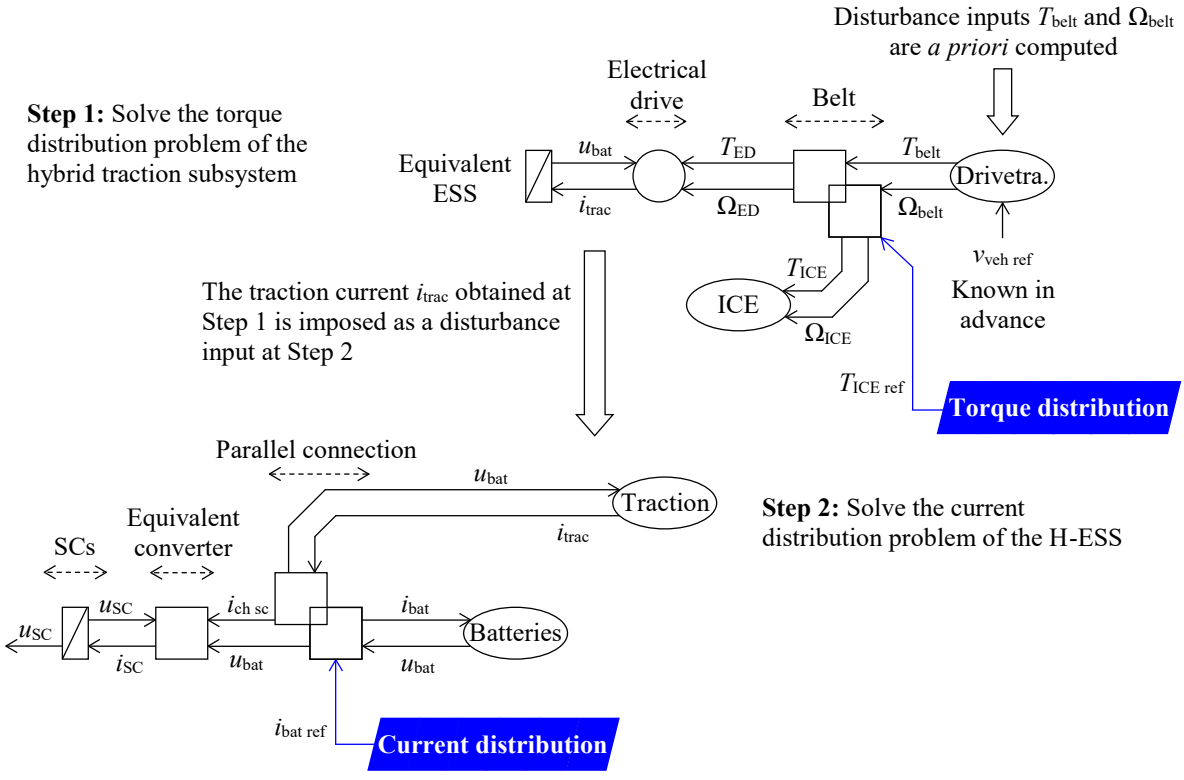

Figure 3.14: Implementation of DP to obtain the off-line optimal torque distribution and optimal current distribution strategies.

The two optimal control problems are solved sequentially in two steps. Firstly, the forward simulation of the drivetrain subsystem is conducted to compute the T_{belt} and the Ω_{belt} in advance. The torque distribution problem is solved based on the knowledge of these disturbance inputs. Secondly, the traction current i_{trac} calculated from this problem solving is employed as the disturbance to solve the current distribution problem of the H-ESS.

3.3. Real-time strategy based on linear quadratic regulator

3.3.1. Approach

Original problem statement

The energy management problem of the parallel hybrid truck can be stated as follows. Find an optimal control law $T^*_{\text{ICE ref}}$ for the system:

$$\frac{d}{dt}SoC_{\text{bat}} = \frac{k_{\text{belt}}\Omega_{\text{ICE}}}{C_{\text{bat eq}}u_{\text{bat}}}(T_{\text{ICE ref}} - T_{\text{belt ref}}) \tag{3.21}$$

to minimize the cost function:

$$J = \int_{t_0}^{t} \dot{m}_{\text{fuel}}(T_{\text{ICE}}, \Omega_{\text{ICE}})dt. \tag{3.22}$$

Applying directly optimal control theory to solve this problem leads to a trivial solution in which $T^*_{\text{ICE ref}} = 0$ [Delprat 2004]. This solution can be intuitively explained as: the best way to save fuel is not to use the ICE. However, it is not an expected solution because the batteries will be fully discharged after few kilometers.

To overcome this issue, two methods are often used in literature. The first one is to add the final constrain of the batteries SoC:

$$SoC_{\text{bat final}} = SoC_{\text{bat init}}. \tag{3.23}$$

Then, optimal control techniques such as DP (see Section 3.2) or PMP [Delprat 2004] are applied. This approach, however, is suitable only for off-line strategies when the driving cycles are known in advance. The final state constrain is warranted only in finite time horizon. There is in fact no way to ensure this constrain in real-time since the final time is unknown. To develop real-time EMSs, λ-control is often applied to adapt the PMP-based optimal solution to real-time operation [Kermani 2011; Castaings 2016a]. The strategies therefore become sub-optimal.

The second approach is to charge the cost of SoC variation by adding to the cost function a penalty like [Borhan 2012]:

$$J = \int_{t_0}^{t} \left[a\left(\dot{m}_{\text{fuel}}(T_{\text{ICE}}, \Omega_{\text{ICE}})\right)^2 + b(SoC - SoC_{\text{ref}})^2\right] dt \tag{3.24}$$

where a and b are weighting factors. This is in fact an ECMS method, in which the batteries energy variation is converted to an equivalent fuel consumption. The problem is then solved by using MPC [Borhan 2012] or PMP [Kim N. 2011] with λ-control scheme [Kessels 2008].

There is a common drawback of these approaches that the fuel consumption rate $\dot{m}_{\text{fuel}}(T_{\text{ICE}}, \Omega_{\text{ICE}})$ must be calculated to develop the strategies. For numerical methods like DP, the look-up table of this map is directly used. For analytical methods like PMP, the map is approximated by polynomial functions of which derivatives can be analytically calculated. It is because PMP method requires analytical expression of the partial derivative. In both cases, a data map of ICE fuel consumption is required. This is a drawback in real-world applications since such data are not often available.

Strategy development using these approaches is also often complicated. Moreover, methods like MPC require strong computational efforts that may prevent them from on-board implementation.

As a consequence, the problem should be reformulated for simplification without requirement of fuel consumption map and low computational efforts.

Problem reformulation

This study proposes an alternative approach, firstly by reformulating the problem. It is known that the fuel consumption rate is mainly proportional to the ICE power [Kessels 2008; Koot 2005]. In other words, for a given speed, the higher the engine torque is, the higher the fuel consumption rate is (e.g., see Figure 3.15). The datasheet of the engine shows an almost linear behavior of the fuel consumption as a function of the torque and the speed.

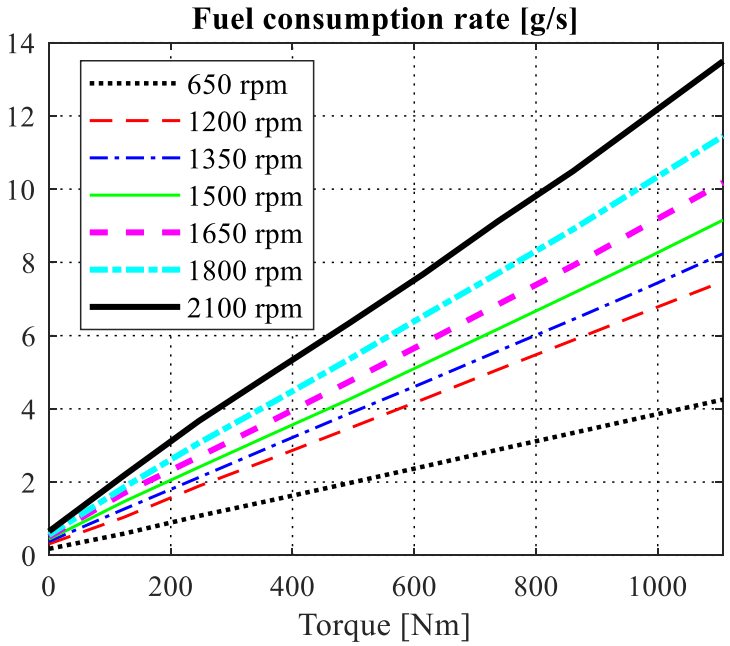

Figure 3.15: An example of fuel consumption rates of the ICE used in this study (Detroit Diesel Corp. Series 50 8.5 (205 kW) Diesel Engine).

Hence, it can be considered that, with the same speed, minimizing the engine torque will minimize the fuel consumption. That means instead of using the original cost function (3.22) of fuel consumption rate $\dot{m}_{\text{fuel}}$, it can be approximated by using the ICE torque as follows:

$$J = \int_{t_0}^{t} T_{\text{ICE ref}}\, dt. \tag{3.25}$$

The approximation may cause some reductions in computational accuracy, which make the strategy sub-optimal. However, this formulation allows deducing analytical solution; whereas the map of $\dot{m}_{\text{fuel}}$ requires numerical computations. The strategy will be therefore simpler for development and easier for real-time implementation.

Additionally, as discussed above, a term of SoC variation should be penalized in order to ensure the charge sustaining of the energy storage as follows:

$$J = \int_{t_0}^{t} [T_{\text{ICE ref}}^2 + Q(t)(SoC_{\text{bat}} - SoC_{\text{bat ref}})^2]dt\,; \tag{3.26}$$

in which $Q(t)$ is an equivalent conversion factor to convert the SoC variation to the engine torque. Thus, the method can be considered as an adaptation of ECMS approach.

Since the reduced mathematical model (3.21) is linear (see Appendix A.3) while the cost function (3.26) is in a quadratic form of state and control variables, the linear quadratic regulator (LQR) method can be employed. That can deduce a simple analytical control law which is suitable for on-board real-time implementation.

3.3.2. Strategy development

Linear quadratic regulator

The LQR control law [Bryson 1975] is developed for the linear system in the following form:

$$\frac{d}{dt}\underline{x} = A\underline{x} + B\underline{u}; \tag{3.27}$$

in which $\underline{x}$ generally denotes state variables vector; $\underline{u}$ the control variables vector; A the dynamical matrix; B the control matrix; with the cost function in the form given by:

$$J = \int_{o}^{\infty} \left(\underline{x}^T Q \underline{x} + \underline{u}^T R \underline{u}\right) dt \tag{3.28}$$

where Q and R are weighting matrices; ∞ denotes infinite time horizon; T the transpose of the matrix. In real-world real-time applications, the final time T_{end} of the driving cycle is unknown. Thus, the formulation with infinite time horizon is suitable.

By applying PMP to this system, the control law is obtained as follows:

$$u = -R^{-1}B^{T}P\left(\underline{x} - \underline{x}_{\text{ref}}\right); \tag{3.29}$$

in which P is the solution of the algebraic Riccati equation:

$$PA + A^{T}P - PBR^{-1}B^{T}P + Q = 0. \tag{3.30}$$

LQR-based strategy development

Applying the reduced mathematical model (3.21) and the reformulated cost function (3.26) to the general form (3.27) and (3.28), the system coefficients are defined by:

$$\begin{cases} A = 0 \\ B = \dfrac{k_{\text{belt}}\Omega_{\text{ICE}}(t)}{C_{\text{bat eq}}u_{\text{bat}}(t)} \\ Q = Q(t) \\ R = 1. \end{cases} \tag{3.31}$$

Replacing (3.31) to (3.30), the Riccati equation for the studied system can be given by:

$$-P(t)^{2}B(t)^{2} + Q(t) = 0. \tag{3.32}$$

Thus,

$$P(t) = \frac{\sqrt{Q(t)}}{B(t)}. \tag{3.33}$$

By replacing (3.33) to the general form (3.29) of the control law, the ICE torque reference can be deduced as follows:

$$\begin{aligned} T_{\text{ICE ref}} &= -\frac{k_{\text{belt}}\Omega_{\text{ICE}}(t)}{C_{\text{bat eq}}u_{\text{bat}}(t)} \frac{\sqrt{Q(t)}}{\dfrac{k_{\text{belt}}\Omega_{\text{ICE}}(t)}{C_{\text{bat eq}}u_{\text{bat}}(t)}} (SoC_{\text{bat}} - SoC_{\text{bat ref}}) \\ &= \sqrt{Q(t)}(SoC_{\text{bat ref}} - SoC_{\text{bat}}). \end{aligned} \tag{3.34}$$

It is seen that, eventually, the LQR-based control law has a form of a proportional (P) controller of the batteries SoC.

Weighting factor determination

The square-root of the weighting factor Q can be determined by using the conventional pole-placement technique for the P controller (Figure 3.16). The system model (3.21) can be rewritten in Laplace domain as follows:

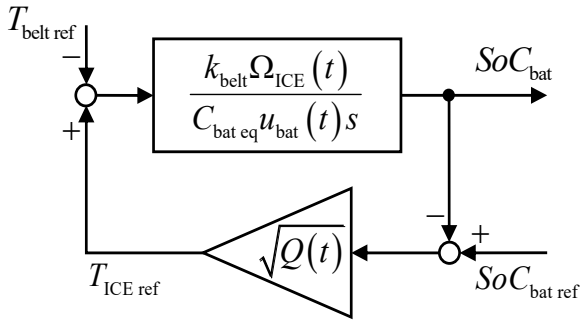

Figure 3.16: P controller form of the LQR control law.

$$SoC_{\text{bat}} = \frac{k_{\text{belt}}\Omega_{\text{ICE}}(t)}{C_{\text{bat eq}}u_{\text{bat}}(t)s}(T_{\text{ICE ref}} - T_{\text{belt ref}}) \tag{3.35}$$

where s is the Laplace operator. Since the belt torque reference $T_{\text{belt ref}}$ is the disturbance of the studied control loop, it is neglected while synthesizing the controller. The closed-loop transfer function is:

$$\begin{aligned} G_{\text{closed-loop}} &= \frac{\frac{k_{\text{belt}}\Omega_{\text{ICE}}(t)}{C_{\text{bat eq}}u_{\text{bat}}(t)s}\sqrt{Q(t)}}{1 + \frac{k_{\text{belt}}\Omega_{\text{ICE}}(t)}{C_{\text{bat eq}}u_{\text{bat}}(t)s}\sqrt{Q(t)}} \\ &= \frac{1}{\frac{C_{\text{bat eq}}u_{\text{bat}}(t)}{k_{\text{belt}}\Omega_{\text{ICE}}(t)\sqrt{Q(t)}}s + 1}. \end{aligned} \tag{3.36}$$

The closed-loop system is a first-order transfer function; in which its response time (to 95% of the step reference) is five times of the time constant, as given by:

$$T_{\text{res}} = 3\frac{C_{\text{bat eq}}u_{\text{bat}}(t)}{k_{\text{belt}}\Omega_{\text{ICE}}(t)\sqrt{Q(t)}} \tag{3.37}$$

where T_{res} is the response time of the closed-loop system. Hence, the square-root of the weighting factor can be determined as:

$$\sqrt{Q(t)} = 3\frac{C_{\text{bat eq}}u_{\text{bat}}(t)}{k_{\text{belt}}\Omega_{\text{ICE}}(t)T_{\text{res}}}. \tag{3.38}$$

The weighting factor $Q(t)$ varies with time and is totally calculated by the measurable variables $u_{\text{bat meas}}$ and $\Omega_{\text{ICE meas}}$. The batteries capacitance $C_{\text{bat eq}}$ and the belt ratio k_{belt} are known parameters. The response time T_{res} is the only parameter needed to be defined by the strategy

developer. It is in fact a trade-off between the fuel consumption reduction (longer T_{res}) and charge sustaining of the batteries (shorter T_{res}).

Finally, by replacing (3.38) to (3.34), the LQR-based control law for the studied parallel hybrid truck is obtained as follows:

$$T_{\text{ICE ref}} = 3\frac{C_{\text{bat eq}}u_{\text{bat}}(t)}{k_{\text{belt}}\Omega_{\text{ICE}}(t)T_{\text{res}}}(SoC_{\text{bat ref}} - SoC_{\text{bat est}}). \tag{3.39}$$

3.3.3. Strategy implementation

The proposed real-time LQR-based strategy is implemented as illustrated in Figure 3.17. The limitations of the electrical drive torque and the batteries SoC are treated by using the conventional switching method. When the system reaches its limitations, the ICE must provide all the demanded traction power. The strategy is simple and straightforward without requiring complex data like engine fuel consumption map. Thus, it is suitable for on-board real-time implementation for real-world applications.

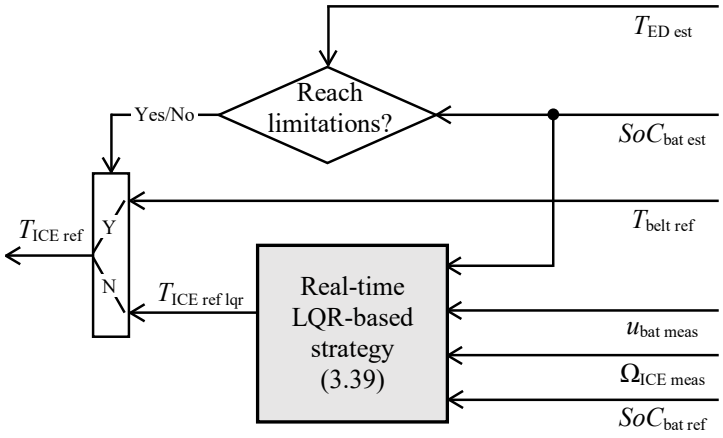

Figure 3.17: Implementation of the proposed LQR-based EMS.

3.4. Simulations and results

3.4.1. Examined system

The studied vehicle is based on a parallel hybrid delivery truck designed in [Hofman 2008] with the main parameters given in Table 3.1. A traditional 6-level gearbox is employed. A 205-kW series 50 8.5 diesel engine of Detroit Diesel Corporation is coupled with a 58-kW permanent magnet synchronous machine (PMSM) drive via a belt with the 1:1 ratio. The electrical drive is originally supplied by a 300-V 62-Ah batteries pack consisting of LiPho A123 20Ah 2010 cells. To form a semi-active H-ESS, a 195-V 13.4-F SCs subsystem is added to the system by using Maxwell BMOD0058 E016 B02 modules.

Table 3.1: Examined system parameters for simulation of the battery/SC hybrid truck.

Parameters		Values
Vehicle (based on the hybrid delivery truck designed in [Hofman 2008])		
Vehicle total mass	M_{veh}	7514 kg
Aerodynamic standard	$c_{\text{x}}A$	0.73×6.9 m^2
Rolling coefficient	k_{roll}	0.008
Final drive ratio	k_{FD}	3.33
Wheel radius	R_{wh}	0.397 m
Gearbox		
Gearbox ratio	k_{gear}	[7.14 4.17 2.50 1.59 1.00 0.78]
Efficiency	η_{gear}	[0.94 0.95 0.9 0.95 0.91 0.91]
Belt		
Belt ratio	k_{belt}	1
Efficiency	η_{belt}	0.95
ICE (Detroit Diesel Corp. Series 50 8.5 Diesel Engine)		
Maximal power	$P_{\text{ICE max}}$	205 kW
Maximal speed	$\Omega_{\text{ICE max}}$	2100 rpm
Idle speed	$\Omega_{\text{ICE idle}}$	650 rpm
Maximal torque	$T_{\text{ICE max}}$	1100 Nm
Mass density of diesel	M_{vol}	850 g/L
Electrical drive (PMSM)		
Maximal power	$P_{\text{ED max}}$	58 kW
Maximal torque	$T_{\text{ED max}}$	400 Nm
Nominal speed	$\Omega_{\text{ED nom}}$	1500 rpm
Maximal speed	$\Omega_{\text{ED max}}$	4000 rpm
Nominal efficiency in traction mode	$\eta_{\text{ED trac}}$	96 %
Nominal efficiency in regenerative mode	$\eta_{\text{ED regen}}$	90 %
Batteries (LiPho A123 20Ah 2010 cells)		
Battery bank capacitance	C_{bat}	62 Ah (equivalent 223.2 kF)
Battery bank resistance (at 70% SoC)	r_{bat}	26 mΩ
Battery bank OCV (at 70% SoC)	$u_{\text{bat OC}}$	300 V (maximum 303.5 V)
SCs subsystem (Maxwell BMOD0058 E016 B02 modules)		
Inductor inductance	L	0.2 mH
Inductor parasitic resistance	r_{L}	10.0 mΩ
SC series resistance	r_{SC}	88 mΩ
SC nominal voltage	$u_{\text{SC nom}}$	195 V
SC nominal capacitance	C_{SC}	13.4 F

This study examines the system with three standard driving cycles:

- Urban Dynamometer Driving Schedule (UDDS) as an American standard driving cycle;
- NEDC as a European standard driving cycle; and
- WLTC class 2 as a statistical combination of standard and real-world driving cycles from different countries in Europe, Asia, and America [Tutuianu 2014].

In fact, WLTC class 2 is developed for testing of light-duty vehicles, including passenger cars and light vans. However, this cycle is used in this study since it reflects real driving behavior with many oscillations in a wide velocity range.

For each driving cycle, three cases are compared:

- Conventional truck driven by ICE only, in which all braking energy is consumed by the mechanical brake;
- Hybrid truck with the proposed LQR-based torque distribution strategy; and
- Hybrid truck with DP-based optimal strategy as an off-line benchmark.

The parameters for DP problem solving is given in Table 3.2 which is implemented by using the dpm function toolbox developed by [Sundström 2009]. The forward simulations are carried out in MATLAB/Simulink™ with the EMR library [EMR 2019] as shown in Figure 3.18.

Table 3.2: Parameters for DP problems solving of the battery/SC hybrid truck.

Parameters		**Range**	**Step**
Time	t	0 to t_f	1 s
Torque distribution problem			
State variable	SoC_bat	20% to 80%	0.1%
Control variable	$T_\mathrm{ICE\ ref}$	0 to 1100 Nm	10 Nm
Initial state	$SoC_\mathrm{bat\ init}$	70%	-
Final state constraint	$SoC_\mathrm{bat\ final}$	70%	-
Current distribution problem			
State variable	u_SC	97.5 to 195 V	1 V
Control variable	$i_\mathrm{bat\ ref}$	−190 to 190 A	1 A
Initial state	$u_\mathrm{SC\ init}$	195 V	-
Final state constraint	$u_\mathrm{SC\ final}$	195 V	-

t_f is the length of the driving cycle under study

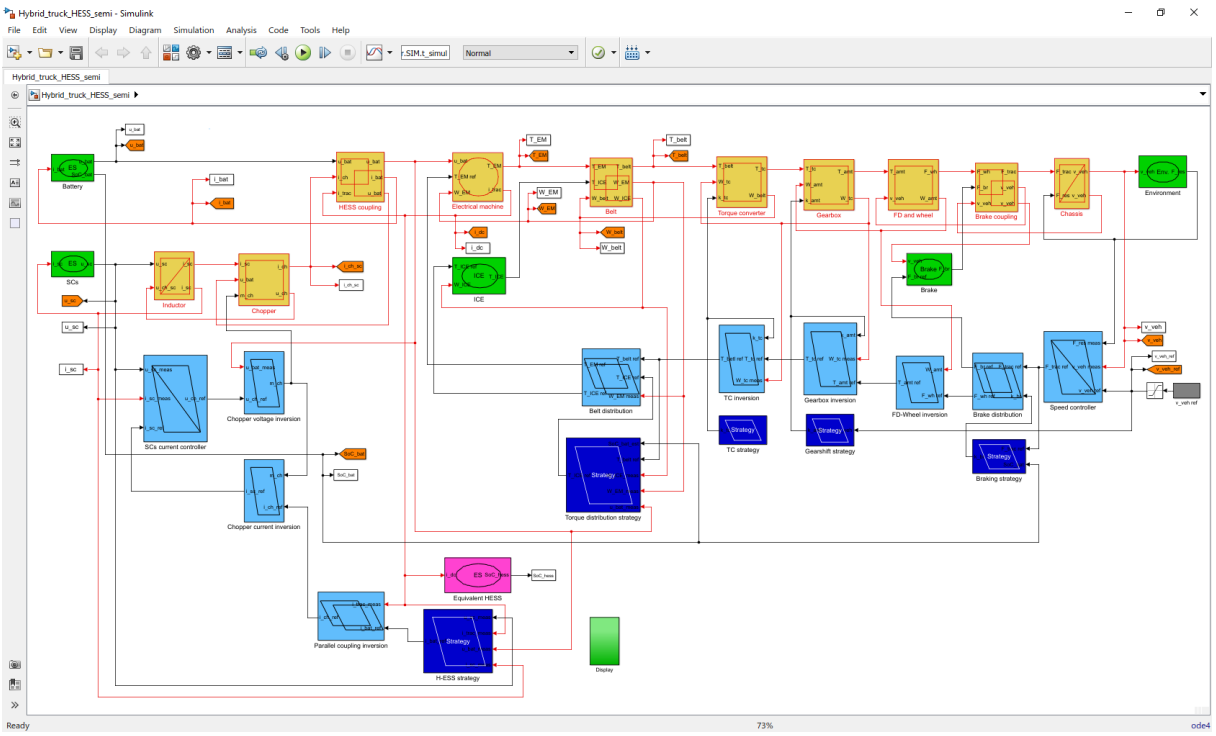

Figure 3.18: Simulation of the studied truck in MATLAB/Simulink™ with the EMR library.

3.4.2. Results and discussions

The objective of the torque distribution strategies is to minimize the engine fuel consumption. Hence, with different driving cycles, fuel consumption per 100 km is the criteria to evaluate and compare the different EMSs. Figure 3.19 shows a comparative evaluation of the proposed LQR-based strategy with the DP-based optimal solution and the case of conventional ICE-only truck as a double benchmark. In comparison to the conventional truck, the hybrid one can save up to 6.8% the fuel consumption with DP in the case of driving with UDDS cycle. Whereas the proposed real-time strategy saves 5.2% without *a priori* knowing the driving cycle. The numbers are 6.7% and 4.5% with NEDC; and 7.8% and 4.6% with WLTC class 2, respectively.

To have better understanding of the system behavior with the proposed torque distribution strategy, the results with NEDC are presented here in detail. NEDC is chosen because it is the simplest cycle among the studied ones. The system behaviors can therefore be seen and analyzed clearly. The main results are presented and discussed in this subsection. Additional results with UDDS and WLTC class 2 are given in Appendix A.5, see Figure A.10 and Figure A.11.

Figure 3.20–Figure 3.23 show the vehicle velocity, the engine torque, the machine torque, and the batteries SoC evolutions, respectively. Figure 3.24 and Figure 3.25 present the evolution of the SCs voltage, and the H-ESS currents, in cases of using the Hamiltonian minimization-based strategy (Chapter 2), correspondingly.

The examined NEDC contains four repeated urban cycles and a highway part (see Figure 3.20). During every urban cycle, the ICE torque (Figure 3.21) and the electrical drive torque (Figure 3.22) perform in the same patterns. That confirms the consistency of the proposed EMS.

The strategy let the machine support the engine as much as possible during the accelerations, then the ICE produce power to recharge the batteries. The electrical drive torque T_{ED} is kept within the torque constraints due to the drive power limitation. It should be noted that the electrical drive torque limitations reduce when its speed is higher than the machine nominal speed. Furthermore, it is seen that the drive torque is balanced in traction and regenerative braking mode. It indirectly shows the charge sustaining of the energy storage which is often a requirement of the non-plug-in HEVs.

The charge sustaining can be witnessed clearly by looking at the SoC evolution, in a comparison with the result deduced by DP (Figure 3.23). DP strategy "knows" that at the end of the cycle there is a huge amount of regenerative energy. Thus, it allows the batteries SoC to continuously reduce after each urban cycle. Meanwhile the real-time EMS does not "know" the driving condition in advance. Hence, it "tries" to ensure the charge sustaining after every urban cycle. The proposed LQR-based EMS perform well in both fuel saving and batteries charge sustaining. Yet the DP-based strategy can save more fuel by *a priori* knowing the driving cycle. At the end of the cycle, the batteries SoC is recovered to exactly the initial value. This is just a "lucky" case for the real-time strategy. In fact, the SoC_{bat} is controlled in real-time so that its final value is close to the initial one. With the other driving cycles, the final SoC can be slightly higher or lower than the initial value (see Appendix A.5 for the results with UDDS and WLTC).

The SCs subsystem supports the batteries by charging and discharging the SCs within their voltage limitations (see Figure 3.24). Figure 3.25 shows that the real-time Hamiltonian minimization-based strategy (Chapter 2) works well in the traction mode to smoothen the batteries current. Meanwhile in the regenerative mode, since the batteries need to be recharged to ensure charge sustaining, they take the most duty of consuming the negative current.

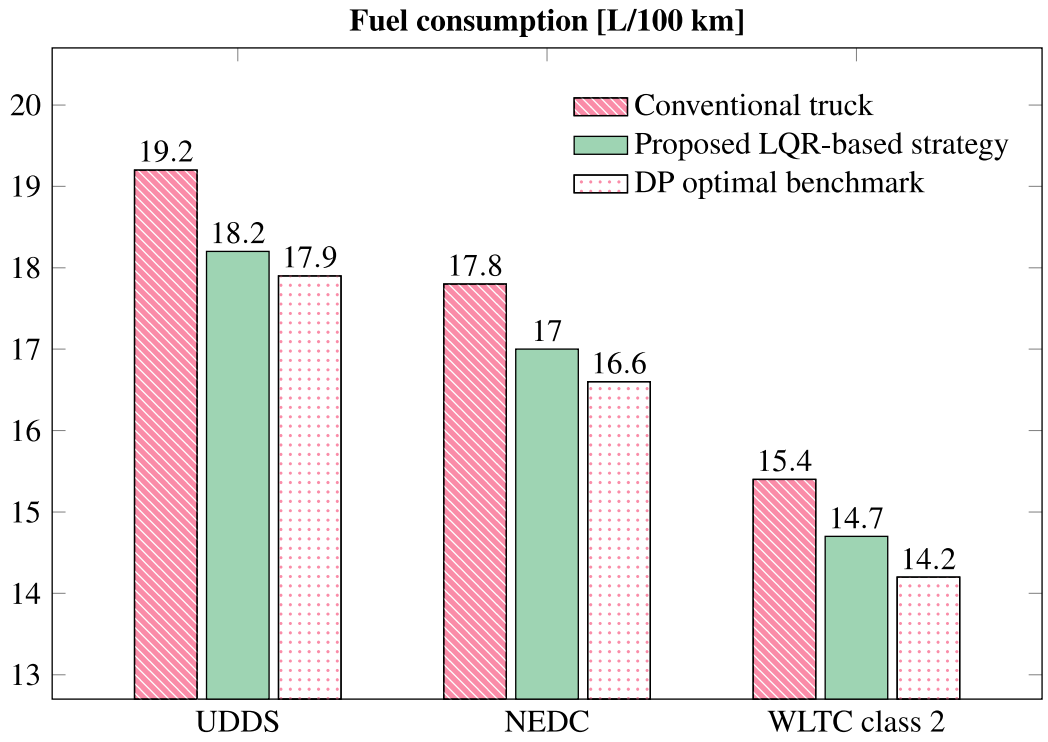

Figure 3.19: Comparative evaluation of the torque distribution strategies by simulation results.

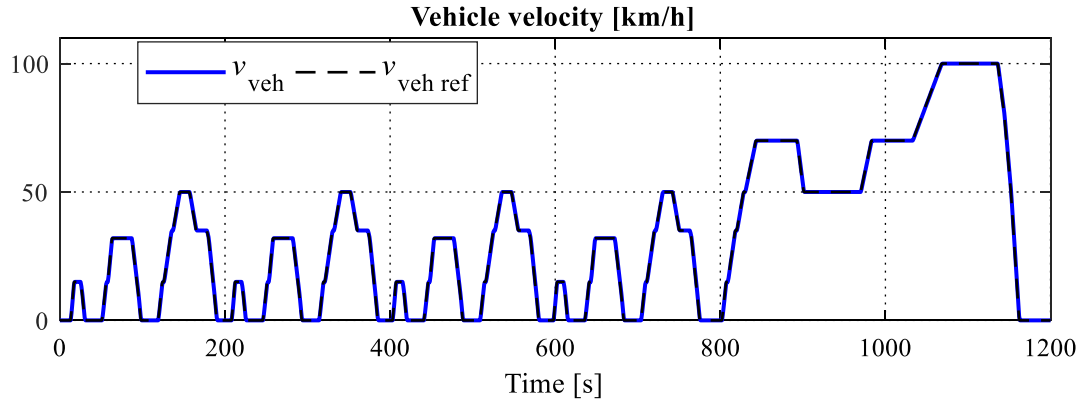

Figure 3.20: (Simulation results) vehicle velocity.

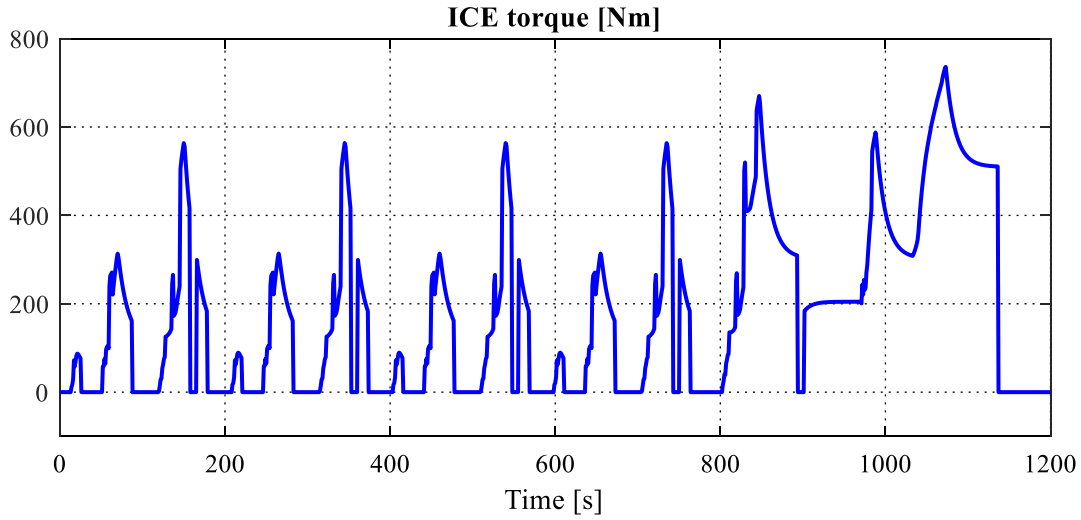

Figure 3.21: (Simulation results) ICE torque with the proposed LQR-based strategy.

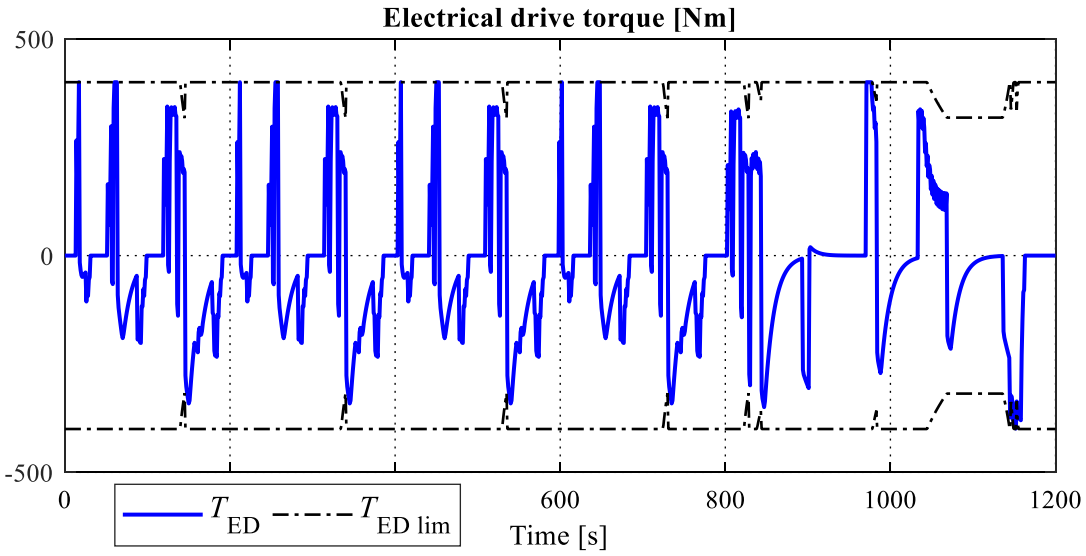

Figure 3.22: (Simulation results) electrical drive torque with the proposed LQR-based strategy.

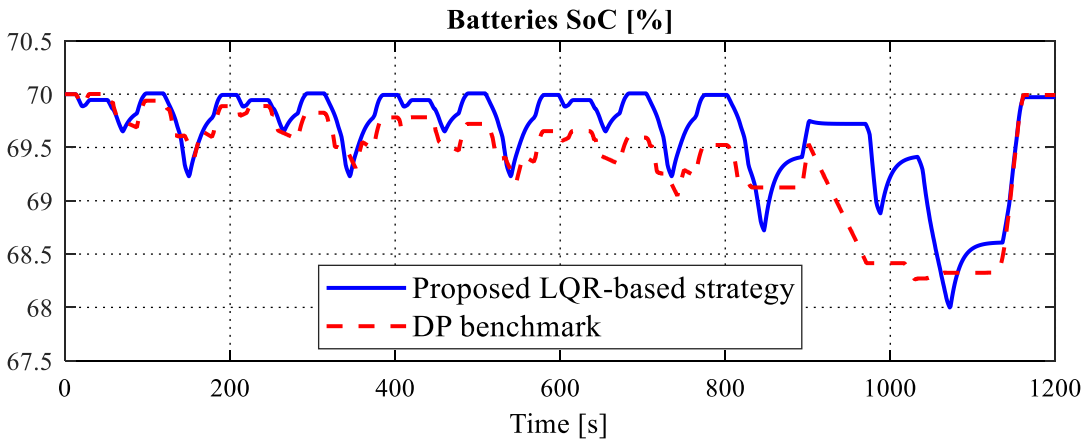

Figure 3.23: (Simulation results) batteries SoC.

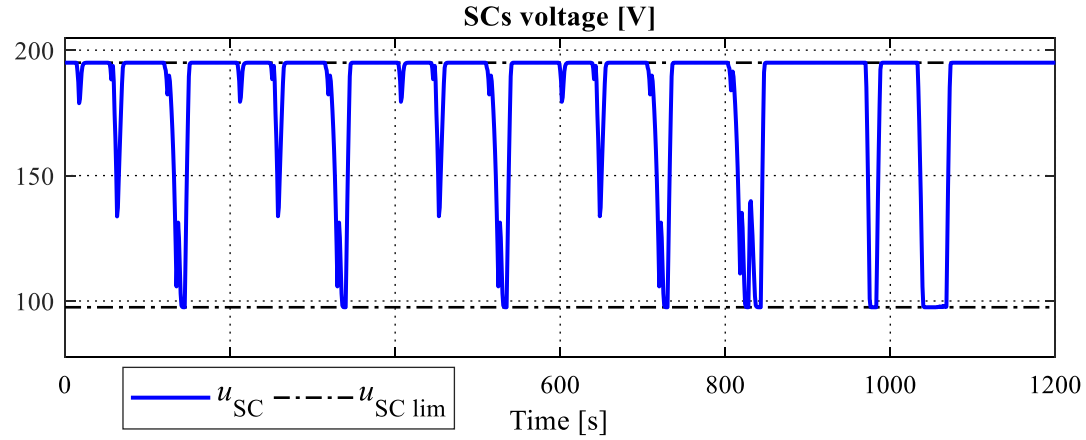

Figure 3.24: (Simulation results) SCs voltage with Hamiltonian minimization strategy (proposed in Chapter 2).

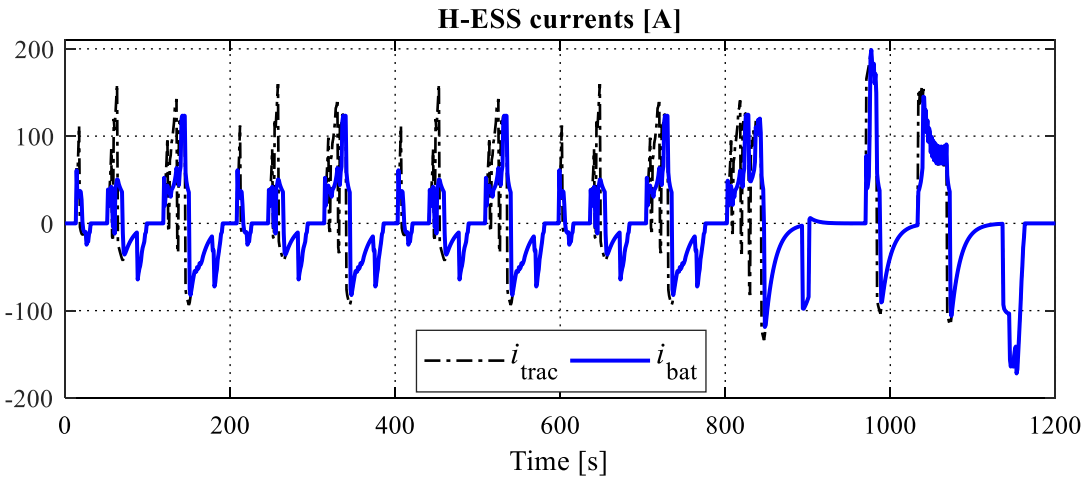

Figure 3.25: (Simulation results) traction and batteries currents with the real-time Hamiltonian minimization strategy (proposed in Chapter 2).

3.5. Experiments and results

3.5.1. Experimental setup

The experiments are conducted to validate the proposed real-time torque distribution strategy by using reduced-scale power HIL simulation [Bouscayrol 2011]. The principle of the HIL of the studied system is illustrated in Figure 3.26. The full-scale studied H-ESS-based hybrid truck is considered as a combination of four subsystems. The traction subsystem, including the ICE, is mechanically coupled with the electrical drive. The drive is electrically coupled with the batteries and the SCs subsystem. The HIL simulation is realized by using reduced-scale power system available in the laboratory to validate the developed EMS. Power adaptation factors are applied to each subsystem.

The electrical drive configuration is remained in the HIL system, while the traction subsystem is emulated. Similarly, the SCs subsystem topology is remained, while the batteries are emulated. The traction emulator should be a controllable mechanical source that imposes the drive rotational speed $\Omega_{ED\ HIL}$ as the reaction of the traction subsystem to the electrical drive. The batteries emulator is a controllable voltage source as already implemented in Section 2.5.

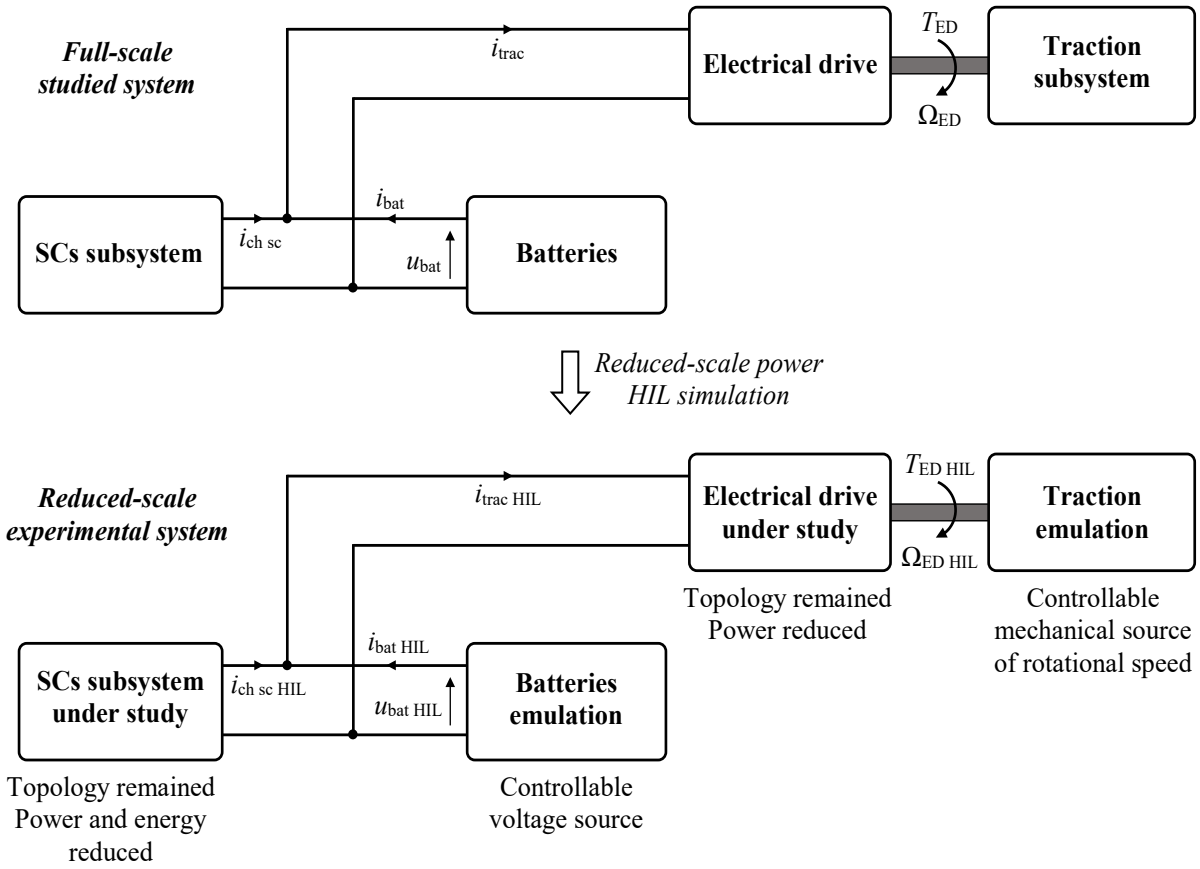

Figure 3.26: Principle of reduced-scale power HIL simulation for the studied system.

Figure 3.27 illustrates the experimental setup that realizes the reduced-scale power HIL simulation. The batteries emulators and the SCs subsystem configurations are the same as described in Section 2.5. The electrical drive is realized by a three-phase wound rotor induction machine (IM) and a voltage-source inverter. The DC bus of the inverter is connected in parallel with the DC bus capacitor of the batteries emulator. The IM is connected in delta-connection scheme to increase the speed range since the emulated batteries voltage $u_{\text{bat HIL}}$ is much lower than the nominal DC bus voltage of the machine. The traction emulation is realized by using a DC machine of which the armature is connected to a chopper to control the armature current i_{DCM}. That DC machine drive is supplied by a voltage source composed by a SCs pack, an inductor, a chopper, and a DC bus capacitor. The SCs pack charges and discharges to consume and to provide the emulated traction power, respectively. The traction DC bus voltage $u_{\text{dc trac}}$ is controlled to be constant. The electrical drive and the traction emulator are mechanically connected via a single shaft with a speed sensor.

The model and control program are implemented in a dSPACE DS1005 card. Via the power adaptation blocks, the full-scale traction model imposes the drive speed and torque references $\Omega_{\text{ED ref}}$ and $T_{\text{ED ref}}$ to the system. The DC machine is controlled by a speed controller to follow the $\Omega_{\text{ED ref}}$; whereas the IM is controlled by a torque controller to follow the $T_{\text{ED ref}}$. The emulated torque $T_{\text{ED HIL}}$ is estimated from the measured currents of the IM. It is then imposed to the full-scale traction model via a power adaptation block. It should be noted that only the most important blocks of the control program are illustrated in Figure 3.27. In fact, the experiments content many other controllers such as IM flux, DC machine current, traction DC bus voltage, etc. There are totally ten state variables to be controlled to realize these experimental tests.

The complexity of the HIL system is dealt with by using EMR as shown in Figure 3.28. The batteries emulation and the SCs subsystem is the same as they are in Subsection 2.5.1. The inverter is depicted by a conversion element. The traction current $i_{\text{trac HIL}}$ is estimated via the model of this inverter, with the measured line currents $\underline{i}_{\text{EM}}$ and the modulation functions $\underline{m}_{\text{inv}}$. The IM is modeled in the rotational d-q frame with the transformation block “abc2dq” represented by a conversion element. The machine armature in d- and q-axes and the magnetization are depicted by accumulation elements which represents the dynamics of the machine to be controlled. The electromagnetic conversion and coupling are depicted by a multi-physical coupling element (overlapped circles). The IM is controlled by using indirect vector control method organized in the inversion-based control scheme with the control (light blue parallelograms) and estimation (purple filled, blue lines) blocks. The common shaft of the IM and the DC machine is represented by an accumulation element which reflects the mechanical dynamics of the machines. The mechanical power is transformed to the electrical power of the DC machine via an electromagnetic conversion block (multi-physical conversion element). Next, the DC machine armature is represented by an accumulation element. Then the chopper of the DC machine is depicted by a conversion element with a modulation tuning input. Finally, the DC/DC converter and the SCs for traction emulation are represented and controlled in the same scheme as the batteries emulation. The full-scale model of the traction subsystem (purple blocks) and its control and strategies impose the references via power adaptation blocks.

The experimental system parameters are given in Table 3.3. Figure 3.29 is the photo of the setup in the laboratory. The software control panel is built in dSPACE ControlDesk as shown in Figure 3.30.

Table 3.3: Reduced-scale power HIL system parameters for the battery/SC hybrid truck.

Parameters		Values
Induction machine (wound rotor, 400 V – 50 Hz – 1.5 kW)		
Stator resistance	r_s	7.7 Ω
Rotor resistance (transformed to stator side)	r_r'	0.264 Ω
Mutual inductance	L_m	0.1061 H
Stator cyclic inductance	L_s	0.7090 H
Rotor cyclic inductance	L_r	0.0189 H
Number of poles pairs	p_p	2
Moment of inertia (common with DC machine)	J	0.00432 kgm^2
DC machine (separated excitation: 220 V – 0.6 A)		
Nominal voltage	$U_{DCM\ nom}$	220 V
Nominal current	$I_{DCM\ nom}$	9 A
Nominal speed	$n_{DCM\ nom}$	1500 rpm
Armature resistance	r_{arm}	3.6 Ω
Armature inductance	L_{arm}	49.3 mH
SCs for the batteries and traction emulators		
SCs capacitance	$C_{SC\ bat/trac}$	260 F
SCs nominal voltage	$u_{SC\ bat/trac\ nom}$	108 V
SCs subsystem		
SCs capacitance	C_{SC}	7.75 F
SCs nominal voltage	$u_{SC\ nom}$	120 V
SCs internal resistance	r_{SC}	146 mΩ
Inductor		
Inductor inductance	L	0.795 mH
Inductor parasitic resistance	r_L	0.20 Ω
Inductor of the batteries emulator		
Inductor inductance	$L_{bat\ emu}$	0.800 mH
Inductor parasitic resistance	$r_{L\ bat\ emu}$	0.20 Ω
Inductor of the traction emulator		
Inductor inductance	$L_{trac\ emu}$	0.831 mH
Inductor parasitic resistance	$r_{L\ trac\ emu}$	0.17 Ω
DC bus capacitors of the batteries and traction emulators		
Capacitor capacitance	$C_{bat/trac\ emu}$	4400 µF

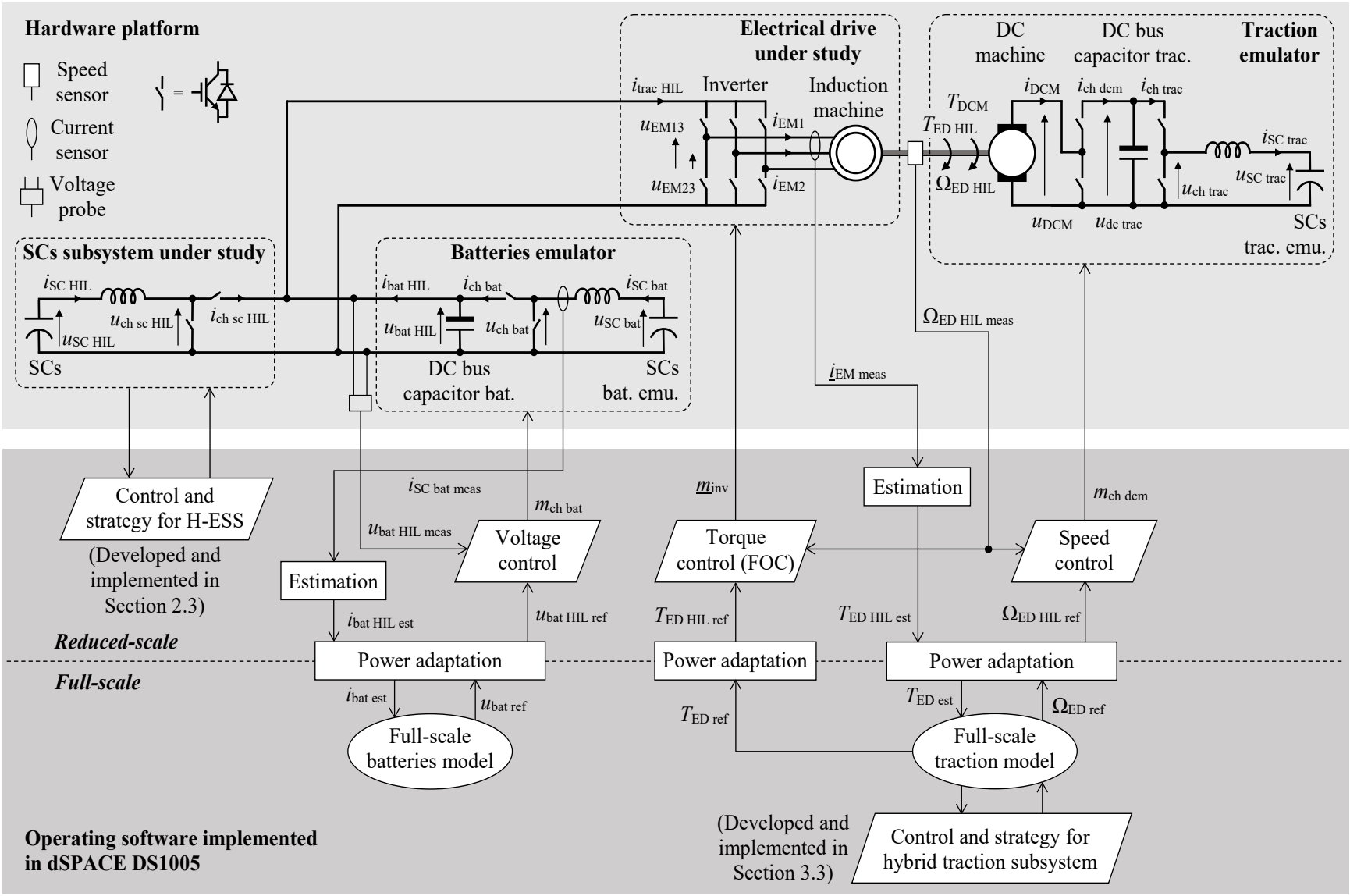

Figure 3.27: Experimental system configuration for the battery/SC hybrid truck.

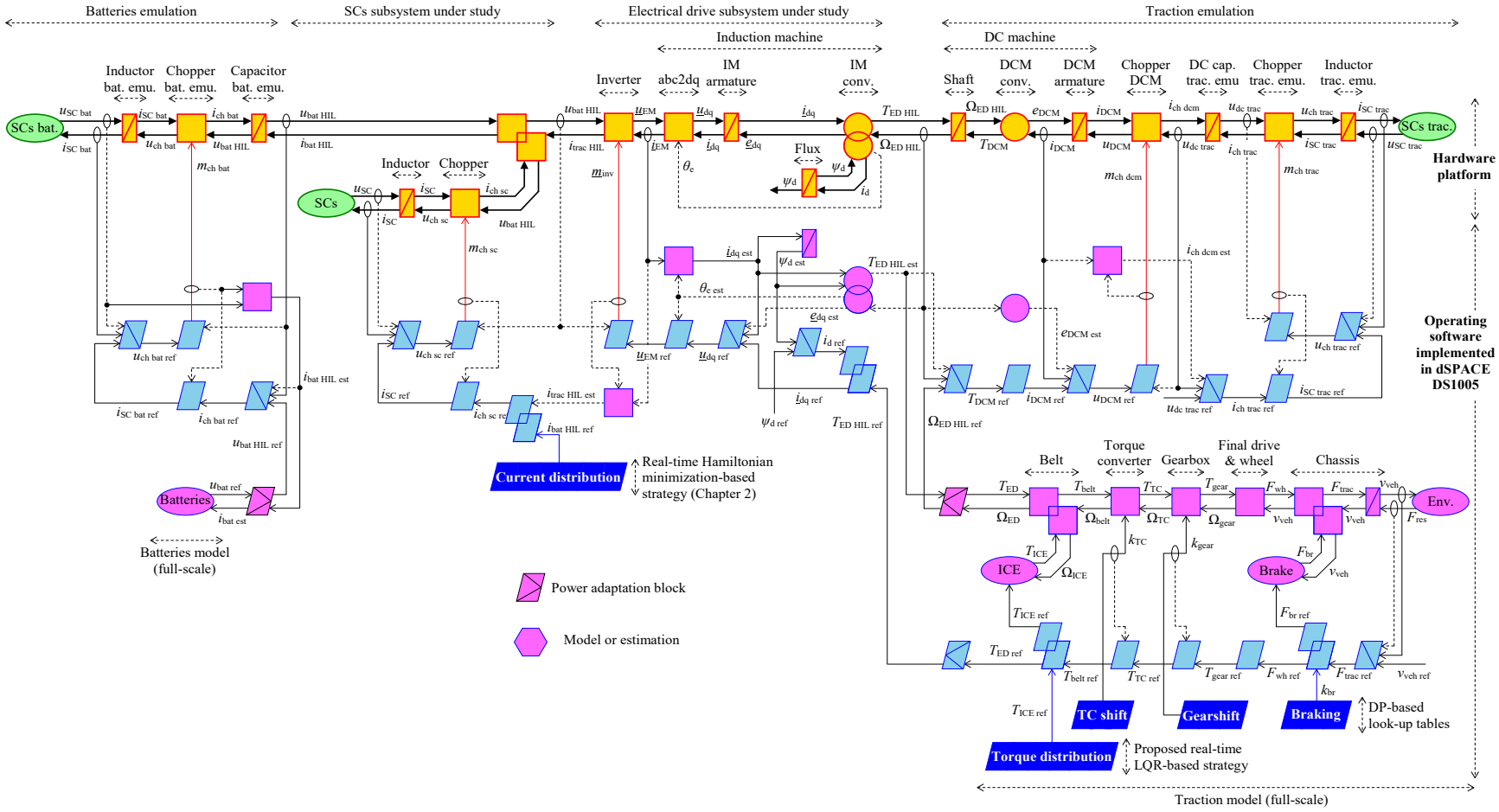

Figure 3.28: EMR of the reduced-scale power HIL experimental system for the battery/SC hybrid truck.

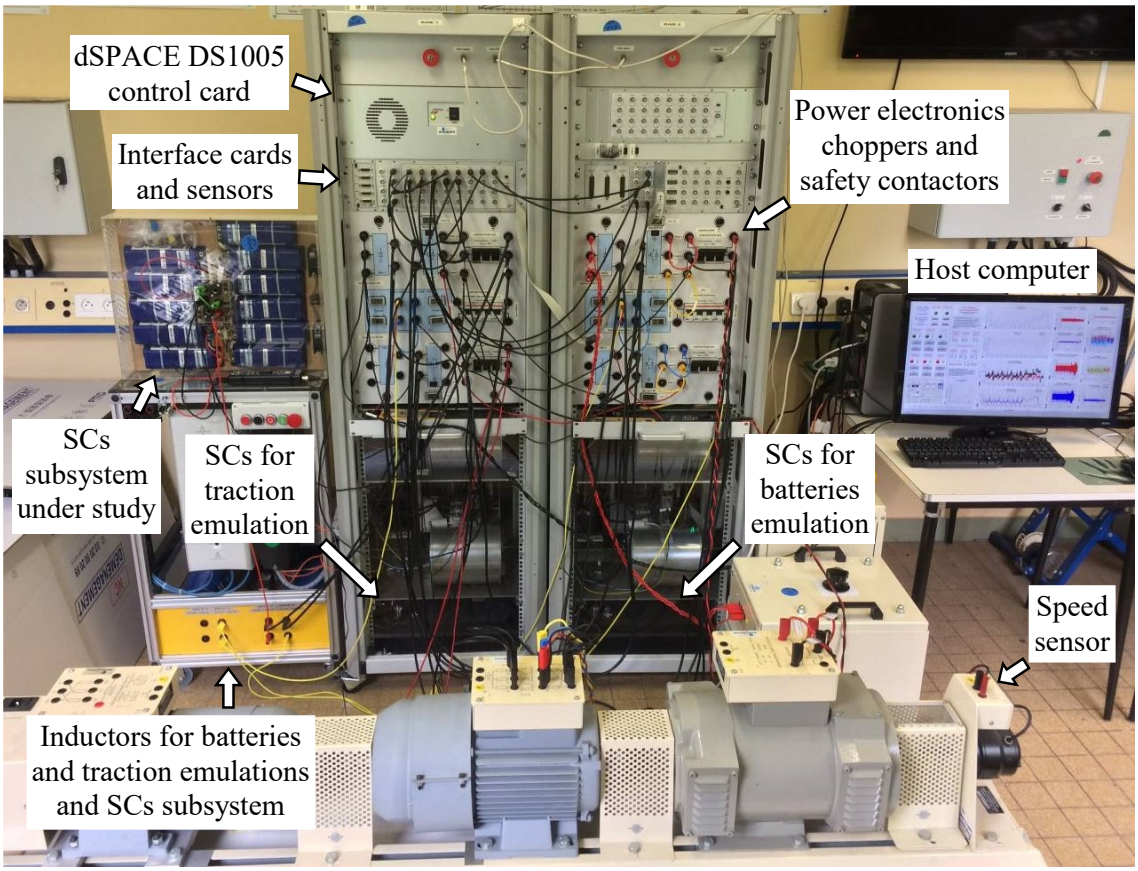

Figure 3.29: Experimental test bench for the battery/SC hybrid truck.

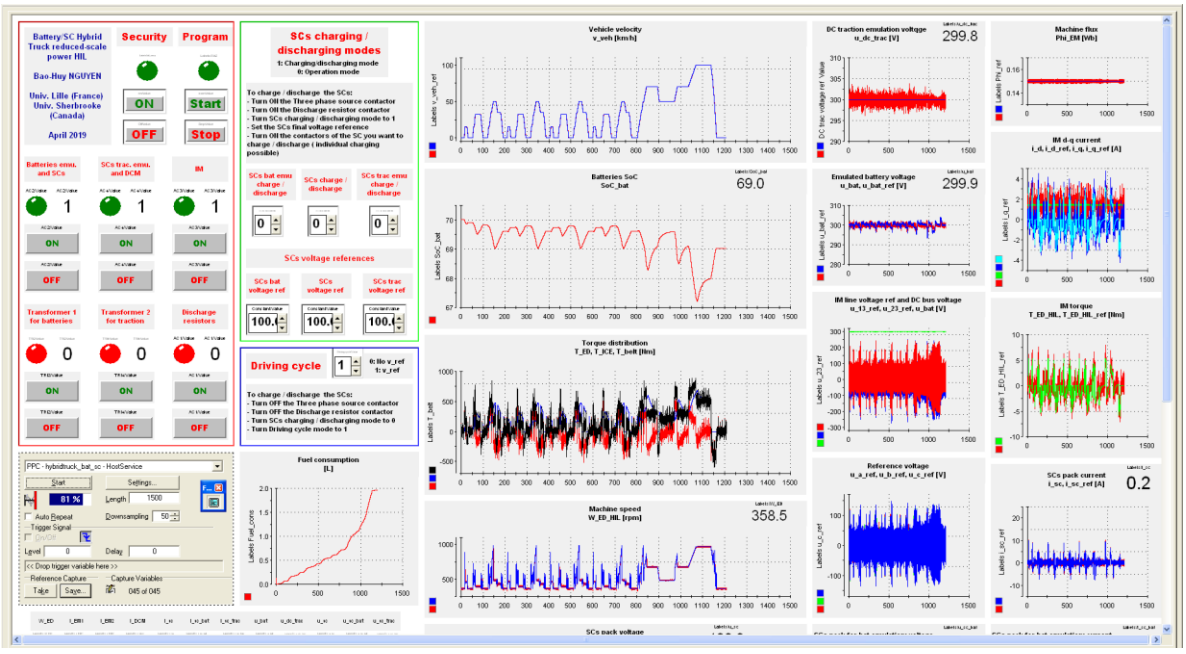

Figure 3.30: Control panel of the experimental system in dSPACE ControlDesk.

3.5.2. Results and discussions

The main results are presented and discussed in this subsection. Additional results are given in Appendix A.5, see Figure A.10 and Figure A.11.

The full-scale model of the traction subsystem is simulated in real-time in the dSPACE rapid prototyping card. The vehicle velocity v_{veh} is controlled by an IP controller to follow its reference $v_{\text{veh ref}}$ as shown in Figure 3.31.

During the driving cycle, the gearbox is shifted by a DP-based look-up table which causes the electrical drive speed, and therefore also the ICE speed, as shown in Figure 3.32. The rotational speed is scaled with the ratio of 1.8 due to the limitations of the electrical machine used for the experiments. The left axis, in blue, indicates the experimental results, while the right axis, in red, shows the simulation results. A period from 580 s to 780 s is zoomed in to show the results in more details. The experimental speed matches with the simulation. Some small differences appear when the engine is shifted too fast. It is because the DP-based gearshift strategy is developed with the assumption that the gearbox can be shifted immediately without any delay. Figure 3.33 presents the emulated batteries voltage which slightly differs from its simulation counterpart.

The results of electrical drive torque with the proposed LQR-based torque distribution strategy are plotted in Figure 3.34. The torque is scaled 80 times by considering the power limitation of the experimental IM drive. The experimental and simulation torques are kept within the boundaries of the electrical drive torque limitations. These torques are the functions of the batteries SoCs plotted in Figure 3.35. It is seen that the evolution of the experimental SoC follows the simulation one. The low efficiency of the IM drive, including mechanical losses by friction, losses of the IM itself, and leakage currents of the inverter causes some gaps between experimental and simulation results. However, the experimental evolution of the estimated batteries SoC follow the simulation one. That confirms the LQR-based strategy works properly in real-time.

Figure 3.36 shows the batteries currents. The difference between the experimental and simulation results are more in the negative quadrant than that in the positive one. Due to the high losses in the regenerative mode, even the machine produces high negative torque, only low negative current regenerated. But in the traction mode, the experimental results fit well with the simulation one. Figure 3.37 also demonstrates the matched results between the power HIL experiment and the computer simulation. In which, the SCs voltage evolution is limited between the higher and lower boundary. Thus, the Hamiltonian minimization-based current distribution strategy proposed in Chapter 2 is confirmed to work in real-time for the H-ESS of the parallel hybrid delivery truck.

The software program of the experiments is implemented in the dSPACE DS1005 card with the sampling time of $T_s = 0.2$ ms. In fact, most of the computational resource of the card is devoted for the complex control schemes of the batteries and traction emulators and for the full-scale model of the traction subsystem. Very little computational effort is required for performing the LQR-based strategy. That proves the real-time ability of the proposed EMS which is the main objective of the experiments.

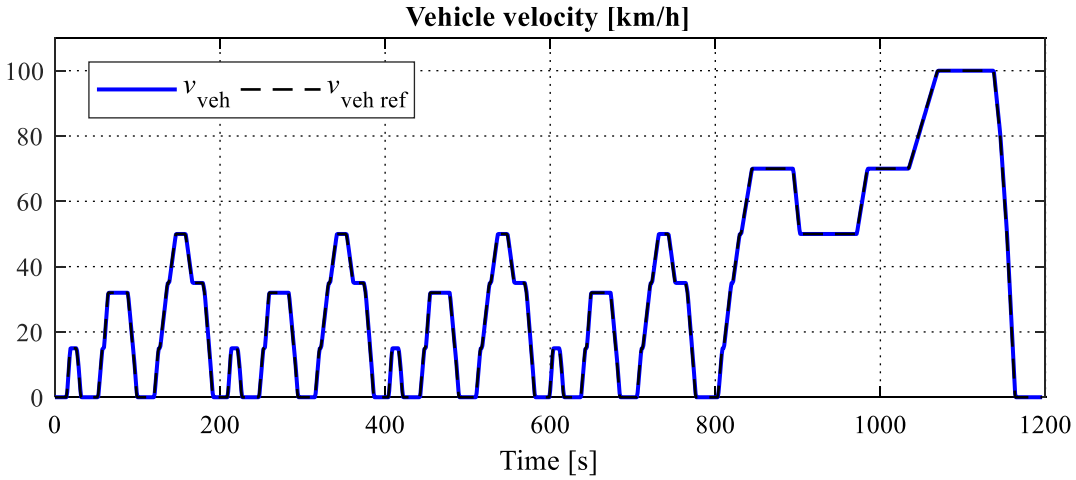

Figure 3.31: (Experimental results) vehicle velocity obtained by real-time simulation in dSPACE DS1005 card.

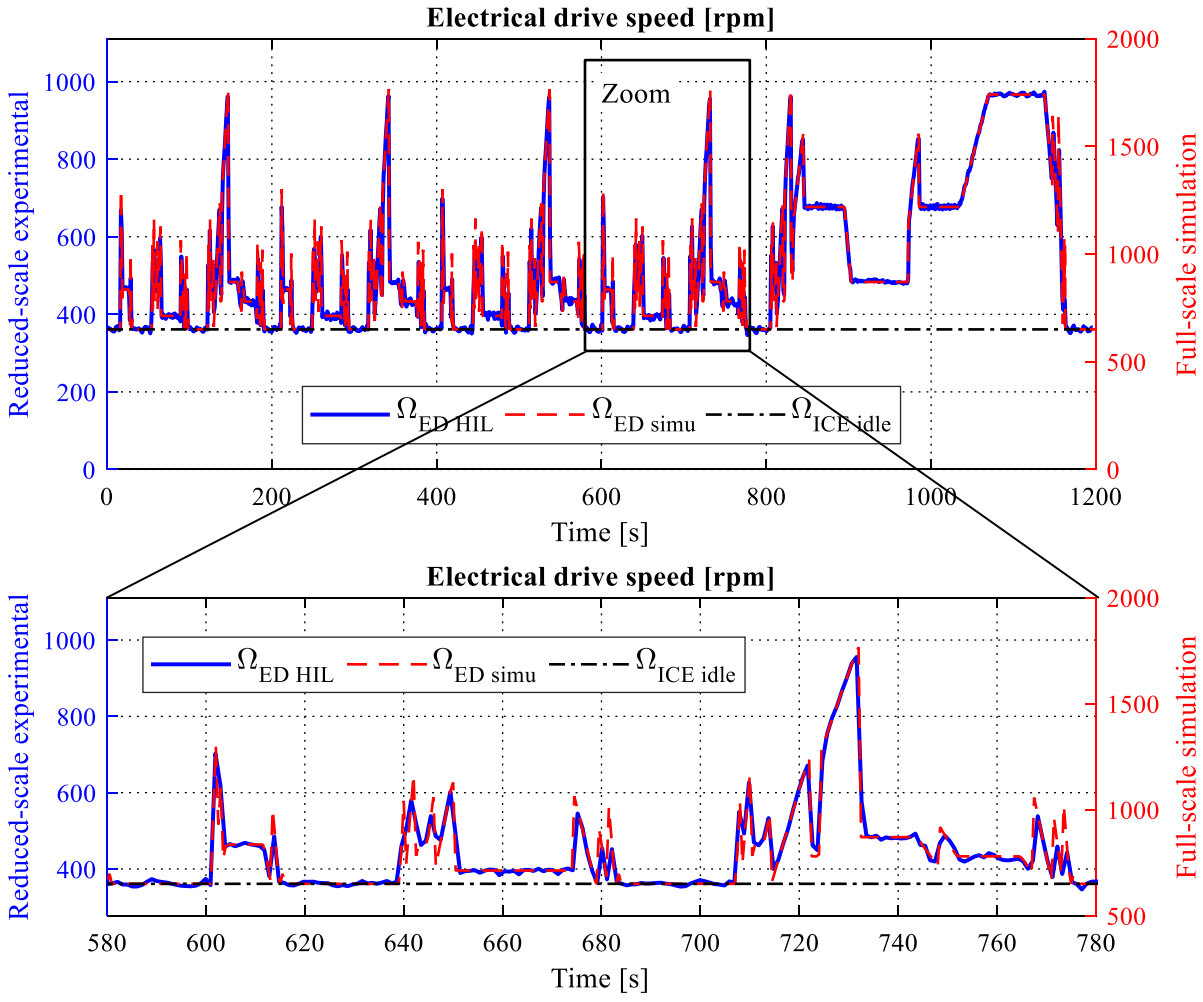

Figure 3.32: (Experimental results) electrical drive speed (also emulated ICE speed) with the DP-based gearshift strategy.

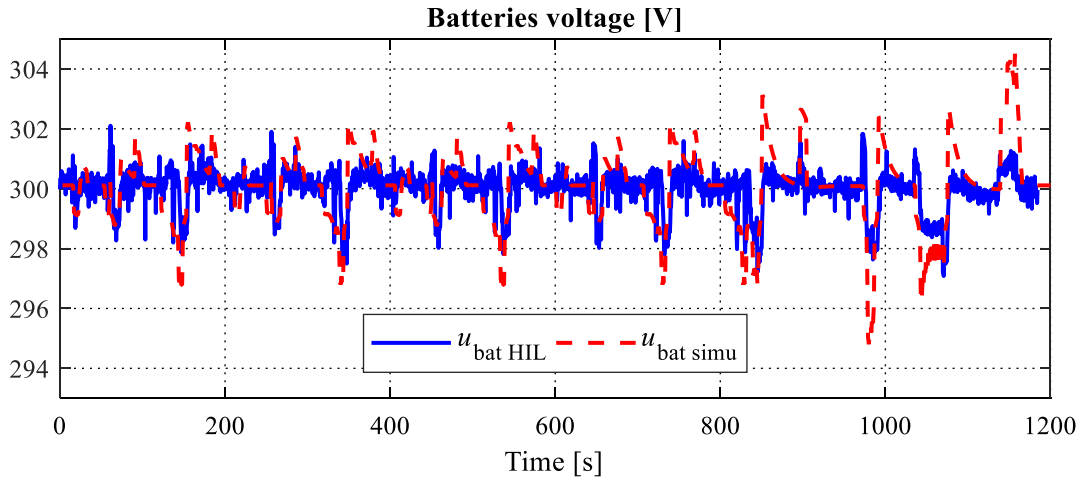

Figure 3.33: (Experimental results) batteries voltage.

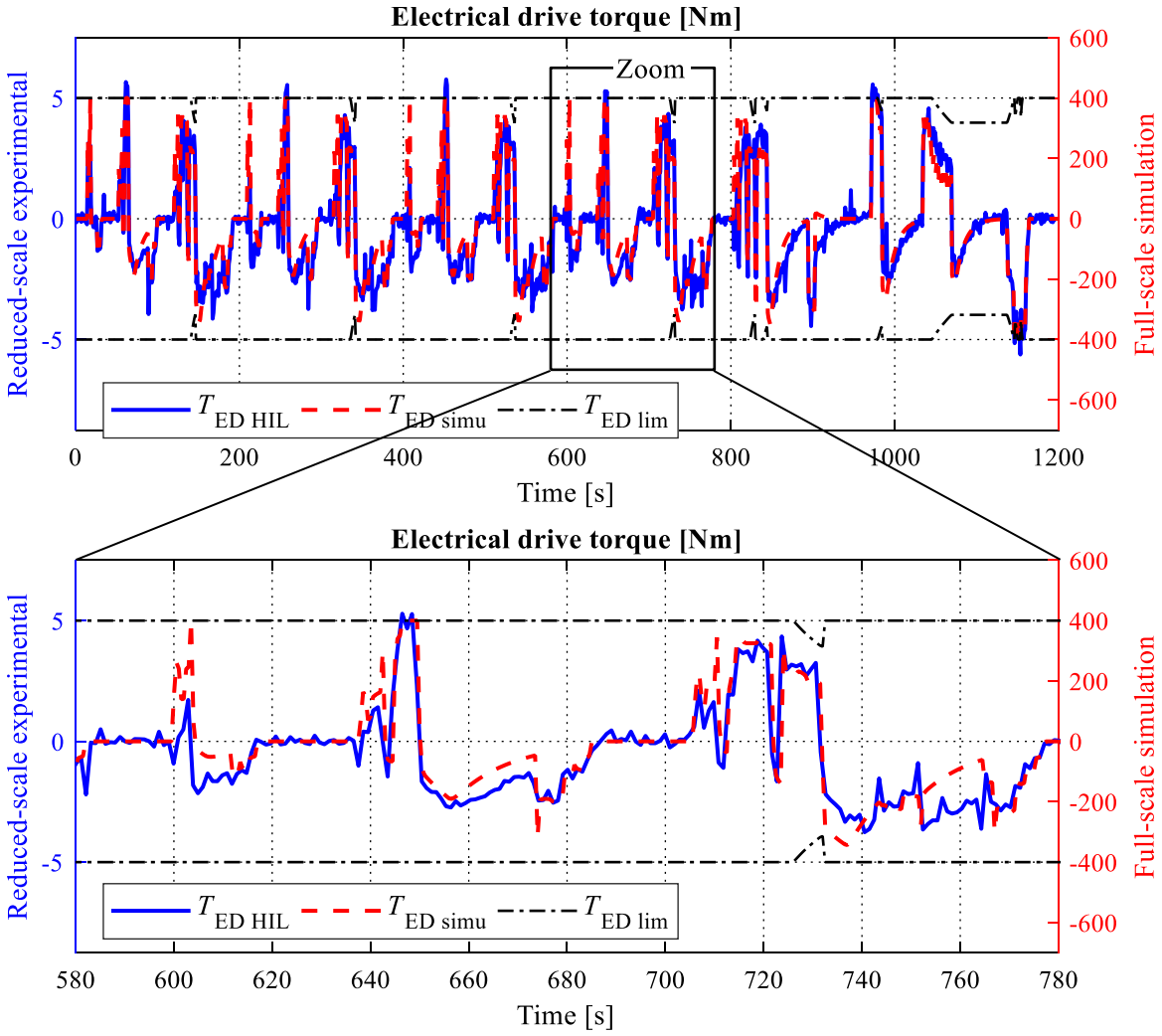

Figure 3.34: (Experimental results) electrical drive torque with the proposed LQR-based torque distribution strategy.

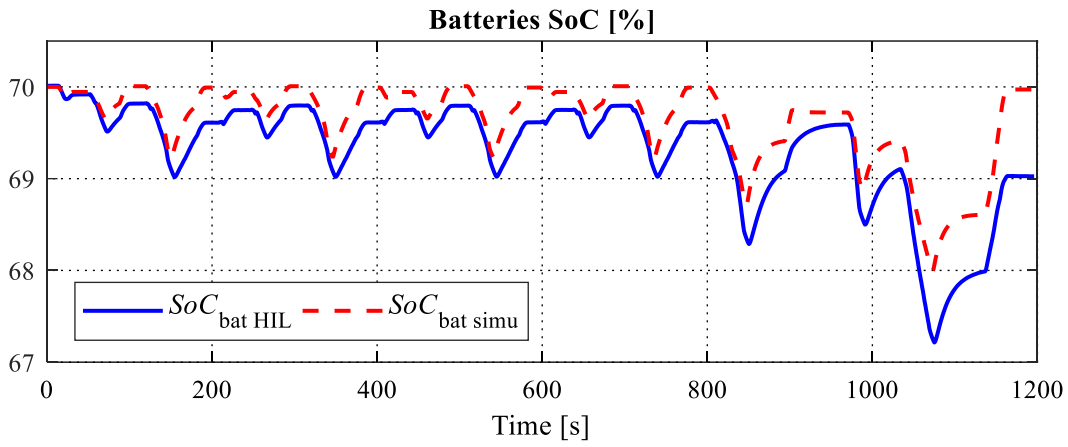

Figure 3.35: (Experimental results) batteries SoC with the proposed LQR-bases strategy.

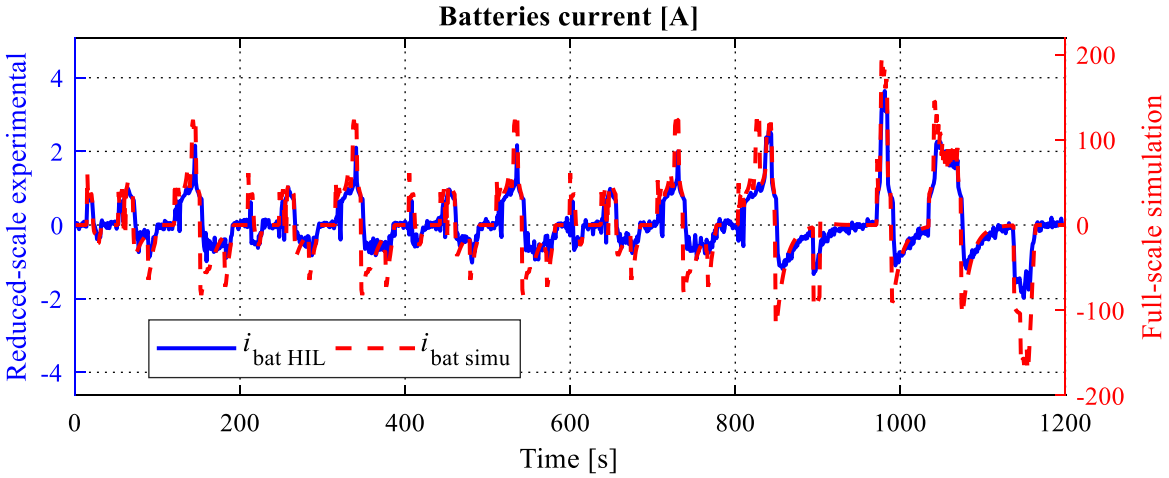

Figure 3.36: (Experimental results) batteries current with the Hamiltonian minimization strategy (proposed in Chapter 2).

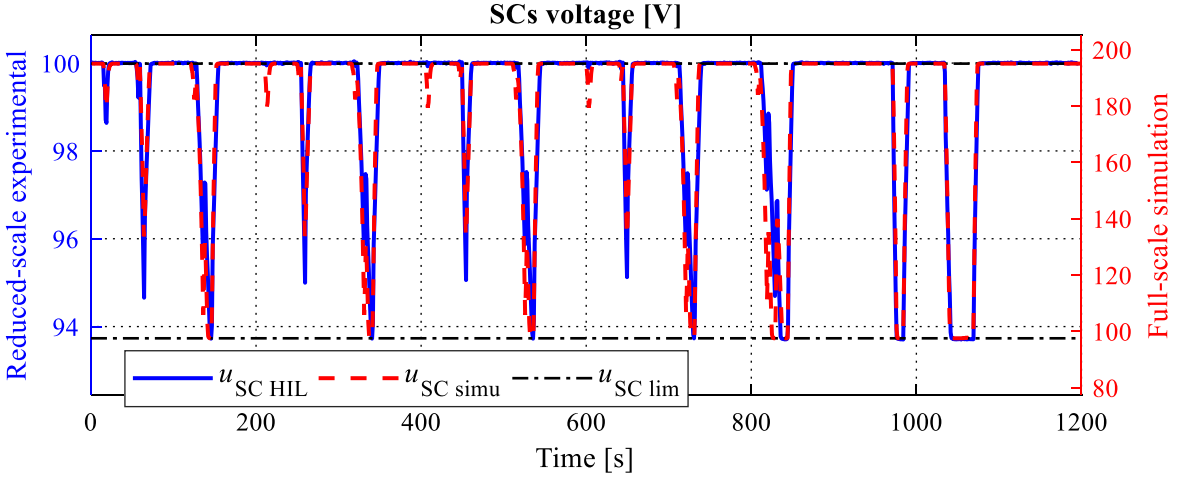

Figure 3.37: (Experimental results) SCs voltage with the Hamiltonian minimization strategy (proposed in Chapter 2).

3.6. Conclusion

In this chapter, a novel real-time torque distribution strategy has been proposed and validated for a parallel hybrid truck supplied by a battery/SC H-ESS. Firstly, the truck has been modeled and controlled considering its full dynamical behaviors. To overcome the complexity of the system, the model, represented by using EMR, has been reduced to obtain a suitable mathematical model. Then optimal control theory has been applied to this reduced mathematical model to deduce the real-time EMS.

To avoid the requirement of using ICE fuel consumption data which is hard to achieve in real-world applications, the cost function has been reformulated. Furthermore, the variation of the batteries SoC has been added to the function as a penalty. Eventually, the cost is in form of a quadratic function of the control and the state variables. Since the reduced model is linear, the LQR method has been applied to obtain the optimization-based control law of the ICE torque reference. The obtained strategy is a closed-loop control scheme of the batteries SoC which is suitable to be implemented in real-time. The development procedure and the strategy implementation require only basic system parameters such as the batteries capacitance and the belt ratio. The proposed EMS is therefore realistic for real-world applications.

The new strategy has been compared to the DP-based off-line optimal solution and the case of the conventional ICE-only truck. Simulation results have verified the performances of the LQR-based strategy. Moreover, reduced-scale power HIL simulation has been used to validate the proposed EMS in experiments. Although the low efficiency of the laboratory setup causes some gaps between simulation and experimental results, it has been figured out that the LQR-based strategy works properly in real-time.

General conclusion

Summary

The objective of the thesis is to develop real-time optimization-based energy management strategies (EMSs) for electric and hybrid vehicles. Two types of hybridizations have been addressed in the thesis: combining battery and supercapacitor (SC) to form a hybrid energy storage subsystem (H-ESS); and combining internal combustion engine (ICE) and electrical machine (EM) to form a hybrid traction subsystem. Based on that, two systems have been studied: a battery/SC electric vehicle (EV) and a battery/SC parallel hybrid truck.

To systematically develop the EMSs, the thesis has been conducted by following a unified approach using Energetic Macroscopic Representation (EMR) and optimal control theory. Firstly, the system is modeled and represented by EMR taking into account all the dynamical behaviors. Then, the inversion-based control scheme is deduced to control the system. Next, the system model is reduced to focus on the dynamics concerned by the EMS at the supervisory level. A mathematical model is then deduced from this reduced model representation. Thereafter, optimal control theory is applied to this reduced model to deduce an analytical control law for a real-time EMS. Due to the fact that real-time strategy is always sub-optimal, an off-line optimal benchmark is of interest for evaluating the strategy performances. Dynamic programming (DP) is employed for this purpose. The real-time EMS is then compared to the DP-based optimal solution by simulation. Finally, the real-time capability of the EMS is experimentally examined by using reduced-scale power hardware-in-the-loop (HIL) simulation. DP and HIL are organized by using EMR. This approach has been consistently followed to develop and validate the EMSs in the thesis.

The aforementioned approach has been figured out in Chapter 1 after the thesis context and a literature review were addressed. The thesis has been conducted in a global context of fuel resource shortage and environmental care. The interests of electric and hybrid vehicles and energy management problems have been figured out within this context. Next, the position of the thesis has been clarified within the scientific network MEGEVH, in a collaboration between the laboratories L2EP and e-TESC, and in the CE2I and Mitacs Accelerate programs. Then the chapter has presented a review on state-of-the-art of EMS development methods for electric and hybrid vehicles. Finally, the objective and approach of the thesis have been pointed out.

Chapter 2 has been dedicated to develop and validate a real-time optimization-based strategy for a battery/SC subsystem in an electric car. The traction subsystem and the H-ESS have been modeled, represented, and controlled with EMR. Since the study focuses on energy management of the H-ESS, the traction subsystem has been considered as an equivalent current source by assuming that its control works perfectly. Moreover, a part of the H-ESS has been reduced assuming its ideal control. That leads to the deduction of the mathematical model of the studied system. The Hamiltonian minimization condition of Pontryagin's minimum principle (PMP) has been then applied to the reduced mathematical model. That has directly conducted an analytical control law containing the measurement of the SCs voltage as a feedback. The control law can

therefore serve as a real-time EMS without requirement of any additional adaptive scheme of the state variable as conventional λ-control method. The proposed EMS has been then compared with the traditional real-time strategies, the DP-based off-line optimal benchmark, and the case of a pure battery EV. The comparative study, carried out by simulation, has confirmed the advantages of the proposed Hamiltonian minimization-based strategy. The new real-time EMS has been then experimentally validated by using reduced-scale power HIL simulation. SCs banks and power electronics bidirectional DC/DC converters have been utilized to emulate the batteries, the traction subsystem, and to examine the SCs subsystem under study. The good match between experimental and simulation results have verified the ability of power HIL simulation in emulating the studied system. The experiments have confirmed the real-time ability of the proposed strategy.

The study in Chapter 3 has developed and validated a real-time optimization-based EMS for a battery/SC parallel hybrid truck. The semi-active configuration of the H-ESS has been inherited as it is in Chapter 2. This chapter has focused in energy management of the parallel hybrid traction subsystem of the truck. Firstly, modeling, EMR, and control scheme of the truck have been developed taking into account the full system dynamics. Then, model reduction steps have been applied by decomposing the strategies and by assuming properly developed control and strategies. As a consequence, the reduced model of the studied system has been obtained with the batteries SoC as the state variable. Based on that, the reduced mathematical model is conducted. Moreover, in order to avoid the disadvantage of using fuel consumption data map as previous works, the optimal control problem has been reformulated to minimize the ICE torque. On the other hand, the SoC variation has been charged as a penalty to ensure batteries charge sustaining. As a result, the problem is a linear system with a quadratic cost function of the control and state variables. Thus, linear quadratic regulation (LQR) has been applied to obtain an analytical solution which is a closed-loop control of batteries SoC. That is the proposed real-time optimization-based torque distribution strategy. Then the EMS has been evaluated by comparing the DP-based off-line optimal solution and the case of conventional ICE truck. The simulation results have confirmed the effectiveness of the strategy in both fuel consumption reduction and batteries charge sustaining. Furthermore, reduced-scale power HIL experiments has validated the real-time ability of the proposed strategy. The configuration of batteries emulation and the SCs subsystem under study have been remained as they are in Chapter 2. An induction machine and a voltage-source inverter have been used as the electrical drive under study. The traction subsystem has been emulated by using a DC machine, a chopper for the machine, a bidirectional DC/DC converter, and a SCs bank. The experimental results have verified that the proposed EMS works properly in real-time. Some differences between the simulation and experimental results have been reported due to the low efficiency of the experimental setup.

To summary, a unified approach has been used in the thesis to develop and validate real-time optimization-based EMSs for an H-ESS-based EV and an H-ESS-based parallel hybrid truck. The two novel strategies of current distribution and torque distribution have been validated via simulations and experiments. These proposed EMSs are simple but effective that can be suitable for implementing in on-board platforms in real-world applications.

Perspectives

The perspectives can be figured out in short-term and long-term outlooks.

There are short-term future works can be carried out. Firstly, there exist notable gaps between experimental and simulation results in Chapter 3, meanwhile the results fit very well in Chapter 2 (see more in Appendix A.4 and A.5). It is because the experimental setup used in Chapter 2 is fast and high-efficiency enough to emulate and examine the full-scale EV. Whereas the efficiency of the experimental setup used in Chapter 3 is much lower and that of the full-scale truck. It should be noted that the full-scale system is modeled with the assumption of high efficiency of the PMSM drive (96% in the traction and 90% in the regenerative mode). Meanwhile, to emulate a high-efficiency system, higher-efficiency devices should be used. Unfortunately, only a low-efficiency IM drive is available in the laboratory. That is why there are gaps between the experimental and simulation results. Thus, experiments with a higher-efficiency setup would better examine the studied system. Moreover, full-scale HIL simulation, in which there is no need of power adaptation, is also of interest.

Secondly, it is seen that even the DP optimal strategy does not save so much fuel of the truck in Chapter 3. The reason might be on the design issue, which is out of the scope of this thesis. However, testing the proposed strategy with a system that can save more fuel could give some more insights. Furthermore, scaling down the ICE in the hybrid traction subsystem to compare with the full-size ICE of the conventional truck could be a fairer comparison.

In a long-term perspective, several research directions could be of interest. Firstly, the decomposition approach has been employed to deal with the multi-objective problem of the battery/SC hybrid truck. This approach has been useful to develop simple but effective strategies. The composition approach, in which a global strategy manages the whole system with multiple objectives, is complex and thus difficult to realized. However, which one is really better? Is there any way to develop such global EMS that is also simple but effective? They are still open questions to be tackled.

Secondly, the work developed in this thesis also shows the limits of non-predictive methods. In Chapter 2, the co-state variable λ has been defined in three driving modes with the assumption that the driver knows the driving condition and can select the proper mode. In Chapter 3, it has been seen that the strategy could work better if it "knows" the driving cycle in advance. In real-world applications, the driving conditions are never known in advance; however, they could be predicted with certain accuracies. Hence, embedding the developed strategies in a predictive framework could improve their performances.

Finally, this thesis has addressed only one objective for each hybrid subsystem; whereas additional objectives can be considered (see Appendix A.2). In such a multi-objective approach, trade-offs between conflicted objectives are essential. For off-line EMSs, all the trade-offs can be taken into account which form the Pareto front of optimal solutions. Yet how to select "the best of the best" from these optimal solutions to serve as a single benchmark? Furthermore, for real-time EMSs, these trade-offs must be dealt with before implementing the strategies. So how to decide these priorities? Can the selections be beyond heuristic, i.e., no need of human expertise? They are also still open questions.

Appendix

A.1. Energetic Macroscopic Representation

Energetic Macroscopic Representation (EMR) is a graphical formalism for modeling and control of energetic systems initiated in 2000s [Bouscayrol 2000, 2013]. EMR is a tool to organize the system model and to develop the control scheme based on three principles.

The system model is represented, i.e., organized, based on the two principles:

- *Principle of causality:* the inputs and the outputs of an energetic system must follow the integral causality; in which the outputs are functional integrals of the inputs. The outputs are delayed with respect to the inputs. For example, a capacitor must have current as its input and voltage as it output since the capacitor voltage is an integral of the capacitor current. A model which imposes a voltage to a capacitor violates this principle of causality.

- *Principle of interaction:* the subsystems of an energetic system interact with each other via pairs of action and reaction variables; in which the product of these variables is the instantaneous power exchanged between these subsystems. For example, when a battery is connected to a resistor, they interact with each other by a pair of variables current and voltage. The battery imposes a voltage to the resistor as an action, while the resistor enforces a current to the battery as a reaction.

The control scheme is deduced from the model representation based on the *principle of inversion*. In which, the control is considered as a functional inversion of the model (see Subsection 2.1.3).

Table A.1 gives EMR elements, their pictograms, and their descriptions. More information and the EMR library can be found in the official website [EMR 2019]. It should be noted that the library is just MATLAB/Simulink^{TM} subsystems with masks to organize the simulation following the EMR rules. The developer has to build his/her own model and control inside each block (Figure A.1).

Table A.1: EMR elements (adapted from [Lhomme 2007]).

Element	Pictogram	Description
Power variable		Pair of action and reaction variables of system model; where s denotes output variable; e input variable. E.g., current and voltage, speed and torque, etc.
Signal variable		Mandatory signal variable in the control scheme; which is often control signal or output feedback in a closed-loop control.
		Optional signal variable; which is often disturbance measurement in the control scheme; or sometimes information in the system model.
Measurement		Measurement of variables for feedback control or disturbance compensation.
Source	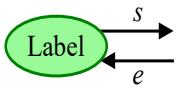	Terminal of the system, which supplies or dissipates energy. Name of the source can be written in the label. E.g., battery, grid, environment, etc.
Accumulation	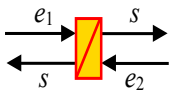	Accumulation of energy; introduce delay to the system; represent dynamics of the system. E.g., an inductor which cause current dynamical delay.
Mono-physical conversion	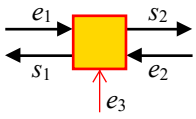	Mono-domain conversion of energy; can be with or without tuning input. E.g., an inverter converts electrical DC energy to electrical AC energy (and vice versa) with modulation functions; a wheel converts mechanical energy to mechanical energy (and vice versa) without tuning input.
Multi-physical conversion	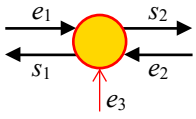	Multi-domain conversion of energy; can be with or without tuning input. E.g., an electrical machine converts electrical energy to mechanical energy (and vice versa) with reference input.
Coupling	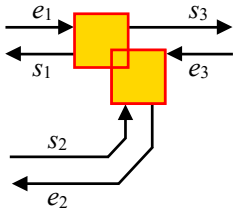	Mono-domain coupling or distribution of energy between more than two subsystems. E.g., parallel connection between two electrical energy storages to supply an inverter of an electrical drive.

	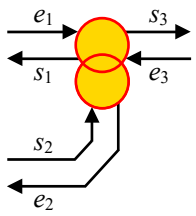	Multi-domain coupling or distribution of energy between more than two subsystems. E.g., electrical power (current) couples with magnetic power (flux) to produce mechanical power (torque) in electrical machine; whereas machine speed couples with flux to produce EMF in the machine.
Accumulation inversion	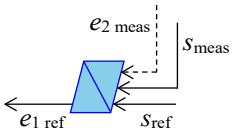	Indirect inversion of the accumulation elements to control its output; which is a closed-loop control with reference, output feedback (mandatory), and disturbance rejection (optional). E.g., closed-loop speed control.
Conversion inversion	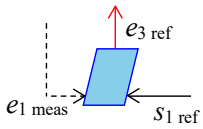	Direct inversion of energy conversion element; the output is the tuning input of that conversion element. E.g., PWM of an inverter.
	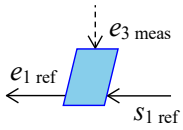	Direct inversion of energy conversion element; the output is the reference for the next control block. E.g., calculation of current reference from torque reference in machine drive.
Coupling inversion	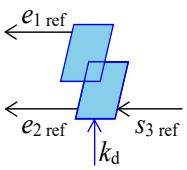	Direct inversion of coupling element (both mono- and multi-domain). A distribution or weighting factor must be introduced to manage the power flow. E.g., to distribute torques in parallel HEVs.
Estimation or model	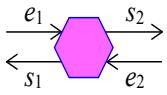	Model copy of the system implemented in the control program; playing the role of estimation of reference model. (Hexagon means any possible block.) E.g., to estimate EMF of electrical machine from its speed and flux.
Strategy		Strategy block to impose reference, distribution, and/or weighting factors to the control scheme. E.g., flux-weakening strategy to impose d-axis current reference in AC machine drive.
Power adaptation	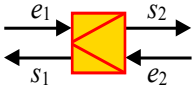	To scale power between subsystems. E.g., a batteries pack can be considered as a scaled equivalence of a battery cell assuming that all the cells behave in the same way. The second example is to scale between a hundred-Nm-torque electrical drive of an EV and a ten-Nm-torque drive in laboratory to emulate the EV.
	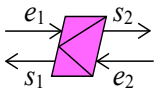	

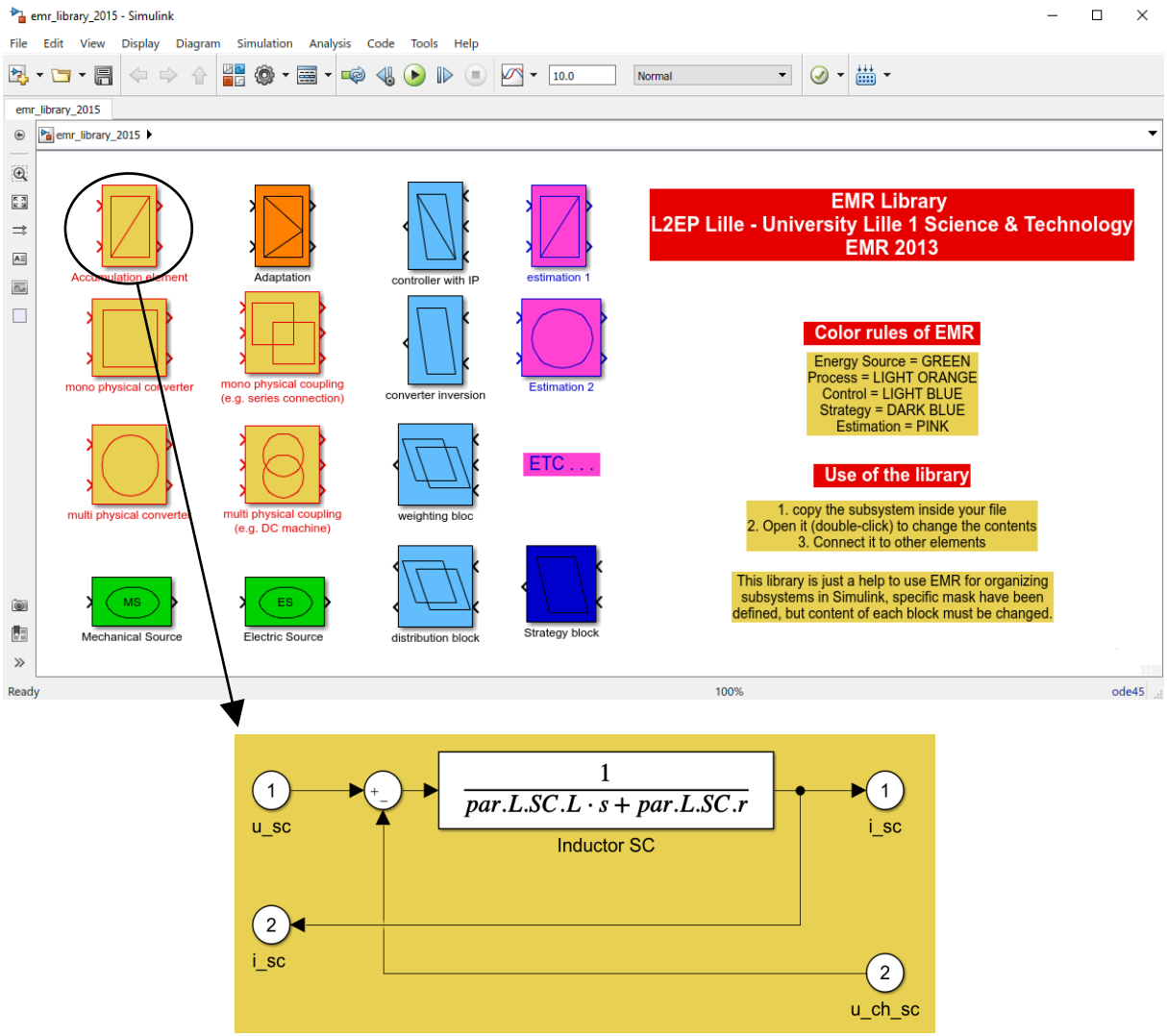

Figure A.1: MATLAB/Simulink™-based EMR library [EMR 2019].

A.2. Additional study on a multi-objective approach for optimal energy management of hybrid energy storage subsystems for electric vehicles

The aim of this work is to develop an off-line multi-objective global optimal EMS for the battery/SC H-ESS to generate a Pareto front benchmark. An approach for developing multi-objective EMS is proposed using EMR which is a graphical formalism [Bouscayrol 2013]. The multi-objective optimization problems can be treated by using the hierarchical structure of strategy [Trovão 2013a]. Weighted sum method is used for scalarization of multiple cost functions [Deb 2014; Kim I. 2006]. Global optimal solutions for the benchmark are deduced by using DP. The EMR-based backward formalism proposed in [Horrein 2015a] is used for integration in DP problem solving. The DP-based Pareto front can serve as a benchmark for evaluating the performances of real-time EMS. In this study, the well-known filtering-based strategy is used as an example with a range of cut-off frequencies.

a. Multi-objective cost functions

Dealing with multiple cost functions is the field of multi-objective optimization [Antunes 2016; Deb 2014]. There are two main groups of multi-objective optimization methods: vectorization and scalarization [Deb 2014; Logist 2010]. It is pointed out that the vectorization is not always suitable for optimal control while the latter group has advantages [Logist 2010]. The vectorization method is more appropriate for optimal design/sizing of the energy storage systems, e.g., a well investigated design in [Song 2014].

The vector of the n cost functions is expressed as:

$$\underline{J} = [\, J_1 \ \cdots \ J_n \,]^T. \tag{A.1}$$

There are several techniques to scalarize the multiple cost functions, in which the most used is the weighted sum method [Deb 2014; Kim I. 2006]. Weighting factors α_i are given to each cost function, then summed to create a single multi-objective cost function. Moreover, it is necessary to make the cost functions dimensionless due to the different units of the performance measurements. Normalization factors are therefore introduced. The choices of these factors depend upon the detailed applications. The weighted sum cost function J_{ws} is therefore expressed as follows:

$$\begin{aligned} J_{\mathrm{ws}} = \alpha_1 \frac{J_1}{J_{1\,\mathrm{nom}}} + (1-\alpha_1) \Bigg\{ \alpha_2 \frac{J_2}{J_{2\,\mathrm{nom}}} + \cdots \\ + \left[\alpha_{n-1} \frac{J_{n-1}}{J_{n-1\,\mathrm{nom}}} + (1-\alpha_{n-1}) \frac{J_n}{J_{n\,\mathrm{nom}}} \right] \Bigg\} \end{aligned} \tag{A.2}$$

where $0 \leq \alpha_i \leq 1$ and $J_{i\,\mathrm{nom}}$ is the normalization factor with $i \in \{1, \ldots, n-1\}$.

In this study, the costs of batteries degradation and SCs system losses are addressed. First, the cost functions of the batteries stresses and SCs system losses are defined. Then, the

scalarization of these multi-objective cost functions is carried out by scalarization. The weighted sum method is used with one weighting factor α.

Batteries stresses

There are a number of stress factors affecting on the batteries life-time [Barré 2013]. For this H-ESS where the battery is the main source, the batteries current is suitable to be examined. The rms, the peak, and the standard deviation of the battery current are sufficient to be considered, e.g., [Florescu 2014; Gomozov 2017; Song 2015].

The rms current causes the long-term stress on the batteries. This is the most used criterion as can be found in the aforementioned literature. It is depicted by:

$$I_{\text{bat rms}} = \sqrt{\frac{1}{t_\text{f} - t_0}\int_{t_0}^{t_\text{f}} i_{\text{bat}}^2 dt}. \tag{A.3}$$

Furthermore, it is figured out that the high frequencies of batteries current cause harmful effects on their life-time [Savoye 2012; Uddin 2016]. A performance index should be defined to investigate this stress. The standard deviation is a statistical measure that indicates the variation of the studied data set. Hence, this index is used to reflect the fluctuation of i_{bat}. It is computed by:

$$\sigma_{\text{bat}} = \sqrt{\frac{1}{N}\sum_{k=1}^{N}[i_{\text{bat}}(k) - \mu_{\text{bat}}]^2}\,; \tag{A.4}$$

in which μ_{bat} is the mean value of batteries current given by:

$$\mu_{\text{bat}} = \frac{1}{N}\sum_{k=1}^{N} i_{\text{bat}}(k). \tag{A.5}$$

Here, statistical performance indexes are utilized. Hence the discrete values are used to calculate instead of the continuous ones. N is the number of the data points of the time series $i_{\text{bat}}(k)$.

The above two criteria measure the long-term impacts of batteries current on the degradation. Short-term extremal effects should be also considered to complete the batteries stresses examination. The peak of batteries current is therefore taken into account [Florescu 2014; Gomozov 2017]. It is given by:

$$I_{\text{bat peak}} = \max(i_{\text{bat}}). \tag{A.6}$$

Hence, a performance index for evaluation of battery stresses can be given by:

$$J_{\text{bat}} = k_{\text{rms}} \frac{I_{\text{bat rms}}}{I_{\text{bat rms}}^{\alpha=0}} + k_{\text{std dev}} \frac{\sigma_{\text{bat}}}{\sigma_{\text{bat rms}}^{\alpha=0}} + k_{\text{peak}} \frac{I_{\text{bat peak}}}{I_{\text{bat peak}}^{\alpha=0}} \tag{A.7}$$

where the denominators are the normalization factors calculated with $\alpha = 0$; k_{rms}, $k_{\text{std dev}}$, and k_{peak} are the weighting factors given to the three performance indexes, respectively. The sum of these weighting factors should equal unit. Here, the normalizations are meant to deduce the dimensionless per unit values of the stress factors for comparisons. For having the cost function $J_{\text{bat}} \leq 1$, the worst case of these factors should be used. That is the reason why the normalization factors are calculated with $\alpha = 0$. Besides, the weighting factors indicate the roles of the stress factors. In fact, the comprehensive impact of stresses factors on the batteries life-time is very complicated [Sarasketa-Zabala 2016]. For energy management evaluation, they can be considered equally [Florescu 2014; Gomozov 2017]. Thus, a common value one-third is given to these weighting factor as follows:

$$J_{\text{bat}} = \frac{1}{3}\left(\frac{I_{\text{bat rms}}}{I_{\text{bat rms}}^{\alpha=0}} + \frac{\sigma_{\text{bat}}}{\sigma_{\text{bat rms}}^{\alpha=0}} + \frac{I_{\text{bat peak}}}{I_{\text{bat peak}}^{\alpha=0}}\right). \tag{A.8}$$

In fact, it is seen that the minimization of i_{bat}^2 will minimize the above performance index. Also, as mentioned in Subsection 2.1.4, the quadratic form is of interest for applying various optimization methods [Bryson 1975]. Hence, the batteries cost function used for calculating in DP program can be given by:

$$J_{\text{bat cal}} = \int_{t_0}^{t_f} i_{\text{bat}}^2 dt. \tag{A.9}$$

Supercapacitors subsystem losses

The losses of SCs subsystem are defined based on its current. Firstly, the SCs current causes the Joule losses on the series resistance of the SCs and the parasitic resistance of the inductor as follows:

$$E_{\text{SC loss}} = \int_{t_0}^{t_f} i_{\text{SC}}^2 (r_{\text{SC}} + r_{\text{L}}) dt. \tag{A.10}$$

Secondly, the high SCs current can cause the saturation of the inductor which reduces the performances and efficiency of the SCs system [Perdigão 2015; Song 2015]. Efficiency map carried out from rigorous equations in [Moreno 2006] shows that the efficiency of DC/DC converter dramatically falls due to the high SCs current. It is therefore reasonable to reduce the SCs peak current:

$$I_{\text{SC peak}} = \max(i_{\text{SC}}). \tag{A.11}$$

Like the batteries stresses, the performance index of the SCs subsystem losses can be defined by:

$$J_{\mathrm{SC}} = \frac{1}{2}\left(\frac{E_{\mathrm{SC\,loss}}}{E_{\mathrm{SC\,loss}}^{\alpha=1}} + \frac{I_{\mathrm{SC\,peak}}}{I_{\mathrm{SC\,peak}}^{\alpha=1}}\right). \tag{A.12}$$

The normalization factors of SCs system losses are calculated with $\alpha = 1$ which is their worst case due to the same reason of the batteries. The priority of 50% is given to each of the two losses factors to consider them equally.

The SCs calculation cost function for the numerical computation procedure is:

$$J_{\mathrm{SC\,cal}} = \int_{t_0}^{t_\mathrm{f}} i_{\mathrm{SC}}^2 dt. \tag{A.13}$$

Scalarization of multi-objective cost functions

The weighted sum cost function of the studied H-ESS for computation is expressed by:

$$J_{\mathrm{ws\,bat/SC}} = \alpha \frac{J_{\mathrm{bat\,cal}}}{J_{\mathrm{bat\,cal\,nom}}} + (1-\alpha)\frac{J_{\mathrm{SC\,cal}}}{J_{\mathrm{SC\,cal\,nom}}}; \tag{A.14}$$

in which the normalization factors can be defined as batteries and SCs rms currents in the cases $\alpha = 0$ and $\alpha = 1$, respectively. Thus, the calculation cost function for the studied battery/SC H-ESS is given as follows:

$$J_{\mathrm{ws\,bat/SC}} = \alpha \int_{t_0}^{t_\mathrm{f}} \left(\frac{i_{\mathrm{bat}}}{I_{\mathrm{bat\,rms}}^{\alpha=0}}\right)^2 dt + (1-\alpha)\int_{t_0}^{t_\mathrm{f}} \left(\frac{i_{\mathrm{SC}}}{I_{\mathrm{SC\,rms}}^{\alpha=1}}\right)^2 dt. \tag{A.15}$$

b. Dynamic programming implementation

This work is conducted based on EMR formalism. EMR is a forward causal formalism while DP is a backward computation method. It is therefore necessary to deduce a backward model based on EMR [Horrein 2015a] (Figure A.2).

Once the backward model is carried out, it is ready to be implemented in backward computation programs. Here, the multi-objective optimization using DP is used as the multi-level strategy composed of the "strategic" and "tactical" layers (adopted from [Trovão 2013a]). The scalarization of the multi-objective problem serves as the strategic layer. It outputs the weighted sum cost function $J_{\mathrm{ws\,bat/SC}}$ which indicates how much priority is given to the objective of battery life-time extension and vice versa.

This cost function is minimized by DP in the tactical layer. Backward computation is implemented in this layer to calculate the optimal control law $i_{\mathrm{bat\,ref}}$ with the feedback of the state variable u_{SC}. The set of generated optimal solutions is the Pareto front benchmark. The procedure is illustrated in Figure A.3.

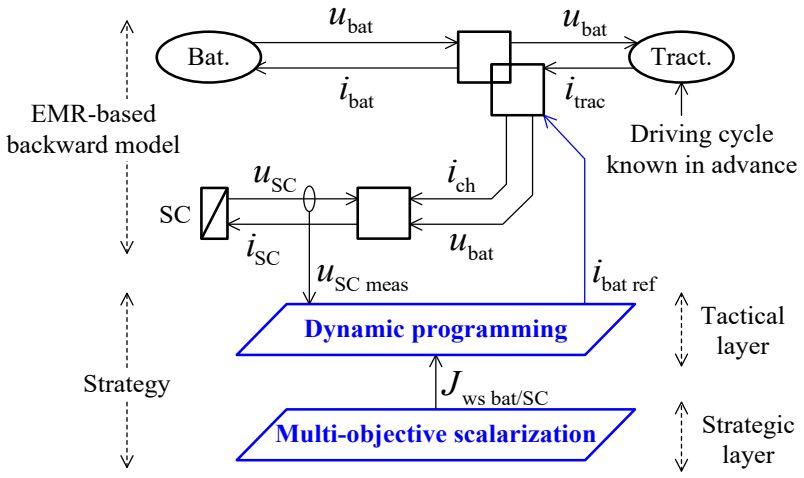

Figure A.2: EMR-based backward model for dynamic programming.

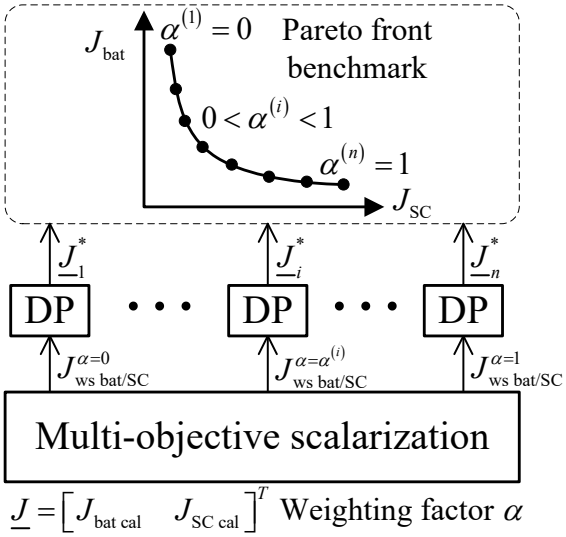

Figure A.3: Illustration of multi-objective optimal benchmark generation.

c. Results and discussions

The simulation is carried out using the parameters of Tazzari Zero as the reference vehicle. DP is realized by using the numerical tool introduced in [Sundström 2009]. The full dynamical model, local control, and filtering-based strategy are simulated in MATLAB/Simulink™ environment using EMR library [EMR 2019]. The ARTEMIS Low Motor Urban Total driving cycle is used as the velocity reference (Figure A.4). This cycle is chosen due to its very fluctuated profile.

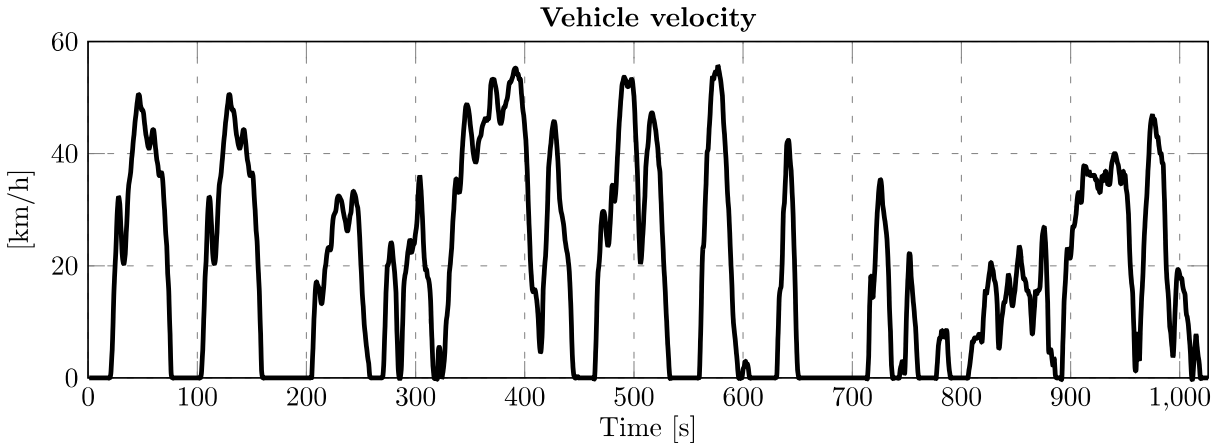

Figure A.4: ARTEMIS Low Motor Urban Total driving cycle.

Two main results are given. First, it is the Pareto front generated with the weighting factor α varying from zero to one. Results of filtering-based strategy are given to illustrate the benchmark role of the generated Pareto front. The second main result is voltage and current evolutions of the studied H-ESS with a specific value of α.

Pareto front as a global optimal multi-objective benchmark

The Pareto front generated from multi-objective optimal EMS is given in Figure A.5. Since DP is the global optimization method, this front can be used as a benchmark to evaluate the performances of sub-optimal strategies.

The well distributed convex form of the generated Pareto front verifies the validation of weighted sum scalarization. It is often argued that this method has drawbacks on the spread of the solutions and the ability to cover non-convex parts [Kim I. 2006; Logist 2010]. However, the results show that they are not the issue for this study.

To give an example for the benchmark role of the generated Pareto front, results of the filtering-based strategy are used. Two well investigated values of the LPF cut-off frequency $f_{c1} = 21$ mHz and $f_{c2} = 4$ mHz proposed by [Florescu 2015] and [Tani 2012] are studied, respectively. With the f_{c1}, the EMS causes low SCs system losses but reduces only a small amount of battery stresses. By contrast, with the f_{c2}, it is better for battery life-time but forces the SCs system working exhaustively. Both are fairly far from the optimal solutions set. For better evaluation of filtering-based strategy, a set of LPF cut-off frequencies from 6 mHz to 20 mHz with a 2-mHz step is examined. Figure A.5 shows that the results of filtering-based strategy keep long distances from the Pareto front. Advanced EMS giving results closer to the Pareto front are therefore preferred. It is supposed that an EMS giving results between the Pareto front and the curve of filtering strategy could be considered as better than this one.

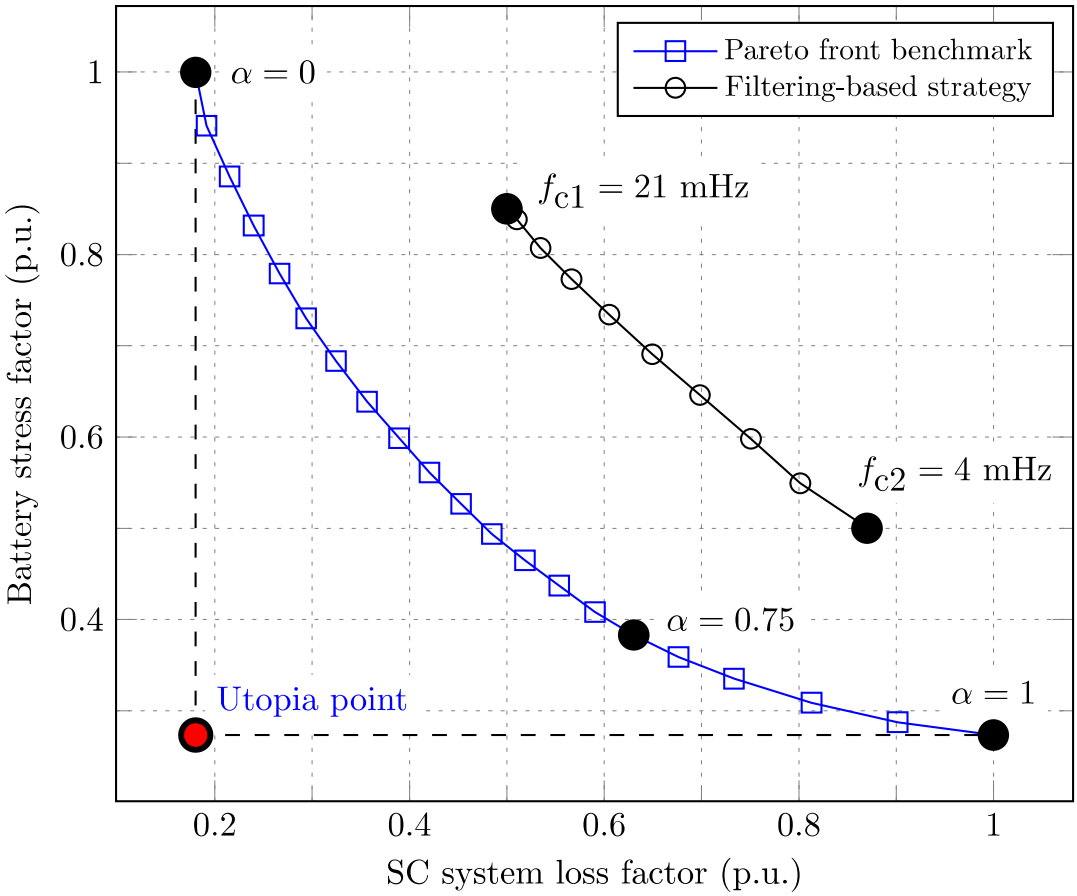

Figure A.5: Pareto front benchmark generated from DP-based multi-objective optimal EMS.

Case study with a particular value of the weighting factor

In this scenario, the weighting factor α is chosen as 0.75 (see the point in Figure A.5). That means the purpose of battery life-time extension is considered with the higher priority (75%) than the SCs subsystem losses reduction (25%).

Figure A.6 shows the SC voltage u_{SC} and the H-ESS currents. They include the i_{bat} (control variable), the chopper current i_{ch} and the traction current i_{trac} (disturbance). The state variable u_{SC} is constrained between the maximal and minimal limitations. The final state $u_{SC}(t_f)$ is controlled to be equal to the initial state $u_{SC}(t_0)$.

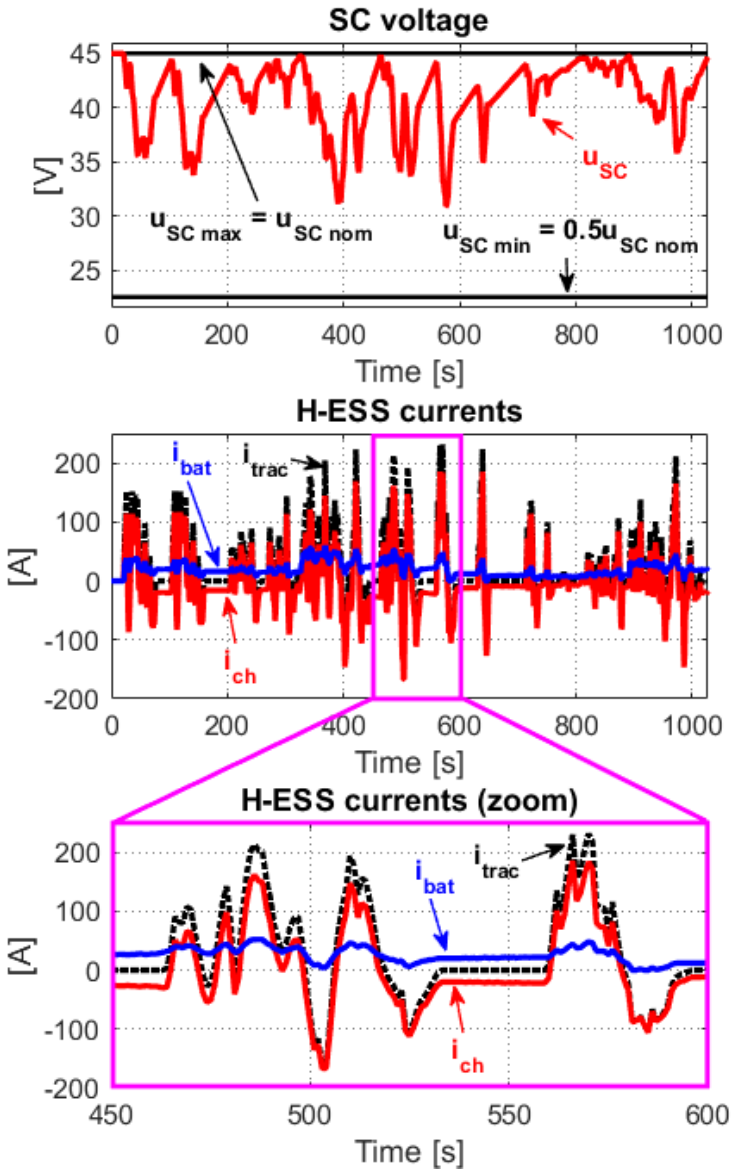

Figure A.6: SCs voltage and H-ESS currents with $\alpha = 0.75$ as a particular testing case.

d. Conclusions

Multi-objective EMS is reasonable for H-ESS-based EVs. A systematic approach to develop off-line multi-objective EMS is deduced. SCs subsystem losses are taken into account in addition to the main objective extending battery life-time. DP is used for problem solving thanks to its ability of giving the global optimal solution. A Pareto front is generated as a benchmark. It could be used in order to evaluate the other on-line strategies for energy management of H-ESS for EVs. The performances of the developed off-line EMS are also validated.

A.3. Linearity and non-linearity of the studied systems models

The linearity of a dynamical system can be examined by using its definition with the principle of superposition [Ogata 2009].

a. The reduced model of the battery/SC H-ESS

The reduced mathematical model of the H-ESS is (from (2.23)):

$$\frac{d}{dt}u_{\mathrm{SC}} = \frac{u_{\mathrm{bat}}}{u_{\mathrm{SC}}C_{\mathrm{SC}}}\left(i_{\mathrm{bat\,ref}} - i_{\mathrm{trac}}\right) \tag{A.16}$$

where $i_{\mathrm{bat\,ref}}$ is the control input; u_{SC} the state variable (output); u_{bat} and i_{trac} the disturbances. Considering the same disturbances, applying the principle of superposition, firstly we have:

$$\begin{aligned}\frac{d}{dt}\left[\alpha u_{\mathrm{SC}}(1) + \beta u_{\mathrm{SC}}(2)\right] \\ = \frac{u_{\mathrm{bat}}}{\alpha u_{\mathrm{SC}}(1)C_{\mathrm{SC}}}\left[i_{\mathrm{bat\,ref}}(1) - i_{\mathrm{trac}}\right] \\ + \frac{u_{\mathrm{bat}}}{\beta u_{\mathrm{SC}}(2)C_{\mathrm{SC}}}\left[i_{\mathrm{bat\,ref}}(2) - i_{\mathrm{trac}}\right]\end{aligned} \tag{A.17}$$

where α and β are arbitrary constants. Whereas

$$\begin{aligned}\alpha\frac{d}{dt}u_{\mathrm{SC}}(1) + \beta\frac{d}{dt}u_{\mathrm{SC}}(2) \\ = \frac{\alpha u_{\mathrm{bat}}}{u_{\mathrm{SC}}(1)C_{\mathrm{SC}}}\left[i_{\mathrm{bat\,ref}}(1) - i_{\mathrm{trac}}\right] + \frac{\beta u_{\mathrm{bat}}}{u_{\mathrm{SC}}(2)C_{\mathrm{SC}}}\left[i_{\mathrm{bat\,ref}}(2) - i_{\mathrm{trac}}\right].\end{aligned} \tag{A.18}$$

From (A.17) and (A.18), it can be seen that:

$$\frac{d}{dt}\left[\alpha u_{\mathrm{SC}}(1) + \beta u_{\mathrm{SC}}(2)\right] \neq \alpha\frac{d}{dt}u_{\mathrm{SC}}(1) + \beta\frac{d}{dt}u_{\mathrm{SC}}(2). \tag{A.19}$$

Thus, the reduced model of the studied battery/SC H-ESS is non-linear.

b. The reduced model of the parallel hybrid truck

The reduced mathematical model of the parallel hybrid truck is (from (3.21))

$$\frac{d}{dt}SoC_{\mathrm{bat}} = \frac{k_{\mathrm{belt}}\Omega_{\mathrm{ICE}}}{C_{\mathrm{bat\,eq}}u_{\mathrm{bat}}}\left(T_{\mathrm{ICE\,ref}} - T_{\mathrm{belt\,ref}}\right); \tag{A.20}$$

in which $T_{\mathrm{ICE\,ref}}$ is the control input; SoC_{bat} the state variable (output); $T_{\mathrm{belt\,ref}}$, u_{bat}, and Ω_{ICE} the disturbances. Here, it is assumed that the batteries voltage u_{bat} is independent on their SoC (in fact, does not vary so much). Considering the same disturbances, applying the principle of superposition, we have:

$$\begin{aligned}\frac{d}{dt}[\alpha SoC_{\text{bat}}(1)+\beta SoC_{\text{bat}}(2)] \\ &= \alpha\frac{k_{\text{belt}}\Omega_{\text{ICE}}}{C_{\text{bat eq}}u_{\text{bat}}}[T_{\text{ICE ref}}(1)-T_{\text{belt ref}}] \\ &+ \beta\frac{k_{\text{belt}}\Omega_{\text{ICE}}}{C_{\text{bat eq}}u_{\text{bat}}}[T_{\text{ICE ref}}(2)-T_{\text{belt ref}}] \\ &= \alpha\frac{d}{dt}SoC_{\text{bat}}(1)+\beta\frac{d}{dt}SoC_{\text{bat}}(2)\end{aligned} \tag{A.21}$$

where α and β are arbitrary constants. Thus, the reduced model of the studied parallel hybrid truck is linear.

A.4. Additional simulation and experimental results of the proposed Hamiltonian minimization-based current distribution strategy for battery/SC EV

More results of the proposed EMS for battery/SC H-ESS-based EV are given here. Figure A.7–Figure A.9 show the simulation and the experimental results of the strategy tested with NEDC, WLTC class 2, and ARTEMIS, respectively. The results reinforce the conclusions that the proposed strategy performs effectively in all the tested driving conditions and the reduced-scale power HIL can emulate well the studied system.

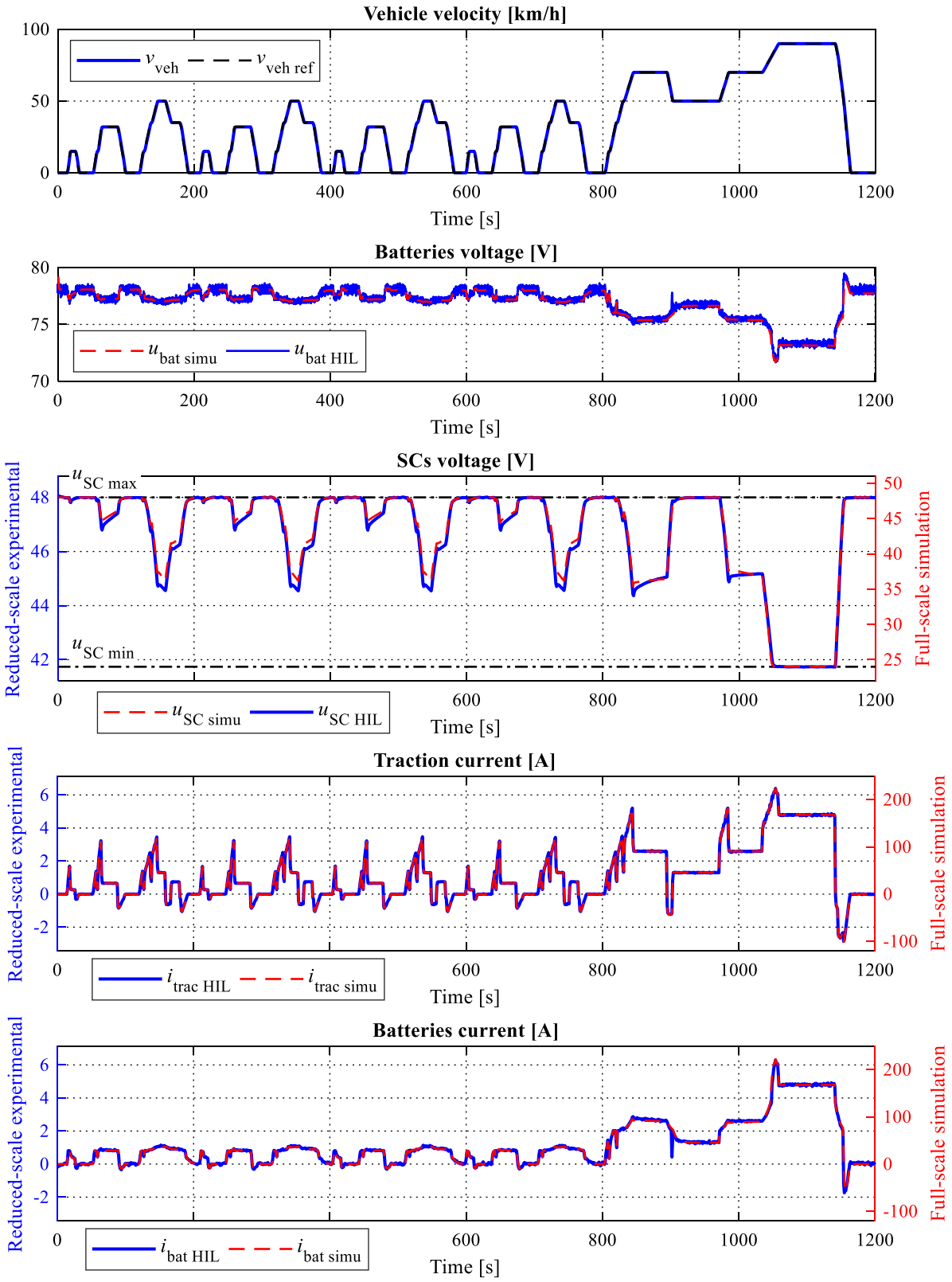

Figure A.7: Simulation and experimental results of the proposed Hamiltonian minimization-based EMS for battery/SC EV with NEDC.

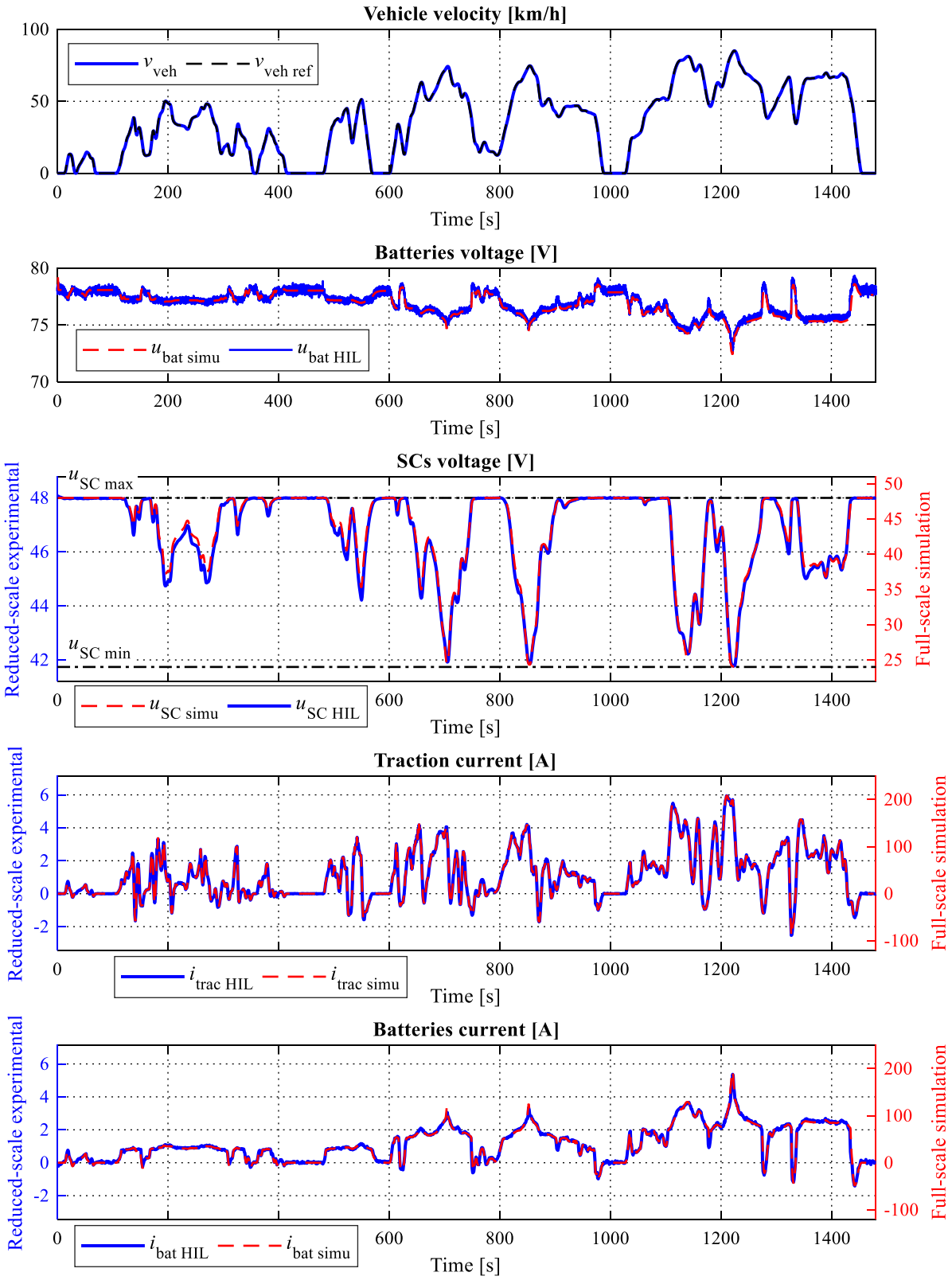

Figure A.8: Simulation and experimental results of the proposed Hamiltonian minimization-based EMS for battery/SC EV with WLTC class 2.

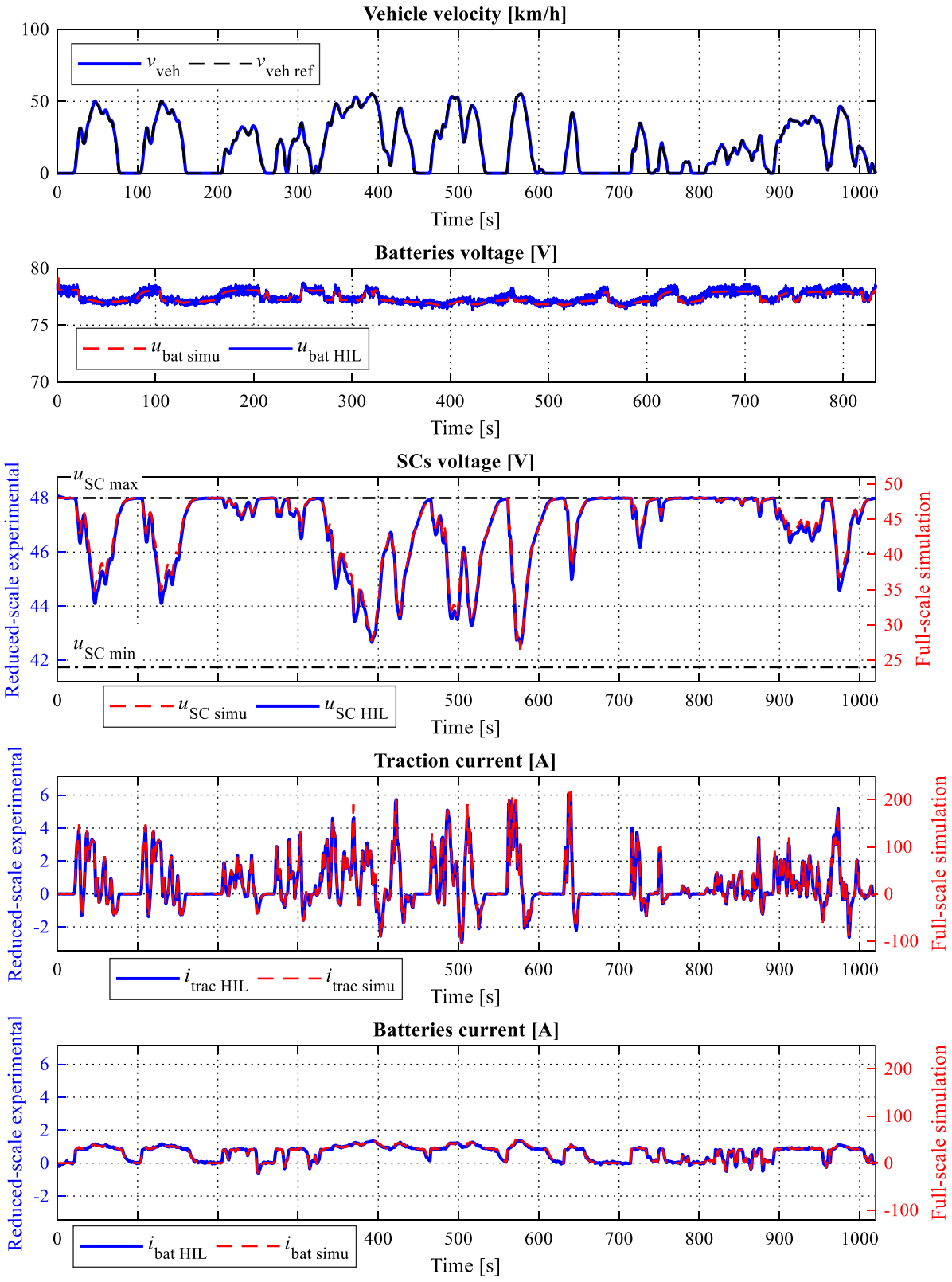

Figure A.9: Simulation and experimental results of the proposed Hamiltonian minimization-based EMS for battery/SC EV with ARTEMIS.

A.5. Additional simulation and experimental results of the proposed LQR-based torque distribution strategy for battery/SC parallel hybrid truck

More results of the proposed EMS for battery/SC H-ESS-based parallel hybrid truck are given here. Figure A.10 and Figure A.11 show the simulation and the experimental results of the strategy tested with UDDS and WLTC class 2, respectively.

The results reinforce the conclusions that the proposed strategy performs effectively in all the tested driving conditions and the reduced-scale power HIL can emulate well the studied system. The differences between simulation and experimental results are due to the low efficiency of the induction machine drive used for these experiments, as explained in Subsection 3.5.2.

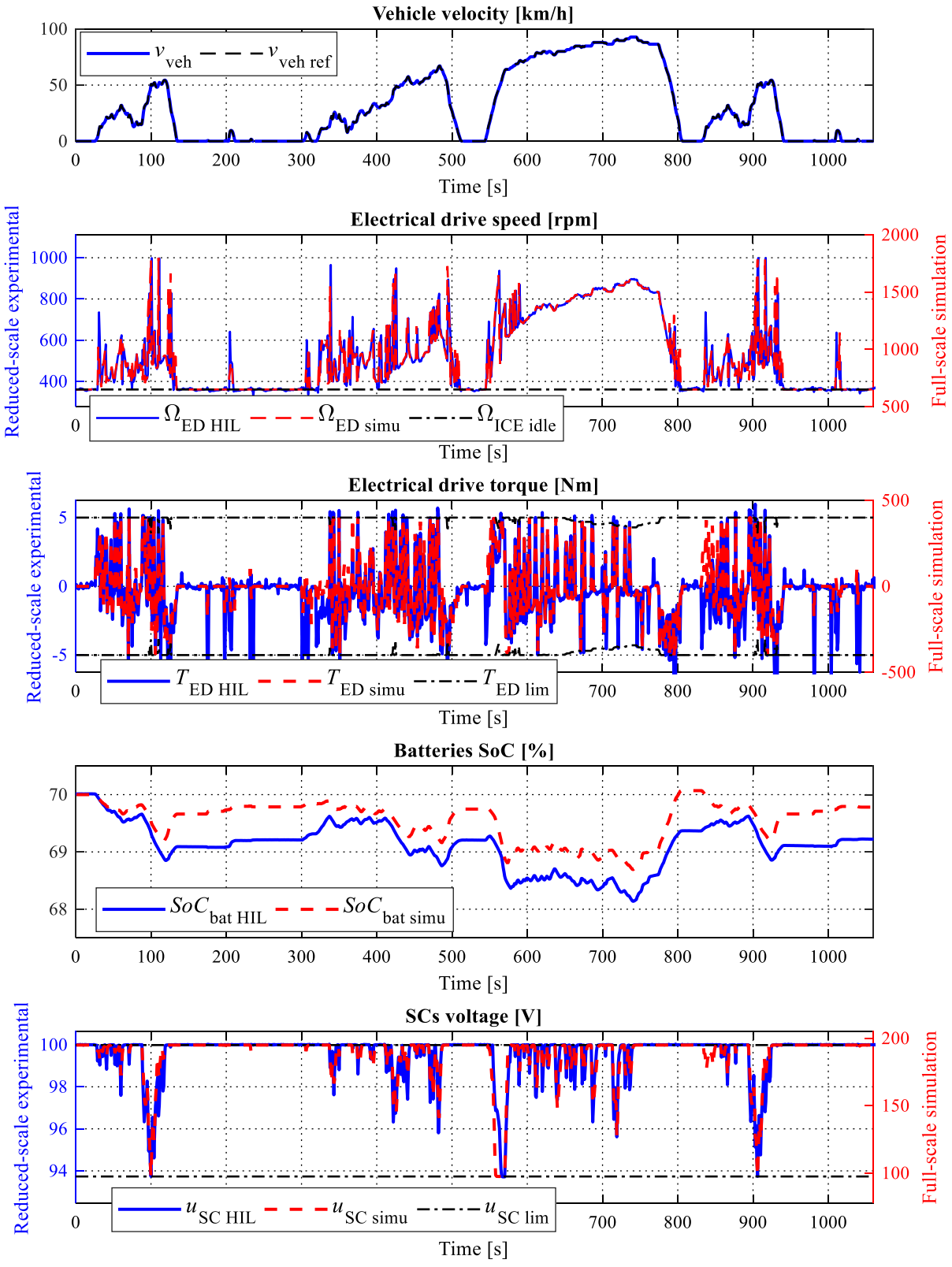

Figure A.10: Simulation and experimental results of the proposed LQR-based EMS for battery/SC parallel hybrid truck with UDDS.

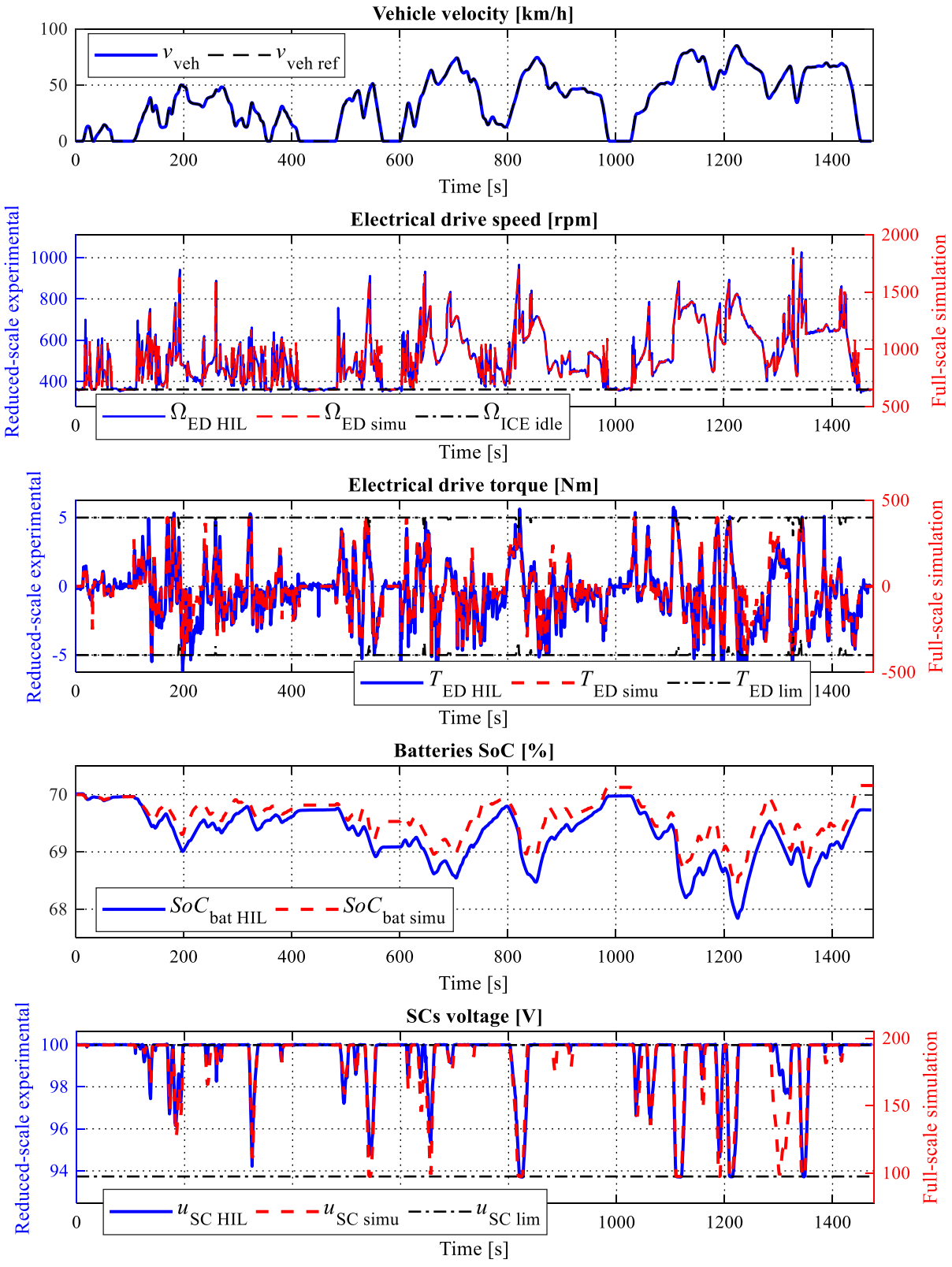

Figure A.11: Simulation and experimental results of the proposed LQR-based EMS for battery/SC parallel hybrid truck with WLTC.

References

[Allègre 2010a] Anne-Laure Allègre. (2010). *Méthodologies de modélisation et de gestion de l'énergie de systèmes de stockage mixtes pour véhicules électriques et hybrides*. PhD thesis (text in French), Université de Lille, France.

[Allègre 2010b] Anne-Laure Allègre, Alain Bouscayrol, Jean-Noel Verhille, Philippe Delarue, Eric Chattot, and Saãd El-Fassi. (2010). Reduced-scale-power hardware-in-the-loop simulation of an innovative subway. *IEEE Transactions on Industrial Electronics*, *57*(4), 1175–1185.

[Allègre 2013] Anne-Laure Allègre, Rochdi Trigui, and Alain Bouscayrol. (2013). Flexible real-time control of a hybrid energy storage system for electric vehicles. *IET Electrical Systems in Transportation*, *3*(3), 79–85.

[Antunes 2016] Carlos Henggeler Antunes, Maria João Alves, and João Clímaco. (2016). *Multiobjective Linear and Integer Programming*. Springer International Publishing.

[Athans 1966] Michael Athans. (1966). The status of optimal control theory and applications for deterministic systems. *IEEE Transactions on Automatic Control*, *11*(3), 580–596.

[Ayad 2010] M. Y. Ayad, M. Becherif, A. Henni, A. Aboubou, M. Wack, and S. Laghrouche. (2010). Passivity-Based Control applied to DC hybrid power source using fuel cell and supercapacitors. *Energy Conversion and Management*, *51*(7), 1468–1475.

[Azib 2010] Toufik Azib, Olivier Bethoux, Ghislain Remy, Claude Marchand, and Eric Berthelot. (2010). An innovative control strategy of a single converter for hybrid fuel cell/supercapacitor power source. *IEEE Transactions on Industrial Electronics*, *57*(12), 4024–4031.

[Baghdadi 2016] Issam Baghdadi, Olivier Briat, Jean Yves Delétage, Philippe Gyan, and Jean Michel Vinassa. (2016). Lithium battery aging model based on Dakin's degradation approach. *Journal of Power Sources*, *325*, 273–285.

[Barré 2013] Anthony Barré, Benjamin Deguilhem, Sébastien Grolleau, Mathias Gérard, Frédéric Suard, and Delphine Riu. (2013). A review on lithium-ion battery ageing mechanisms and estimations for automotive applications. *Journal of Power Sources*, *241*, 680–689.

[Bauer 2016] Nico Bauer, Ioanna Mouratiadou, Gunnar Luderer, Lavinia Baumstark, Robert J. Brecha, Ottmar Edenhofer, and Elmar Kriegler. (2016). Global fossil energy markets and climate change mitigation – an analysis with REMIND. *Climatic Change*, *136*(1), 69–82.

[Benmouna 2018] A. Benmouna, M. Becherif, C. Dépature, Loïc Boulon, and D. Depernet. (2018). Experimental study of energy management of FC/SC hybrid system using the Passivity Based Control. *International Journal of Hydrogen Energy*, *43*(25), 11583–11592.

[Beraki 2017] Mebrahtom Woldelibanos Beraki, João Pedro F. Trovão, Marina S. Perdigao, and Maxime R. Dubois. (2017). Variable Inductor Based Bidirectional DC-DC Converter for Electric Vehicles. *IEEE Transactions on Vehicular Technology*, *66*(10), 8764–8772.

[Biasini 2013] Riccardo Biasini, Simona Onori, and Giorgio Rizzoni. (2013). A near-optimal rule-based energy management strategy for medium duty hybrid truck. *Int. J. Powertrains*, *2*(2/3), 232–261.

[Bolloré 2012] Bolloré. (2012). *Business Report 2012*. Available: https://www.bollore.com/bollo-content/uploads/2018/12/mel_bol_ra-gb_04-06.pdf

[Borhan 2012] Hoseinali Borhan, Ardalan Vahidi, Anthony M. Phillips, Ming L. Kuang, Ilya V. Kolmanovsky, and Stefano Di Cairano. (2012). MPC-based energy management of a power-split hybrid electric vehicle. *IEEE Transactions on Control Systems Technology*, *20*(3), 593–603.

[Boulon 2010] Loïc Boulon, Daniel Hissel, Alain Bouscayrol, Olivier Pape, and Marie-Cécile Péra. (2010). Simulation model of a military HEV with a highly redundant architecture. *IEEE Transactions on Vehicular*

Technology, *59*(6), 2654–2663.

[Boulon 2013] Loïc Boulon, Alain Bouscayrol, Daniel Hissel, Olivier Pape, and Marie-Cécile Péra. (2013). Inversion-Based Control of a Highly Redundant Military HEV. *IEEE Transactions on Vehicular Technology*, *62*(2), 500–510.

[Bouscayrol 2000] Alain Bouscayrol, B. Davat, B. de Fornel, B. François, Jean Paul Hautier, F. Meibody-Tabar, and M. Pietrzak-David. (2000). Multi-converter multi-machine systems: application for electromechanical drives. *The European Physical Journal - Applied Physics*, *10*(2), 131–147.

[Bouscayrol 2005] Alain Bouscayrol, Ph Delarue, and X. Guillaud. (2005). Power strategies for maximum control structure of a wind energy conversion system with a synchronous machine. *Renewable Energy*, *30*(15), 2273–2288.

[Bouscayrol 2011] Alain Bouscayrol. (2011). Hardware-in-the-Loop Simulation. In Bogdan M. Wilamowski & J. david Irwin (Eds.), *The Industrial Electronics Handbook: Control and Mechatronics* (2nd ed.). CRC Press.

[Bouscayrol 2013] Alain Bouscayrol, Jean Paul Hautier, and Betty Lemaire-Semail. (2013). Graphic Formalisms for the Control of Multi-Physical Energetic Systems: COG and EMR. In Xavier Roboam (Ed.), *Systemic Design Methodologies for Electrical Energy Systems: Analysis, Synthesis and Management* (pp. 89–124). ISTE Ltd.

[Bryson 1975] Arthur E. Bryson and Yu-Chi Ho. (1975). *Applied Optimal Control: Optimization, Estimation, and Control*. John Wiley & Sons.

[Castaings 2016a] Ali Castaings, Walter Lhomme, Rochdi Trigui, and Alain Bouscayrol. (2016). Comparison of energy management strategies of a battery/supercapacitors system for electric vehicle under real-time constraints. *Applied Energy*, *163*, 190–200.

[Castaings 2016b] Ali Castaings. (2016). *Gestion d'énergie de véhicules multi-sources électriques et hybrides au travers de la Représentation Energétique Macroscopique*. PhD thesis (text in French), Université de Lille, France.

[Chan 2009] C. C. Chan, Y. S. Wong, Alain Bouscayrol, and Keyu Chen. (2009). Powering Sustainable Mobility: Roadmaps of Electric, Hybrid, and Fuel Cell Vehicles. *Proceedings of the IEEE*, *97*(4), 603–607.

[Chan 2010] C. C. Chan, Alain Bouscayrol, and Keyu Chen. (2010). Electric, hybrid, and fuel-cell vehicles: Architectures and modeling. *IEEE Transactions on Vehicular Technology*, *59*(2), 589–598.

[Chen S. 2015] Syuan Yi Chen, Yi Hsuan Hung, Chien Hsun Wu, and Siang Ting Huang. (2015). Optimal energy management of a hybrid electric powertrain system using improved particle swarm optimization. *Applied Energy*, *160*, 132–145.

[Chen Ze. 2015] Zeyu Chen, Rui Xiong, Chun Wang, and Jiayi Cao. (2015). An on-line predictive energy management strategy for plug-in hybrid electric vehicles to counter the uncertain prediction of the driving cycle. *Applied Energy*, *185*, 1663–1672.

[Chen Zh. 2014] Zheng Chen, Chunting Chris Mi, Jun Xu, Xianzhi Gong, and Chenwen You. (2014). Energy management for a power-split plug-in hybrid electric vehicle based on dynamic programming and neural networks. *IEEE Transactions on Vehicular Technology*, *63*(4), 1567–1580.

[Christen 2000] Thomas Christen and Martin W. Carlen. (2000). Theory of Ragone plots. *Journal of Power Sources*, *91*(2), 210–216.

[Cipek 2013] Mihael Cipek, Danijel Pavković, and Joško Petrić. (2013). A control-oriented simulation model of a power-split hybrid electric vehicle. *Applied Energy*, *101*, 121–133.

[CRC 2017] Canada Research Chair. (2017). Canada Research Chair in Efficient Electric Vehicles with Hybridized Energy Storage Systems. Available: http://www.chairs-chaires.gc.ca/chairholders-titulaires/profile-eng.aspx?profileId=3428

[Dai 2016] Ping Dai, Sébastien Cauet, and Patrick Coirault. (2016). Disturbance rejection of battery/ultracapacitor hybrid energy sources. *Control Engineering Practice*, *54*, 166–175.

[Daouda 2018] Mande Daouda, João Pedro F. Trovão, Ruben Gonzalez Rubio, and Minh C. Ta. (2018).

Comparison of Bidirectional Quasi Z-Source- and Bidirectional Conventional Two-Stage-Inverter for Electric Traction System. *2018 IEEE Vehicle Power and Propulsion Conference (VPPC)*, 1–6.

[De Castro 2012] Ricardo De Castro, Rui Esteves Araujo, João Pedro F. Trovão, Paulo G. Pereirinha, Pedro Melo, and Diamantino Freitas. (2012). Robust DC-link control in EVs with multiple energy storage systems. *IEEE Transactions on Vehicular Technology*, *61*(8), 3553–3565.

[Deb 2014] Kalyanmoy Deb. (2014). Multi-objective Optimization. In Edmund K. Burke & Graham Kendall (Eds.), *Search Methodologies: Introductory Tutorials in Optimization and Decision Support Techniques* (2nd ed., pp. 403–449). New York: Springer.

[Delprat 2002] Sebastien Delprat, T. M. Guerra, and J. Rimaux. (2002). Optimal control of a parallel powertrain : From global optimization to real time control strategy. In *2002 Vehicular Technology Conference* (pp. 2082–2088).

[Delprat 2004] Sebastien Delprat, J. Lauber, T. M. Guerra, and J. Rimaux. (2004). Control of a parallel hybrid powertrain: optimal control. *IEEE Transactions on Vehicular Technology*, *53*(3), 872–881.

[Denis 2018] Nicolas Denis, Maxime R. Dubois, João Pedro F. Trovão, and Alain Desrochers. (2018). Power Split Strategy Optimization of a Plug-in Parallel Hybrid Electric Vehicle. *IEEE Transactions on Vehicular Technology*, *67*(1), 315–326.

[Dépature 2017] Clément Dépature. (2017). *Commandes par inversion d'un véhicule à pile à combustible et supercondensateurs*. PhD thesis (text in French), Université de Lille, France and Université du Québec à Trois-Rivières, QC, Canada.

[Dépature 2018a] Clément Dépature, Samir Jemei, Loïc Boulon, Alain Bouscayrol, Neigel Marx, Simon Morando, and Ali Castaings. (2018). Energy management in fuel-cell/battery vehicles: Key issues identified in the ieee vehicular technology society motor vehicle challenge 2017. *IEEE Vehicular Technology Magazine*, *13*(3), 144–151.

[Dépature 2018b] Clément Dépature, Walter Lhomme, Pierre Sicard, Alain Bouscayrol, and Loïc Boulon. (2018). Real-Time Backstepping Control for Fuel Cell Vehicle Using Supercapacitors. *IEEE Transactions on Vehicular Technology*, *67*(1), 306–314.

[Devillers 2014] Nathalie Devillers, Samir Jemei, Marie-Cécile Péra, Daniel Bienaimé, and Frédéric Gustin. (2014). Review of characterization methods for supercapacitor modelling. *Journal of Power Sources*, *246*(0), 596–608.

[DoE 2014] Department of Energy (USA). (2014). The History of the Electric Car. Available: https://www.energy.gov/articles/history-electric-car

[Ehsani 2006] Mehrdad Ehsani and Yimin Gao. (2006). Parametric design of the traction motor and energy storage for series hybrid off-road and military vehicles. *IEEE Transactions on Power Electronics*, *21*(3), 749–755.

[Ehsani 2010] Mehrdad Ehsani, Yimin Gao, and Ali Emadi. (2010). *Modern Electric, Hybrid Electric, and Fuel Cell Vehicles: Fundamentals, Theory, and Design* (2nd ed.). CRC Press.

[EMR 2019] EMR. (2019). EMR Website. Available: http://www.emrwebsite.org

[Ettihir 2016] K. Ettihir, Loïc Boulon, and K. Agbossou. (2016). Optimization-based energy management strategy for a fuel cell/battery hybrid power system. *Applied Energy*, *163*, 142–153.

[Fares 2015] Dima Fares, Riad Chedid, Ferdinand Panik, Sami Karaki, and Rabih Jabr. (2015). Dynamic programming technique for optimizing fuel cell hybrid vehicles. *International Journal of Hydrogen Energy*, *40*(24), 7777–7790.

[Florescu 2014] Adrian Florescu, Antoneta Iuliana Bratcu, Iulian Munteanu, Axel Rumeau, and Seddik Bacha. (2014). LQG Optimal Control Applied to On-Board Energy Management System of All-Electric Vehicles. *IEEE Transactions on Control Systems Technology*, *23*(4), 1–13.

[Florescu 2015] Adrian Florescu, Seddik Bacha, Iulian Munteanu, Antoneta Iuliana Bratcu, and Axel Rumeau. (2015). Adaptive frequency-separation-based energy management system for electric vehicles. *Journal of Power Sources*, *280*, 410–421.

[Fontaine 2013] C. Fontaine, Sebastien Delprat, S. Paganelli, and T. M. Guerra. (2013). Optimal control of a parallel hybrid vehicle equipped with a dual electrical storage system. In *7th IFAC Symposium on Advances in Automotive Control* (pp. 512–517). IFAC.

[Garcia 2010] Pablo Garcia, Luis M. Fernandez, Carlos Andres Garcia, and Francisco Jurado. (2010). Energy management system of fuel-cell-battery hybrid tramway. *IEEE Transactions on Industrial Electronics*, *57*(12), 4013–4023.

[Gauchia 2011] L. Gauchia, Alain Bouscayrol, J. Sanz, Rochdi Trigui, and P. Barrade. (2011). Fuel Cell, Battery and Supercapacitor Hybrid System for Electric Vehicle: Modeling and Control via Energetic Macroscopic Representation. In *Vehicle Power and Propulsion Conference (VPPC'2011)*.

[Gomozov 2017] Oleg Gomozov, João Pedro F. Trovão, Xavier Kestelyn, and Maxime Dubois. (2017). Adaptive Energy Management System Based on a Real-Time Model Predictive Control with Non-Uniform Sampling Time for Multiple Energy Storage Electric Vehicle. *IEEE Transactions on Vehicular Technology*, *66*(7), 5520–5530.

[Grbovic 2011] Pj Grbovic, Philippe Delarue, Philippe Le Moigne, and Patrick Bartholomeus. (2011). Modeling and Control of the Ultracapacitor-Based Regenerative Controlled Electric Drives. *IEEE Transactions on Industrial Electronics*, *58*(8), 3471–3484.

[Greenwell 2010] W. Greenwell and A. Vahidi. (2010). Predictive Control of Voltage and Current in a Fuel Cell - Ultracapacitor Hybrid. *IEEE Transactions on Industrial Electronics*, *57*(6), 1954–1963.

[Han 2014] Jihun Han, Youngjin Park, and Dongsuk Kum. (2014). Optimal adaptation of equivalent factor of equivalent consumption minimization strategy for fuel cell hybrid electric vehicles under active state inequality constraints. *Journal of Power Sources*, *267*, 491–502.

[Hannan 2012] M. A. Hannan, F. A. Azidin, and A. Mohamed. (2012). Multi-sources model and control algorithm of an energy management system for light electric vehicles. *Energy Conversion and Management*, *62*, 123–130.

[Hautier 2004] Jean Paul Hautier and P. J. Barre. (2004). The causal ordering graph - a tool for modelling and control law synthesis. *Studies in Informatics and Control Journal*, *13*(4), 265–283.

[Hemi 2015] Hanane Hemi, Jamel Ghouili, and Ahmed Cheriti. (2015). Combination of Markov chain and optimal control solved by Pontryagin's Minimum Principle for a fuel cell/supercapacitor vehicle. *Energy Conversion and Management*, *91*, 387–393.

[Henson 2008] William Henson. (2008). Optimal battery/ultracapacitor storage combination. *Journal of Power Sources*, *179*(1), 417–423.

[Hilairet 2013] M. Hilairet, Malek Ghanes, Olivier Béthoux, Valentin Tanasa, Jean Pierre Barbot, and D. Normand-Cyrot. (2013). A passivity-based controller for coordination of converters in a fuel cell system. *Control Engineering Practice Journal*, *21*, 1097–1109.

[Hofman 2008] Theo Hofman, M. Steinbuch, R. M. Van Druten, and A. F. A. Serrarens. (2008). Hybrid component specification optimisation for a medium-duty hybrid electric truck. *International Journal of Heavy Vehicle Systems*, *15*(2/3/4), 356–391.

[Horrein 2015a] Ludovic Horrein. (2015). *Gestion d'energie decomposee d'un vehicule hybride integrant les aspects thermiques via la representation energetique macroscopique*. PhD thesis (text in French), Université de Lille, France.

[Horrein 2015b] Ludovic Horrein, Alain Bouscayrol, Yuan Cheng, and C. Dumand. (2015). Hybrid Energy Management Strategy for Hybrid Electric Vehicle. In *Vehicle Power and Propulsion Conference (VPPC'15)*.

[Hou 2014] Cong Hou, Minggao Ouyang, Liangfei Xu, and Hewu Wang. (2014). Approximate Pontryagin's minimum principle applied to the energy management of plug-in hybrid electric vehicles. *Applied Energy*, *115*, 174–189.

[Hredzak 2014] Branislav Hredzak, Vassilios G. Agelidis, and Minsoo Jang. (2014). A model predictive control system for a hybrid battery-ultracapacitor power source. *IEEE Transactions on Power Electronics*, *29*(3), 1469–1479.

[Hu 2014] Xiaosong Hu, Nikolce Murgovski, Lars Mårdh Johannesson, and Bo Egardt. (2014). Comparison of three electrochemical energy buffers applied to a hybrid bus powertrain with simultaneous optimal sizing and energy management. *IEEE Transactions on Intelligent Transportation Systems*, *15*(3), 1193–1205.

[Hu 2015a] Xiaosong Hu, Lars Johannesson, Nikolce Murgovski, and Bo Egardt. (2015). Longevity-conscious dimensioning and power management of the hybrid energy storage system in a fuel cell hybrid electric bus. *Applied Energy*, *137*, 913–924.

[Hu 2015b] Xiaosong Hu, Jiuchun Jiang, Bo Egardt, and Dongpu Cao. (2015). Advanced Power-Source Integration in Hybrid Electric Vehicles: Multicriteria Optimization Approach. *IEEE Transactions on Industrial Electronics*, *62(12)*, 7847–7858.

[Ibrahim 2016] Mona Ibrahim, Samir Jemei, Geneviève Wimmer, and Daniel Hissel. (2016). Nonlinear autoregressive neural network in an energy management strategy for battery/ultra-capacitor hybrid electrical vehicles. *Electric Power Systems Research*, *136*, 262–269.

[Iwasaki 1994] Yumi Iwasaki and Herbert A. Simon. (1994). Causality and model abstraction. *Artificial Intelligence*, *67*, 143–194.

[Jaafar 2009] A. Jaafar, C. R. Akli, B. Sareni, X. Roboam, and A. Jeunesse. (2009). Sizing and Energy Management of a Hybrid Locomotive Based on Flywheel and Accumulators. *IEEE Transactions on Vehicular Technology*, *58*(8), 3947–3958.

[Johnson 2000] Valerie H. V. H. Johnson, Keith B. K. B. Wipke, and David J. D. J. Rausen. (2000). HEV control strategy for real-time optimization of fuel economy and emissions. *SAE Transactions*, *109*, 1677–1690.

[Kermani 2009] Saida Kermani. (2009). *Gestion énergétique des véhicules hybrides: de la simulation à la commande temps réel*. PhD thesis (text in French), Université de Valenciennes et du Hainaut-Cambresis, France.

[Kermani 2011] Saida Kermani, Rochdi Trigui, Sebastien Delprat, Bruno Jeanneret, and Thierry Marie Guerra. (2011). PHIL implementation of energy management optimization for a parallel HEV on a predefined route. *IEEE Transactions on Vehicular Technology*, *60*(3), 782–792.

[Kessels 2008] J. T. B. A. Kessels, Michiel Koot, P. P. J. van den Bosch, and D. B. Kok. (2008). Online Energy Management for Hybrid Electric Vehicles. *IEEE Transactions on Vehicular Technology*, *57*(6), 3428–3440.

[Kim I. 2006] I. Y. Kim and O. L. De Weck. (2006). Adaptive weighted sum method for multiobjective optimization: A new method for Pareto front generation. *Structural and Multidisciplinary Optimization*, *31*(2), 105–116.

[Kim M. 2007] M. J. Kim and H. Peng. (2007). Power management and design optimization of fuel cell/battery hybrid vehicles. *Journal of Power Sources*, *165*(2), 819–832.

[Kim N. 2011] Namwook Kim, Sukwon Cha, and Huei Peng. (2011). Optimal Control of Hybrid Electric Vehicles Based on Pontryagin's Minimum Principle. *IEEE Transactions on Control Systems Technology*, *19*(5), 1279–1287.

[Kim Y. 2014] Youngki Kim, Ashwin Salvi, Jason B. Siegel, Zoran S. Filipi, Anna G. Stefanopoulou, and Tulga Ersal. (2014). Hardware-in-the-loop validation of a power management strategy for hybrid powertrains. *Control Engineering Practice*, *29*, 277–286.

[Kirk 1970] Donald E. Kirk. (1970). *Optimal control theory: An introduction*. Prentice-Hall.

[Kollmeyer 2014] Phillip J. Kollmeyer, Larry W. Juang, and T. M. Jahns. (2014). Loss optimization and ultracapacitor pack sizing for vehicles with battery/ultracapacitor hybrid energy storage. In *2014 IEEE Transportation Electrification Conference and Expo (ITEC)* (pp. 1–8).

[Koot 2005] Michiel Koot, J. T. B. A. Kessels, Bram de Jager, W. P. M. H. Heemels, P. P. J. van den Bosch, and Maarten Steinbuch. (2005). Energy Management Strategies for Vehicular Electric Power Systems. *IEEE Transactions on Vehicular Technology*, *54*(3), 771–782.

[LeBel 2018] Félix-Antoine LeBel, João Pedro F. Trovão, Loïc Boulon, Ali Sari, Serge Pelissier, and Pascal Venet. (2018). Lithium-Ion Cell Empirical Efficiency Maps. In *2018 IEEE Vehicle Power and Propulsion*

Conference (VPPC).

[Letrouvé 2013] Tony Letrouvé. (2013). *Structuration de la commande de la simulation au prototype d'un véhicule hybride double parallèle au travers de la Représentation Energétique Macroscopique*. PhD thesis (text in French), Université de Lille, France.

[Lhomme 2007] Walter Lhomme. (2007). *Gestion d'énergie de véhicules électriques hybrides basée sur la représentation énergetique macroscopique*. PhD thesis (text in French), Université de Lille, France.

[Lhomme 2008] Walter Lhomme, Rochdi Trigui, Philippe Delarue, Bruno Jeanneret, Alain Bouscayrol, and François Badin. (2008). Switched causal modeling of transmission with clutch in hybrid electric vehicles. *IEEE Transactions on Vehicular Technology*, *57*(4), 2081–2088.

[Lhomme 2009] Walter Lhomme, Philippe Delarue, Alain Bouscayrol, Philippe Le Moigne, Philippe Barrade, and Alfred Rufer. (2009). Comparison of control strategies for maximizing energy in a supercapacitor storage subsystem. *EPE Journal*, *19*(3), 5–14.

[Lhomme 2017] Walter Lhomme, Alain Bouscayrol, Sajjad Syed, Sebastien Roy, Frederic Gailly, and Olivier Pape. (2017). Energy Savings of a Hybrid Truck using a Ravigneaux Gear Train. *IEEE Transactions on Vehicular Technology*, *66*(10), 1–1.

[Li J. 2017] Jun-qiu Li, Xin Jin, and Rui Xiong. (2017). Multi-objective Optimal Energy Management Strategy and Economic Analysis for an Range-Extended Electric Bus. *Applied Energy*, *194*, 798–807.

[Li X. 2009] Xiangjun Li, Liangfei Xu, Jianfeng Hua, Xinfan Lin, Jianqiu Li, and Minggao Ouyang. (2009). Power management strategy for vehicular-applied hybrid fuel cell/battery power system. *Journal of Power Sources*, *191*(2), 542–549.

[Lin 2011] Wei Song Lin and Chen Hong Zheng. (2011). Energy management of a fuel cell/ultracapacitor hybrid power system using an adaptive optimal-control method. *Journal of Power Sources*, *196*(6), 3280–3289.

[Liu 2008] Jinming Liu and Huei Peng. (2008). Modeling and Control of a Power-Split Hybrid Vehicle. *IEEE Transactions on Control Systems Technology*, *16*(6), 1242–1251.

[Logist 2010] Filip Logist, Boris Houska, Moritz Diehl, and Jan Van Impe. (2010). Fast Pareto set generation for nonlinear optimal control problems with multiple objectives. *Structural and Multidisciplinary Optimization*, *42*(4), 591–603.

[Machado 2016] Felipe Machado, João Pedro F. Trovão, and Carlos Henggeler Antunes. (2016). Effectiveness of Supercapacitors in Pure Electric Vehicle Using a Hybrid Meta-Heuristic Approach. *IEEE Transactions on Vehicular Technology*, *65*(1), 29–36.

[Martinez 2011] Javier Solano Martinez, Daniel Hissel, Marie-Cécile Péra, and Michel Amiet. (2011). Practical Control Structure and Energy Management of a Testbed Hybrid Electric Vehicle. *IEEE Transactions on Vehicular Technology*, *60*(9), 4139–4152.

[Marx 2017] Neigel Marx. (2017). *Gestion énergétique et dimensionnement des systèmes hybrides multi-pile à combustible et batterie pour application au transport automobile*. PhD thesis (text in French), Université du Québec à Trois-Rivières, QC, Canada.

[Mayet 2014a] Clément Mayet, Ludovic Horrein, Alain Bouscayrol, Philippe Delarue, Jean-Noel Verhille, Eric Chattot, and Betty Lemaire-Semail. (2014). Comparison of Different Models and Simulation Approaches for the Energetic Study of a Subway. *IEEE Transactions on Vehicular Technology*, *63*(2), 556–565.

[Mayet 2014b] Clément Mayet, Julien Pouget, Alain Bouscayrol, and Walter Lhomme. (2014). Influence of an energy storage system on the energy consumption of a diesel-electric locomotive. *IEEE Transactions on Vehicular Technology*, *63*(3), 1032–1040.

[Mayet 2019] Clément Mayet, J. Welles, Alain Bouscayrol, T. Hofman, and B. Lemaire-semail. (2019). Influence of a CVT on the fuel consumption of a parallel medium-duty electric hybrid truck. *Mathematics and Computers in Simulation*, *158*, 120–129.

[MEGEVH 2019] MEGEVH. (2019). MEGEVH - French network on HEV. Available: http://megevh.univ-lille1.fr/

[Melosi 2010] Martin V. Melosi. (2010). The Automobile and the Environment in American History. Available: http://www.autolife.umd.umich.edu/Environment/E_Overview/E_Overview3.htm

[Montazeri-Gh 2015] Morteza Montazeri-Gh and Mehdi Mahmoodi-k. (2015). Development a new power management strategy for power split hybrid electric vehicles. *Transportation Research Part D: Transport and Environment*, *37*, 79–96.

[Moreno 2006] Jorge Moreno, Micah E. Ortúzar, and Juan W. Dixon. (2006). Energy-management system for a hybrid electric vehicle, using ultracapacitors and neural networks. *IEEE Transactions on Industrial Electronics*, *53*(2), 614–623.

[Moura 2013] Scott J. Moura, Jeffrey L. Stein, and Hosam K. Fathy. (2013). Battery-health conscious power management in plug-in hybrid electric vehicles via electrochemical modeling and stochastic control. *IEEE Transactions on Control Systems Technology*, *21*(3), 679–694.

[Mullem 2010] Dominique Van Mullem, Thijs Van Keulen, J. T. B. A. Kessels, Bram de Jager, and Maarten Steinbuch. (2010). Implementation of an Optimal Control Energy Management Strategy in a Hybrid Truck. In *6th IFAC Symposium Advances in Automotive Control* (pp. 61–66). Munich, Germany.

[Murphey 2012] Yi Lu Murphey, M. L. Kuang, M. a. Masrur, and a. M. Phillips. (2012). Intelligent hybrid vehicle power control—Part I: Machine learning of optimal vehicle power. *IEEE Transactions on Vehicular Technology*, *61*(8), 3519–3530.

[Murphey 2013] Yi Lu Murphey, Jungme Park, Leonidas Kiliaris, Ming L. Kuang, M. Abul Masrur, Anthony M. Phillips, and Qing Wang. (2013). Intelligent Hybrid Vehicle Power Control—Part II: Online Intelligent Energy Management. *IEEE Transactions on Vehicular Technology*, *62*(1), 69–79.

[Ngo 2012] Viet Ngo, Theo Hofman, Maarten Steinbuch, and Alex Serrarens. (2012). Optimal control of the gearshift command for hybrid electric vehicles. *IEEE Transactions on Vehicular Technology*, *61*(8), 3531–3543.

[Nguyen 2014] Anhtu Nguyen, Jimmy Lauber, and Michel Dambrine. (2014). Optimal control based algorithms for energy management of automotive power systems with battery/supercapacitor storage devices. *Energy Conversion and Management*, *87*, 410–420.

[Nguyễn 2016] Bảo-Huy Nguyễn, Ronan German, João Pedro F. Trovão, and Alain Bouscayrol. (2016). Improved Voltage Limitation Method of Supercapacitors in Electric Vehicle Applications. In *2016 IEEE Vehicle Power and Propulsion Conference, VPPC 2016 - Proceedings*. Hangzhou, China.

[Nguyễn 2017a] Bảo-Huy Nguyễn, João Pedro F. Trovão, Ronan German, and Alain Bouscayrol. (2017). An Optimal Control-Based Strategy for Energy Management of Electric Vehicles Using Battery/Supercapacitor. In *2017 IEEE Vehicle Power and Propulsion Conference, VPPC 2017 - Proceedings* (pp. 1–6). Belfort, France.

[Nguyễn 2017b] Bảo-Huy Nguyễn, João Pedro F. Trovão, Ronan German, and Alain Bouscayrol. (2017). Energy management of hybrid energy storage systems for electric vehicles: A multi-objective approach. In *ElectrIMACS*. Toulouse, France.

[Nguyễn 2018a] Bảo-Huy Nguyễn, Ronan German, João Pedro F. Trovão, and Alain Bouscayrol. (2018). Bi-level Optimal Energy Management of a Hybrid Truck Supplied by Batteries and Supercapacitors. In *The 15th IEEE Vehicle Power and Propulsion Conference (VPPC'18)*. Chicago, IL, USA.

[Nguyễn 2018b] Bảo-Huy Nguyễn, Ronan German, João Pedro F. Trovão, and Alain Bouscayrol. (2018). Merging control of a hybrid energy storage system using battery/supercapacitor for electric vehicle application. In *Proceedings of the IEEE International Conference on Industrial Technology* (pp. 2066–2071). Lyon, France.

[Nguyễn 2018c] Bảo-Huy Nguyễn, João Pedro F. Trovão, Ronan German, Alain Bouscayrol, and Yves Goulet. (2018). Optimal energy management of a parallel hybrid truck for fuel consumption comparative study. In *IEEE Vehicular Technology Conference* (pp. 1–5). Porto, Portugal.

[Nguyễn 2019] Bảo-Huy Nguyễn, Ronan German, João Pedro F. Trovão, and Alain Bouscayrol. (2019). Real-Time Energy Management of Battery/Supercapacitor Electric Vehicles Based on an Adaptation of Pontryagin's Minimum Principle. *IEEE Transactions on Vehicular Technology*, *68*(1), 203–212.

[Nüesch 2014] Tobias Nüesch, Alberto Cerofolini, Giorgio Mancini, Nicolò Cavina, Christopher Onder, and Lino Guzzella. (2014). Equivalent consumption minimization strategy for the control of real driving NOx emissions of a diesel hybrid electric vehicle. *Energies*, *7*(5), 3148–3178.

[Ogata 2009] K. Ogata. (2009). *Modern control engineering*. Prentice Hall.

[Paganelli 2000] Gino Paganelli, T. M. Guerra, Sebastien Delprat, J. J. Santin, M. Delhom, and E. Combes. (2000). Simulation and assessment of power control strategies for a parallel hybrid car. *Proceedings of the Institution of Mechanical Engineers, Part D: Journal of Automobile Engineering*, *214*(7), 705–717.

[Paganelli 2002] Gino Paganelli, Sebastien Delprat, T. M. Guerra, J. Rimaux, and J. J. Santin. (2002). Equivalent consumption minimization strategy for parallel hybrid powertrains. In *IEEE 55th Vehicular Technology Conference. VTC Spring 2002* (Vol. 4, pp. 2076–2081).

[Pagano 2007] Mario Pagano and Luigi Piegari. (2007). Hybrid electrochemical power sources for onboard applications. *IEEE Transactions on Energy Conversion*, *22*(2), 450–456.

[Pam 2017] Abdoulaye Pam, Alain Bouscayrol, Philippe Fiani, and Frederic Noth. (2017). Rule-based energy management strategy for a parallel hybrid electric vehicle deduced from dynamic programming. In *2017 IEEE Vehicle Power and Propulsion Conference, VPPC 2017 - Proceedings* (pp. 1–6).

[Pant 2014] YV Pant. (2014). Peak power reduction in hybrid energy systems with limited load forecasts. In *American Control Conference*.

[Pelletier 2018] Louis Pelletier, Félix-Antoine LeBel, Ruben Gonzalez Rubio, Marc-Andre Roux, and João Pedro F. Trovão. (2018). Design of a High Performance Battery Pack as a Constraint Satisfaction Problem. In *2018 IEEE Vehicle Power and Propulsion Conference (VPPC)*.

[Perdigão 2015] Marina S. Perdigão, João Pedro F. Trovão, J. M. Alonso, and E. S. Saraiva. (2015). Large-Signal Characterization of Power Inductors in EV Bidirectional DC-DC Converters Focused on Core Size Optimization. *IEEE Transactions on Industrial Electronics*, *62*(5), 3042–3051.

[Qiuming 2008] Gong Qiuming, Li Yaoyu, and Peng Zhong-Ren. (2008). Trip based optimal power management of plug-in hybrid electric vehicles using gas-kinetic traffic flow model. *IEEE Transactions on Vehicular Technology*, *57*(6), 3393–3401.

[Rajabzadeh 2016] Mahdi Rajabzadeh, Seyed Mohammad Taghi Bathaee, and Masoud Aliakbar Golkar. (2016). Dynamic modeling and nonlinear control of fuel cell vehicles with different hybrid power sources. *International Journal of Hydrogen Energy*, *41*(4), 3185–3198.

[Ross 2015] I. Michael Ross. (2015). *A Primer on Pontryagin's Principle in Optimal Control*. Collegiate Publishers.

[Salmasi 2007] Farzad Rajaei Salmasi. (2007). Control strategies for hybrid electric vehicles: Evolution, classification, comparison, and future trends. *IEEE Transactions on Vehicular Technology*, *56*(5), 2393–2404.

[Santucci 2014] Alberto Santucci, Aldo Sorniotti, and Constantina Lekakou. (2014). Power split strategies for hybrid energy storage systems for vehicular applications. *Journal of Power Sources*, *258*, 395–407.

[Sarasketa-Zabala 2016] E. Sarasketa-Zabala, E. Martinez-Laserna, M. Berecibar, I. Gandiaga, L. M. Rodriguez-Martinez, and I. Villarreal. (2016). Realistic lifetime prediction approach for Li-ion batteries. *Applied Energy*, *162*, 839–852.

[Savoye 2012] François Savoye, Pascal Venet, Michael Millet, and Jens Groot. (2012). Impact of periodic current pulses on Li-ion battery performance. *IEEE Transactions on Industrial Electronics*, *59*(9), 3481–3488.

[Schaltz 2009] Erik Schaltz, Alireza Khaligh, and Peter Omand Rasmussen. (2009). Influence of battery/ultracapacitor energy-storage sizing on battery lifetime in a fuel cell hybrid electric vehicle. *IEEE Transactions on Vehicular Technology*, *58*(8), 3882–3891.

[Sciarretta 2004] Antonio Sciarretta, Michael Back, and Lino Guzzella. (2004). Optimal control of parallel hybrid electric vehicles. *IEEE Transactions on Control Systems Technology*, *12*(3), 352–363.

[Sciarretta 2007] Antonio Sciarretta and Lino Guzzella. (2007). Control of hybrid electric vehicles. *IEEE Control*

Systems Magazine, *27*(2), 60–70.

[Sechilariu 2013] Manuela Sechilariu, Baochao Wang, and Fabrice Locment. (2013). Building Integrated Photovoltaic System With Energy Storage and Smart Grid Communication. *IEEE Transactions on Industrial Electronics*, *60*(4), 1607–1618.

[Shah Mohammadi 2018] Ahmad Shah Mohammadi, João Pedro F. Trovão, and Maxime R. Dubois. (2018). Hybridisation ratio for hybrid excitation synchronous motors in electric vehicles with enhanced performance. *IET Electrical Systems in Transportation*, *8*(1), 12–19.

[Song 2014] Ziyou Song, Jianqiu Li, Xuebing Han, Liangfei Xu, Languang Lu, Minggao Ouyang, and Heath Hofmann. (2014). Multi-objective optimization of a semi-active battery/supercapacitor energy storage system for electric vehicles. *Applied Energy*, *135*, 212–224.

[Song 2015] Ziyou Song, Heath Hofmann, Jianqiu Li, Xuebing Han, and Minggao Ouyang. (2015). Optimization for a hybrid energy storage system in electric vehicles using dynamic programing approach. *Applied Energy*, *139*, 151–162.

[Song 2017] Ziyou Song, Jun Hou, Heath Hofmann, Jianqiu Li, and Minggao Ouyang. (2017). Sliding-mode and Lyapunov function-based control for battery/supercapacitor hybrid energy storage system used in electric vehicles. *Energy*, *122*, 601-612.

[Sun 2015] Chao Sun, Scott Jason Moura, Xiaosong Hu, J. Karl Hedrick, and Fengchun Sun. (2015). Dynamic Traffic Feedback Data Enabled Energy Management in Plug-in Hybrid Electric Vehicles. *IEEE Transactions on Control Systems Technology*, *23*(3), 1075–1086.

[Sundström 2009] Olle Sundström and Lino Guzzella. (2009). A generic dynamic programming Matlab function. In *Proceedings of the IEEE International Conference on Control Applications* (pp. 1625–1630).

[Suzuki 2008] Masahiro Suzuki, Pongsathorn Raksincharoensak, and Masao Nagai. (2008). Fuel Economy Improvement Strategy for Light Duty Hybrid Truck Based on Fuel Consumption Computational Model Using Neural Network. In *Proceedings of the 17th World Congress The International Federation of Automatic Control* (pp. 10719–10725). Seoul, Korea.

[Sylvas 2017] Emilia Silvas, Theo Hofman, Nikolce Murgovski, L. F. Pascal Etman, and Maarten Steinbuch. (2017). Review of Optimization Strategies for System-Level Design in Hybrid Electric Vehicles. *IEEE Transactions on Vehicular Technology*, *66*(1), 57–70.

[Tani 2012] Abdallah Tani, Mamadou Baïlo Camara, and Brayima Dakyo. (2012). Energy Management Based on Frequency Approach for Hybrid Electric Vehicle Applications: Fuel-Cell/Lithium-Battery and Ultracapacitors. *IEEE Transactions on Vehicular Technology*, *61*(8), 3375–3386.

[Thounthong 2009] Phatiphat Thounthong, Stephane Raël, and Bernard Davat. (2009). Energy management of fuel cell/battery/supercapacitor hybrid power source for vehicle applications. *Journal of Power Sources*, *193*(1), 376–385.

[Thounthong 2010] Phatiphat Thounthong, Serge Pierfederici, Jean Philippe Martin, Melika Hinaje, and Bernard Davat. (2010). Modeling and control of fuel cell/supercapacitor hybrid source based on differential flatness control. *IEEE Transactions on Vehicular Technology*, *59*(6), 2700–2710.

[Tian 2016] He Tian, Ziwang Lu, Xu Wang, Xinlong Zhang, Yong Huang, and Guangyu Tian. (2016). A length ratio based neural network energy management strategy for online control of plug-in hybrid electric city bus. *Applied Energy*, *177*, 71–80.

[Tie 2013] Siang Fui Tie and Chee Wei Tan. (2013). A review of energy sources and energy management system in electric vehicles. *Renewable and Sustainable Energy Reviews*, *20*, 82–102.

[Trovão 2013a] João Pedro F. Trovão, Paulo G. Pereirinha, Humberto M. Jorge, and Carlos Henggeler Antunes. (2013). A multi-level energy management system for multi-source electric vehicles - An integrated rule-based meta-heuristic approach. *Applied Energy*, *105*, 304–318.

[Trovão 2013b] João Pedro F. Trovão, Victor D. N. Santos, Paulo G. Pereirinha, Humberto M. Jorge, and Carlos H. Antunes. (2013). A simulated annealing approach for optimal power source management in a small EV. *IEEE Transactions on Sustainable Energy*, *4*(4), 867–876.

[Trovão 2015a] João Pedro F. Trovão and Carlos Henggeler Antunes. (2015). A comparative analysis of meta-heuristic methods for power management of a dual energy storage system for electric vehicles. *Energy Conversion and Management*, *95*, 281–296.

[Trovão 2015b] João Pedro F. Trovão, Victor D. N. Santos, Carlos Henggeler Antunes, Paulo G. Pereirinha, and Humberto M. Jorge. (2015). A Real-Time Energy Management Architecture for Multisource Electric Vehicles. *IEEE Transactions on Industrial Electronics*, *62*(5), 3223–3233.

[Trovão 2016] João Pedro F. Trovão, Felipe Machado, and Paulo G. Pereirinha. (2016). Hybrid electric excursion ships power supply system based on a multiple energy storage system. *IET Electrical Systems in Transportation*, *6*(3), 190–201.

[Trovão 2017] João Pedro F. Trovão, Marc Andre Roux, Eric Menard, and Maxime R. Dubois. (2017). Energy- and power-split management of dual energy storage system for a three-wheel electric vehicle. *IEEE Transactions on Vehicular Technology*, *66*(7), 5540–5550.

[Tutuianu 2014] Monica Tutuianu, Alessandro Marotta, Heinz Steven, Eva Ericsson, Takahiro Haniu, Noriyuki Ichikawa, and Hajime Ishii. (2014). *Development of a World-wide Worldwide harmonized Light duty driving Test Cycle (WLTC)*. *Technical Report* (Vol. 03).

[Uddin 2016] Kotub Uddin, Andrew D. Moore, Anup Barai, and James Marco. (2016). The effects of high frequency current ripple on electric vehicle battery performance. *Applied Energy*, *178*, 142–154.

[Uzunoglu 2008] M. Uzunoglu and M. S. Alam. (2008). Modeling and Analysis of an FC/UC Hybrid Vehicular Power System Using a Novel-Wavelet-Based Load Sharing Algorithm. *IEEE Transactions on Energy Conversion*, *23*(1), 263–272.

[Van Keulen 2014] Thijs Van Keulen, Jan Gillot, Bram De Jager, and Maarten Steinbuch. (2014). Solution for state constrained optimal control problems applied to power split control for hybrid vehicles. *Automatica*, *50*(1), 187–192.

[Vinot 2013] Emmanuel Vinot and Rochdi Trigui. (2013). Optimal energy management of HEVs with hybrid storage system. *Energy Conversion and Management*, *76*, 437–452.

[Vinot 2014] Emmanuel Vinot, Rochdi Trigui, Yuan Cheng, Christophe Espanet, Alain Bouscayrol, and Vincent Reinbold. (2014). Improvement of an EVT-Based HEV Using Dynamic Programming. *IEEE Transactions on Vehicular Technology*, *63*(1), 40–50.

[Vulturescu 2013] Bogdan Vulturescu, Rochdi Trigui, Richard Lallemand, and Gérard Coquery. (2013). Implementation and test of a hybrid storage system on an electric urban bus. *Transportation Research Part C: Emerging Technologies*, *30*, 55–66.

[Waldmann 2014] Thomas Waldmann, Marcel Wilka, Michael Kasper, Meike Fleischhammer, and Margret Wohlfahrt-Mehrens. (2014). Temperature dependent ageing mechanisms in Lithium-ion batteries - A Post-Mortem study. *Journal of Power Sources*, *262*, 129–135.

[Wang B. 2016] Bin Wang, Jun Xu, Binggang Cao, and Bo Ning. (2016). Adaptive mode switch strategy based on simulated annealing optimization of a multi-mode hybrid energy storage system for electric vehicles. *Applied Energy*, *194*, 596–608.

[Wang L. 2011] Lei Wang, Emmanuel G. Collins, and Hui Li. (2011). Optimal design and real-time control for energy management in electric vehicles. *IEEE Transactions on Vehicular Technology*, *60*(4), 1419–1429.

[Wei 2017] Shouyang Wei, Yuan Zou, Fengchun Sun, and Onder Christopher. (2017). A pseudospectral method for solving optimal control problem of a hybrid tracked vehicle. *Applied Energy*, *194*, 588–595.

[Werkstetter 2015] Stefan Werkstetter. (2015). *Ultracapacitor Usage in Wind Turbine Pitch Control Systems*. Maxwell Technologies.

[Whittingham 2012] M. S. Whittingham. (2012). History, Evolution, and Future Status of Energy Storage. *Proceedings of the IEEE*, *100*(Special Centennial Issue), 1518–1534.

[Wu 2014] Guoyuan Wu, Kanok Boriboonsomsin, and Matthew J. Barth. (2014). Development and evaluation of an intelligent energy-management strategy for plug-in hybrid electric vehicles. *IEEE Transactions on*

Intelligent Transportation Systems, *15*(3), 1091–1100.

[Xiang 2017] Changle Xiang, Feng Ding, Weida Wang, and Wei He. (2017). Energy management of a dual-mode power-split hybrid electric vehicle based on velocity prediction and nonlinear model predictive control. *Applied Energy*, *189*, 640–653.

[Yin 2017] Changjie Yin, Hongwei Wu, Fabrice Locment, and Manuela Sechilariu. (2017). Energy management of DC microgrid based on photovoltaic combined with diesel generator and supercapacitor. *Energy Conversion and Management*, *132*(4), 14–27.

[Yoo 2008] H. Yoo, Sul Seung-Ki, Park Yongho, and Jeong Jongchan. (2008). System Integration and Power Flow Management for a Series Hybrid Electric Vehicle using Super-capacitors and Batteries. *IEEE Transactions on Industry Applications*, *44*(1), 108–114.

[Zhang 2008] Xi Zhang, Chris Chunting Mi, Abul Masrur, and David Daniszewski. (2008). Wavelet-transform-based power management of hybrid vehicles with multiple on-board energy sources including fuel cell, battery and ultracapacitor. *Journal of Power Sources*, *185*(2), 1533–1543.

[Zhou 2019] Yang Zhou, Alexandre Ravey, and Marie-Cécile Péra. (2019). A survey on driving prediction techniques for predictive energy management of plug-in hybrid electric vehicles. *Journal of Power Sources*, *412*(2019), 480–495.